L-Università ta' Malta
Faculty of Engineering

DOCTOR OF PHILOSOPHY IN ENGINEERING DISSERTATION

Development of the Mechanical Framework for a Minimal Anthropomorphic Prosthetic Hand

YESENIA AQUILINA

Supervised by:
PROF. MICHAEL A. SALIBA

Co-supervised by:
PROF. ALEXIEI DINGLI
DR. JESMOND ATTARD

A dissertation submitted in partial fulfilment of the requirements for the degree of Doctor of Philosophy in Engineering

by the

Faculty of Engineering

October 2023

FACULTY OF ENGINEERING

DECLARATION OF AUTHENTICITY FOR DOCTORAL STUDENTS

(a) Authenticity of Thesis/Dissertation

I hereby declare that I am the legitimate author of this Thesis/Dissertation and that it is my original work.

No portion of this work has been submitted in support of an application for another degree or qualification of this or any other university or institution of higher education.

I hold the University of Malta harmless against any third party claims with regard to copyright violation, breach of confidentiality, defamation and any other third party right infringement.

(b) Research Code of Practice and Ethics Review Procedure

I declare that I have abided by the University's Research Ethics Review Procedures. Research Ethics & Data Protection form code 2903_02102019_Yesenia Aquilina.

□ As a Ph.D. student, as per Regulation 66 of the Doctor of Philosophy Regulations, I accept that my thesis be made publicly available on the University of Malta Institutional Repository.

□ As a Doctor of Sacred Theology student, as per Regulation 17 (3) of the Doctor of Sacred Theology Regulations, I accept that my thesis be made publicly available on the University of Malta Institutional Repository.

□ As a Doctor of Music student, as per Regulation 26 (2) of the Doctor of Music Regulations, I accept that my dissertation be made publicly available on the University of Malta Institutional Repository.

□ As a Professional Doctorate student, as per Regulation 55 of the Professional Doctorate Regulations, I accept that my dissertation be made publicly available on the University of Malta Institutional Repository.

COPYRIGHT NOTICE

ABSTRACT

Upper limb amputation may severely affect the quality of life of amputees, as it hinders their ability to perform daily activities, especially bimanual activities. For this reason, numerous prosthetic solutions have been developed throughout the years. Unfortunately, amputees sometimes reject such devices, with the most common reason being dissatisfaction with various aspects of their design, such as appearance, function, and ease of control. However, designing an anthropomorphic prosthetic hand that replicates the human hand in its control, form and mechanical behaviour is exceedingly difficult, due to weight and size constraints. Hence, prosthetic hands either lack dexterous capabilities or make use of complex structures and subcomponents, resulting in bulky and heavy designs that are less usable. This incongruence regarding simplicity, dexterity and usability is one of the key issues in the development of commercial prosthetic hands.

Thus, the aim of this work is to carry out a systematic exercise to seek a practical solution that optimizes the trade-off involving these three attributes. Previous research found in the literature has shown that despite the complexity of the human hand, the variance in the patterns of human hand configuration and movements can be described by a few parameters, giving rise to postural synergies (that is, common patterns of hand configurations). It implies that effective coupling of joints can simplify the control of the prosthetic hand as well as its design, while maintaining high dexterity. This work exploits this concept through an innovative approach to develop a non-dominant, minimal anthropomorphic prosthetic hand (that is, three active digits: the thumb, the index, and the middle finger), for additional support during bimanual activities.

The postural synergies of the minimal anthropomorphic hand when carrying out bimanual activities were determined through a principal component analysis of new experimental data. These synergies were then exploited by means of extensive analytical and simulation work to develop a simple kinematic hand structure that exhibits an acceptable and optimum dexterity while maintaining high usability of the device. The effectiveness of the approach was then evaluated by developing and constructing a prototype of a prosthetic hand based on the resulting kinematic architecture. The final prototype, despite its simplicity, was able to execute various daily activities using only four fundamental motions that are highly usable and intuitive to the amputee.

ACKNOWLEDGEMENTS

The completion of this project would not have been possible without the support and guidance of several individuals to whom I would like to express my warmest thanks.

Foremost, I would like to thank my supervisor, Prof. Ing. Michael A. Saliba, for sharing his wisdom on the subject, as well as providing the necessary guidance to achieve the targeted goals.

My sincere gratitude also goes to my other co-supervisors, Prof. Alexiei Dingli and Dr Jesmond Attard, for their valuable insight into their respective fields, which was crucial for the success of this research.

A heartfelt thanks also goes to all the subjects that took part in the experiment that was carried out in this work, without whom this study would not have been possible.

I am also extremely grateful to Mr. Fabrizio Cali for his expertise and time dedicated to this work by modelling a realistic human hand in Blender.

A special thanks also goes to Mr Manuel Aquilina, the Robotic Systems Lab Officer, for his diligence and help during my work, together with the entire technical staff of the University Workshop for their work and advice.

Regarding the financial aspect of the research, my appreciation goes to the Malta Council for Science & Technology for funding this project.

Finally, I would also like to express my deepest gratitude to my caring, loving parents, Sebastian, and Sandra Aquilina, for their continuous moral support, patience, and guidance.

CONTENTS

LIST OF FIGURES

LIST OF TABLES

LIST OF ABBREVIATIONS

ABD	Abduction
ADD	Adduction
ADLs	Activities of Daily Living
AHAP	Anthropomorphic Hand Assessment Protocol
BADLs	Basic Activities of Daily Living
B-Grasp	Body Cream Container Grasp
CAD	Computer Aided Design
C-grasp	Toothpaste Cap Grasp
CMC	Carpometacarpal
CNS	Central Nervous System
CoM	Correlation Matrix
CvM	Covariance Matrix
Cyl	Cylindrical Grasp
DC	Direct Current
D-H	Denavit-Hartenberg
DIP	Distal Interphalangeal
DOA	Degrees of Actuation
DOF	Degrees of Freedom
EADLs	Enhanced Activities of Daily Living
EMG	Electromyography
EXT	Extension
FDM	Fusion Deposition Modelling
FEA	Finite Element Analysis
FLEX	Flexion
FP	Flexpoint Sensor Systems, Inc.
FSR	Force Resistive Sensor
GR	Gear Ratio
GA	Genetic Algorithm
GAS	Grasping Ability Score
GRG	Generalised Reduced Gradient
HCA	Hierarchical Cluster Analysis
Hook	Hook Grasp
IADLs	Instrumental Activities of Daily Living

IF	Interactivity of Fingers
IntPP	Intermediate Power-Precision Grasp
IP	Interphalangeal
KHS	Kinematic Hand Structure
LatP	Lateral Pinch
Lum	Lumbrical Grasp
MAProHand	Minimal Anthropomorphic Prosthetic Hand
MCP	Metacarpophalangeal
M-grasp	Medium-Sized Cup Grasp
MRL	Middle-Ring-Little Finger
N-grasp	Neutral Position
NBDM	Non-backdriveable Mechanism
NonP	Non-Prehensile
Obl	Oblique Palmar Grasp
O-grasp	Fully open hand configuration
PC	Principal Component
PCA	Principal Component Analysis
PG	Proto-Gesture
P-Grasp	Paper Grasp
Pinch	Pinch Grasp
PIP	Proximal Interphalangeal
PLA	Polylactic Acid
PM	Proto-Motion
PWM	Pulse-Width Modulation
RFS	Resistive Flex Sensor
ROM	Range of Motion
SF	Safety Factor
SD	Standard Deviation
sEMG	Surface Electromyography
S-grasp	A variation of the SP-grasp
SPG	Shift of the Proto-Grasps
SP-Grasp	Sewing-Pin Grasp
SpP	Special Pinch
SS	Spectra Symbol
T-grasp	Tablet Grasp

GLOSSARY OF SYMBOLS AND NOTATIONS

$a_{D_{i_D}}$	the link length, the distance between z_{i-1} and z_i about the x_i, m
b	face width of a gear, mm
c	Cosine function
cp_{1m_d}	Fingertip points that can attain three-finger pinch
cp_{m_d}	Fingertip points that can attain two-finger pinch
C	A set of kinematic constraints
CJ	Coupled Joint
CR	Coupling Ratio
d	The number of variables analysed using PCA
$\vec{d}_{c_i}$	The positional vector between the active joint of digit, D, and the contact force, $\vec{F}_{c_i}$, in terms of the coordinate axes of the active joint, which was obtained from Unity, m
$d_{D_{i_D}}$	the link offset, the distance between x_{i-1} and x_i about the z_i, m
$\vec{d}_i$	The vector quantifying the position of the i^{th} contact point with respect to the fixed frame, m.
D	Indicates the digit being considered, with T, I, and MRL referring to the Thumb, the Index and the MRL, respectively
D_c	The core distance of a bevel gear, m
$D_{MCP_{pulley}}$	The diameter of the pulley located at the MCP joint of the finger, mm
$D_{PIP_{pulley}}$	The diameter of the pulley located at the PIP joint of the finger, mm
DJ	Driving Joint
$etac$	Distribution index for crossover
$etam$	Distribution index for mutation
$\bar{E}$	The weights or loadings of the set of d-dimensional PCs
$\vec{F}_{c_i}$	Refers to the contact-force vector corresponding to one of the phalanges of the digit, D, in terms of the coordinate system of the active joint, which was obtained from Unity, N
$\vec{f}_i$	The force applied at each contact point relative to a local reference frame, N
$\vec{f}_{n_i}$	The vector component along the normal direction, N
$\vec{f}_{t_i}$	The vector component along the surface of the object, N
F_{A_1}, F_{A_2}	The external loads present when peeling a potato, N
$F_{B_1}, F_{B_2}, F_{B_3}$	The external loads present when opening a packaged-food box, N
F_f	The force required for the cart to overcome friction and start moving, N
F_{fk}	The external load present on the fork when eating food with a fork and a knife, N

F_k, T_k	The external loads present on the knife when eating food with a fork and a knife
F_{k_1}, F_{k_2}	The components of F_k in the vertical and horizontal direction, respectively, N
$\mathcal{F}_i$	The set of admissible forces that can be transmitted through a particular contact, N
F_{SB}	The maximum force recorded on the spring balance during the external-loads experiments, N
F_{Sh}, T_{Sh}	The external loads present when sharpening a pencil
FA	Fixed Angle, °
g	The gravitational pull, m/s^2
G	The grasp map which defines the linear mapping of an f_i to the corresponding w_i, together with the transformation from the local-contact reference frame to the object-defined fixed frame
GR_{AG_F}	The additional gear reduction required for the fingers
GR_{AG_T}	The additional gear reduction required for the thumb
GR_{gb_F}	The gear reduction of the finger gearbox
GR_{gb_T}	The gear reduction of the thumb gearbox
h_{m_d}	The distance between the position of the MCP of the m_d^{th} finger and the base of the thumb, mm
i	Refers to one of the contact points that make up the grasp
i_D	the number of the joint being considered for a particular joint
I	The moment of inertia around the neutral axis, m^4
I_F	The moment of inertia of the system, m^4
I_{Load_F}	The current drawn, mA
$I_{No_{load_T}}$	The rated no-load current of the thumb motor, mA
I_{stall_F}	The rated stall current of the finger motor, mA
I_{stall_T}	The rated stall current of the thumb motor, mA
j	The number of observations considered in the PCA
J	The polar second moment of area, m^4
$J_{C_i}^T$	The transpose of the hand Jacobian matrix, which relates the torque required at the active joint of digit D to the i^{th} contact force with reference to the local-contact frame.
k	The compensation coefficient that keeps the effect of v_{m_d} and v_{1m_d} balanced
l_{D_x}	The distance between x_0-axis and x_{D_1} -axis, m
l_{D_y}	The distance between y_0-axis and y_{D_1} -axis, m
l_{D_z}	The distance between z_0-axis and z_{D_1} -axis, m
L_f	The length of the fingers, mm
L_t	The length of the thumb, mm

M_b	Bending Moment, Nm
$M_{b_{max_{\{x,y\}}}}$	The maximum M_b observed in both the x- and y-directions, Nm
m_d	It can have a value from 1 to 4 in the IF, representing the four fingers, from the index to the little finger
m_{gear}	Gear module, mm
m_{MRL}	The mass of the MRL, kg
$m_{weights}$	The weights required to sharpen a pencil
n_d	The number of digits
$\vec{n}_{m_T}$	Unit vector in the direction of $\vec{T}_{m_T}$
$\vec{n}_T$	Unit vector in the direction of $\vec{T}_T$
N	The normal force, N
N_a	The number of active digits
Np	The size of the population used in the genetic algorithm
p_d	Pitch-circle diameter, mm
p_{m_d}	The fingertip points of the m_d^{th} finger
p_t	The fingertip points of the thumb
P	Posture matrix used for PCA
Pc	Probability of Crossover
Pm	Probability of Mutation
Q	The first moment of area of the section above the point of shear stress, with reference to the neutral axis, m^3
Q_k	Principal Component Scores for one of the observations
r	The radius between the point mass and the axis of rotation of the motor, m
r_{mean}	The mean pitch radius for a bevel gear, m
r_n	Random number generating during the crossover and mutation process
R_{Fixed}	The resistor connected in series with the RFS, Ω
R_p	The reaction force between the shaft and the phalange, N
R_s	The reaction force acting on the shaft due to the structure, N
R_{shaft}	The radius of the thumb CMC shaft, m.
R_{Sensor}	Electrical resistance across an RFS, Ω
s	Sine function
t	The thickness of the shaft at a particular point of shear stress, m
T	Torsion, Nm
$\vec{T}_c$	The torque applied by the intact hand to open a water bottle, Nm
T_{cable}	The tensions that the cable would need to withstand during the execution of different activities, N
$\vec{T}_D$	The torque required at the active joint of digit, D, Nm

$T_{D_i}^{i-1}$	Represents the homogenous transformation from frame $i-1$ to frame i of a particular digit
T_{D_k}	The component of $\overrightarrow{T_D}$ in the z-axis, Nm
$T_{D_{k_s}}$	The scaled-down torque applied by the $\overrightarrow{F_p}$ about the fingers' active joint, taking into consideration the maximum torque that can be applied by the thumb, Nm
T_{Load_F}	The load on the finger motor when actuating the fingers at constant speed, Nm
$\overrightarrow{T_{m_f}}$	The resulting output torque from the transmission system of the fingers, Nm
$\overrightarrow{T_{m_T}}$	The torque that needs to be applied by the thumb motor, Nm
T_O	Desired output torque of a gear, Nm
$T_{O_{gb_T}}$	The output torque of the thumb gearbox, Nm
T_P	The moment applied by $\vec{F}_{c_1}$ around the thumb CMC joint axis, Nm
$\overrightarrow{T_s}$	The "unnecessary" torque applied at the thumb CMC Joint against the structure of the finger, Nm
T_{Stall_F}	The rated stall torque of the finger motor, Nm
T_{Stall_T}	The rated stall torque of the thumb motor, Nm
T_{ww}	The torque that the worm wheel would need to withstand during the execution of different activities, Nm
$T_{TC_{PIP}}$	The torque created by T_{cable} around the PIP joint, Nm
V	Shear Force, N
V_{in}	The supply voltage of a voltage divider, V
V_{out}	The voltage across R_{Fixed}, V
V_{sensor}	The voltage across R_{sensor}, V
V_{sp}	The supply voltage of the finger motor, V
$\vec{w}_e$	External wrench applied on the object
$\vec{w}_i$	A vector which quantifies the force and torques applied by a contact force on the object with respect to a global reference frame fixed on the object
w_{m_d}	A weighting factor which reflects the importance of each finger in the robot hand
W	The normal load present between two gears, N
W_a	The axial Force applied on the teeth of the gear, N
$\vec{W}_{bt}$	The weight of a water bottle, N
W_g	Grasp Wrench Space
W_{gh}	Grasp Wrench Hull
W_{object}	The weight of the object considered for the experiment estimating μ_{rubber}, N

W_r	The radial force applied on the teeth of the gear, N
W_t	Tangential force applied on the teeth of the gear, N
$W_{t_{LF}}$	The maximum allowable force that can be applied, tangential to the tooth, N
x_1^c, x_2^c	Parameters of two offspring solutions
x_1^p, x_2^p	Parameters of two parent chromosomes
y	The vertical distance away from the neutral axis, m
Y	The Modified Lewis form factor
z_1	The number of teeth on the driver gear
z_2	The number of teeth on the driven gear
z_{e_b}	The spur gear equivalent number of teeth for a bevel gear
z_{e_w}	The spur gear equivalent number of teeth for a worm wheel.
$\bar{Z}$	The grand mean computed over the entire observations
α	The assumed angular acceleration of the fingers, rad/s^2
$\alpha_{D_{i_D}}$	the link twist, the angle between z_{i-1} and z_i about the x_i, rad
$\alpha_{i,j}$	The weighting of each of the forces that approximates the friction cone at contact point i
β	A parameter calculated during the crossover process
β_{1_i}, β_{2_i}	The frictional weightings for $\vec{f}_{t_{1_i}}$ and $\vec{f}_{t_{2_i}}$, respectively
γ	The lead angle of the worm and wheel, °
γ_T	The angle between T_{m_T} and $\overrightarrow{T_T}$, °
δ	A parameters calculated during the mutation process
δx	Small element along the face width of a bevel gear, m
$\Delta\theta$	Sample Degree of each joint, °
$\frac{\Delta\omega}{\Delta T}$	The slope of the speed vs torque of the selected finger motor, rpm/Nm
ε	The pitch cone angle, °
η_{AG_F}	The efficiency of the additional gear reduction
η_{AG_T}	The efficiency of the thumb additional gear reduction, %
η_{gb_F}	The efficiency of the finger gearbox %
η_{gb_T}	The efficiency of the thumb gearbox, %
η_{ww}	The efficiency of the worm and wheel, %
θ_{A_1}	1st rotation when modelling the thumb CMC joint with Angle Pair A,°
θ_{A_2}	2nd rotation when modelling the thumb CMC joint with Angle Pair A,°
θ_{B_1}	1st rotation when modelling the thumb CMC joint with Angle Pair B,°
θ_{B_2}	2nd rotation when modelling the thumb CMC joint with Angle Pair B,°
θ_{C_1}	1st rotation when modelling the thumb CMC joint with Angle Pair C,°
θ_{C_2}	2nd rotation when modelling the thumb CMC joint with Angle Pair C,°

$\theta_{D_{i_D}}$	The joint angle, the angle between x_{i-1} and x_i about the z_i, rad
θ_{slope}	Inclination angle of the plane, °
θ_{total}	The sum of the ROM of all joints, °
η_{m_F}	The efficiency of the finger motor, %
μ_{rubber}	The friction coefficient between the rubber chosen for the frictional covers and different materials applicable to day-to-day activities
μ_s	The static friction coefficient associated with the surface at the point of contact.
μ_{s1}	The static coefficient of rolling friction between the cart and the scale
μ_{ww}	The static friction coefficient between the worm and wheel
v_{1m_d}	The volume of intersection between the thumb and index fingertips and each of the other fingertips, mm^3
v_{m_d}	The volume of intersection between the workspace of the thumb fingertip and the fingertip of the m_d^{th} finger, mm^3
σ	Normal Stress, MPa
σ_y	The yield strength of the material from which the gears are manufactured; usually, it is steel, brass, aluminium or nylon, for commercial gears. MPa
τ	Shear Stress, MPa
τ_{normal}	The torque that soft-finger contact models can apply around the normal axis, Nm
τ_T	The maximum τ build up on the cross-section of the shaft due to T_P, MPa
$\tau_{V_{\{x,y\}}}$	The maximum τ build up on the cross-section of the shaft due to $V_{\{x,y\}}$, MPa
ϕ	The pressure angle of the gear teeth, °
ω_F	The angular speed of the fingers, rad/s
$\omega_{gb_{In_F}}$	The angular input speed of the finger gearbox, rpm
$\omega_{gb_{In_T}}$	The angular input speed of the thumb gearbox, rpm
ω_{load_F}	The angular speed of the motor when rotating the fingers at constant speed, rad/s
ω_{R_F}	The resulting speed of the finger after taking into account the load applied on the thumb motor, rpm
ω_T	The angular speed of the thumb, rpm

CHAPTER 1: INTRODUCTION

The human hand is a versatile, powerful tool which gives a vital contribution to the dexterity of the human body. In fact, the upper extremities are an integral part of an individual’s activities, communication, identity, and social interactions with others. It follows that upper-limb loss is not only disruptive to one’s body image, it also affects the amputee’s quality of life, including the psychological and social aspects [1]. Approximately, 22 million people worldwide suffer from upper-limb amputation [2]. Just in the United States, 541,000 amputees with upper-limb loss were reported in 2005, with the number of cases expected to double by 2050 [3]. Meanwhile, in the UK and Italy, 5200 and 3500 upper-limb amputees are reported each year [4].

An effective artificial hand can help amputees regain the independence and functionality that they had prior to the limb loss. For this reason, the field of prosthetics has attracted a lot of interest over the years, especially when it comes to developing an anthropomorphic prosthetic hand that mimics the human hand in its control and function. In fact, a simple online search indicates that up to 2022, 17,100 publications related to prosthetic hands were available, with 91% being published in the last decade [5]. However, despite the technical and clinical advancement made regarding upper-limb prosthetics, 24% to 70% of amputees are still abandoning their prosthetic devices, which is a considerable percentage [6]. There are several factors that contribute to this decision, with one of the most common factors being the device itself. This indicates that there are still aspects of the prosthetic hands currently available that need to be improved upon, such as the weight, cost, and ease of use.

One of the major engineering challenges encountered in this field is the difficulty to develop a device that excels in each of the following important but contradictory attributes related to prosthetic hands [7]:

- *Simplicity*, which refers to a design with the smallest possible number of components incorporated in a compact design, each component having minimal geometrical features and design variations whilst reducing the design constraints on other components. This aims to develop a device resembling the human hand in terms of weight and size that is reliable, affordable, and easily manufactured.
- *Dexterity*, which is associated with the Degrees of Freedom (DOF) (i.e., the maximum number of independent joints) and the compliance of a device that

allow it to perform a wide range of movements and force-related functions. It ensures that the user can use such device to perform several daily activities.

- *Usability*, which refers to the qualities of the device that allow the user to perform the required function with minimal effort and inputs. This ensures an intuitive and reliable control system.

A sensible balance between these three attributes is crucial for a device to be effective and accepted by the amputees. Therefore, the primary research objective of this work is to carry out a systematic exercise to develop a practical solution that optimises the trade-off between these attributes, while taking into consideration also the anthropomorphism of the hand.

Previous research at the University of Malta had already tackled this issue with the development of a minimal anthropomorphic artificial hand which includes only the essential features of the human hand, (three active digits: the thumb, the index and the middle finger) [8]. Hence, this work seeks to exploit and build on these results to develop a mechanical device, referred to as MAProHand (Minimal Anthropomorphic Prosthetic Hand), which is dexterous yet simple and with minimal control inputs required. This should then facilitate the design of an intuitive and reliable control system, based on Surface Electromyography (sEMG) signals (i.e., signals generated in the skeletal muscles), which was developed concurrently in a separate study [9], as part of the project entitled *The Development of the Mechanical and control Framework for a Minimal Anthropomorphic Prosthetic Hand (MAProHand)* [10]. The MAProHand project was carried out at the University of Malta in collaboration with the company, Orthopaedic Centre Malta [11]. This project was funded by the Malta Council for Science and Technology under the 2018 Fusion Technology Development Programme [10].

The primary objective of this research was divided into smaller goals as follows:

- Familiarization with the prosthetic hands available on the market and the discussion in the literature of the different techniques implemented to reduce the dimensionality of the prosthetic hand, with the aim of reducing the number of control inputs required, while maintaining a high dexterity and a simple design (Chapter 2).

- Identification of the required specifications of the prosthetic hand with reference to the amputee's needs, which will make it more acceptable to amputees (Chapter 3).
- Identification, through experiments on human volunteers and analytical work, of the bare minimum movements/grasps (i.e., the smallest possible number of control inputs) that a minimal anthropomorphic prosthetic hand must be capable of, to perform a range of daily activities. This step optimises the balance between dexterity and usability, while it paves the way for a simple design (Chapter 4).
- Development of a simple hand model capable of attaining the identified movements/grasps, while taking into consideration also the overall aesthetic of the hand. This ensures that the hand has sufficient dexterity for day-to-day activities, and that its design is simple and natural as much as possible (Chapter 5).
- Practical manifestation of the approach considered in this project by designing and constructing a prototype of MAProHand, based on the previously developed hand model (Chapter 6).
- Investigation of the effectiveness of the approach by evaluating the general characteristics and performance of MAProHand in different daily activities, and where possible, comparing it with other prosthetic hands available (Chapter 7).

As can be seen from the above, this thesis is structured in a way that each of the above objectives is addressed in a separate chapter.

CHAPTER 2: LITERATURE REVIEW

2.1 INTRODUCTION

This chapter examines the autonomy of the human hand, its importance in everyday tasks and the wide range of prosthetic hands currently available to compensate for upper-limb loss. However, as with any technology, current prosthetic hands have their own limitations. Thus, through a thorough literature review, the challenges encountered in the development and the strategies employed to overcome them will be discussed to offer a comprehensive understanding of this evolving field.

2.2 ANATOMY OF THE HUMAN HAND

The hands are responsible for most of a human being's mechanical interactions with their surroundings. They allow humans with different occupations and lifestyles to perform a considerable number of different activities, from exerting high forces to performing very precise movements. This dexterity is highly attributed to the complex architecture of the human hand. [12], [13].

The human hand is made up of twenty-seven bones, divided into three groups: eight *carpal* bones, five *metacarpal* bones, and fourteen *phalanges*, Figure 2.1. The nomenclature that will be used to refer to the position of these hand elements with respect to the three spatial directions can be found in Figure 2.2 [12], [13].

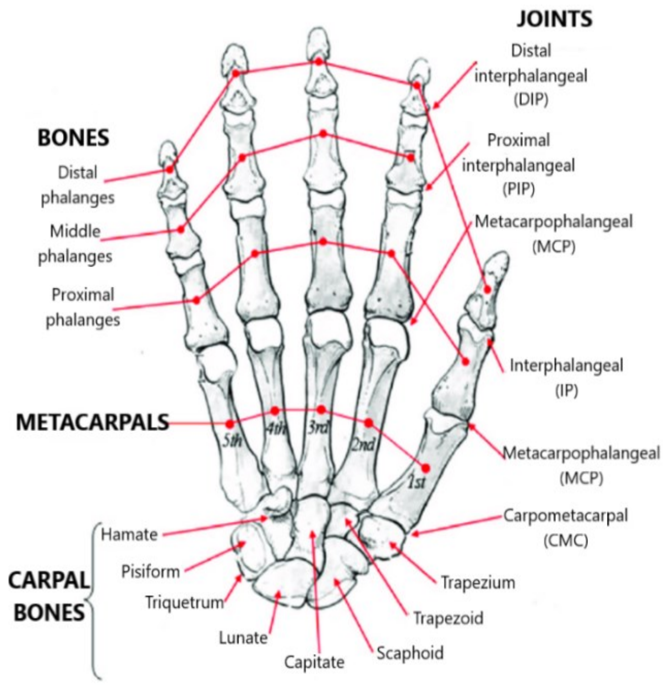

Figure 2.1: Palmar view of the bones and joints of the right hand [13]

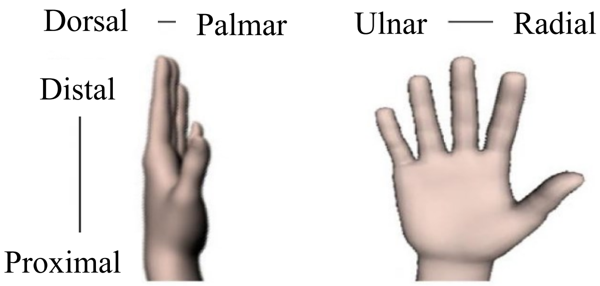

Figure 2.2: The terminology used to identify the position of the hand elements with respect to the three spatial directions [12]

The carpal bones are in the wrist and connect the bones in the forearm with the base of the five metacarpal bones, where four of these metacarpals form the palm of the hand. Each finger (i.e., the index, the middle, the ring and the little finger) then consists of three phalanges: proximal, middle, and distal phalanges, which become progressively smaller towards the end of the hand. On the other hand, the thumb only has two phalanges, with the middle one missing. These phalanges have a semicircular cross section with the palmar surface being almost flat, as opposed to the cylindrical shape of the metacarpals [12], [13].

These bones are linked together by different joints. From Figure 2.1, one can observe that each digit has four joints; *Carpometacarpal (CMC), Metacarpophalangeal (MCP), Proximal Interphalangeal (PIP)* and *Distal Interphalangeal (DIP)* joints, except for the thumb, which has only one *Interphalangeal Joint (IP)*. These joints are of the *synovial* type, which is the only type of joint present in the human hand, due to its structural characteristics which allow for smooth movement between the adjacent bones. In fact, these joints have a complex internal structure, Figure 2.3, which is comprised of the ends of the bone, the articular cartilage, synovial membrane, the articular capsule synovial fluid and in some cases also the bursae. Outside of their articulating surfaces, ligaments support the joint by connecting the bones together and preventing excess or abnormal joint movement [14].

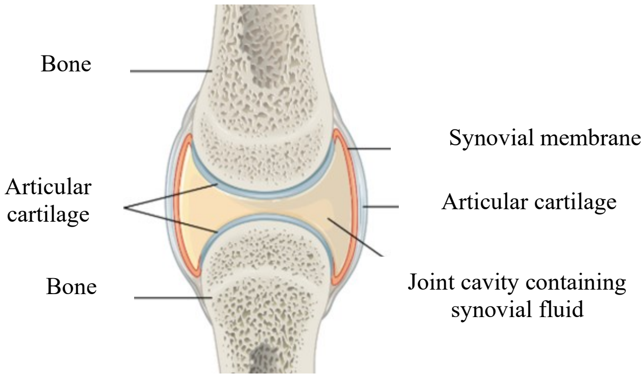

Figure 2.3: Synovial Joint [14]

Synovial joints can be further divided into six types: *pivot, hinge, saddle, plane, ball and socket,* and *condyloid joints*. Each type has its own function which defines the motion of the body/human hand and its limitation. The four types of synovial joints found in the human hand are outlined in Table 2.1; these allow the digits to perform different movements, some of which are shown in Figure 2.4 [15].

Table 2.1: Summary of the joints found in the human hand (adapted from [14],[15])

Joint Type		***Degrees of Freedom***	***Allowable Movements***	***Joints***
Plane Joints	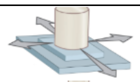	2	Flexion/Extension Lateral Deviation	Intercarpal joints of the wrist and palm
Saddle Joints	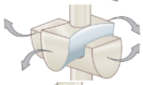	2	Abduction/Adduction Circumduction	Carpometacarpal joint of the thumb
Condyloid Joints		2	Flexion/Extension Abduction/Adduction Limited Circumduction	Wrist joint and Metacarpophalangeal joints
Hinge Joints	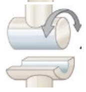	1	Flexion/Extension	Distal-Interphalangeal joints and Proximal Interphalangeal joints

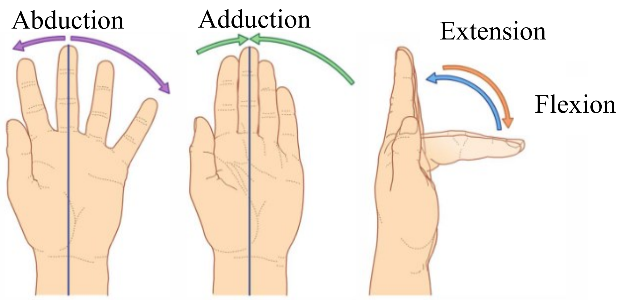

Figure 2.4: Some of the allowable movements of the digits [15]

Hence, each finger has four DOFs: two DOFs at the MCP joint (Flexion (FLEX)/Extension (EXT) and Abduction (ABD)/Adduction (ADD)), one DOF at the PIP joint (FLEX/EXT) and another DOF at the DIP joint (FLEX/EXT). The DOF (FLEX/EXT) at the CMC joint of the fingers is nominal, with the mobility of the joint decreasing to nil, from the fifth to the second CMC joint. Although the Range of Motion (ROM) of the fourth and fifth CMC joint is limited, it is necessary for the ring and little finger to oppose the thumb [16].

Meanwhile, the thumb has five DOFs: one FLEX/EXT movement at the IP joint and two DOFs (FLEX/EXT and ABD/ADD) for both the MCP joint and the CMC joint, with the mobility of the MCP joint being limited in the ABD/ADD direction. It is important to note that in literature the plane of the FLEX/EXT and ABD/ADD of the CMC joint is sometimes interchanged. This work will make use of the terminology shown in Figure 2.5. The thumb also exhibits pronation and supination, which is the twisting motion of the digit. However, Cooney et al. [17] demonstrated that this twist is not another DOF and that its magnitude is dependent on the amount of FLEX and ABD of the CMC joint. Hollister et al. [18] then showed that this is because the CMC joint consists of two non-intersecting, non-orthogonal axes.

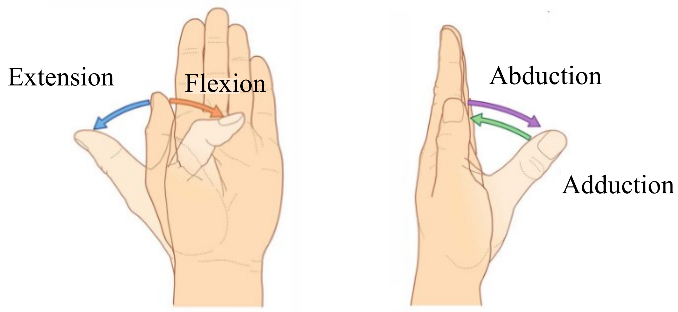

Figure 2.5: The two degrees of freedom of the thumb CMC joint [15]

The typical ROM of each of these DOFs are listed in Table 2.2, and it considers only the motion that can be achieved without any external forces [19]. By combining these DOFs, the hand is then able to formulate different movements, such as thumb opposition, and various postures to grasp and manipulate different objects [20].

Table 2.2: Typical range of motion of the degrees of freedom of the human hand [19]

Joint	***DOF***	***Typical ROM (°)***
Thumb CMC	EXT/FLEX	0-65
	ADD/ABD	0-80
Thumb MCP	EXT/FLEX	0-45
Thumb IP	EXT/FLEX	0-90
#2-5 Finger MCP	EXT/FLEX	0-90
	ADD/ABD	0-20
#2-5 Finger PIP	EXT/FLEX	0-120
#2-5 Finger DIP	EXT/FLEX	0-90

The joints are actuated by muscles, which are connected to multiple bones, through tendons and a tough band of fibrous connective tissue. These muscles are found in the forearm, wrist, and hand, and can be divided into two main groups: *extrinsic* and *intrinsic*. The extrinsic muscles originate primarily in the forearm and are used to move the digits of the hand and provide strength. The intrinsic muscles are smaller and originate primarily in the hand itself; they are responsible for providing precise coordination for the fingers. Hence, for good coordination of hand movements, each digit is actuated by both types of muscles. However, various joints experience mechanical coupling due to biomechanical constraints, such as interconnections between tendons, interdigit webbings and multidigit insertions of extrinsic finger muscles. A common example is the dynamic coupling between the PIP and the DIP joint, where the DIP joint expresses some degree of movement when the PIP joint is moved. For this reason, the human hand is often considered an underactuated system [14], [15]. The hand is said to be in the *relaxed posture* when all its muscles are not working [12], [13].

A human being is able to instruct the muscles to move the arm, hand, fingers, and thumb by transmitting singles from the Central Nervous System (CNS) (i.e., the brain and the spinal cord) to the muscles via the motor neurons that pass through the nervous system of the hand. The three main nerves innervating the hand are the *radial, median* and *ulnar* nerves. All these nerves travel together from the shoulder to the wrist where they split up into numerous minor branches to innervate separate and distinct areas of the hand. They also carry signals back to the brain that have to do with sensation, such as temperature, touch, and pain. The neurons that transmit these signals are known as sensory neurons [15].

This section highlights the complex architecture of the human hand and demonstrates the astounding ability of the CNS, which can effortlessly select appropriate muscles to perform specific hand movements despite the several DOFs available.

2.3 THE LOSS OF THE HUMAN HAND

In the light of the description of the human hand in the previous section, it is understandable that upper-limb loss may be perceived as a traumatic event. It has lifelong consequences that affect both the personal and the social aspects of the individual's life.

The upper extremities allow human beings to perform anything from gross to fine motor skills, that, when combined, enable the execution of crucial activities for independent living [21]. These activities are known as *Activities of Daily Living* (ADLs), which can be divided into *Basic Activities of Daily Living* (BADLs), *Instrumental Activities of Daily Living* (IADLs) and *Enhanced Activities of Daily Living* (EADLs). BADLs refer to basic activities one performs to take care of oneself; they include grooming, feeding, dressing, transferring/ambulation, toileting, and bathing. Meanwhile, IADLs are higher-functioning activities which include shopping, housekeeping, transportation, telephone use, food preparation, laundry, the handling of finances and responsibility for one's own medications. On the other hand, EADLs include participation in social and enriching activities such as learning a new skill [22]. Hence, the human hands are an integral part of an individual's communication, activities, self-identity, and social interactions with others.

It follows that upper-limb loss adversely affects the amputee's lifestyle and quality of life, by reducing their level of autonomy when performing these ADLs. In fact, Jang et al. [23] found that 69% of respondents became unemployed or changed occupation mainly because they could not perform as well. All these factors may have negative implications on one's sense of self-esteem and psychology [1], [24].

However, living with the loss of an upper limb may be inevitable as a result of congenital anomaly, trauma (such as accidental injury and severe crush injury) or medical conditions (such as malignant tumour and vascular/infectious diseases). Depending on the case, the hand may be amputated at various anatomic levels, which include *transcarpal, wrist disarticulation, transradial, elbow disarticulation, trans-humeral, shoulder disarticulation* and *forequarter*, Figure 2.6. As a general rule, a longer limb is preferred due to the number of joints that remain intact, which means higher functionality for the amputee [25]. The most common type of upper-limb loss is transcarpal, with 61%, followed by trans-humeral and transradial with 16% and 12%, respectively. Only 3% suffered bilateral limb loss, which refers to the loss of both limbs [4]. Thus, this work focuses primarily on unilateral amputees, namely, people who had one of their hands amputated.

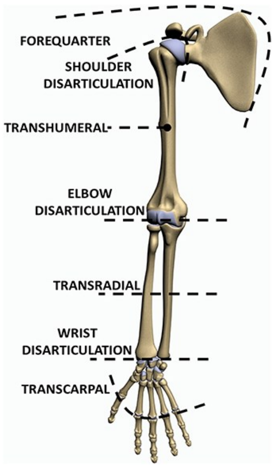

Figure 2.6: Levels of Upper-limb Loss [27]

After surgical recovery, amputees tend to go through three different stages, similar to grieving, which are disbelief, realisation and adaptation [26]. The realisation stage is the most important step as the amputee is faced with the chance to start accepting this loss and adapting accordingly. Therefore, it is crucial that during this period amputees are provided with effective rehabilitation aimed at helping them adjust and giving them the best opportunity to regain maximal function in tasks of daily living as quickly as possible [21], [27].

People with limb loss tend to rely heavily on their intact limb during everyday life, but the importance of both human hands and arms in daily activities should not be underestimated [28], [29]. This is because we live in a two-handed world, where a lot of daily activities require participation of both hands, each hand helping the other in a harmonious manner. In fact, problems for amputees usually arise from the inability to execute tasks which require the use of both hands, such as tying shoe laces, cutting food and buttoning clothes, rather than from predominantly one-handed activities such as writing (in the latter case, even if the amputee is missing his/her previously dominant hand, the function of the residual hand can be vastly improved through targeted training [30]). As a result, one-handed people may seek less public contact or vocational and social places to avoid embarrassing situations related to the difficulty in performing tasks requiring both hands; this will gradually lead to a loss of one's own security and self-pride in all tasks [31].

To help with this transition, two hands, or at least a substitute, are needed, such as the prosthetic hands designed to maintain the appearance and function of a regular hand. While it is possible that amputees try to adapt and manage daily tasks using only one hand and aids such as non-slip mats and fixating boards, a functional prosthesis offers greater independence through an increased activity level, which in turn may improve one's mental health [21], [32]. This highlights the importance of an effective prosthetic hand that caters to the amputee's needs.

2.4 UPPER-LIMB PROSTHETIC DEVICES

2.4.1 Introduction to Upper-Limb Prosthetic Devices

Throughout the years several prosthetic solutions have been developed to help amputees restore the function and form of their lost extremity, with the earliest example being a toe belonging to an Egyptian noblewoman, dated to between 950-710 B.C [33]. Given the importance of the human hand, several upper-limb prostheses are currently available for either research or commercial purposes. Typically these prostheses consist of four major components, which include *a terminal device, a wrist, a socket* and *a control system* [34], [35], Figure 2.8, which can then be covered with a flesh-tone cosmetic glove. Differences in these main components give rise to three main types of upper-limb prosthesis; *passive, active* and *hybrid* prostheses, which can be further divided as shown in Figure 2.7 [21], [27].

All these types of upper-limb prosthesis have their benefits and limitations. The most common type of prosthesis, based on a survey carried out by Ostlie et al. [32], was the myoelectric (34%), followed by body-powered (30%) and cosmetic (23%) prostheses, with the majority of the amputees wearing their prosthesis more than four hours daily.

The following sub-sections will discuss in more detail the different types of prosthetic hands available.

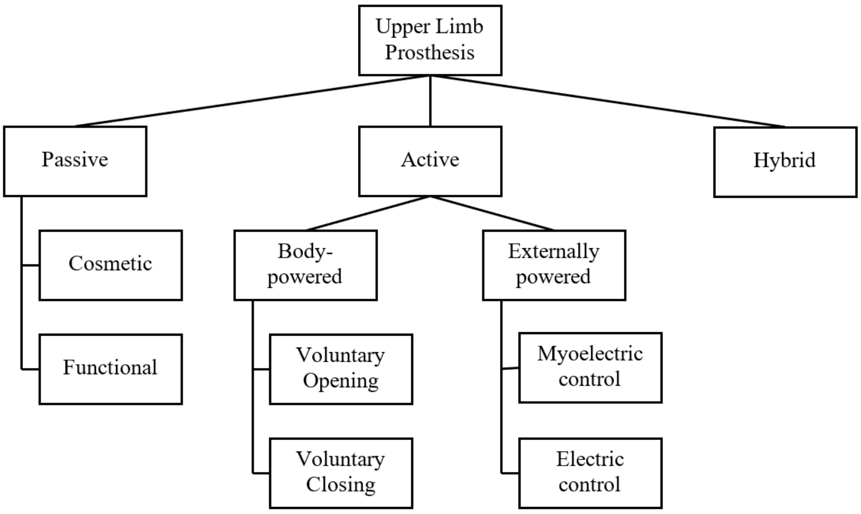

Figure 2.7: Classification of Upper-limb Prostheses (adapted from [21], [27])

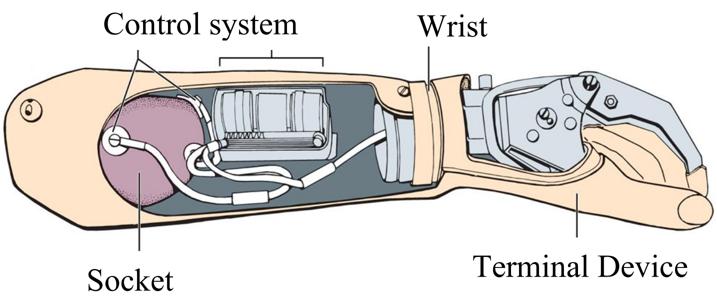

Figure 2.8: Typical components of a prosthetic hand (adapted from [33])

2.4.2 PASSIVE PROSTHESES

Passive prostheses are prosthetic hands which do not have any electronically or mechanically moving parts. They can be classified as cosmetic and functional prostheses. Cosmetic prostheses, Figure 2.9(a), aim at providing a life-like appearance of the missing body part. Thus, they are lightweight, and may be covered with high-definition silicone that closely matches the person's skin tone, or with a more basic-production glove. Even though cosmetic prostheses do not have any active moving joints, they may improve the person's functional capabilities such as pulling, pushing, supporting, and stabilizing. Meanwhile, functional prostheses, Figure 2.9(b), have a more mechanical appearance as they are designed to facilitate one specific activity (usually related to sport or work). This type of prosthesis is especially required for activities where two hands are needed but using the residual limb or even other types of prostheses is not a viable option, due to fear of injury/damage and/or lack of functionality regarding the intended activity. Both types of prosthesis can be either static (i.e., they do not move at all) or adjustable. This adjustability offers the amputee the option to orient various parts of the prosthesis or to adjust the grasping mechanism to improve its function [21], [27], [36].

(a) (b)

Figure 2.9: Cosmetic prosthesis [37] [38]

2.4.3 Active Prostheses

2.4.3.1 Body-Powered Prostheses

The body-powered prostheses are controlled by the movement of the amputee’s sound limb, which is captured through a harness and a cable, Figure 2.10. Various terminal devices may be fitted on the prostheses, such as a hook or a hand. The amputee may then opt to interchange the different devices, depending on the situation. For example, a hand would be preferred in a social setting. Specialised work devices may also be used to maximise the actions of the amputee, especially in cases of activities where traditional devices are not adequate.

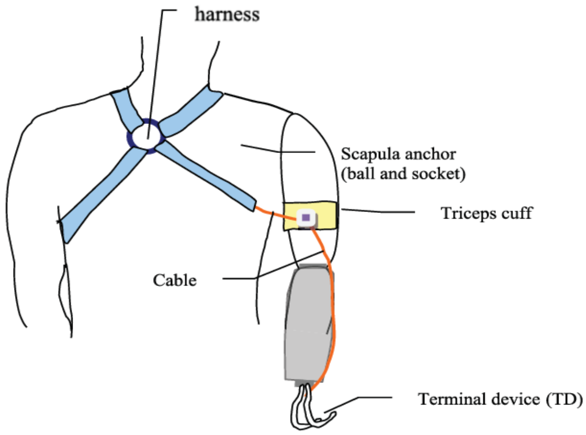

Figure 2.10: Body-powered system [40]

However, to maintain the simplicity of the body-powered prostheses, only one cable is used. This means that only one joint can be controlled, and in one direction. Consequently, a decision must be made on how to best use the active force generated by the user. There are two ways how this can be implemented, which are *voluntary opening* and *voluntary closing* [39]. Voluntary-opening terminal devices are the most common; they open when the cable is pulled, while a rubber band or a spring causes them to close again. On the other hand, the spring in a voluntary-closing device keeps it open; it closes by means of the cable.

Body-powered prostheses may be found lacking as regards cosmetic appearance, but they are lightweight, low-cost and durable. They can also provide some feedback through the tension in the control cable, and can be made waterproof. However, for the amputee to be able to use the device in all positions, especially overhead, s/he must have the ROM and strength to adequately pull the cable, which leads to high expenditure of energy. Nonetheless, people engaged in manual labour may favour such prostheses due to their basic function and durability [21], [27], [40].

2.4.3.2 Externally Powered Prostheses

Externally powered prostheses exploit an external power source (e.g., a battery pack) and actuators to provide power and movement to the prostheses. There are two main categories, *electric* and *myoelectric* prostheses, where the main difference is in the way they are operated.

For electric prostheses, people use external controllers, such as buttons, to operate the device. Thus, they are more suitable for people who have short/malformed limbs [27]. Meanwhile, myoelectric prostheses capture the amputee's intent through Electromyography (EMG) signals read from different muscles of the residual limb or upper body, depending on the level of amputation. This gives myoelectric devices a more 'natural control' when compared to other prostheses, which is why such devices are most used and will be the focus of this project.

Similar to body-powered systems, several terminal devices are available for myoelectric prostheses, with the most popular being motorized hands. These can be further grouped into two classes: *single-degree-of-freedom* and *multiarticulating*. Single-degree-of-freedom hands are the most durable type of myoelectric hands and can exert the most pinch force. This is because they only have one motor to open and close the hand. However, due to their simple design they are limited in the number of tasks whereby they can help the user. Examples of single-degree-of-freedom hands are the VASI hand [41] and the SensorHand Speed by Ottobock [42]. On the other hand, multiarticulating hands closely replicate the shape and size of the human hand, with commercial devices usually being available in different sizes. Due to their anthropomorphic nature, multiarticulating hands will be the focus of this work.

Examples of commercially available myoelectric multiarticulating hands include the Michelangelo Hand [43], the i-Limb Quantum [44] and the BeBionic Hand V3 [45], Figure 2.11.

(a) (b) (c)

Figure 2.11:(a) The Michelangelo Hand [43], (b) the i-Limb Quantum [44] and (c) BeBionic Hand V3 [45]

Commercial multiarticulating hands have different joints resembling the human hand. In fact, the fingers of such devices typically consist of a proximal joint, equivalent to the human MCP joint, and a single distal joint that emulates the shape of the PIP and DIP joint of the human hand. However, other kinematic designs do exist. In fact, the Michelangelo finger only has one joint, which corresponds to the MCP joint of the human hand. Meanwhile, the thumb in most prostheses is actuated in the FLEX/EXT direction and along the circumduction axis, with the distal joint also being actuated in some cases [46]. These joints are usually *rigid* (i.e., fixed, mechanical elements, such as pins, are used to connect the different links), but novel solutions, such as *flexible* and *dislocatable* joints, where elastic and flexible elements (e.g., springs), are used to introduce compliance in the joints, are gaining more popularity [47]. Examples of prosthetic hands that make use of these types of joints include the Pisa/IITSoftHand [48] and the Alpha Hand [49].

The different joints of the prosthetic hand are then driven by multiple actuators, which can also be combined with stiffness or impedance modulation to introduce compliance in the actuation mechanism. However, rigid actuation is more commonly used [47]. This involves an actuator, placed in either the palm or the proximal phalange, for a more compact design, that can reach and hold a specific position even in the presence of external loads applied to its output. Commercial prostheses tend to utilise Direct Current (DC) motors due to their weight and size. There are two types of DC motors available, namely, *brushed,* and *brushless*. Brushed motors are more common due to their ease of control, but brushless motors tend to provide higher torque-to-weight capabilities and generate less noise. Regardless of the type of DC motor utilised, a drive reduction, such as gears and even a harmonic drive, is usually required to reduce the speed and increase the torque supplied by the actuator. Many prostheses also include Non-Backdriveable Mechanisms (NBDMs) to hold the position of the digits, and thus, the high grip forces, without continuously draining the battery. Examples of common NBDMs include worm gears and leads screws. Compliant features, such as collapsible linkages, can then be introduced in the design as a precaution against breaking the fingers due to unexpected, excessive force [46].

However, to simplify the mechanical design, the number of motors in a prosthetic hand is usually smaller than the number of joints. Thus, some prostheses may manually power one of the joints, usually the thumb circumduction joint as in the BeBionic Hand [45]. Otherwise, several joints, such as the MCP and the PIP joints of the fingers, are coupled together [46]. Mechanisms used to couple the different joints will be discussed in more detail in Section 2.8.2 (on p.27).

Despite the resulting reduction in dimensionality when compared to the human hand, these devices can still offer a wide selection of grasp patterns which the amputee can exploit during daily activities. For example, the BeBionic Hand, with only six DOFs and five actuators, can attain fourteen different types of grasp, Figure 2.12, [50]. Depending on the actuation and transmission system, the prostheses may even allow the amputee to customise grasps that suit their lifestyle and preferences through software and wireless technology located within the hand [45]. Combined with the

Figure 2.12: The different grasp types that can be attained by the BeBionic hand v3 [50]

various wrist options currently available, this further increases the functionality of the hand, as it allows amputees to place the hand in a better position relative to the object.

To ensure that the task object is grasped with ease, some prostheses integrate soft finger pads, wide thumb profile, and padded palm (other benefits of the padded palm include protection of the internal mechanism and the grasped object, as well as reduction in the noise generated by the motors); this enhances the grip on the object. Features such as *proportional speed control* (i.e., precise control, suitable for delicate activities, such as holding an egg), *auto grip* function (i.e., the grip is automatically adjusted when it senses that the gripped item is slipping) and *sense of touch* (i.e., vibrations in the forearm that give the amputee cues when the prosthetic hand is in contact with the object) might also be included in the device for better control [45], [51]. Thus, the amputee only needs to make sure not to damage the device, by being careful not to exceed its maximum carrying capacity, which is highly dependent on its construction. In fact, the carrying capacities of the Michelangelo Hand and the BeBionic hand are $20kg$ [52] and $45kg$ [45], respectively.

For the amputee to be able to exploit these grip patterns, s/he must be able to give the prosthetic hand distinct and reliable commands based on his/her intentions. Given that individuated movements are not that critical for day-to-day activities, each grip pattern can be associated with a specific command, which is less tedious than having to actuate each finger individually. As discussed previously, in myoelectric prostheses, EMG signals are used to capture the amputee's intent. Techniques such as *Surface Electrodes, Targeted Muscular Re-innervation* [53] and *Intra-Muscular Wireless EMG transceivers* [54] can be used to read these EMG signals. Surface electrodes are the most common interface used in commercial products as they are less invasive [46], [47].

However, the information conveyed by the EMG signals is limited compared to the large number of grip patterns available. For this reason, commercial prostheses make use of different control schemes such as sequential schemes and movement triggers. External sources of information for grip selection have also been used, such as a mobile phone app, gesture control and passive radio frequency identification tags [21], [27], [55], [57]. In recent years, control systems based on pattern recognition have also been developed, where several electrodes are used to detect several repeatable signal patterns for different human contractions. There are only a few pattern recognition systems available on the market, with the Coapt Complete Control [58] being the first system commercialised in 2014 followed by the Ottobock Myo Plus System [59]. The state of the prosthetic hand is then communicated to the amputee through visuals, audible sounds, and vibrations.

However, state-of-the-art prostheses with multi-DOF, feedback and myoelectric control, are very expensive, and can range from around 20,000Eur to 100,000Eur [60]. This is in addition to the required maintenance required, which will also be expensive. Thus, in recent years, with the innovation of 3D printing (an additive manufacturing process which will be discussed in more detail in Section 6.4.1.1 (on p.155)), 3D-printed prosthetics are gaining popularity as an inexpensive alternative. Other benefits of 3D-printed prostheses may include customisation, better fit and light weight, but they tend to be inferior in performance and robustness when compared to the traditional commercial prosthesis [61], [62]. While there are not a lot of 3D-printed prostheses available on the market, examples of such prosthetic hands are shown in Figure 2.13, and include the Hero Arm [63] and the TrueLimb [51], while Limbitless [64] is currently in the clinical trial phase.


(a) (b) (c)

Figure 2.13: (a) the Hero Arm [63], (b) the TrueLimb [51], and (c) Limbitless [64]

Table 2.3 compares the general characteristics of the different anthropomorphic prosthetic hands currently available [21], [27].

2.4.4 Hybrid Prostheses

Hybrid prostheses, as the name indicates, combine externally powered and body-powered components into one device. They are typically used for shoulder disarticulation or transhumeral prostheses, where a myoelectric terminal device is attached to a body-powered elbow. Hybrid prostheses allow the user to operate both components simultaneously, while taking advantage of the higher gripping force of the powered hand and the light weight of the body-powered elbow [21].

Table 2.3: Published general characteristics of commercially available prosthetic hands

	Michelangelo Hand **[43]**	***i-limb Quantum [44]***	***BeBionic Hand v3*** **[45]**	***The Hero Arm*** **[63]**	***The TrueLimb*** **[51]**
Developer	Ottobock	Touch bionics	Ottobock	Open bionics	Unlimited Tomorrow
Weight without battery (g)	460	432-518	402-689	277-336	450-680 (including socket)
Height (mm)	160	154-183	162-188	165-178	customized
Width (mm)	-	72-86	72-85	70-80	customized
Thickness (mm)	-	35-39	50	48-55-	customized
Number of joints	6	11	11	10	14
No of actuators	2	6	5	3-4	-
No of DOFs	2	6	6	8/10	14
Passive DOFs	-	-	Thumb CMC joint	Thumb IP joint	Thumb CMC joint
Actuation Method	-	DC motor – Worm Gear	DC motor – lead screw	DC motor- tendons	-
Joint Coupling mechanism	Cam design with links to all fingers	Tendon linking MCP to PIP	Linkage spanning MCP to PIP	Tendon linking to MCP to the fingertip	Tendon linking to MCP to the fingertip
No. of grip patters	7	24	14	4/6	6
Maximum applied force	$70N$	Hold up to $90kg$	Hold up to $45kg$	Hold up to $8kg$	Hold up to $6.8kg$
Adaptive grip	No	Yes	Yes	Yes	Yes
Movement command	Different Switching modes available, in 4-channel control	Hold open, double impulse, triple, impulse, co-contraction	Co-contraction/open-open signals	Flexing and relaxing the wrist	Hold and pulse signals
Feedback	No	No	Audible beeps and/or Vibration	LEDs and Vibration	Vibration

2.5 ACCEPTANCE AND REJECTION OF PROSTHESES

From cosmetic hands to myoelectric multiarticulating hands, prosthesis design aims to satisfy the various needs and desires of people with upper-limb absence. Nonetheless, the percentage of amputees that abandon their prosthesis is high [6], [65]. The reason for this may be a lifestyle choice based on one's values, needs and perspective. However, it may also be the result of external factors, which include availability, insurance, and limited technology. Understanding the motivating factors behind the use and abandonment of prostheses is important for researchers trying to improve the design of the prostheses [66], [67], [68], and thus it will be discussed in further detail in this section.

The Anderson behavioural model for healthcare-service utilization was adapted by Biddiss and Chau to the rehabilitation of individuals with upper-limb deficiency,

Figure 2.14. It explains and/or predicts the utilization of prostheses through the influence of the following roles: (1) *the predisposing characteristics of an individual*; (2) *the established need*; (3) *the enabling resources* [66], [67].

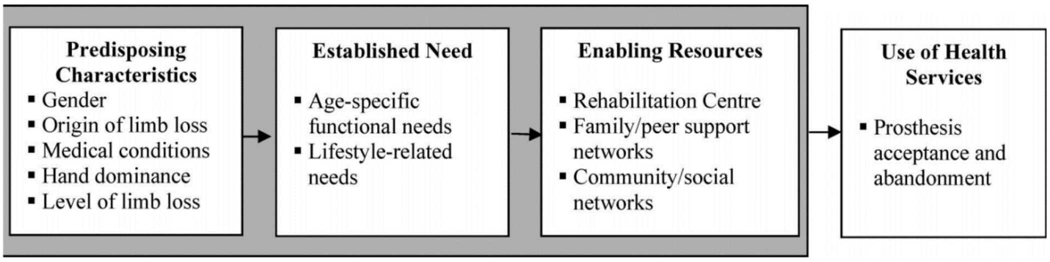

Figure 2.14: The adaptation of the Anderson behaviour model of health service utilization to the management of upper-limb deficiency [67]

From a review of twenty-five years of literature, the predisposing characteristics that define an individual (e.g., gender) and his/her condition (e.g., level of limb loss) could be factors that influence prosthesis acceptance and use. One of the most widely studied predisposing characteristics is the level of limb loss, which emerged as a primary disposing factor in prostheses usage. Acceptance of prostheses tends to diminish with a higher level of limb loss, where the prosthetic devices are usually heavier and require more energy to operate, and partial hand amputations, due to the lack of sensory feedback for grasp control and tactile sensation. Gender and age also play a role in the selection and usage of prostheses. In fact, females tend to opt for more anthropomorphic devices, but usage of prostheses tends to diminish with age [6]. Still, there was a lack of correlation between the loss of the dominant hand and the acceptance of the prostheses. This could be due to the fact that in unilateral limb loss, the remaining hand is the best substitute for manipulation, while the prosthesis usually assumes the functional role of the non-dominant hand [66], [67].

However, unless the amputees regard prostheses as a need to continue taking part in life activities, they will not justify their usage [67]. Prostheses are required in particular for difficult daily activities, which include those that require both hands, delicate movements and/or significant force from the distal extremities. In fact, unilateral amputees tend to make more use of their prostheses for bilateral activities such as tying shoelaces, opening a bottled beverage, using scissors, buttoning shirts, and closing a jacket zipper. Meanwhile, the prosthesis is less utilised in unimanual activities, such as moving a PC mouse [32] [23], [69]. Table 2.4 lists the challenging activities reported by the participants in the Biddiss et al. survey [70]. Nonetheless their lifestyle will also play a vital role in their choice of prostheses. For example, people who have occupations which require interaction with others and are concerned about their body image may reject prosthetic devices which may be more functional in favour of those that improve their appearance. Also, not all the amputee's functional needs may be met by just one prosthesis. Hence, it is good clinical practice to use several different prostheses that can complement each other [66], [67].

Table 2.4: The challenging activities reported by participants that took part in the Biddiss et al. survey [70]

Activity	Detailed description	Frequency
Household chores	Repairs and household maintenance (i.e., car repairs, shoveling snow, gardening, electrical work); general housework (i.e., vacuuming, dishes, cleaning); use of tools (i.e., hammer, power tools, shovels); heavy lifting; climbing (i.e., ladders)	40%
Sports	Cycling; swinging sports (i.e., golf, baseball, tennis); monkey bars/climbing; swimming; exercising; rock climbing; boating (i.e., canoeing, kayaking); ball sports (i.e., basketball, volleyball)	30%
Hobbies	Playing a musical instrument (i.e., guitar, piano); motorbike and airplane control; woodworking and crafts	22%
Activities of daily living	Food preparation and eating (cutting food, peeling, slicing); dressing (i.e., zippers, buttons, laces, pantyhose, ties); hair styling; typing; washing/personal hygiene; childcare; driving	19%
Social activities	Intimacy (i.e., sex, hugging); clapping; shaking hands; passing through airport security; dancing	8%
Occupational activities	Operating heavy machinery and large vehicles (i.e., farming equipment, trucks); training to be a doctor, surgeon, chemist etc.; law enforcement	6%

Amputees also live in a complex environment (i.e., the physical, social, and attitudinal environment). An environment with facilitating factors has the potential to positively influence the adaptation of prosthetic devices by limiting the effect of certain barriers. Hence, in addition to the need for a prosthesis and predisposition, there must also be constructs that facilitate prosthesis acceptance. These environmental factors can be mainly categorised as: (1) *products and technology*, (2) *attitudes*, (3) *support and relationships* [66], [67], [68].

The prosthesis itself is one of the environmental factors most commented on. It can facilitate everyday life for people with upper- . However, if the prosthesis does not satisfy the individual's needs regarding its efficiency, relevance, and learnability, s/he will not use it as it will not be worth the effort. The amputee community is dissatisfied with various aspects of the prosthetic design, including, *appearance* (i.e., life-like appearance under clothing), *comfort* (i.e., weight, comfort of harness and heat/perspiration), *function* (i.e., grip strength, noise, dexterity, grasp of big and soft objects, greater finger movement, longer-lasting batteries and wrist movement), *ease of control* (i.e., sensory feedback, frequency of unplanned movements, ability to keep objects from slipping, coordination of multiple joints, and physical effort needed to use), *maintenance* (i.e., glove staining and tearing, ease of cleaning, resistance to moisture/sand/dirt and frequency of minor repairs) and *cost* (i.e., cost of prosthesis and repairs) [68], [71], [72].. Addressing these issues would benefit all users and could also reduce rejection rates. In fact, in [66], 74% of the prosthesis rejecters stated that they would reconsider the use of a prosthesis if advancements were made at a reasonable price.

Ultimately, the acceptance of the prosthesis depends on the individual's positive attitude toward the prosthesis itself and their approach to the new lifestyle. Widehammar et al in [68] observed that the users of a prosthesis on a daily basis felt more comfortable wearing the prosthesis in public as it drew attention away from their disability. Meanwhile, the non-daily users felt that the prosthesis itself drew unwanted attention, as they did not incorporate it into their body image. It was also noted that these non-daily users experience reduced level of participation due to the rejection of the prosthesis, which is a problem [68]. Thus, positive support from family, society and healthcare is important for an amputee to have a more positive outlook. This is especially true during the rehabilitation process, which can be intimidating as amputees learn to cope and adapt to their prostheses. However, prosthesis use may also depend on societal support networks, such as local resources, accessibility, and funding, which may vary from one country to another. Thus, prosthesis use may be limited to a small part of the population for various reasons, ranging from lack of prosthetic equipment and government support to unsuitable amputation practices [66], [67], [68].

Unfortunately, these issues defeat the purpose of prosthetic devices. However, with an understanding of the factors that facilitate or hinder prosthesis usage, efforts can be made to provide the amputees with the required support and resources. As a result, this project focuses on improving the design of the prosthetic hand to best satisfy the needs of the amputee.

2.6 DESIGN REQUIREMENTS

Researchers improving the design of a prosthesis must first understand the design requirements to guide the research efforts. These design requirements can be determined from customer feedback, which helps track the user's needs and satisfaction, with Kejlaa (1993) [73] and Atkins et al. (1996) [74] being among the most notable.

The user's needs for upper-limb prosthesis may vary considerably, which is understandable, given that the amputee's reasons for the use of a prosthetic hand may vary from one individual to another. Consequently, individual solutions for the type of prosthesis, socket, control and training should always be considered. However, there are requirements that are common among different users, and thus, myoelectric prosthesis should aim to satisfy these requirements to improve their usefulness and acceptability. These requirements were extracted by Cordella et al. [27] and can be summarised as follows:

1. Allow the execution of important and complex daily activities by facilitating basic grasping actions (e.g., lateral, pinch, and neutral) and simple manipulation operations (e.g., rotating and pushing a coin). Several attempts such as [75], [76] have been made to classify the full range of grasps that can be executed by the human hand. For this reason, Feix et al. [77] developed a comprehensive taxonomy of thirty-three distinct prehensile grasps found in literature, Figure 2.15. However, certain grasps are used more frequently than others, making them more important. This is evident from an analysis of the grasps used in food preparation, housekeeping, laundry and the work of a machinist, which showed that a subset of the grasps shown in Figure 2.15 accounted for approximately 80% of the total duration [78], [79]. In this light, the relevance of the following nine different grasp types, namely, *cylindrical* (Cyl), *oblique* (Obl), *pad-to-pad pinch* (PpP), *lumbrical* (Lum), *hook* (Hook), *special pinch* (SpP), *non-prehensile* (NonP), *intermediate*

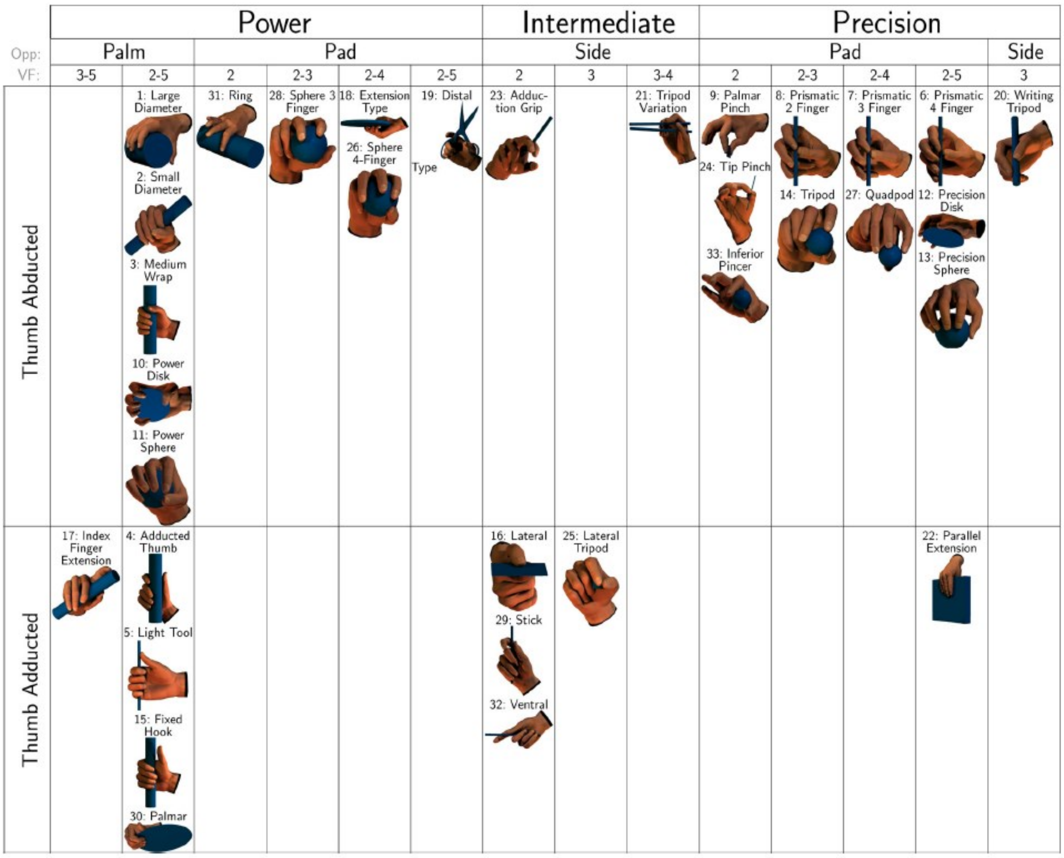

Figure 2.15: The comprehensive-grasp taxonomy developed by Feix et al. [77]

power-precision (IntPP), and *lateral pinch* (LatP) grasps, based on Edwards et al.'s [80] classification, in the achievement of autonomy was quantified by Gracia-Ibáñez et al. [81]. From this study, it was observed that the relevance of the grasp types depends on whether the hand is the dominant or the non-dominant one, and on whether the activity is unimanual or bimanual. In general, the most relevant grasp types are PpP (31.9%), NonP (18.6%), Lum (15.4%), Cyl (12%), SpP (7.3%); these highlight what a prosthesis should at least be able to execute.

2. Achieve a high level of anthropomorphism, in terms of weight, shape, size, colour, noise, number of digits and DOF.
3. Integrate a tactile sensorization system composed of sliding, contact, force, and temperature sensors.
4. Provide an effective control system that regulates the position of and force exerted by each finger, reducing the role of visual feedback, and giving more importance to sensory feedback.
5. Increase the variety of grasp types and move toward manipulation tasks required in day-to-day activities.
6. Increase the number of controlled DOFs of both the wrist and the hand digits to improve the dexterity of the prosthesis.
7. Reduce the cost of the prosthetic device and the cost to maintain it.

These requirements then dictate the mechanical design of an anthropomorphic hand. Belter et al. [46] proposed the following design criteria:

- The total weight of the prosthesis should not be more than $500g$, and a lighter prosthesis is desirable, especially for high-level amputation. In fact, amputees using a prosthesis weighing around $400g$ (i.e., the average weight of the human hand) have reported the hand as being too heavy and uncomfortable to use in daily activities [82]. This is because the weight of the prosthetic hand is borne by the stump's soft tissue rather than by the skeletal system as in the intact hand, thus yielding a higher perceived weight. For this reason, the weight of the prosthesis should be reduced as much as possible.
- The kinematics of the finger should be simple and robust.
- Powered circumduction of the thumb is desirable to be able to switch between palmar to lateral prehension.
- Brushless motors are preferred to brushed motors due to their performance-to-weight ratio.

- Maximum pinch force at the fingertips should be $65N$ when executing palmar prehension.
- The angular speed of the prosthesis should be between $115°/s$ and $230°/s$, but studies such as [82] have also stated that a closing speed of $90°/s$ is still adequate.
- The mechanical design of the prosthesis should be compliant with the object by using conforming fingertips/palmar pad, compliant joints, and other methods.
- The number of actuators embedded in the prosthetic hand should be reduced as much as possible.

These customer priorities and mechanical design criteria guide researchers in designing innovative prostheses that best address the requirements which are critical for amputees to reconsider using a prosthesis.

2.7 ENGINEERING CHALLENGES

Several researchers have addressed the challenge of developing a functional prosthetic hand that satisfies the amputee's needs. However, despite the technological advancements made in recent years, a prosthesis that satisfies all the customer requirements in one single device remains a difficult goal [57]. This section delves deeper into the engineering challenges encountered.

Prosthetic hands with a single DOF have simple mechanical and control systems which make them durable and robust but limited in the number of tasks in which they can help the user (i.e., low dexterity). Meanwhile, multiarticulating prostheses are capable of various grasping patterns, but make use of complex structures and subcomponents to embed multiple actuators, sensors and other components required in a prosthesis [27]. The number of components required greatly affects the size, weight and cost of the prostheses, Figure 2.16 [83]. The latter two parameters can be minimised with the use of 3D printing instead of conventional manufacturing processes. The issue that arises is that 3D-printed parts tend to have lower material strength. Thus, to prevent mechanical failure, a fairly bulky design is required, with the result that limitations on the objects that can be grasped or manipulated successfully become inevitable [84].

Additionally, the low performance of the techniques currently being used to detect the user's intentions hinders the full utilization of this increased dexterity in practical use. In fact, most of the existing control strategies (such as ON/OFF, and/or sequential scheme) are robust and reliable, but they are not intuitive as they do not correspond to the movement required by the prosthesis and may also require the amputee to carry

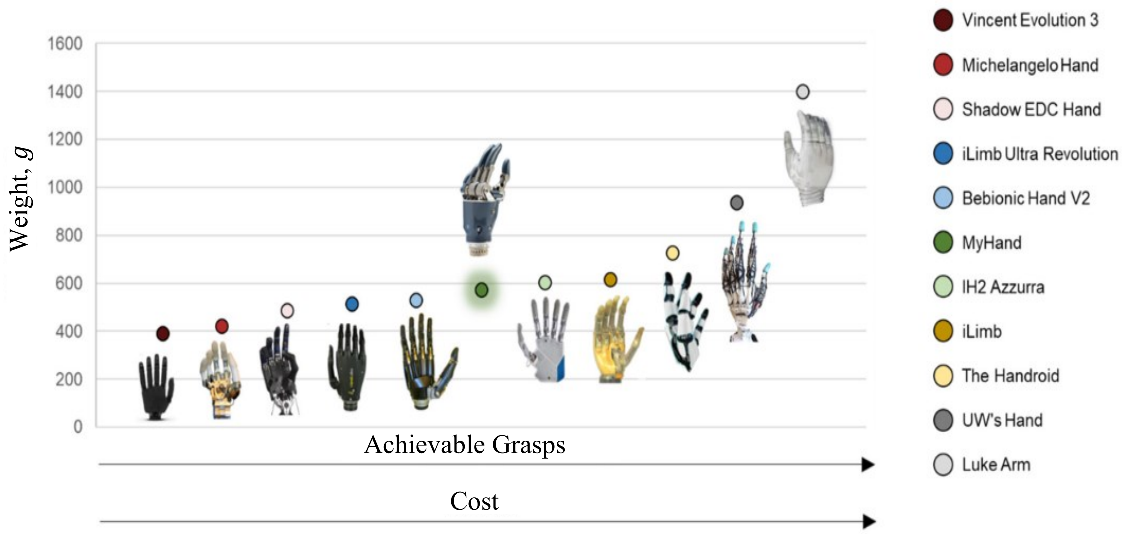

Figure 2.16: The comparison between the weight and the cost and achievable grasps of eleven anthropomorphic prosthetic hands [83]

additional devices with their intact hand. This means that controlling the prosthesis can be incredibly challenging to learn and mentally draining to operate. Short-range beacons such as radio-frequency identification tags can be used to reduce the cognitive load on the amputee, but the requirement for prior adaptation to the environment means that the use of the prosthesis is limited to specific areas [85]. Difficulty in controlling these devices also arises from signal degradation (due to sweating, scar tissue, and incorrect positioning of the socket) or involuntary co-contraction of residual limb muscle that leads to unplanned movements. On the other hand, control systems based on pattern recognition, such as the Coapt Complete Control [58], offer great potential for intuitive multi-function prostheses control, but their performance is also affected by electrode positioning, inherent cross-talk in the surface electrodes, fatigue, modification of arm posture, changes in temperature and muscles displacement during contraction. Therefore, apart from the extensive training required to obtain the best results, reliability issues make it difficult for the amputee to use the device effectively [36], [86], [87], [88].

This shows that if priority is given to the simplicity of the overall mechanical and control systems (thus aiming for lower cost and higher reliability), it is likely that a mechanical system with lower dexterity will be set up. Meanwhile, if the dexterity of the system is prioritised (aiming for a hand with increased grasping capabilities), the likely result will be an overly complex (i.e., lower simplicity) device whose usability is also reduced due to the challenges encountered by the user of such device. If system usability is the focus in the design process (aiming for a device that can be operated with ease), the likely yield will be a less dexterous device (i.e., lower dexterity) and a more complex control system (i.e., lower simplicity) [10]. This incongruence involving simplicity, dexterity and usability has proven to be a major engineering challenge in the design of prosthetic hands.

The key to obtain an anthropomorphic prosthetic hand that is as functional as possible, and at the same time simple, light, and convenient to use by the amputee, is to balance these three attributes in the best possible way. One way to contribute to this balance is to try to improve simplicity and usability by reducing in a systematic and studied manner the number of joints that can be controlled independently, thereby reducing the number of actuators and signals required while maintaining a high level of dexterity.

2.8 REDUCTION IN DIMENSIONALITY OF THE PROSTHETIC HAND

2.8.1 Minimal Anthropomorphic Hand

Depending on which joints are not controlled independently, the versatility of the hand may be significantly affected.

In view of this, an empirical study was carried out in [8] to quantify the relevance of the various hand attributes for dexterity (e.g., the presence of each finger) so as to provide a set of design guidelines for a simplified, yet dexterous, artificial hand. A series of standard tests were conducted on normal human subjects to measure manual dexterity in humans when different hand attributes were physically constrained. In the light of the results of that study, the authors proposed a minimal anthropomorphic hand that should include the following features:

- The thumb and two fingers (i.e., the index and the middle finger) with an overall size and phalanx length comparable to that of the human hand;
- Both the MCP and PIP joints of both fingers to be present, with ranges of motion and force capabilities comparable to those of the human hand; (Meanwhile, the DIP joint might need to be coupled to the PIP joint.)
- An ABD/ADD joint between the two fingers with a ROM comparable to that of the human counterpart;
- A thumb comparable to the human counterpart in terms of DOFs, ROM and force capabilities;
- An effective sense of touch.

The authors showed that a dexterity level (as defined and measured in the experiments) of about 84% could be attained by the minimal anthropomorphic hand, provided that the control, actuation/transmission, compliance, vision, and tactile processing systems of the device are comparable to those of the natural hand. Robotic hands that were developed at the University of Malta, based on the proposed kinematic configuration, are the UM-Mar Hands I and II, Figure 2.17, where both hands demonstrated high-level of dexterity [89], [90].

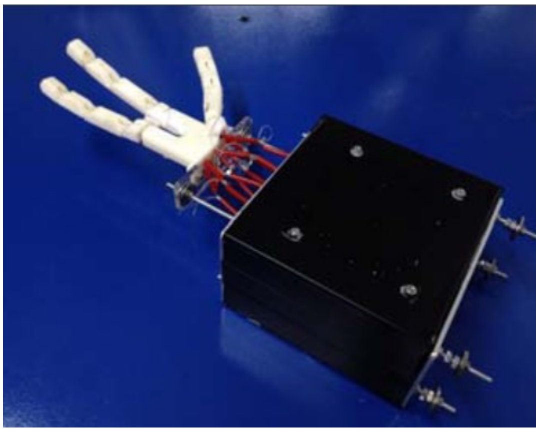

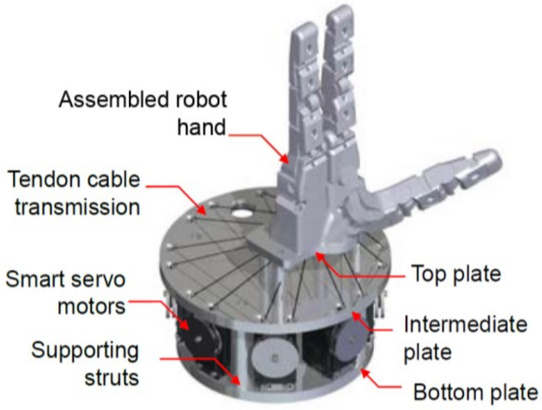

(a) (b)

Figure 2.17: Robotic hands based on the minimal anthropomorphic hand: (a) UM-Mar Hands I [89] and (b) UM-Mar Hands II [90]

The proposed kinematic architecture of the minimal anthropomorphic hand would have up to eleven joints, nine of which are independently actuated, assuming the ADD/ABD of the thumb MCP joint is neglected due to its limited movement. This means that nine actuators would be required which would very likely result in a bulky prosthetic hand, especially if they were to be embedded in the palm to cater for amputees with a shorter limb. This is evident from the size of the housing of the actuation systems in Figure 2.17.

2.8.2 Underactuation

To further simplify the kinematic architecture of the human hand, the concept of underactuation can be applied to the minimal anthropomorphic hand.

Underactuation is a common approach utilised in prosthetic hands, where the Degrees of Actuation (DOA) (i.e., the number of actuators) is reduced to save space, weight, and cost without reducing the number of joints. This approach is possible, mainly, through *rigid coupling* or *adaptive underactuation*. In rigid coupling, the joints are coupled to act as one compound movement, where only the actuator position is required to determine the position of all the other joints. Here, the movement is considered as one DOF regardless of the number of joints coupled. This can be realized with differential transmissions, such as gears, and linkages. Figure 2.18(a) shows an example of different four-bar linkages that are utilised in commercial prosthetic hands [46]. Meanwhile, in adaptive underactuation, several independent DOFs are controlled by a single actuator. This allows the phalanges of the hand to passively adapt to the shape of the object and distribute the grasping force. A typical example of adaptive underactuation is a single cable routed through multiple joints, Figure 2.18(b) [91], [92], [93].

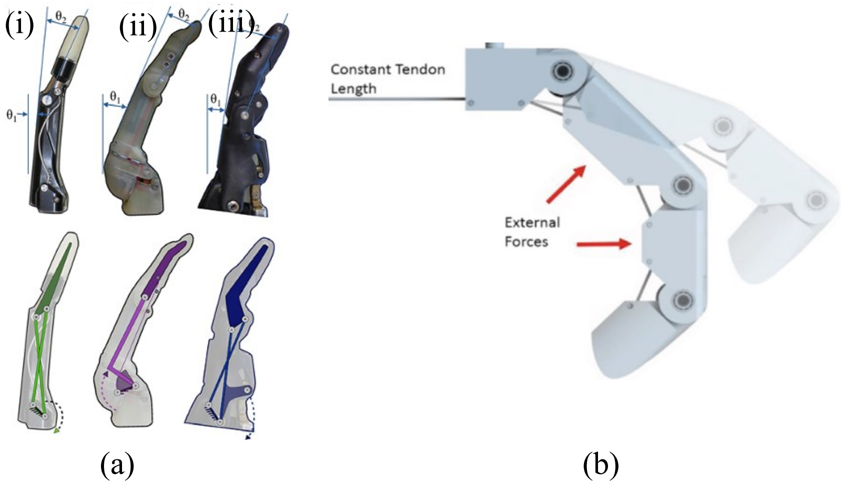

Figure 2.18: (a) The different forms of the four-bar linkage coupling the PIP joint to the MCP joint in the following commercial prosthetic hands: (i) Vincent, (ii) i-Limb and i-Limb Pulse and (iii) BeBionic v2 and BeBionic [82] and (b) An example of an adaptive underactuation mechanism [91].

However, the use of underactuation does not necessarily imply a light and compact prosthetic hand, as this will depend on the mechanical complexity required to implement the coupling system. In fact, Figure 2.19 shows that the weight of the prosthetic hands with the same number of actuators varies. This shows the importance of the coupling mechanism utilised in the design of prostheses.

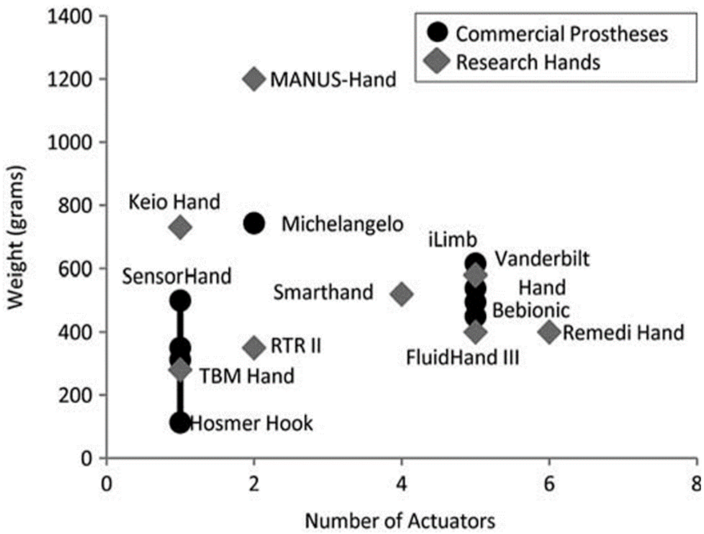

Figure 2.19: The relationship between the weight of the prosthetic hand and the number of actuators [46]

Throughout the years several underactuated hands have been proposed in the literature, such as the fifteen-DOF anthropomorphic hand actuated by a single actuator [94]. However, the taxonomies of everyday grasps, such as Feix et al. [77], do not provide a clear indication of how to assign actuation and couple the movements of the joints in an underactuated prosthetic hand. This is because for a particular grasp type, the relationship of the hand joints relative to one another may differ, depending on the properties of the grasped object. An alternative approach that better guides the development of underactuated prosthetic hands is required, which will be discussed in the next section.

2.8.3 Postural Synergies

2.8.3.1 Definition of Postural Synergies

Despite the biomechanical complexity of the hand, the CNS manages to handle all hand movements effortlessly and dexterously. This has intrigued researchers and motivated them to investigate the approach utilised by the CNS to possibly apply the findings to simplify the complexity in controlling and actuating a dexterous prosthetic hand [95], [96].

Several hypotheses have been proposed in the literature, as in [97], [98]. One of them is Bernstein’s hypothesis [97], who proposed in 1967 that instead of controlling each DOF individually, the CNS uses a simplified strategy. He hypothesised that the CNS uses a single variable, referred to as “synergy”, to control the different aspects of the hand as a single functional unit [97]. Therefore, these synergies can be viewed as fundamental building blocks for any hand movement, including coordination between the two hands [99]. There is substantial evidence to support this hypothesis. In fact, Häger-Ross and Schieber [100] have shown that the movement of neighbouring fingers are not independent, even when the intention is to individuate each joint movement, such as when playing a piano or typing. This could be the result of mechanical coupling, as discussed in Section 2.2 (on p.4), as well as the repetition of several day-to-day tasks, that result in the brain activating the muscles in a predictable pattern [95].

This synergistic control of the CNS is included in various levels of the hand, with common patterns being observed in the behaviour of joints [95], forces [101], muscles [102], etc. Among them, postural synergies are the most important for the design of a prosthesis, as they explain the patterns at the joint-displacement level. An example of a postural synergy might be the co-contraction of all fingers, as when forming a fist.

Hence, these synergies provide a solution that allows greater dexterity by overcoming the redundancy of the motor system through effective coupling of joints. Meanwhile, the number of active DOFs that the amputee would need to control is reduced [46].

The study of postural synergies is not limited to prostheses. In fact, it has a wide range of other applications, such as the study of human-hand grasps [103], gesture recognition [104] and rehabilitation [105], which is why this research field has gained popularity along the years.

2.8.3.2 Measuring Different Hand Postures

The study of postural synergies involves the analysis of different hand postures that captures the variance of the human-hand movements in the best way. Thus, a device is required to measure the different joint angles of the human hand.

Hand therapists typically use a universal goniometer, Figure 2.20(a) [106], to quantify the ROM of a joint, as it is simple, economical, non-invasive, and portable. Goniometers consist of two connecting arms placed on the joint; one is manually held in a fixed position as the other one moves with the finger, indicating on a protractor the angular position of that joint. Even though these instruments are clinically accepted, they are limited to static-hand postures and the process to measure all the DOFs of the hand can be time consuming and tedious for both the participant and the assessor [40]. On the other hand, electro-goniometers, Figure 2.20(b), allow a limited number of joints to be measured concurrently. However, their application is limited due to their size, and consequently the MCP and PIP cannot be measured simultaneously [107]. In fact, a data glove, also known as an instrumented glove, Figure 2.20(c), is typically used in studies of postural synergies, as in [103], [108]. The glove is a hand-shaped sensing device which is embedded with several sensors, usually Resistive Flex Sensors (RFSs) (these will be discussed in more detail in Section 4.3.4.1 (on p.60)), placed over the different joints of the hand [109]. Throughout the years,

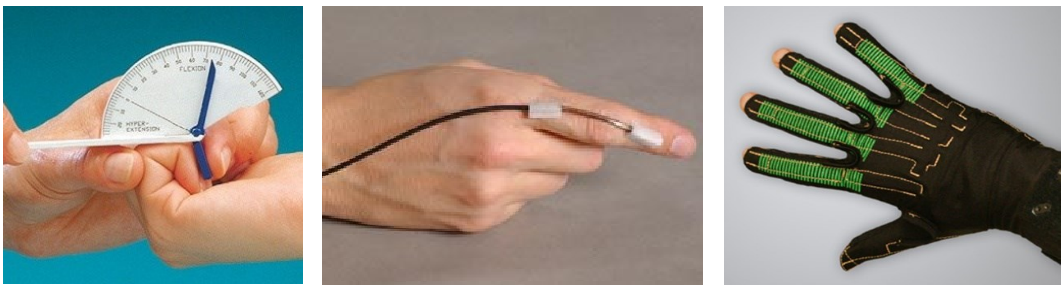

(a) (b) (c)

Figure 2.20: (a) Universal Goniometer [106], (b) Electro-goniometer [107] and (c) CyberGlove III, Data glove [110]

several data gloves have been developed by academia and industry for application in fields such as virtual reality, sign language recognition and robotics. Examples of data gloves include the CyberGlove III (Cyber Glove Systems, San Jose, CA) [110], the 5th Glove (Fifth Dimension Technologies, Irvine, CA) [111], and the Shadow Monitor [112].

Other non-glove systems that can record hand motion, such as the vision-based motion analysis system and the electromagnetic tracking system [113], have also been used in studies of postural synergies, as in [96]. However, they are not used as frequently, due to the cost of the system, the possible occlusion of markers during measurement and the interference in the electromagnetic field from objects in the environment [114].

2.8.3.3 Extraction of Postural Synergies

Postural Synergies can be extracted from a posture matrix (i.e., a dataset consisting of the joint angles of the hand for different hand postures) using several linear and non-linear dimensionality reduction techniques, such as singular-value decomposition, Principal Component Analysis (PCA) and gaussian process latent variable model [115]. PCA has been shown to provide good results in hand kinematics as it captures global patterns as well as physical constraints that constitute most of the common patterns of hand movements [116] [117]. In fact, this method has been widely used in studies on postural synergies, as in [103], [118]. For this reason, PCA was also adopted in this work.

PCA is a well-known statistical technique developed by Pearson [119] and Hotelling [120]. It attempts to represent, as accurately as possible, a multivariate data in a low-dimensional space through an orthogonal linear transformation, where the data are projected in the directions of maximum variance. The result of this transformation is shown in Figure 2.21 [121], where a set of highly correlated variables (in this case, the DOF of the human hand) are converted into Principal Components, PCs, (also known as postural synergies or eigenvectors). The PCs are a set of uncorrelated variables which are a *linear* combination of the original variables [122].

For a dataset P (with d variables in columns and j observations in rows), d PCs are required to reproduce the total variance of the data. Mathematically, each observation of P, P_i, can be mapped to a new vector of principal component scores, $Q_k = (q_1, q_2, \dots., q_d)_k$, as follows [122]:

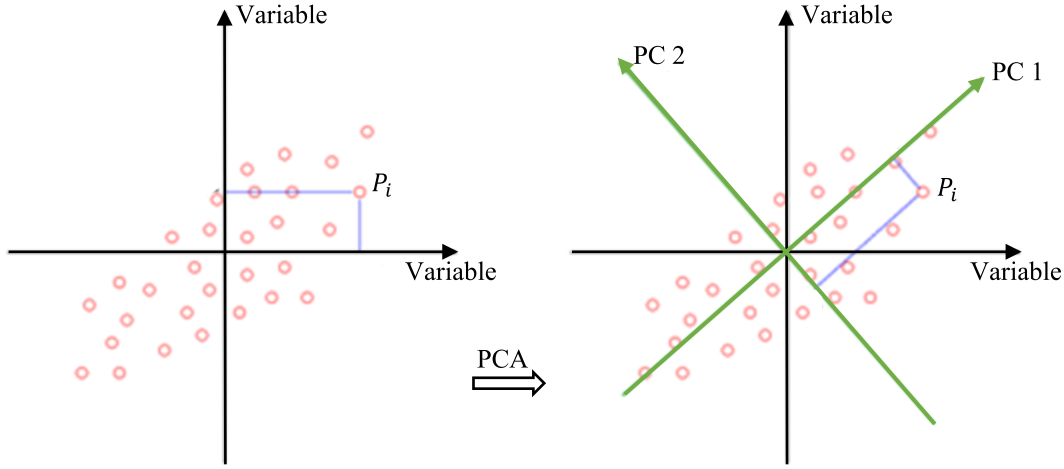

Figure 2.21: Graphical Interpretation of a principal component analysis applied to a sample dataset [121]

$$P = \begin{bmatrix} q_{1,1} \cdots q_{1,k} \cdots q_{1,d} \\ \vdots \\ q_{i,1} \cdots q_{i,k} \cdots q_{i,d} \\ \vdots \\ q_{j,1} \cdots q_{j,k} \cdots q_{j,d} \end{bmatrix} \begin{bmatrix} E_1 \\ \vdots \\ E_k \\ \vdots \\ E_d \end{bmatrix}^t + \begin{bmatrix} \bar{z}_1 \ldots \bar{z}_k \ldots \bar{z}_d \\ \vdots \\ \bar{z}_1 \ldots \bar{z}_k \ldots \bar{z}_d \\ \vdots \\ \bar{z}_1 \ldots \bar{z}_k \ldots \bar{z}_d \end{bmatrix} \quad 2.1$$

Here,

- $\bar{E}$ is the weights or loadings of the set of d-dimensional PCs, where $E_k = (e_1, e_2, \ldots, e_d)_k$
- $\bar{Z}$ is the grand mean computed over the entire observations.

The PCs are ranked, with the first PC accounting for most of the variability in the data. Each succeeding component, orthogonal to the preceding components, has the highest variance from among the remaining components. Very often in physical systems, a subset of these PCs can account for most of the variance in the original data. As a result, by considering only the first few synergies instead of the original d variables, the original dataset P can still be approximated with reasonable accuracy [122]. However, unless there is a significant difference in the percentage of variance explained by consecutive PCs, it is difficult to decide the number of PCs that should be retained. A common rule of thumb typically used in studies on postural synergies is to consider the PCs that explain about 80% or more of the total variance.

2.8.3.4 Major Findings in Literature on Postural Synergies

Throughout the years several researchers have investigated the influence that different factors might have on the structure of postural synergies. This section discusses some of these studies.

Findings in neurology have shown that most of the variance of the human hand posture can be described by a few postural synergies. Santello et al. [103], who were among the first to study postural synergies, observed that the first two synergies, Figure 2.22(a), accounted for over 80% of the information in fifty-seven different static hand postures (e.g. miming holding an apple, a jar lid and a wrench) across five healthy subjects. The first synergy represented the correlation of the FLEX/EXT of the MCP joint and ADD/ABD at all fingers, as well as the ABD/ADD and rotation of the thumb. This motion of the thumb is also accounted for by the second synergy, together with the FLEX/EXT of the PIP and MCP joints. Meanwhile, higher-order PCs accounted for a small amount of the overall variance which contributed subtle information about the shape of the hand irrespective of the object [103]. Similar results were also obtained by Mason et al. [96], who further demonstrated that tactile contact was not a dominant factor in the shaping of the hand, as suspected by Santello et al. [103], who did not make use of physical objects to avoid influencing the resulting hand posture.

Given the high percentage of information transmitted by the first two PCs, the different hand postures could be approximated quite well by just varying the weighting of these synergies. This implies a significant reduction from the fifteen DOFs measured during the experiments. The lack of clustering of the reconstructed static hand postures in the reduced PC space, Figure 2.22(b), suggests that despite the wide range of grasp types considered in the experiment, the hand postures are not discrete; they vary along a continuum based on the weighting of a small number of postural synergies. In fact, objects held with a power grasp could evoke dissimilar hand shapes, while objects which are often associated with distinctive grasps (e.g., precision and power grips)

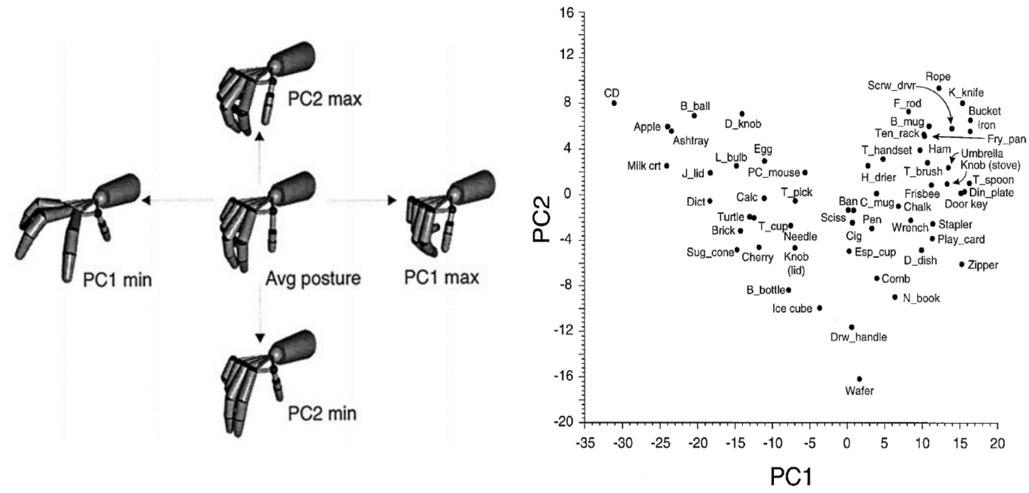

(a) (b)

Figure 2.22: (a) Postural synergies defined by the first two principal components and (b) the distribution of the different hand postures in the plane of the first two principal components [103]

could evoke similar hand postures. This does not refute other studies which have attempted to classify the hand grips, such as Napier's [75], Cutkosky's [76] and Feix et al. [77] grasp taxonomies. It all goes to show that these latter schemes are based on the control of the contact forces (i.e., which part of the finger(s) contact and apply force on the object) rather than the control of static hand postures, which are separate but not independent. This is because different contact forces may be applied to an object which is held with the same hand posture (i.e., the relationship between force and posture control is not one-to-one) [103].

A similar set of postural synergies can also describe the evolving shape of the hand throughout the reach phase, which is an integral part of the coordination of day-to-day activities closely related to hand grasp. Mason et al. [96] studied the reach-to-grasp movement of sixteen objects on five subjects, demonstrating that the first synergy accounts for more than 97% of the total variance. Temporal weightings of the first synergy show the evolution of the hand shape during three distinct periods of the reach-to-grasp movement, which include the hold, reach and object grasp phases. In general, a common pattern was observed, with the weightings first increasing during the reach phase and then decreasing as the hand closes, in preparation for the grasp stage. The variability of the weightings in these three different phases implies that subjects begin to control the shape of the hand prior to the reach phase and continue slightly after the object is grasped, reflecting minor modifications in the grasp.

Slight differences might be present, depending on whether the right- or left-hand side is used. In fact, Jarrassé et al. [123] observed that hand dominance played a role in the definition of the postural synergies despite encouraging symmetric grasping through a grasp-give-receive task.

However, the actual hand posture used to grasp an object may vary, depending on the activity. Upon further analyses, a combination of *extrinsic* (its orientation and location), *intrinsic* (the shape and size of the object) and *contextual* (grasp type and task goal) object properties have been shown to influence the definition of these synergies [124] [108]. In fact, Touvet et al. [124] showed that when these factors were varied during several visually guided reach-to-grasp movements carried out by eleven subjects, the first four PCs were required to describe 76.2% of the variance. The first PC primarily described the distal joints, with the second PC affecting primarily the MCP joints. The third PC described to a lesser extent the FLEX/EXT of all joints, while the fourth PC described the finger and thumb ADD/ABD. Even though the first two PCs did not transmit the same level of information as in Santello et al. [103], a reduction in dimensionality was still observed compared to the twenty DOFs measured during the experiment.

This reduction in dimensionality observed in these studies has the potential to simplify the control strategy of redundant biomechanical systems, but only if the number of synergies is small and task-independent. Otherwise, if the synergies were to be adapted to a new task, they would introduce a synergy-learning problem having the same dimensionality as the original control problem. Studies such as [125], [126] have observed that the synergies are, in fact, task dependent, thus highlighting the need to adjust the synergy strategy based on the task requirements. Figure 2.23 highlights the difference observed by Todorov et al. [125] in the structure of the first two PCs of several complex hand-manipulation tasks (e.g. flipping through the pages of a book and turning a pair of Chinese balls). This study also observed that the number of synergies required to explain a particular percentage of the variance is dependent on the number of DOFs considered in the analysis, since eliminating certain DOFs has the effect of reducing the variance in the data.

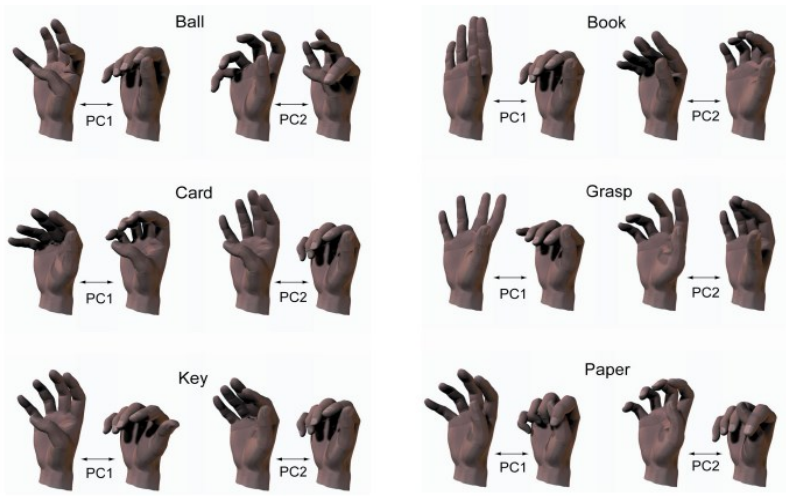

Figure 2.23: Depiction of the first two principal components in each task [125]

On the other hand, studies such as [127] [128], have argued that task-dependent synergies are based on a limited number of tasks, such that the full range and frequency of daily movements evoked by the hand are not captured. Thus, specific tasks occupy isolated parts in the reduced dimensionality, which is defined by synergies that generalise across tasks. A true representation of the underlying task-independent synergies can only be obtained if all hand postures possible are considered. For this reason, Thakur et al. [127] asked eight participants to carry out an unconstrained haptic exploration (a good representation of most of the naturalistic postures evoked during object manipulation) of fifty different objects, using their dominant hand. The PCA revealed that nine synergies, similar across different subjects, described more than 90% of the overall variance. The same set of synergies could also accurately describe simple reach-to-grasp movements and skilled precision pinching, except for the thumb-and-ring pinch, which is rarely used in task exploration. Hence, according to Thakur et al., these nine synergies are a close estimate to the true underlying task-independent synergies, deviating by at least one vector, which can serve as basic building blocks for natural-human-hand motion. This is evident from the fact that synergies observed in previous studies are qualitatively similar to some of these nine synergies. For example, the first synergy was qualitatively similar to the open-hand configuration found by Santello et al. and other studies [127].

However, most of these studies are based on a small number of subjects. As a result, the synergies extracted are usually not distinguished by the subjects and their generalization to a larger population is limited. Hence, Jarque-bou et al. [118] carried out a PCA on the NinaPro database [129], which consists of the kinematic data of twenty-two DOFs, for seventy-seven subjects executing twenty day-to-day grasps. The result of this analysis revealed that on average, the number of synergies required for each subject to describe 82-84% of the variability was between five and six. However, a hierarchical clustering analysis, which grouped similar synergies, showed that twelve synergies were required to explain 80% of variance across the different subjects. Synergies one to three were repeated quite frequently among the subjects. Meanwhile, synergies from four to twelve were less common and only used by a small percentage of the subjects. This implies that only synergies for fine and precise movements are subject-dependent. Nevertheless, some of the synergies found were qualitatively similar to synergies reported in the literature; a good example is the first synergy, which is comparable to the first synergy reported in previous studies [95], [96], but with slight differences as it does not account for the FLEX of the index finger. There were also synergies that were quite novel, due to the introduction of joints; such was the case with the palmar arch and wrist FLEX, which are not typically measured during these studies.

In general, most of these studies instruct participants to use their dominant hand to either grasp or explore a large number of typical day-to-day objects, with the aim of identifying the set of generic postural synergies that account for most of the variance of the hand postures across different subjects. The results of these studies have shown that the information transmitted by the first few synergies decreases as the size and variance of the dataset increases. This means that for the different hand postures to be accurately described in a lower-dimensional space, a larger number of synergies is required; this can be up to ten synergies or even more.

2.8.3.5 Implementation of postural synergies in prosthetic hands

The design of a prosthetic hand can be directed towards the implementation of the postural synergies observed in literature. However, replicating the human grasping features that can be controlled intuitively in a self-contained and compact mechanism has always been a challenging task in the field of artificial hands.

Most of the synergies extracted during these studies express complex relationships between the measured synergies and the human-hand joints. Such synergies can be easily implemented in fully actuated anthropomorphic hands, such as the DLR Hand [130], by reproducing the synergies digitally in the controller, as in [131],[132], based on two bio-signal channels which serve as synergy inputs. This approach is straightforward, allowing the prosthetic hand to easily implement and switch between different sets of synergies. Nevertheless, utilising artificial hands with several actuators to produce only a reduced number of DOFs means unnecessary complexity, expense, energy, and weight. A better alternative would be to reproduce these synergies at the mechanical level.

Hence, for each synergy, the rotational input from the actuator is converted into the motion of each joint (i.e., the output of the system) through the implemented mechanism. Researchers have attempted to use several different types of mechanisms, such as the cam mechanism [133], planetary gears [134], and differential pulleys [135]. Figure 2.24 is an example of an artificial hand developed by Brown and Asada [135] where the postural synergies were mechanically implemented through differential pulleys.

Figure 2.24: Mechanical implementation of the postural synergies in a prosthetic hand [135]

The mechanisms employed are usually complex and too bulky to fit in the palm, as shown in Figure 2.24. This is due to the significant number of outputs and the high contribution of each input to each output. Two main solutions have been proposed in the literature: (1) reducing the number of output joints by implementing the synergies in the intra-finger and inter-finger separately as in [136] or (2) simplifying the mapping relationship by using a compliant mechanism as in [137]. These solutions offer an indirect implementation of the postural synergies and compromise accuracy in replicating the motion of the human hand and/or the ability to control the hand intuitively. To overcome these limitations, a novel design framework was proposed in [138]. In this design, the number of output joints was reduced through the grouping of joints into modules, where each module is actuated by a separate actuator. Further improvements are still required in terms of weight and size, but the design was able to accurately replicate the first two synergies observed by Santello et al. [103], with the first synergy having a mean reproduction error of only 2.3° [138].

Although motion-replication accuracy is important, especially for within-hand manipulation, a problem that may arise with purely replicating the kinematic model of synergies is that contact between some of the phalanges and the object may be attained before that of the other phalanges. Thus, the hand will not necessarily conform to the shape of the grasped object, and as a result the area of contact between the hand and the object will not be sufficient to support a successful grasp. This can be visualised in Figure 2.25, where a fifteen-DOF hand is shown closing on a spherical object according to Santello et al.'s first synergy [139]. Contact involving the thumb, the index and the object first occurs when the weighting of the first synergy is 0.75. If contact is to be achieved with the other phalanges, the weighting of the first synergy will need to be increased, which implies that the phalanges of the thumb and the index fingers will penetrate the object's surface.

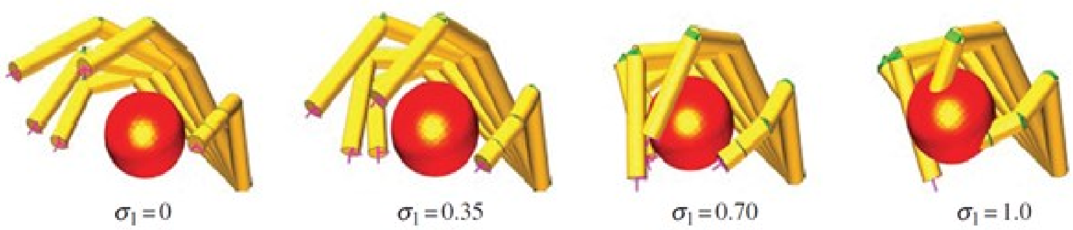

Figure 2.25: A rigid configuration of the hand enclosing a spherical object [139].

This will be an unacceptable behaviour of the model and will not correctly emulate the performance of the human hand, since the latter is not rigid and has compliance in the musculoskeletal system and in the skin. Solutions such as ceasing the motion of each finger separately when it encounters the object, or modifying the shape of the synergies by introducing a complementary actuation system may be applied [48].

Whilst these techniques simplify the design of the pre-grasp phase, they do not take advantage of the synergies to control the grasping forces. Hence, the concept of *soft synergies* was introduced in [139] to better describe the adaptability of the human hand when grasping and manipulating objects. In this model, the synergies only describe the movement of a virtual reference hand, towards which the physical hand is elastically attracted. The resulting hand posture emerges as the equilibrium between hand compliance and the manipulated environment prevents penetration from the motion of the hand. At equilibrium, the difference in position between the real and the reference hand generates the joint torques required to balance the interaction forces of the hand and the object. Figure 2.26(a) depicts the conceptual mechanical design of the implementation of soft synergies, where a spring is used in series with the transmission mechanism that actuates the joints in synergy. Despite the elegant solution provided by soft synergies, its actual physical implementation was not simple, as observed in [48].

For a simpler implementation, adaptive synergies were proposed in [140], which combine soft synergies with under-actuation. This idea exploits the ability of underactuated hands to adapt to the shape of the grasped object to compensate for the reduction in the number of synergies implemented. A concept hardware implementation of adaptive synergies actuation is shown in Figure 2.26(b), where a spring is used in parallel to the actuation mechanism rather than in series.

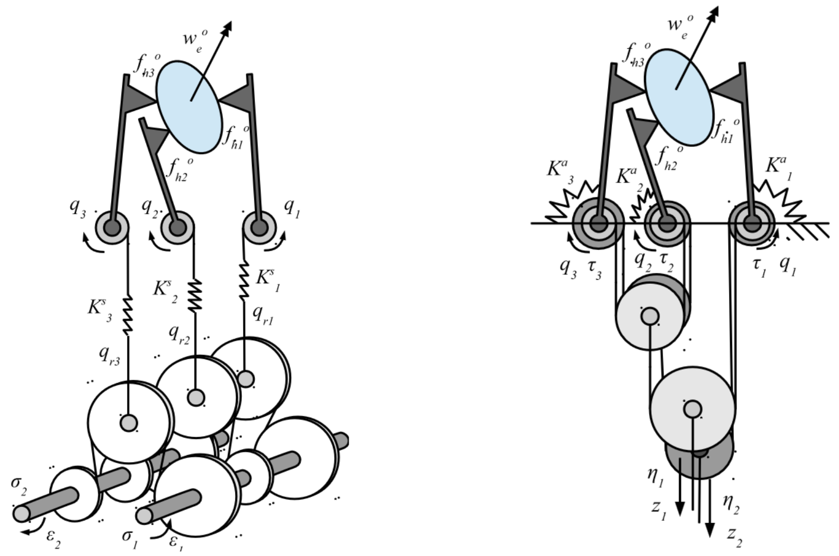

(a) (b)

Figure 2.26: Conceptual hardware implementation of: (a) Soft Synergies and (b) Adaptive Synergies [48]

An interesting implementation of adaptive synergies is the Pisa/IIT SoftHand [48], Figure 2.27 (a). It is a nineteen-DOF anthropomorphic hand simulating Santello et al.'s first synergy, and actuated by a transmission system that involves one tendon, two levels of pulleys and one motor. The Pisa/IIT SoftHand demonstrated effective grasping skills in many different situations but given that only one synergy was implemented, there were still some limitations when compared to the human hand, especially in the completion of complex tasks such as fine pre-shaping and in-hand manipulation. More synergies could easily be added to the the Pisa/IIT SoftHand, by replicating the routing path of the tendon and placing several independent sets of pulleys in parallel at the expense of size and weight. Hence, the challenge becomes finding a design that adds dexterity to the hand without an excessive increase in the mechanical complexity to implement the coupling.

In this regard, the Pisa/IIT SoftHand 2, Figure 2.27(b), a self-contained, compact design with two DOAs, was proposed in [141]. It incorporates the second synergy with little additional complexity by utilising a mechanism that exploits friction effects. This provided the hand with better grasp adaptability and in-hand manipulation skills (e.g. pouring a cup of coffee without compensation from the wrist) compared to the original hand [141].

(a) (b)

Figure 2.27: (a) the Pisa/IIT SoftHand [48] and (b) the Pisa/IIT SoftHand 2 [141]

However, even though the hand could perform several pinch/power grasps, it could not execute a lateral pinch (instead using non-intuitive grasps to hold a banknote and a card, Figure 2.28). This is because in lateral pinch, the position of the thumb relative to the index finger is different from pinch/power grasps, and has troubled even commercial prosthetic hands. This is also true of the BRL/Pisa/IIT SoftHand [142], which is the most recently developed, low-cost hand, based on the original Pisa/IIT

SoftHand. Thus, while it can still grasp various everyday-life objects, the dexterity of both prototypes is still less than the level required to execute ADLs.

Figure 2.28: Multiple ways how the Pisa/IIT SoftHand 2 grasps a banknote and a card [141]

For this reason, Lafranchi et al. [143] used a more holistic design approach that takes into consideration human-like grasping, anthropomorphism and biometric performance to develop a prosthesis called Hannes, Figure 2.29, that has high potential for embodiment. Hannes, with an overall weight of $480g$, is comparable to the dimensions of the 50th percentile of human hands. Furthermore, it is able to actuate most of the DOFs of the human hand in a synergistic manner, except for the distal joints of the digits which are fixed and the rotation of the thumb which is passive. These different DOFs are actuated through a cable-pulley-system driven by a high-power-density DC motor, which in turn is controlled by two sEMG sensors placed over the amputee's stump. These sensors not only allow the amputee to open and close the device, but also to adjust its force and velocity accordingly, which are superior to those found in other prosthesis. Using PCA, it was observed that Hannes, with just one synergy, was able to achieve various human-like motions. This means that the authors were able to achieve their requirements, but further research is required to implement more DOAs, especially since the thumb rotation is still passive.

Figure 2.29: Hannes hand [143]

2.8.3.6 Intuitiveness of surface electromyography control

To operate each synergy in both directions, two distinct sEMG signals are then required. For a more natural and intuitive control system, the sEMG signals that correspond to the movements that closely resemble the movements performed by the prosthetic hand should be chosen. This was the case in [144], where a Myo Armband from Thalmic labs [145], a low-cost myoelectric input device, was used to control the two DOAs of the Pisa/IIT SoftHand 2, Figure 2.30. Postures that constitute both synergies can be attained as a result of the compliance of the hand.

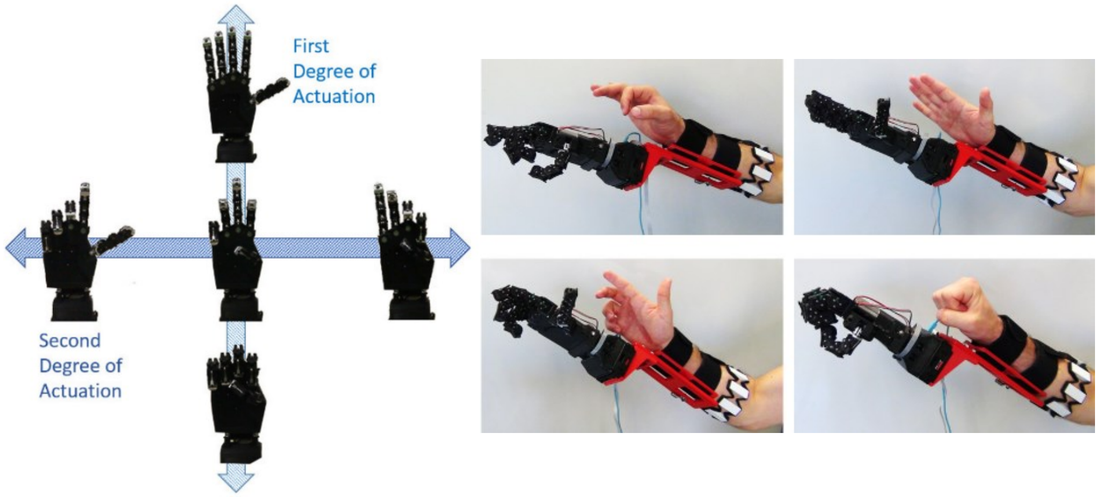

(a) (b)

Figure 2.30: (a) the two DOAs of the Pisa/IIT SoftHand 2 and (b) the hand postures used to control these two DOAs [144]

Thus, the extent of the intuitiveness of the control system depends on whether the extreme hand postures of each synergy can be readily attained by the hand. This is usually the case with the first synergy, since several studies have shown that it resembles the opening and closing of the hand. However, typical postures associated with higher-order synergies are simply postures orthogonal to the previous ones, and thus, not natural. In fact, from Figure 2.30, one can observe that some of the hand postures are not commonly used in daily activities. This limits the effectiveness of the developed controlled system [144].

2.9 RESEARCH GAPS

Postural synergies have the potential to optimise the balance involving simplicity, dexterity and usability if the number of synergies required to accurately reconstruct different hand postures in the reduced dimension is small and they are task-independent.

The studies on postural synergies, discussed in Section 2.8.3.4 (on p.32), have shown that while a reduction in dimensionality is observed compared to the twenty-one DOFs of the human hand, the synergies depend on the dataset considered, with the information transmitted by the first few synergies decreasing as the size and variance of the dataset increase. Hence, for the prosthetic hand to truly replicate the function of the human hand, several synergies would have to be implemented, which is a complex task for both the mechanical (as discussed in Section 2.8.3.5 (on p.37)) and the control (as discussed in Section 2.8.3.6 (on p.42)) systems. This implies that the intact hand and its use, given the current technology, will always be superior to an artificial device. In fact, after amputation of the dominant hand, the intact hand usually becomes the dominant hand through targeted training [146].

Therefore, a more appropriate strategy for prosthetic-hand development would be that of considering the intact hand as the dominant hand and designing the prosthetic hand for a non-dominant role as applicable to bimanual activities (since they are typically impossible or very challenging to execute with one hand). This means that the postural synergies considered for the design only need to account for the variance of the movements produced by the non-dominant hand during bimanual activities even if they cannot be generalised for all the daily tasks. In doing so, the size and variability of the required dataset is significantly reduced, since the non-dominant hand is typically used for grasping tasks (as opposed to within-hand manipulation tasks), which involve less individuated movements, especially if performed with the minimal anthropomorphic hand.

Hence, the postural synergies discussed in Section 2.8.3.4 (on p.32) were not optimised for the needs of the amputees to live a full and autonomous life. Further research is therefore still required to identify the postural synergies that are optimised for the design of a non-dominant prosthetic hand. Meanwhile, there is still room to improve both the hardware and the control system of a multi-synergistic prosthetic hand that optimises the balance involving simplicity, dexterity, and usability. Further literature on the components required to construct a prosthetic hand and any additional equipment that might be required can be found in the coming chapters.

CHAPTER 3: PRODUCT DESIGN SPECIFICATIONS

Based on the literature review, the approach chosen to optimise the balance involving the simplicity, dexterity, and usability of MAProHand was to develop a non-dominant, minimal anthropomorphic myoelectric prosthesis actuated through a control system based on postural synergies. However, to make sure that the developed prosthesis would satisfy the needs of the amputees, the design requirements discussed in Section 2.6 (on p.21) were used to establish a set of specifications to guide the design process. These requirements, in particular the mechanical ones, will be discussed in this chapter.

MAProHand is targeted at unilateral amputees who require a prosthetic hand, with transradial amputees being the main focus, as intuitive sEMG signals can be read from the forearm while allowing sufficient space for additional components that might be required for the prosthetic hand, such as the power source. Depending on the side of the hand lost, a left-hand or a right-hand model is required. In this work, only one model is developed, which will assume the role of the non-dominant hand. Given the prevalence of right-handed people, a left-hand model was chosen to facilitate the selection of participants in subsequent analyses. However, a mirrored version of the developed prosthetic hand is envisaged to be applicable as a right prosthetic hand taking a non-dominant role, since the left- and right-hand can approach most task objects in the same way, especially if there are no contextual constraints that dictate the configuration of the hand, such as the direction in which a door may open.

Regardless of the model chosen, a high level of anthropomorphism in terms of size, colour, number of fingers and joints is also required to resemble the intact hand. Hence, even though MAProHand is based on the minimal anthropomorphic hand, which consists of only three active digits, the "middle" finger must have the appearance of the middle, ring and little fingers (i.e., the MRL finger); this would also provide additional support to the grasped objects. However, human hands vary from one person to another. In fact, commercially available prostheses tend to be available in different sizes, usually small, medium, and large, so that amputees can choose the one that best suits them. Each hand size has its own challenges, with weight being a greater concern in larger models, while space is more limited in smaller models. Hence, as a compromise between these two extremes, this work focuses on developing a medium prosthetic hand with a length of $181mm$, a breadth of $81mm$ and finger thickness of

$20mm$. These dimensions were based on the average of the anthropometric data of the 50th and 95th percentile for women, and the 5th and 50th percentile for men (i.e., the percentile of the population that would make use of a medium-sized prosthetic hand) in a population of British adults aged between nineteen and sixty-five years [147].

The main goal of this prosthesis is to provide a helping hand when performing ADLs, especially bimanual activities, such as carrying an object and cutting food, but excluding specific activities such as sports. For this reason, the prosthetic device must facilitate various grasping motions and postures which the amputee can use to perform these activities in addition to the neutral position, when the hand is not in use. However, as discussed in Section 2.4.3.2 (on p.13), the information transmitted by sEMG signals is limited. Thus, for the amputee to be able to control the prosthesis reliably and intuitively with the limited number of control inputs available, the device must facilitate the execution of a small set of movements and grasps that are most relevant for the non-dominant hand.

These movements/grasps must be done in a natural and timely fashion. The recommended angular speed for ease of approach, without compromising the overall time required to grasp an object, is between $90°/s$ and $230°/s$. Some form of compliance is also required in the design to allow the prosthesis to better conform to the shape of the object. As a result, the gripping force, which the amputee should be able to adjust so as not to damage the grasped object, can be applied more efficiently. The required gripping force should be further reduced, to lower the demands on the actuation system, by utilising materials with good frictional properties to line the prehension surfaces. The integration of feedback about this force should then allow the amputee to operate the prosthetic hand more easily by reducing the role of visual feedback when operating the prosthetic hand.

Regardless of the advanced functionality of the prosthesis, its architecture must remain as simple and robust as possible to ensure that the device is lightweight, compact, inexpensive, yet reliable and resistant to any unplanned impacts during normal use. Therefore, the different hand postures should be attained with the smallest possible number of actuators, without opting for any passive joints (i.e., joints that are operated manually by the user), so that they can be easily embedded in a device that caters for amputees with different levels of amputation. Furthermore, the design of the device should minimise the number of different components, where each component has the smallest number of design features and dependencies.

Ideally, the overall weight of MAProHand, including a simple wrist attachment without any rotation which weighs around $17g$ [148], remains below $400g$, as discussed in Section 2.6 (on p.21). This means that the weight of each component of the hand must also be taken into consideration during the design process, especially the structure of the prosthesis, which is responsible for a significant portion of the weight due to its size. The position of each component is also important since the weight distribution of the hand greatly affects its perceived weight. Thus, for the hand to appear lighter, its weight should be evenly distributed along the width of the palm at the proximal side (i.e., the side closer to the wrist).

The developed design must also consider the ease of manufacturing. Hence, off-the-shelf components should be used whenever possible, which can then be modified locally, if necessary. However, this is not always possible, and customised parts, such as the phalanges, would need to be manufactured. There are several manufacturing processes available, with each process having its own set of materials. Given the cost and weight reduction observed with other 3D printing prostheses, additive manufacturing should be resorted to, especially for complex or small parts. To ensure that these components can withstand the required loads, a Safety Factor (SF) of 1.5, suitable for applications where weight is important [149], should be considered for all structural and functional aspects of the design process.

Whilst the objective of this research is to develop a prosthetic hand that can be tested in a laboratory setting, performance requirements regarding heat and power consumption, as well as the maintenance required, must also be taken into consideration when selecting a component. This is to ensure that the amputee will be able to use the final product for at least a typical day (i.e., around sixteen hours) without creating any discomfort or the need to recharge the battery. For example, the design may include a mechanism that maintains the force applied on the object in the absence of a control signal and power to the motor. Furthermore, it will ensure that maintaining the device in good condition is simple and cost effective.

In the end, the prototype will be a proof-of-concept, and it will need to be assembled and disassembled multiple times. Therefore, the design must also take into consideration the ease of assembly.

All these requirements must be met at a reasonable price. However, given that they will not be purchased in bulk, the parts may be slightly more expensive, especially if any modification is required. For this reason, the cost to construct this prototype should be limited to 5,000Eur. While this is higher than the starting price of the Hero Arm [63], 2,600Eur [150], which also includes other expenses such as labour, it is still significantly less than other prosthetic hands found on the market, which can cost over 25,000 Eur [62].

These requirements, which can be summarised as follows, will serve as a guide during the design process to make sure that the developed prototype achieves the objective of this research:

- The device should assume the role of a left non-dominant hand.
- There should be a high level of anthropomorphism, with the "middle" finger having the appearance of the middle, ring and little fingers.
- The overall size of the device should be 181mm, 81mm and 20 mm.
- Allowance should be made for the execution of a small set of grasping motions and postures relevant to the non-dominant hand in bimanual activities.
- The angular speed of the prosthetic hand should lie between 90°$/s$ and 230°$/s$.
- The device should comply with the shape of the grasped object.
- The gripping force must be minimised, while still being able to hold the object within the grasp without damaging it.
- The device should provide the amputee with feedback on the gripping force.
- The architecture of the device should be reliable and robust.
- The number of actuators required must be minimised.
- The actuators must be embedded in the palm.
- The use of passive joints should be avoided.
- The overall weight of the prosthetic hand should be less than 400g, with the centre of mass lying in middle of the palm towards the proximal side.
- The design should utilise, as much as possible, off-the-shelf components.
- Customised parts should be manufactured using 3D printing.
- A SF of 1.5 should be considered during the design process.
- The device should last the amputee a typical workday before recharging.
- The device must not cause the amputee any discomfort, especially in terms of heat.
- The maintenance of the device should be simple and cost effective.
- The device must be easily assembled and disassembled.
- The cost to construct the prototype should be less than 5,000Eur.

However, if the prosthesis is to be commercialised, which is beyond the scope of this work, other requirements might have to be included, such as food safety, especially if the hand is to be used in food preparation.

CHAPTER 4: IDENTIFICATION OF AN INCLUSIVE SET OF GRASPING MOTIONS AND/OR POSTURES

4.1 INTRODUCTION

A minimal anthropomorphic prosthesis assuming the role of the non-dominant hand must facilitate a number of grasping motions and/or postures used in daily activities, as discussed in the previous chapter.

Identifying this set of grasping motions and/or postures is a challenging task, especially since a comprehensive taxonomy of day-to-day grasps consists of over thirty distinct grasps, Figure 2.15 (on p.22) [77]. Although some of these grasps inherently cannot be attained with the minimal anthropomorphic hand (as this only includes three distinct fingers), developing a prosthetic hand that can perform all of the remaining grasps is, still, not practical. This is not only due to mechanical and control constraints discussed in Section 2.7 (on p.24), but also because some of these grasps may rarely be used in ADLs [151].

Fortunately, Santello et al. [95] have shown that these different grasp types might not be as distinct from each other as portrayed in these taxonomies. In fact, a small number of postural synergies can account for most of the variance in these different hand postures. Hence, this chapter exploits this concept with an innovative approach to identify, using PCA, the set of grasping motions and postures most relevant for a non-dominant prosthetic hand in bimanual activities.

4.2 METHODOLOGY

For the identification of this set of grasping motions and postures based on the relevant postural synergies, a dataset of everyday hand postures in the minimal anthropomorphic condition was required. Consequently, an experiment was carried out on human volunteers to capture the different hand postures employed by the constrained non-dominant hand during a number of representative bimanual activities. The reach-and-release phase is an integral part of the coordination of daily-life activity, but Mason et al. [96] have shown that the hand shape evolves gradually throughout the reach phase and reaches its peak when the hand conforms to the object. This implies that only the final hand postures are necessary for this work, especially since, for a prosthesis assuming the role of the non-dominant hand, what is more important in the first instance is that the applicable grasps *can* be achieved, rather than *how* they are achieved.

The bimanual activities included in the experiment can be based on the activities which are most challenging for the amputee to perform, such as the ones listed in Table 2.4 (on p. 20). However, such activities might not capture the frequency and the full range of daily movements produced by the non-dominant hand when performing bimanual ADLs. Thus, as discussed in Section 2.8.3.4 (on p.32), the structure of the postural synergies derived from this list may not be generalized as to apply to other activities. This means that the specific tasks that the participants are asked to execute during the experiment must be selected very carefully and systematically.

For a true representation of the hand postures utilized by the non-dominant hand, all the hand postures possible must be considered by asking the participants to perform a long list of randomly chosen bimanual activities. However, it was not considered practical to do this due to the long duration and difficult implementation of such an experiment. Therefore, it was essential to understand the relevance of the different grasp types for autonomy. This has been quantified by Gracia-Ibáñez et al. in [81]. In that study, one hundred and twenty-eight tasks that are representative of day-to-day activities were selected (e.g., reading a book and clearing the table), and subsequently, 145 videos of thirty-two right-handed people performing these tasks were analysed to extract 320 elementary grasp actions. These were then used to identify the various grasp types used by each hand for each task and the duration of each grasp. They were based on a nine-type classification shown in Figure 4.1 [81]. Although the taxonomy used to classify the different grasps was relatively simple when compared to the taxonomy of Feix et al. [77], the authors of [81] considered it sufficient to characterize most of the human grasp types used in the real environment, especially since studies

Name	Description
Cylindrical grasp (Cyl)	The palm is involved. The thumb is in direct opposition to the fingers (in abduction or neutral)
Oblique palmar grasp (Obl)	Variation of the Cylindrical grasp. The palm is involved, but the thumb is adducted
Hook grasp (Hook)	Palm and thumb are not involved. The object's weight is borne by fingers
Lumbrical grasp (Lum)	Thumb and proximal part of the fingers are involved, but the palm is not involved
Intermediate power-precision grasp (IntPP)	The palm is somewhat involved but both the thumb and index stabilize the grasp
Pinch grasp (Pinch)	Thumb and fingertips (one or more) are used
Lateral Pinch (LatP)	The lateral part of the fingers (one or more) are used, and usually the thumb as well
Special pinch (SpP)	The thumb, lateral part of some finger and the fingertips of another/others are involved
Non-prehensile grasp (NonP)	Objects are manipulated without grasping them

(a)

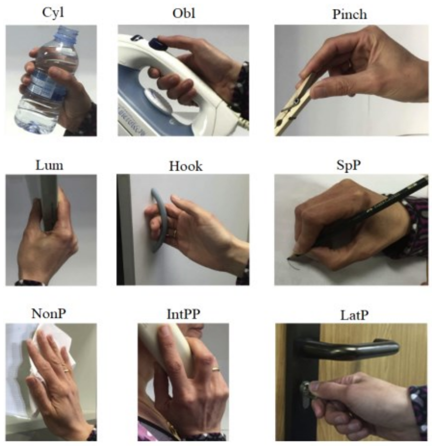

(b)

Figure 4.1: (a) Description of the nine-grasp taxonomy and (b) examples of the grasp types [81]

such as [78], [79], have shown that only a subset of these grasps is actually used during different activities.

The importance of the task for which each grasp was used should also be taken into consideration when determining the relevance of the different grasp types. The importance of such activities was quantified by Querejeta [152] according to the frequency of each activity appearing in twenty-three disability scales, such as Barthel [153] and the Katz Index [154] . It must be noted that the importance of the different activities varies, depending on one’s roles, habits, and responsibility, and that the way the relative importance of these activities was calculated reflects mainly the perception about autonomy of the evaluators of the hand function, which may be different from the amputee’s perception [81] .

Hence, the relevance of the grasp types shown in Figure 4.1(a) was calculated by weighting time with the importance of the activity estimated by Querejeta [152], considering by the hand involved (left/right) and noting whether the task was unimanual or bimanual, Figure 4.2. For the non-dominant hand (i.e., the left-hand in this cited study) in bimanual activities, the most relevant grasp types were pinch (26%), non-prehensile (23.9%) and lumbrical (20.8%) grasps.

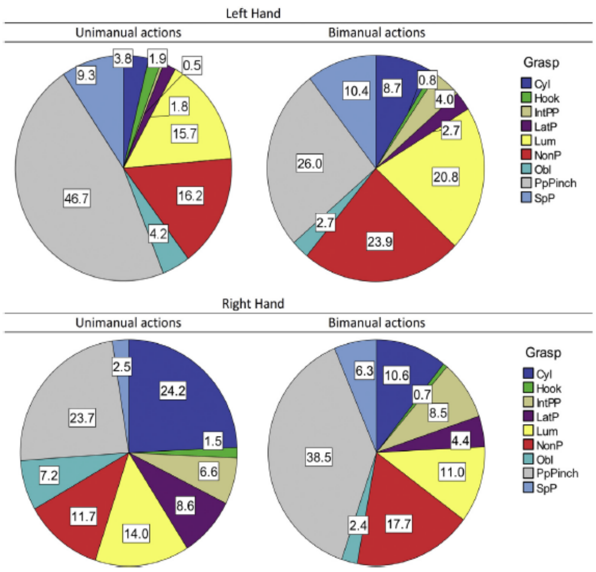

Figure 4.2: Relevance of different grasped distinguished by hand and by the type of task [81]

By reflecting on the relevance of each of these grasps in the dataset, a better representation of the hand postures utilised during daily bimanual activities can be obtained, especially if it is assumed that the relevance of the grasp types remains valid for the minimal anthropomorphic condition. This assumption was considered reasonable because, as shown in [8], the first three digits give the greatest contribution to dexterity, and by inference are the most used in daily grasps. To this end, the experiment should focus on the grasps used by the participants rather than the activity performed. This implies that the participants could have been simply asked to grasp random objects using the different grasp types. However, Touvet et al. [124] observed that the structure of the synergies depends not only on the grasp type, but also on the extrinsic, intrinsic and contextual object properties. For this reason, each grasp type was considered within the context of a bimanual activity to ensure a natural hand posture when grasping a physical object. This also ensures that the grasp variant being considered is actually one that is used in daily activities.

A natural approach would then be for the number of activities chosen for each grasp type to be based on the relevance of that particular grasp. However, using this approach for an experiment of not very long duration, the least relevant grasp types would not even be represented. Meanwhile, the grasp types at the opposite end would be overrepresented such that finding activities that involved different hand postures that still fall under the same type of grasp would be difficult. Consequently, during the experiment, a good representation of all the nine grasp types was collected, and then during the subsequent analysis each grasp type could be weighted according to its prevalence discussed above.

For each grasp type, three bimanual activities which require the non-dominant hand to grasp everyday objects of different shape, size and texture with that particular grasp were chosen. Other factors, such as personal space, ease of implementation in the laboratory, and the safety of the participants, were also considered during the selection. Table 4.1 lists the bimanual activities chosen and the hand posture in the minimal anthropomorphic condition required to grasp the task object. Although the list of activities analysed by Gracia-Ibáñez et al. was used as a reference, some difficulty was encountered in finding different activities suitable for the lab, that evoked a particular type of grasp while making use of the entire workspace of the hand. For this reason, some activities were repeated across different grasp types. However, this was not an issue, since the focus of the experiment is the grasp type used by the participants, but it highlights the importance of the participants using the correct grasp type when performing the activity.

The analysis of these different hand postures should reveal a dimensionally reduced set of synergies that account for most of the variance present when executing the chosen, as well as other daily bimanual activities, resulting in an inclusive set of grasping motions and postures required for the prosthetic hand.

Table 4.1: List of everyday tasks objects and bimanual activities chosen for the experiment

	Cylindrical Grasp (Cyl)	
Sweeping	***Peeling a potato***	***Opening a hand-tightened bottle***
Broom	*Potato*	*Large Water Bottle*
Ø22x1220***mm***	60x40x80*mm*	Ø95*x*340*mm*
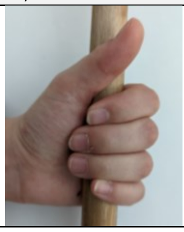		
	Oblique Palmar Grasp (Obl)	
Putting toothpaste on a toothbrush	***Opening the zipper of a purse***	***Pouring from a frying pan***
Toothbrush	*Purse*	*Frying Pan Handle*
13x190x7***mm***	47x75x100*mm*	32x125x16*mm*
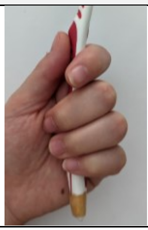		
	Pinch Grasp (Pinch)	
Passing a thread through a needle	***Opening a hand-tightened cap***	***Pouring water into a cup***
Sewing Pin	*Soap Bottle Cap*	*Medium-Sized Cup*
negligible	Ø50x42*mm*	Ø80x120*mm*
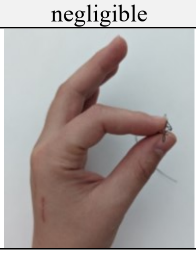		
	Lumbrical Grasp (Lum)	
Playing Cards	***Carrying a tray***	***Opening a packaged-food box***
Cards	*Tray*	*Cracker box*
Negligible thickness	306x432x32*mm*	68*mm*
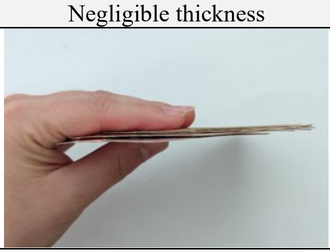		
	Hook Grasp (Hook)	
Carrying a shopping bag	***Pulling a drawer***	***Carrying a briefcase***
Shopping bag	*Cabinet handle*	*Briefcase*
/	20x6*mm*	104x36x16*mm*
		.

Table 4.1: List of everyday tasks objects and bimanual activities chosen for the experiment (cont.d)

Special Pinch (SpP)		
Sharpening a pencil	***Opening a hand-tightened toothpaste cap***	***Opening a hand-tightened body cream cap***
Small Sharpener	*Toothpaste Cap*	*Body Cream Container*
23x25x45***mm***	Ø33x20*mm*	72x17*mm*
		
Non-Prehensile Grasp (NonP)		
Putting glue on a paper	***Using a tablet***	***Throwing a ball***
Paper	*Tablet*	*Beach Ball*
/	171x262x9*mm*	Ø23*mm*
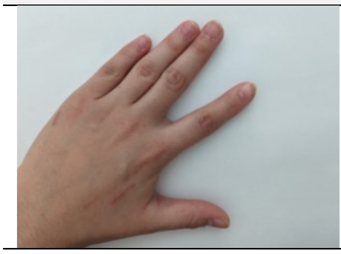	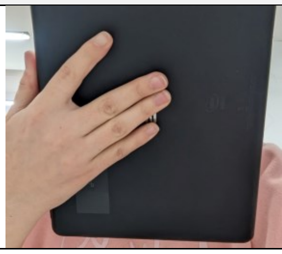	
Intermediate Power-precision Grasp (IntPP)		
Eating with a fork and a knife	***Dialling a telephone number***	***Spraying a detergent while wiping a surface***
Fork	*Telephone*	*Spray Bottle*
11x1***mm***	180x45x15*mm*	40x32*mm*
		
Lateral Pinch (LatP)		
Cutting with scissors	***Opening a hand-tightened bottle Cap***	***Opening the flip top of a toothpaste tube***
Paper	*Water Bottle Cap*	*Toothpaste Cap*
Negligible	27*mm*	Ø33*mm*
	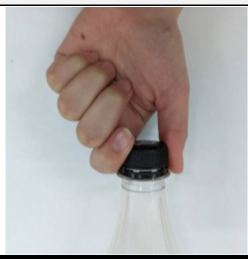	

4.3 MEASURING DIFFERENT HUMAN-HAND POSTURES IN THE MINIMAL ANTHROPOMORPHIC CONDITION

4.3.1 INTRODUCTION

In the upcoming sections, attention will be focused on the complex task of measuring the hand postures in Table 4.1 (on p.52). This undertaking necessitates a thorough exploration into the definition of the Kinematic Hand Structure (KHS) of the minimal anthropomorphic hand, establishing the foundation for the specifications required for the measuring device. Notably, the data gloves currently available in the market have proven unsuitable, prompting the necessity to develop, calibrate and characterize a data glove tailored to the unique demands of the study. These sections will highlight the complexities inherent in the measurement of various hand postures and outline the steps taken to overcome such challenges.

4.3.2 ESTABLISHING A PRELIMINARY KINEMATIC STRUCTURE OF THE MINIMAL ANTHROPOMORPHIC HAND

A KHS is a mathematical description of the functional dimensions and DOFs of a hand. It defines the positional capabilities and constraints of the hand and, as a result, its workspace. Hence, understanding the KHS of the minimal anthropomorphic hand is important to accurately measure and model different hand postures in this condition.

The method most commonly used to describe a KHS is the Denavit-Hartenberg (D-H) convention [155]. Using a set of four parameters based on the geometry of the system, Figure 4.3, it describes how each subsequent reference frame, attached to links of the kinematic chain, relates to the one before it through the following series of homogeneous transformations around and along the x and z axes:

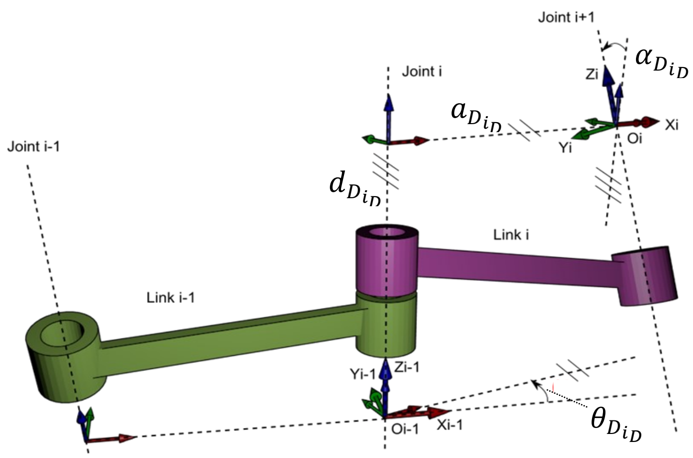

Figure 4.3: D-H parameters [159]

$$T_{D_i}^{i-1} = Rot\left(0,0,\theta_{D_{i_D}}\right) \rightarrow Trans\left(0,0,d_{D_{i_D}}\right) \rightarrow Trans\left(a_{D_{i_D}},0,0\right) \rightarrow Rot(\alpha_{D_{i_D}},0,0) \quad 4.1$$

Where,

- D, indicates the digit being considered, with T, I, and M referring to the Thumb, the Index and the Middle finger, respectively.
- ${T_D}_i^{i-1}$, represents the homogeneous transformation from frame $i-1$ to frame i of a particular digit.
- i_D, is the number of the joint being considered for a particular digit.
- $\theta_{D_{i_D}}$, is the joint angle, the angle between x_{i-1} and x_i about the z_{i-1}, rad.
- $d_{D_{i_D}}$, is the link offset, the distance between x_{i-1} and x_i about the z_{i-1}, m.
- $a_{D_{i_D}}$, is the link length, the distance between z_{i-1} and z_i about the x_i, m.
- $\alpha_{D_{i_D}}$, is the link twist, the angle between z_{i-1} and z_i about the x_i, rad.

This convention models the hand as a series of rigid links that rotate about an ideal revolute joint. This means that the compliance in the joints and bones, as well as the non-ideal rotation of joints cannot be modelled with the D-H convention, but it simplifies the kinematic model for easier implementation and simpler analytical solutions [157].

The minimal anthropomorphic hand consists of two fingers and a thumb. Due to their structural differences, two distinct cases need to be modelled with the D-H convention. Hence, to simplify the overall model, for each case, the reference coordinate system (i.e. the 1st frame for that particular case) is taken to be at the base joint, whose position with respect to the global 0th frame (located at the bottom of the palm beneath the centre of the middle finger, with the z_0-axis facing away from the palm and the x_0-axis along the middle finger) is given by the following transformation:

$$T_{D_0}^{1} = Trans\left(l_{D_x}, l_{D_y}, l_{D_z}\right) \quad 4.2$$

Where,

- l_{D_x}, is the distance between x_0-axis and x_{D_1} -axis, m.
- l_{D_y}, is the distance between y_0-axis and y_{D_1} -axis, m.
- l_{D_z}, is the distance between z_0-axis and z_{D_1} -axis, m.

Using the D-H convention, the kinematic model for the fingers is shown in Figure 4.4, with the first frame located at the knuckle of either the index or the middle finger, since the CMC joint is not included in the model due to its limited mobility [16]. In this kinematic structure, the MCP joint is modelled by two orthogonal revolute joints, while the DIP and the PIP joints are each modelled by one revolute joint. The order of the two DOFs of the MCP joint is not that critical, since the ROM of the ADD/ABD reduces as the finger is flexed. In the literature, the ADD/ABD tends to be modelled first, as in [156], [158], but in this work, the FLEX/EXT was instead modelled first, as in [159], to simplify the measurement and the modelling of the ADD/ABD joint; this will be discussed in Section 4.3.4.2 (on p.63). The D-H parameters for the fingers are shown in Table 4.2.

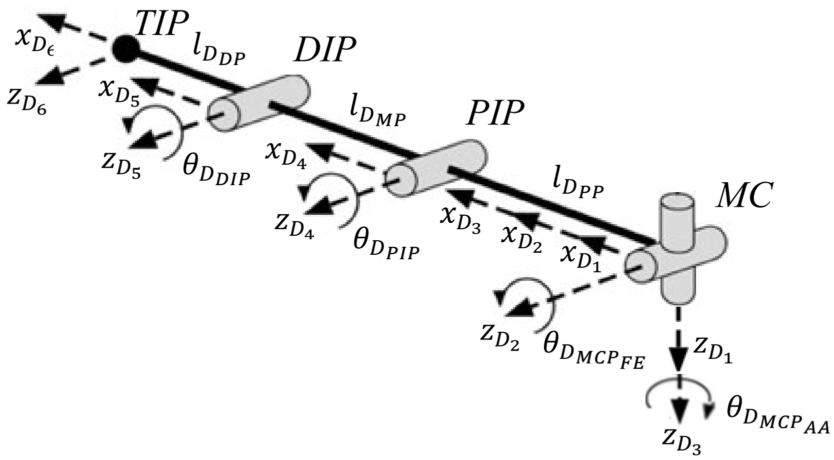

Figure 4.4: Kinematic Model for the finger in the initial position

Table 4.2: The D-H Parameters of the fingers

Transformation	$\boldsymbol{i_D}$	$\boldsymbol{\theta_{D_{i_D}}}$	$\boldsymbol{d_{D_{i_D}}}$	$\boldsymbol{a_{D_{i_D}}}$	$\boldsymbol{\alpha_{D_{i_D}}}$
$\boldsymbol{T_{D_2}^{1}}$	2	0	0	0	$\pi/2$
$\boldsymbol{T_{D_3}^{2}}$	3	$\theta_{D_{MCP_{FE}}}$	0	0	$-\pi/2$
$\boldsymbol{T_{D_4}^{3}}$	4	$\theta_{D_{MCP_{AA}}}$	0	$l_{D_{PP}}$	$\pi/2$
$\boldsymbol{T_{D_5}^{4}}$	5	$\theta_{D_{PIP}}$	0	$l_{D_{MP}}$	0
$\boldsymbol{T_{D_6}^{5}}$	6	$\theta_{D_{DIP}}$	0	$l_{D_{DP}}$	0

The model of the thumb is slightly more complex due to the two non-intersecting, non-orthogonal axes present at the CMC joint, which allow the motion of the thumb to take place in three anatomical planes [18]. Nonetheless, orthogonal, intersecting axes are often used to model this joint, especially models whose primary objective is to closely reproduce the motions of the hand rather than to replicate its intrinsic structure. Three orthogonal revolute joints are theoretically required to completely define the position and the twist of the thumb in 3D-space, but studies, such as [160], [161], have successfully modelled the thumb CMC joint with just two orthogonal joints.

A similar approach was considered in this work to reduce the variance of the hand postures in the dataset. However, this means that the twist of the thumb in 3D-space will depend on the orientation of the two revolute joints. Given that the axes of the pair of revolute joints that best model the twist of the thumb are not known, both the orientation of the revolute joints and the twist of the thumb will have to be optimized to ensure that the thumb looks natural in different positions, as will be discussed in Chapter 5 (on p. 88).

For the preliminary model, a coordinate system that can be easily visualized relative to the human hand was chosen to facilitate the measurement process of these joint angles, as will be discussed in Section 4.3.4.2 (on p.63). For this coordinate system, three alternative pairs of revolute joints, which are listed below, could then be used to model the thumb CMC joint, as shown in Figure 4.5. Given that there was no clear preference and that the results obtained, although meaningful, might be slightly different, each angle pair was analysed separately, as will be discussed in subsequent sections:

- Angle Pair A: refers to θ_{A_1} and θ_{A_2};
- Angle Pair B: refers to θ_{B_1} and θ_{B_2};
- Angle Pair C: refers to θ_{C_1} and θ_{C_2}.

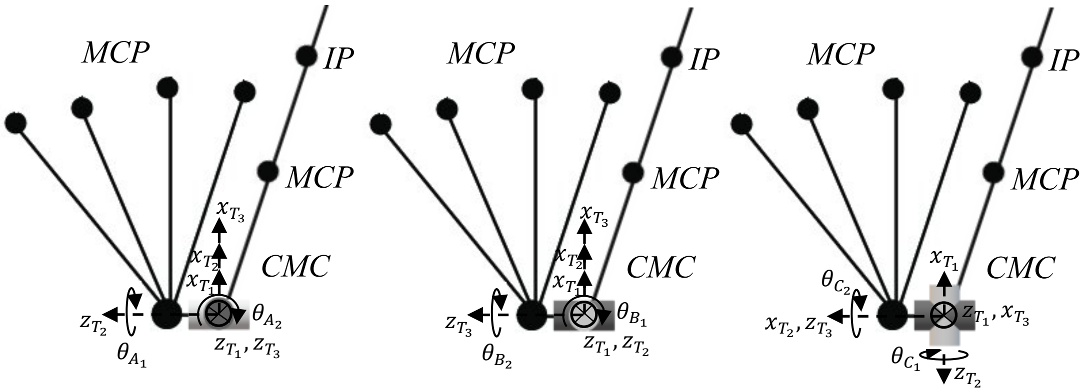

Figure 4.5: The three angle pairs considered for the modelling of the thumb CMC joint with the thumb in the natural position

Meanwhile, the thumb MCP and IP joints were each modelled by a revolute joint, on the assumption that the ADD/ABD of the thumb MCP joint would be negligible due to its limited ROM. The D-H parameters of the thumb model then depend on the angle pair used to model the CMC joint. Taking Angle Pair A as an example, the kinematic model of the thumb is shown in Figure 4.6, while the D-H parameters are listed in Table 4.3.

Combining the D-H parameters of both cases, a preliminary model of the minimal anthropomorphic hand was established and modelled in SketchUp, using simple shapes, as shown in Figure 4.7. The dimensions of the hand, such as the length of the phalanges, were based on the hand dimensions of the participants in the experiment. Meanwhile, a good approximation of the location of the thumb CMC joint was provided in [161].

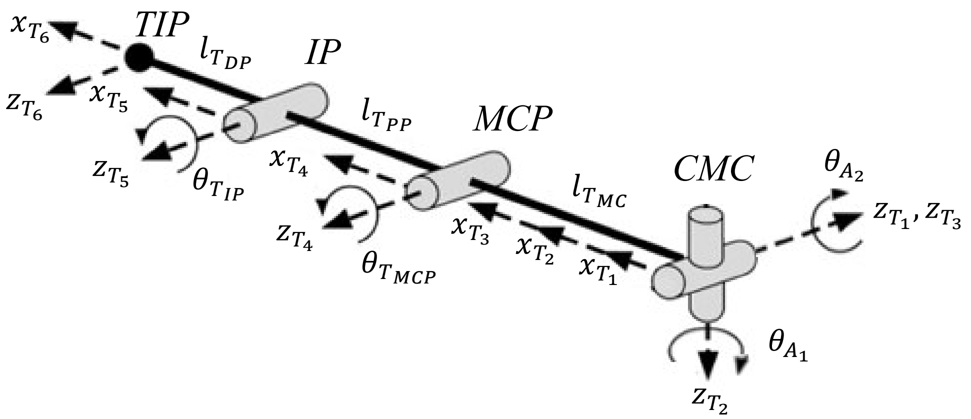

Figure 4.6: Kinematic Model of the Thumb in the initial position with the CMC joint modelled by Angle Pair A

Table 4.3: The D-H Parameters of the thumb for Angle Pair A

Transformation	i_T	$\theta_{T_{i_T}}$	$d_{T_{i_T}}$	$a_{T_{i_T}}$	$\alpha_{T_{i_T}}$
$T_{T_2}^{\;1}$	*2*	*0*	0	0	$\pi/2$
$T_{T_3}^{\;2}$	3	θ_{A_1}	0	0	$-\pi/2$
$T_{T_4}^{\;3}$	4	θ_{A_2}	0	$l_{T_{MC}}$	π
$T_{T_5}^{\;4}$	5	$\theta_{T_{MCP}}$	0	$l_{T_{PP}}$	$-\pi/18$
$T_{T_6}^{\;5}$	6	$\theta_{T_{IP}}$	0	$l_{T_{IP}}$	0

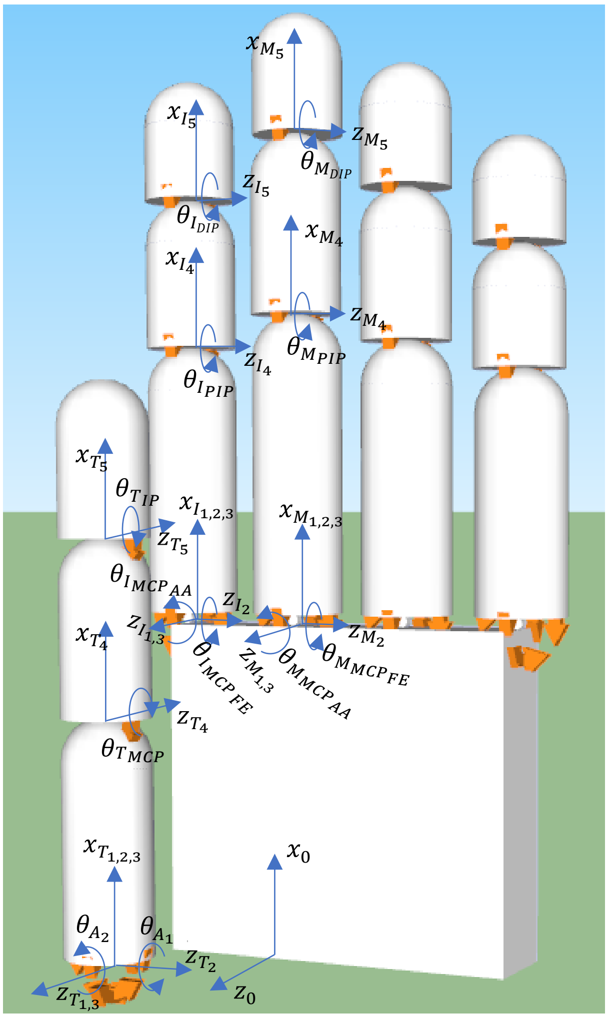

Figure 4.7: The preliminary kinematic model of the minimal anthropomorphic hand where angle pair A is used to model the thumb CMC joint

4.3.3 Requirements for a device measuring hand postures

A device capable of measuring the different joint values in Figure 4.7 during various, static-hand postures in the minimal anthropomorphic condition was required. As discussed in Section 2.8.3.2 (p.30), there are several types of equipment that could be used. This work, like other studies on postural synergies, opted for data gloves due to the ease in measuring several joints simultaneously. This meant that a left data glove that fits various hand sizes was required.

The data glove must at least be able to measure, accurately and repeatably, the following nine DOFs which comprise the minimal anthropomorphic hand:

- One of the angle pairs considered to model the thumb CMC joint in the KHS;
- FLEX/EXT of the thumb MCP joint, $\theta_{T_{MCP}}$;
- FLEX/EXT of the thumb IP joint, $\theta_{T_{IP}}$;
- FLEX/EXT of the index finger MCP joint, $\theta_{I_{MCP_{FE}}}$;
- FLEX/EXT of the index finger PIP joint, $\theta_{I_{PIP}}$;
- FLEX/EXT of the middle finger MCP joint, $\theta_{M_{MCP_{FE}}}$;
- FLEX/EXT of the middle finger PIP joint, $\theta_{M_{PIP}}$;
- ADD/ABD between the index and the middle fingers, where a commonly adopted constraint in human modelling can be used, which states that the middle finger displays little ABD/ADD motion [162] (thus, the measured angle is $\theta_{I_{MCP_{AA}}}$, while $\theta_{M_{MCP_{AA}}}$ is zero).

Note that the DIP joint was omitted, since several studies, as in [162], have shown that a linear, angular relationship exists between the DIP and PIP joints of each finger, which is given by Equation 4.3.

$$\theta_{D_{DIP}} = 2\theta_{D_{PIP}}/3 \quad (4.3)$$

However, given that the minimal anthropomorphic hand consists of only three active digits, the participant's individuated movements of the ring and little fingers must be constrained, without interfering with the workspace of the hand and the final hand posture.

The presence of the sense of touch is also important as it provides a critical contribution to the hand, especially during dexterous tasks [8]. Hence, the data glove should minimise any loss of sensitivity to ensure that the hand posture recorded is realistic, especially at the fingertip.

While several data gloves are available on the market, the use of such devices in conjunction with the constraints necessary on the middle, ring and little fingers was not possible without adversely affecting the outputs of the position sensors of the glove. As a result, a custom-designed left data glove was required for use in the experiments.

The developed data-glove must be durable and able to fulfil its required function without creating any discomfort to the participants, neither during the donning and removing of the glove nor during the experiment. This means that the glove must be stretchable and lightweight, without presenting any hazard to the participant or the glove itself. Due to the fact that during the experiment the participants will be stationary in the lab, the portability of the device is not that important as long as it does not interfere with the participant's execution of the day-to-day activities.

The design and construction of the data glove, as well as its characterisation, will be discussed in the following sections.

4.3.4 Design and Construction of the Data Glove

4.3.4.1 Selecting the sensing technology for angular joint displacement

Various sensing technologies, such as RFSs [110], strain gauges [163] and fibre optics [164], have been used in data gloves to measure, directly or indirectly, the angular joint displacement of a singular joint [165]. RFSs offer a lightweight, inexpensive, compact and reliable alternative [112], suitable for low-cost instrumented gloves, as in [166], [167], and the data glove developed in this work.

The RFSs consist of a thin conductive layer, typically made from a carbon-based ink, placed on top of a polymer substrate, such as polyvinylchloride, as shown in Figure 4.8. Over-laminates, such as a layer of polyamide or polyester, can be added on top of

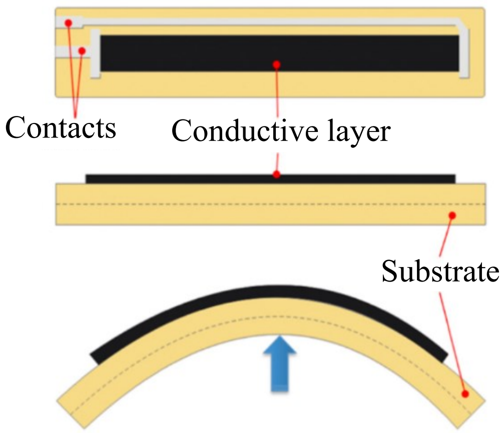

Figure 4.8: (a) A schematic view of a resistive flex sensor [171]

the conductive one for added environmental protection against mechanical scratches [168]. As the RFS is bent, the micro-cracks present in the conductive layer move away from each other, causing the electrical resistance across it, R_{Sensor}, to increase. The entire process is reversible, with the micro-cracks returning to their initial position when the sensor is returned to its flat condition. This means that a proper calibration of the RFS allows the joint angles to be mapped to the particular R_{Sensor} [168].

RFSs are commercialised by several brands, but those most commonly used and reported on in the literature are those from Flexpoint Sensor Systems, Inc. (FP) [169] and Spectra Symbol (SS) [170]. They come in different sizes to cater for several applications, as shown in Figure 4.9. FP also offer the option of polyester- or polyamide- overlamination. As with any other product, the behaviour of the sensor in terms of sensitivity, repeatability, stability and linearity of response varies from one brand to another, making one brand more suitable for certain applications. Hence, a detailed study was carried out in [171] to identify the characteristics of the RFSs from these two brands, taking into consideration different lengths and overlamination.

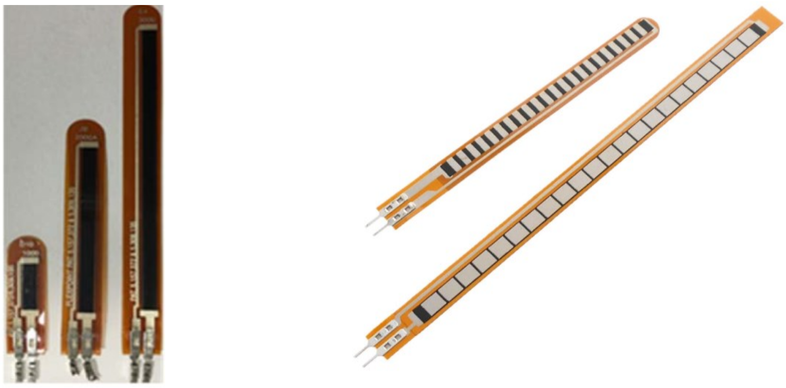

(a) (b)

Figure 4.9: (a) Flexpoint Resistive flex sensors with different lengths of 1- inch, 2- inch and 3- inch [171] and (b) Spectra Symbol Resistive 2.2-inch and 4.5- inch flex sensors [171]

In that study, each sensor was placed on a hinge, as shown in Figure 4.10, where one of its leaves was rotated by a stepper motor to make sure that the correct angle was reached. The electrical resistance of each RFS was then measured, using a digital multimeter, for bending angles starting from 0° up to 120°, in steps of 10°. This was repeated for ten times [171] in order to obtain the curve of resistance against angle.

The different FP RFSs exhibited a non-linear behaviour represented by a unique polynomial function, in which sensitivity at lower angles was reduced, especially for polyamide-laminated RFSs. However, the sensitivity at different angles was lower for the coated versions. This is due to the protective layer which not only provides

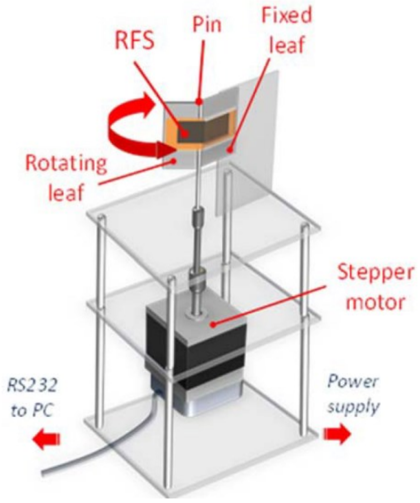

Figure 4.10: Set-up used in [171] to characterise different commercial RFSs

mechanical and environment protection, but also limits the distance that the micro cracks in the conductive layer can be separated from each other. As a result, there is a reduction in the variance in the resistance, with the polyamide-coated version being more effective in this regard. The protective layer had a similar effect on the repeatability of the sensor, with higher Standard Deviations (SDs) observed for the coated versions, in particular the middle angles.

Nonetheless, all the FP RFSs offered good repeatability. Meanwhile, the SS RFSs exhibited a higher degree of linearity in their response, with a high-level of repeatability across the tested angles, which is evident from the low and relatively constant SD. However, it had a low, meaningful variation in resistance comparable to the sensitivity of the FP RFSs at lower angles. Meanwhile, the hysteresis was considered practically irrelevant for all brands [171].

Signal stability over time is also important for an accurate and repeatable measurement of human-hand movement, otherwise a single angle will correspond to a wide range of resistance values. The step response decay (i.e., the variation in the resistance value over time following a step transition to a different bending angle) of most of the sensors stabilized at a resistance value of 90-93% of the initial value, with the uncoated FP RFSs exhibiting a lower signal stability in the long run. This means that measurement of the sensor must take place after an established period of time from when it was bent [171].

For this application, the RFSs from FP were preferred due to their higher sensitivity, while still offering good repeatability, despite their non-linear behaviour. Different techniques have been proposed in the literature in an attempt to increase the linearity of these sensors, such as the introduction of a fixed-value resistance in parallel to the RFS [166] or the modification of the shape of the sensor [172], but at the expense of its sensitivity. Hence, instead of trying to increase the linear behaviour of the sensors, which goes beyond the scope of this research, a detailed calibration protocol that defines the non-linear relationship between the resistance of the sensor and the joint angle should be carried out. The RFS with the polyester coating was eventually chosen as a compromise between the sensitivity of the sensor at lower angles and the stability of the signal over time. The size of the sensor chosen varied, depending on which size best covered the joint being measured.

4.3.4.2 Identifying the placement of the Sensing Technology on the human hand

An RFS is required for each DOF that needs to be measured by the data glove. The position of these sensors relative to the joint being measured is important for the sensors to provide meaningful data.

For the FLEX/EXT of the MCP and PIP joints, a singular 2-inch RFS is placed towards its middle length, over the dorsal aspect of the joint, as is the case with other data gloves found in the literature [110]. It is important that the conductive layer of the sensor is placed on the convex side of the bent surface so that when the joint is flexed, the micro-cracks are separated from one another instead of compressed.

On the other hand, effectively locating the position of the RFSs for the measurement of the ABD/ADD between the two fingers, and the two DOFs of the thumb CMC joint proved to be more of a challenge. For the ABD/ADD angle, the sensor between the index and the middle finger is typically laid on its narrow side on top of the hand-web space, Figure 4.11(a), as in [110], or placed in a half circle configuration with both sides sewn to the dorsal part of the fingers, Figure 4.11(b), as in [166]. Meanwhile, for

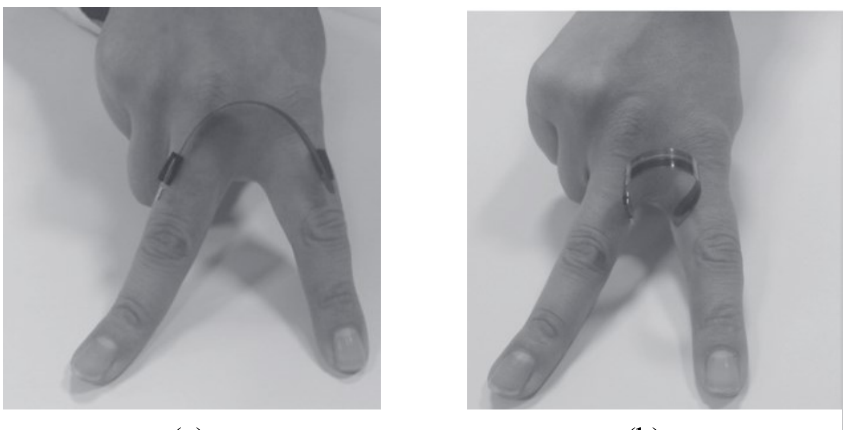

(a) (b)

Figure 4.11: The different methods proposed in literature for the measurement of the ABD/ADD between the fingers [168]

the two DOFs of the thumb CMC joint, commercial data gloves typically have the sensors placed as shown in Figure 4.12; one sensor is laid on its narrow side on the hand-web space between the thumb and the index, while the other one is placed horizontally across the 1st and 2nd metacarpal bones, either on the dorsal or palmar part of the hand.

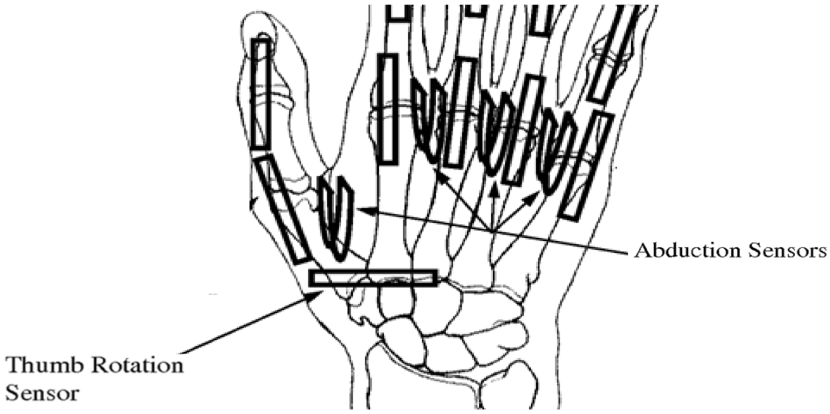

Figure 4.12: The position of the sensors used to measure the two DOFs of the thumb CMC joint in a commercial data glove [176]

Unfortunately, studies such as [173] and [174], as well as some preliminary tests carried out in the lab, have shown that cross-talk is present between the different sensors in these locations. Cross-talk occurs when the resistance value of a particular sensor depends not only on the position of the joint being measured, but also on the position of the adjacent joints. For example, the ABD/ADD sensor in either method is stretched when either neighbouring joint is flexed; this will affect its response. Unless a sophisticated algorithm is used to calibrate the sensors, a time-consuming calibration is required to determine the relationship as regards output of the different sensors involved.

Hence, to eliminate the risk of inaccuracies stemming from sensor cross-talk, the approach used by hand therapists was adopted for these DOFs (i.e., a mechanical goniometer was used instead of the RFS), especially since only the static posture needs to be analysed and the objects identified in Table 4.1 (on p.52) do not interfere with the measurement process. The ABD/ADD angle is measured in the plane of the proximal phalange of the index finger with reference to the position of the middle finger projected onto this plane, as shown in Figure 4.13(a). The middle finger is used as a reference since it provides the experimenter with a visual guide. Hence, modelling the ABD/ADD angle after the FLEX/EXT of the MCP joint, as discussed in Section 4.3.2 (on p.54) means that the measured ABD/ADD angle can be directly modelled in the KHS.

For the two DOFs of the thumb CMC joint, the goniometer is used as shown in Figure 4.13(b) and (c), where the angles measured are θ_{B_1} and θ_{C_2} in Figure 4.5 (on p.57). As one can observe, these two angles do not define an angle pair. Hence, in the situation where the thumb is in the open-hand position only one measurement is noted. Using the D-H convention, as discussed in Appendix A (on p.217), the two measured angles can then be converted to each of the angle pairs shown in Figure 4.5.

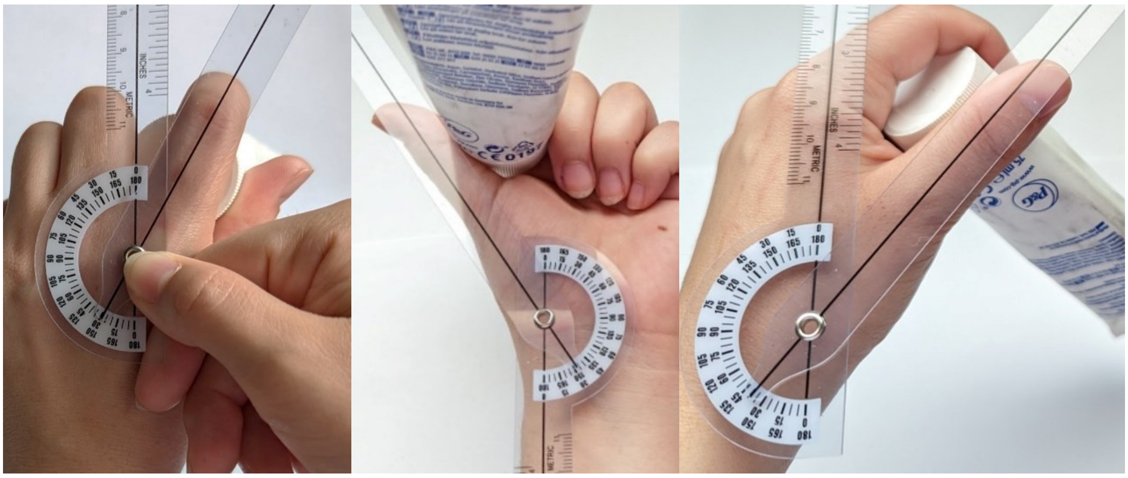

(a) (b) (c)

Figure 4.13: Measuring: (a) the ADD/ABD between the fingers (b) θ_{B_1} and (c) θ_{C_2}

4.3.4.3 Designing the support for the Sensing Technology to be worn by the participants

The RFSs then need to be mounted on some fabric that, when worn by the participants, keeps the sensors in the appropriate positions relative to the joints of the hand so that their movements are consistent and repeatable.

The supporting fabric does not necessarily have to be in the shape of a glove. For example, the study in [175] developed a data glove which measured the five MCP joints, where each sensor was placed in a thin sleeve attached to the back of the fingers via double-sided toupee-tape adhesive. The advantage of this design is that it can be adjusted for participants with different hand sizes, since the sensors can be positioned according to their hand without any loss of sensitivity. However, given that multiple sensors need to be mounted on the same digit, gloves in different hand sizes were considered more appropriate for this application.

Each glove must fit tightly on the participants' hands to ensure a consistent and repeatable movement of the FSRs that closely follow the hand movement so as to minimise measurement errors, as observed in [176], [177]. Several materials have been considered in the literature, but usually they are Lycra-based, such as Lycra/Cotton combination (i.e. spandex) [178] and Lycra/polyamide combination [109]. This is because Lycra is a lightweight material known for its stretching property, which ensures a tight fit for different participants with similar hand sizes while facilitating the donning and removal of the glove without restricting any finger movements. Hence, a stretchable grade of Lycra, found at a local shop, was used in this work.

A glove was then made from this material, with the fingertips exposed to minimise loss of sensitivity. The individuated movements of the ring and little fingers could then be constrained by either tucking these two fingers in the palm (as in the study carried out on the minimal anthropomorphic hand [8]) or constraining them to the middle finger. The latter option was preferred because it does not interfere with the workspace of the hand, which could potentially alter the final hand posture, especially when the palm is involved in the grasp. Furthermore, given that the ring and little finger are to be incorporated in the final design of the prosthetic hand, the latter approach is a better representation, especially if these two fingers are to provide additional support when grasping the object. Hence, a single pocket was sewn for the ring and little finger which was in turn sewn to the pocket of the middle finger, thus making the middle, ring, and little fingers move together.

The six 2-inch RFSs, Figure 4.14, placed over the MCP and PIP joints of the index and middle finger, as well as the MCP and IP joints of the thumb were then embedded in the glove. The distal end of each MCP sensor overlapped the proximal end of the corresponding IP sensor, so that each sensor could be placed on the appropriate joint. To avoid side drifting and contact between each pair of sensors, two layers of Lycra were sewn on the upper side of the glove (for a more stable environment since it would prevent rubbing against the skin of the participants), forming separate sleeves into

Figure 4.14: The developed data glove equipped with six 2-inch RFSs

which these sensors could be inserted. The proximal end of each sensor was sewn to the glove to ensure that the sensors were not displaced during operation and the distal end could slip into the sleeve.

This glove was to be sewn in three different sizes to cater for participants with different hand sizes. However, only the medium-sized glove had been developed and characterised, before restrictions were implemented as a result of COVID-19 (e.g., people not allowed or afraid to venture away from their home to meet other people, and contractual obligations precluding an indefinite halt to the research project). These restrictions forced the experiments to be held as early as possible with a limited number of willing participants so that the research could proceed. Although this limitation may possibly have resulted in a slightly reduced spread of the work, the results obtained from medium-sized hands are still expected to be applicable to prosthetic hands of different sizes, since Mason et al. [96] had observed that whilst there were slight differences in the postural synergies observed from people with different hand sizes, (e.g., smaller hands had their fingers extended more than larger hands), the similarity indicated that a common strategy could be used regardless of the hand size.

4.3.4.4 Front-End Conditioning Circuity

The resistance values of the RFSs need to be read and processed by a microcontroller so that meaningful data can be outputted to a computer for further processing. Hence, a front-end conditioning circuitry was needed to prepare the R_{Sensor} for the next processing stage.

The front-end circuitry adopted in this work is a simple voltage divider, which is suggested by manufacturers and commonly used by different authors, as in [179], [109]. In this circuit, the RFS is connected in series with a fixed resistor, R_{Fixed}, as shown in Figure 4.15. This produces a variable voltage, V_{out}, proportional to the R_{Sensor}. The relationship between these two parameters is shown in Equation 4.4:

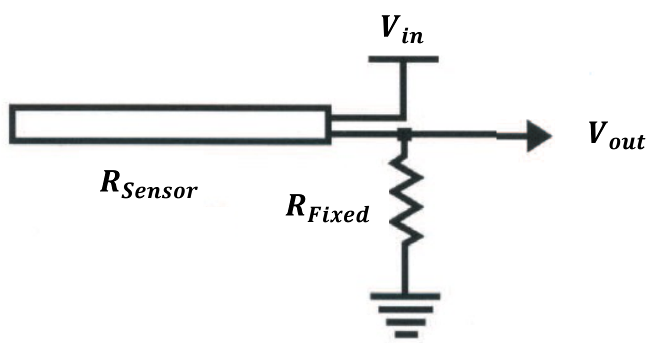

Figure 4.15: Voltage Divider

$$V_{out} = V_{in}\left(\frac{R_{Fixed}}{R_{Sensor} + R_{Fixed}}\right) \quad 4.4$$

In this configuration, V_{out} decreases as the RFS is bent (i.e., as the R_{Sensor} increases). This means that the maximum value V_{out} corresponds to when the sensor is not bent, which should be the same for different participants irrelevant of their joint ROM. In this way, it ensures that the maximum allowable input range of the microcontroller analogue input is not exceeded. The voltage across the sensor, V_{sensor}, can then be determined by subtracting the V_{out} from the supply voltage, V_{in}.

As a result, the relationship between V_{sensor} and the joint angles is a function of both R_{Fixed} and V_{in}. This means that the signal range can be maximised by optimising these two parameters. Saggio et al. [179] recommended that the value of R_{Fixed} should correspond to the geometric mean of the minimum and maximum values observed for the R_{Sensor} during operation. To investigate the effect that R_{Fixed} has on V_{sensor}, a simple experiment was carried out in the lab, in which the V_{sensor} at different bent angles was noted for several values of R_{Fixed}. For easier comparison, the graph of normalised V_{sensor} against joint angle was plotted for each value of R_{Fixed}, as shown in Figure 4.16, where $21.2k\Omega$ is the geometric mean.

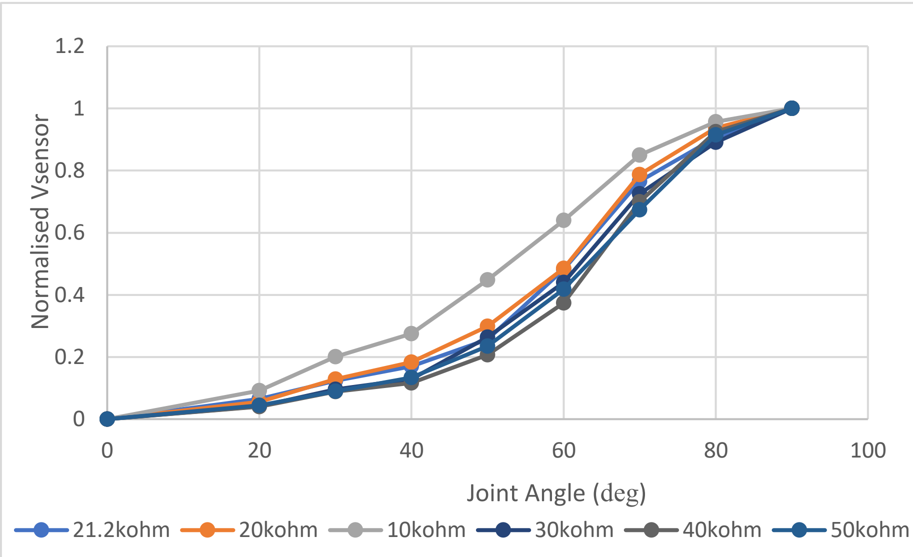

Figure 4.16: The graph of normalised V_{sensor} against different angles for several R_{Fixed}

From Figure 4.16, one can observe that decreasing the value of R_{Fixed} beyond the geometric mean increases the sensitivity of the lower angles at the expense of the higher ones. Increasing the value of R_{Fixed} had the opposite effect. Hence, as a compromise between the two extremes, the value of R_{Fixed} was set to the geometric mean as recommend by Saggio et al. [179]. This parameter may vary slightly from one participant to another, depending on their ROM and bend radius. However, to avoid the need to change the value of R_{Fixed} during the experiments, it was set to the geometric mean observed during testing, especially since Figure 4.16 has shown that the difference in shape of V_{sensor} against joint angle for $21.2k\Omega$ and $20k\Omega$ is not that large.

To further increase the sensor resolution of the RFSs, Oess et al. [109] also suggested increasing the voltage of the power supply. In fact, as with the results noted in [109], the sensor dynamic range was observed to increase significantly when the supply voltage was increased from $5V$ to $10V$, as shown in Figure 4.17. Hence, the maximum V_{in} suggested by the manufacturers of the sensors was used, which was $12V$.

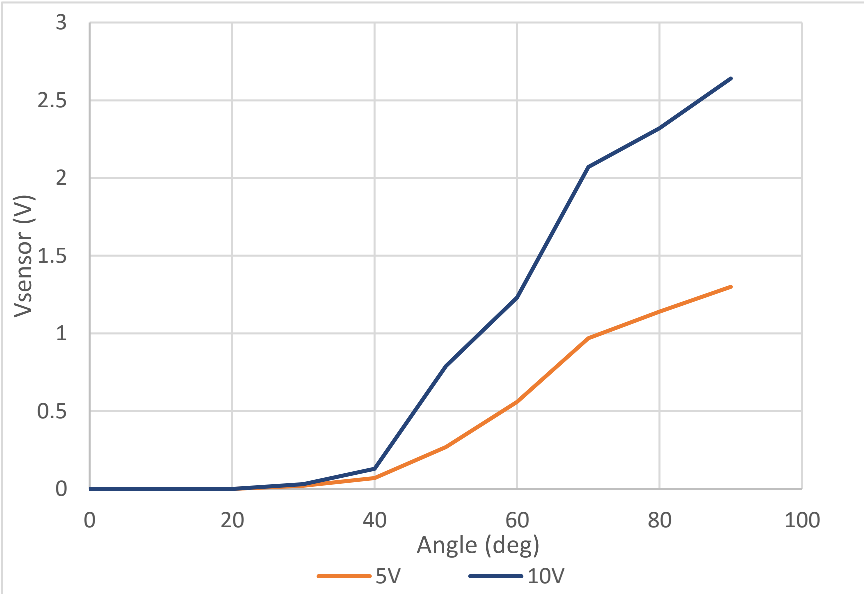

Figure 4.17: The graph of V_{sensor} against joint angle for two different values of V_{in}

The V_{sensor} of each RFS could then be processed by a microcontroller combined with an analogue-to-digital converter, which converts the analogue voltage to a digital value for further processing by a computer. The LabJack U6 microcontroller (LabJack Corporation , Lakewood, CO, USA) [180], Figure 4.18, was chosen, together with the CB37 terminal board [181] that replaces the connector on the microcontroller with

Figure 4.18: LabJack U6 [180]

screw terminals. The microcontroller has fourteen 16-bit analogue inputs available, with a large input range of $\pm\ 10V$; these inputs provide a good quality digital signal for the V_{sensor} of the six RFSs.

The digital signal was then logged on a computer, using DaqFactory [182] (a software developed by Azeotech Inc, Oregon for the design of custom applications such as collecting input data) via the USB cable. Hence, two graphical user interfaces were developed in DaqFactory to facilitate the collection of data during the calibration protocol of the data glove (which will be discussed in a later section) and the measurement of the minimal anthropomorphic hand postures, including the logging of the ADD/ABD angle between the two fingers and the two DOFs of the thumb CMC joint, Figure 4.19.

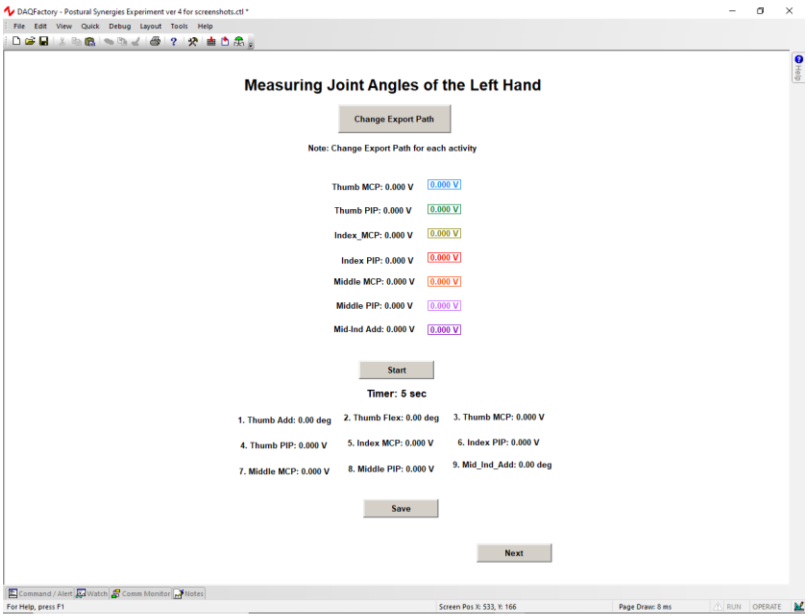

Figure 4.19: Graphical User interface for the measurement of the minimal anthropomorphic hand postures

However, the voltage supplied by the microcontroller is only $5V$. Hence, an external power supply was used to provide the $12V$ to the front-end circuit, since the portability of the data glove was not important for our application.

4.3.4.5 The Constructed Data Glove

Each sensor was connected to its physically separated signal-conditioning circuit, which were mounted on a printed-circuit board and secured inside an enclosure box. The circuits were then powered by an external source and wired to the LabJack U6 microcontroller, which was connected to a computer via a USB cable. The complete set-up of the data glove is shown in Figure 4.20(a).

The enclosure box together with the LabJack U6 and CB37 terminal block were then secured in a backpack, which the participants were able to wear during the experiment. This facilitated the donning and the removal of the data glove; it also ensured that the different components were not in the way during the execution of the different bimanual activities. The wires between the sensors and the enclosure box were then secured to the forearm of the participant, using Velcro, Figure 4.20(b). To ensure that this did not affect the ROM of the participants and that the sensors were not being pulled during motion, which could alter their position and even damage them, the wires were made long enough so that they would not be taut.

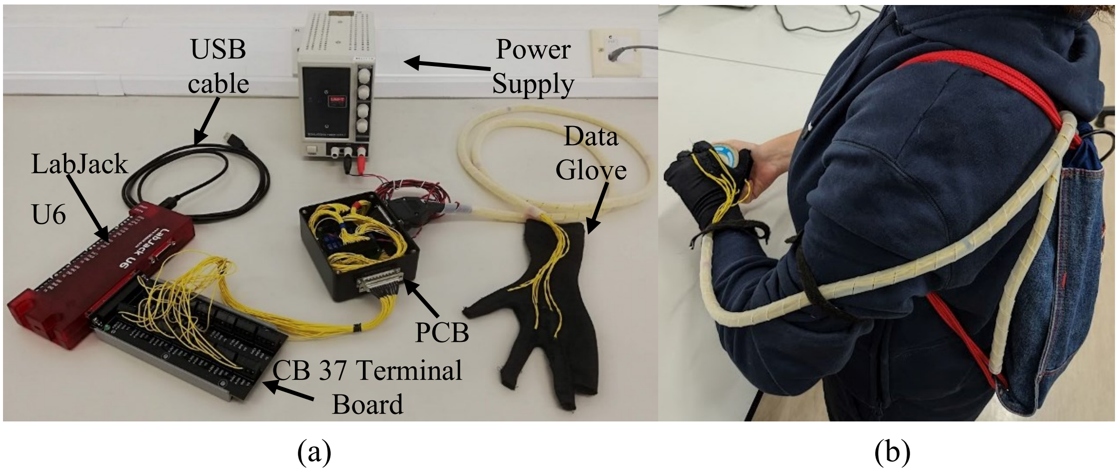

Figure 4.20: (a) The complete setup of the designed data glove and (b) the data glove worn by a participant

4.3.5 Calibration Protocol

A calibration protocol to determine the conversion factors from V_{sensor} to joint angles was required. This was to be carried out in every measuring session to take into account the variation in the bent position and radius from one session to another due to the different participants and the removal of the glove.

This protocol consisted of a set of calibration blocks and a mechanical goniometer, shown in Figure 4.21, to bend the joints of the hand to specific angles ranging from 0°

Figure 4.21: Calibration tools

to the maximum ROM of the participant (up to 120º), in increments of 10°. For each angle, sufficient time was allowed for the signal to stabilise before noting the corresponding V_{sensor} through DaqFactory [182]. Hence, calibration blocks were preferred for most joints, as they provided a steady surface on which the participant could lean their finger. This meant that the participant could maintain a more constant angle while the corresponding V_{sensor} was measured. However, this was not possible for the thumb MCP joint due to the limited space available under the joint; in that case a mechanical goniometer was used.

For each RFS, this procedure was to be carried out once before and once after each experiment; it offered a compromise between keeping the duration of calibration as low as possible and maintaining adequate accuracy of the relationship between the output voltage of each sensor and the corresponding joint angle. From each voltage-angle pair (averaged over the two calibration runs), a non-linear relationship was obtained by fitting the best polynomial curve, which could be used to convert V_{sensor} into the corresponding joint angle. A typical calibration curve is shown in Figure 4.22.

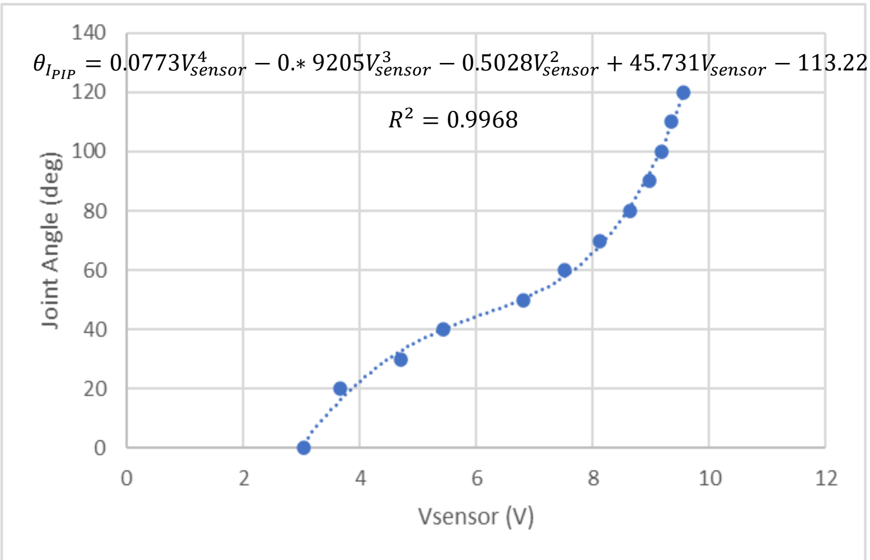

Figure 4.22: A typical calibration curve of the index PIP joint

4.3.6 Characterization of the Data Glove

Measurement repeatability (i.e., the variation present in repeated measurements taken on the same subject, using the same method) and accuracy (i.e., the closeness of the measurement to the actual value) are important for the developed data glove. Hence, multiple tests were carried out to evaluate its characteristics.

The first test established the repeatability of multiple measurements taken during a single measuring session, and was based on a repeatability testing protocol proposed by Dipietro et al. [177]. This test quantified the repeatability of the fist posture and of the flat hand position. Hence, the hand was first closed in a fist for a couple of seconds and then placed flat on the tabletop for another couple of seconds, as shown in Figure 4.23. Each time, the stabilized output voltage of each sensor was logged and converted to its corresponding joint angle. This open/close cycle was repeated for ten times to form a single data block. In total ten data blocks were obtained. Each phase was then analysed separately, where, for each joint angle, the range and SD of the average value observed in each of the ten data blocks was calculated and listed in Table 4.4. These statistics provide an approximate measure of the repeatability of the data glove.

(a)

(b)

Figure 4.23: Repeatability test of (a) fist and (b) flat-hand posture

Table 4.4: The range and SD obtained for each joint in the repeatability test.

	Index MCP	***Index PIP***	***Middle MCP***	***Middle PIP***	***Thumb MCP***	***Thumb IP***	***Average***
Fist Posture							
Range (°)	8.24	7.42	5.81	6.65	2.79	4.50	5.90
SD (°)	2.51	2.35	1.44	1.82	0.79	1.41	1.72
Flat Hand Posture							
Range (°)	0.82	5.62	0.70	5.25	4.20	5.55	3.69
SD (°)	0.23	1.62	0.23	1.56	1.32	1.83	1.13

The results observed for the different joints were similar, with the average range across the joint angles and postures being 4.80±1.43°. This is comparable to the reliability of the mechanical goniometer [176] and other designed gloves whose reliability has been systematically addressed, such as the Wü-Glove [166], whose reliability was observed to be 4.35±1.40°. The range and SD in Table 4.4 tended to be higher for the fist than for the open hand. This is because the measurement error that was investigated may be influenced by the technical characteristics of the glove, such as glove instability and glove inaccuracies, and by factors such as movement variation of the thumb and finger, wrist movement and grip strength. Identifying the weight that each of these factors has on the total measured error would be quite complicated. Instead, a Force Test and a Wrist FLEX/EXT Test, based on additional tests described by Dipietro et al. [177], were carried out to investigate their effect on V_{sensor}.

In the Force Test, three objects of different shapes, namely, a piece of wood, a screwdriver, and a bottle of water, were grasped with the maximum force possible for a couple of seconds, then the force was released for another couple of seconds without moving any of the hand and wrist joints. This strong/light grip cycle was repeated for ten times. Meanwhile, in the Wrist FLEX/EXT Test, the same three objects were held with the wrist flexed for a couple of seconds and then with the wrist extended for another couple of seconds, as shown in Figure 4.24. This was also repeated for ten times. For each test, the sensors' output voltages logged for each object were converted to joint angles, and the range of angles observed across the ten trials was noted. Table 4.5 lists for each of these tests the range of angles observed for each joint, averaged across the different objects.

(a) (b)

Figure 4.24:The Wrist Flex/Ext Test for the bottle of water

Table 4.5: The average range of angles observed for each joint in the Force and Wrist Flex/Ext tests

	Index MCP	***Index PIP***	***Middle MCP***	***Middle PIP***	***Thumb MCP***	***Thumb IP***	***Average***
				Force Test			
Range (°)	5.11	9.80	5.69	11.38	2.24	7.56	6.96
SD (°)	0.09	7.18	2.83	6.80	0.83	4.72	3.74
				Wrist Flexion/Ext test			
Range (°)	4.23	5.73	6.31	8.66	2.69	6.98	5.53
SD (°)	1.53	2.48	1.97	5.06	1.87	2.88	2.58

As with the results obtained by Dipietro et al. [177], both grip strength and wrist movement were found to influence the measurements, especially the middle PIP joint.

Hence, to mitigate these factors, during the calibration of the data glove and the measurement of the hand postures, the participants were asked to apply minimal force and keep the wrist straight as much as possible.

Meanwhile, the accuracy of the data glove was evaluated by comparing the joint angle returned by the data glove to the actual angle set by the calibration tools, as shown in Figure 4.25. For each joint, five V_{sensor}readings were noted for each angle between 0° and the maximum ROM of that joint in increments of 10°. These voltages were then converted into angles and the difference between the measured angle and the actual joint angle was computed. Table 4.6 lists for each joint the difference in joint angle, averaged across the ROM of the joint and the repeated readings, together with the SD and the 95% confidence interval. On average, the 95% agreement limits for each joint were within ±5°, which are comparable to other gloves evaluated, such as the one in [109].

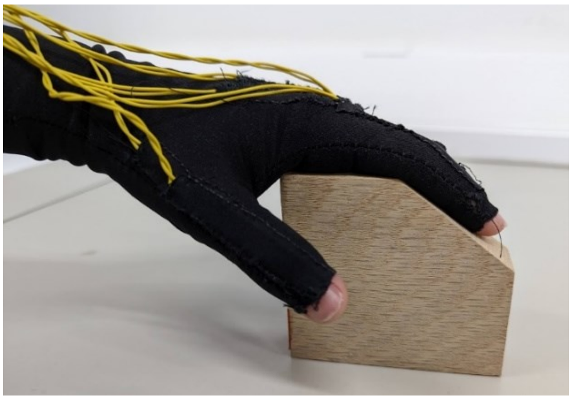

Figure 4.25: Accuracy Test

Table 4.6: The average accuracy of each of the joints of the data glove

Finger Joint	***Mean difference (º)***	***SD of differences (º)***	***95% confidence interval (º)***
Index MCP	-0.21	3.87	-5.02 to 4.59
Index PIP	-1.33	1.90	-3.69 to 1.04
Middle MCP	0.07	3.93	-4.81to 4.95
Middle PIP	0.64	1.76	-1.74 to 3.02
Thumb MCP	1.38	1.50	-0.49 to 3.24
Thumb PIP	-1.22	2.79	-4.69 to 2.25
Mean	**-0.11**		**-3.41 to 3.18**

The repeatability and accuracy of the data glove was comparable to traditional goniometers and other gloves, and thus considered acceptable for the objective of this research. A limitation regarding the characterization of the data glove is that the tests discussed in this section were only carried out by one subject. However, given the number of times that the RFSs had to be bent during this testing process and that the performance of the RSFs may decay with time and usage [171], the characteristics of the data glove obtained from one subject were considered sufficient, especially since the designed data glove caters for similar hand sizes.

4.4 EXPERIMENTAL PROTOCOL

After the successful development and characterization of the data glove, an experiment was conducted to capture the variance of the non-dominant, minimal anthropomorphic hand in bimanual activities.

Three right-handed participants (25-49 years old) with medium-sized hands took part in the experiment. Although, as indicated previously, this number was smaller than originally planned, it can still be considered sufficient, since this experiment focused on a pre-determined representative set of standard grasp postures, which for the most part would be executed in the same way by all the participants under the strict supervision of the researcher. All the subjects were self-reported to be in good health, with no neurological history or motor disorders. The consent form in Appendix B (on p.219), was filled in by all the participants before starting the experiment, as required by the Faculty of Engineering Research Ethics Committee of the University of Malta.

Each participant wore the data glove on their left hand (i.e., their non-dominant hand) and underwent the calibration protocol. For the actual experiment, the participants executed the twenty-seven representative grasps in Table 4.1 (on p.52), where for each grasp the participants were asked to:

1. Place their non-dominant hand flat on the table;
2. Grab the object as explained by the experimenter, who ensured that the correct grasp type was being used;
3. Hold the object and wait for the output signals of the sensors to stabilize so that the experimenter could log, in DaqFactory, the output voltage of each sensor;
4. Keep holding the object while the experimenter used a mechanical goniometer to measure the ABD/ADD of the fingers and the two DOFs of the thumb CMC joint.

For each grasp, the average voltage of each sensor was then converted into joint angles using the calibration curves obtained during that specific session, while the two angles measured for the thumb CMC joint were converted into the three angle pairs as discussed in Appendix A (on p.217).

4.5 IDENTIFYING THE POSTURAL SYNERGIES OF THE NON-DOMINANT, MINIMAL ANTHROPOMORPHIC HAND

The analysis of the hand postures captured during the experiment is elaborated upon in this section.

First, the grasp postures measured during the experiment were modelled in SketchUp [183], using the preliminary kinematic hand model discussed in Section 4.3.2 (on p.54). Each posture was then checked in the simulation environment, and corrected for any obvious measurement errors, to further improve the accuracy of the analyses.

The experimental data were subsequently analysed, using PCA, a dimension-reduction technique that has provided very good results in the field of postural synergies [116]. However, the variability of the dataset depends on the angle pair used to define the position of the thumb metacarpal bone, yielding slightly different but meaningful results. Hence, each angle pair was analysed separately (i.e., three different datasets were obtained from each participant, where, in each dataset, one of the angle pairs was used to define the position of the thumb metacarpal).

Before performing the PCA using SPSS statistics [184], the suitability of the data was first checked, using Bartlett's Test of Sphericity [185], to determine whether there is actually any redundancy in the data that can be expressed by a few parameters. This is determined by noting whether the Correlation Matrix (CoM) of the dataset diverges significantly from the identity matrix, which would indicate that the variables are not orthogonal (therefore, they are correlated). The result of this test revealed that the probability that the variables measured in this work are orthogonal is less than 0.01, thus confirming the appropriateness of the data for PCA.

For the prosthetic hand to then be able to reconstruct as effectively as possible the representative set of everyday postures, different weightings were applied to the grasp types within the analysis in accordance with their relevance to the non-dominant hand in bimanual ADLs, as shown in Figure 4.2 (on p.50). In view of the fact that the individual participants had slightly different hand dimensions, and might have also or consequentially adopted grasping postures ("strategies") that were slightly different from each other, the PCA was applied separately on the dataset of each participant. This is because the PCA applied globally (i.e., the recorded hand postures of all the participants are included in the PCA) as in [103], is hypothesized to be susceptible to subtle differences in hand use by different people [186]. Thus, for each participant and angle pair, the dataset consisted of a [27x9] matrix (i.e., twenty-seven postures and nine measured kinematic DOFs), with each posture weighted according to its prevalence in ADL use.

The synergies extracted can then be the eigenvectors of either the Covariance Matrix (CvM) or the CoM [186]. The CvM is typically used when the units of measurement are the same for the different variables, as it is quite sensitive to the variance of the original data. However, this means that variables with larger ranges of variation may dominate the small ranges and hide the coordination of the DOF with the lowest ROM. To ensure that each DOF of the hand contributes equally to the analysis, the experimental data are standardized (i.e., for each DOF the mean = 0 and SD = 1) before applying the PCA to the CvM; this is equivalent to applying the PCA to the CoM. However, for the prosthetic hand, the important thing is that it can reconstruct the representative set of everyday postures, which were carefully chosen to utilise the entire ROM of most joints, as shown in Table 4.7, with the skewness parameter indicating whether the joint is more often FLEX/ABD (i.e. negative skew) or EXT/ADD (i.e. positive skew). For this reason, the significance of the motion of a joint should not be inflated if that joint has a small total ROM. Therefore, as with other studies on postural synergies, such as [103], [187], the PCA was applied to a CvM without standardizing the data prior to the analysis so as to preserve the variance of the original data.

Table 4.7: Basic statistics of the joint angles across all postures and all subjects

Joint Angle	***Mean*** (°)	***SD*** (°)	***Minimum*** (°)	***Maximum*** (°)	***Skewness***
$\boldsymbol{\theta_{A_1}}$	27	20	0	78	0.54
$\boldsymbol{\theta_{A_2}}$	25	11	0	52	0.04
$\boldsymbol{\theta_{B_1}}$	24	18	0	74	0.65
$\boldsymbol{\theta_{B_2}}$	20	12	0	52	-0.12
$\boldsymbol{\theta_{C_1}}$	41	13	15	78	0.88
$\boldsymbol{\theta_{C_2}}$	50	26	0	90	0.16
$\boldsymbol{\theta_{T_{MCP}}}$	6	6	0	30	1.60
$\boldsymbol{\theta_{T_{IP}}}$	12	17	0	74	1.53
$\boldsymbol{\theta_{I_{MCP_{FE}}}}$	29	20	0	89	0.51
$\boldsymbol{\theta_{I_{MCP_{AA}}}}$	12	8	0	35	0.47
$\boldsymbol{\theta_{I_{PIP}}}$	47	32	0	110	0.17
$\boldsymbol{\theta_{M_{MCP_{FE}}}}$	39	21	0	90	0.28
$\boldsymbol{\theta_{M_{PIP}}}$	57	32	0	120	-0.14

The results of the PCA applied to each of the nine datasets (i.e., three datasets for each of the three participants) were consistent with those of the literature. In fact, a reduction in dimensionality, similar to the one shown in Figure 4.26, was observed for all the datasets, with the first three PCs of each participant accounting for a mean variance of 85.5±1.8% across the different angle pairs and the different participants. This reduction in dimensionality implies that the number of sEMG signals required is reduced, meaning that a more usable sEMG control system can be developed. Such reduction can also simplify the mechanical design, if this reduction in dimensionality is implemented through effective coupling of joints and a reduced number of actuators.

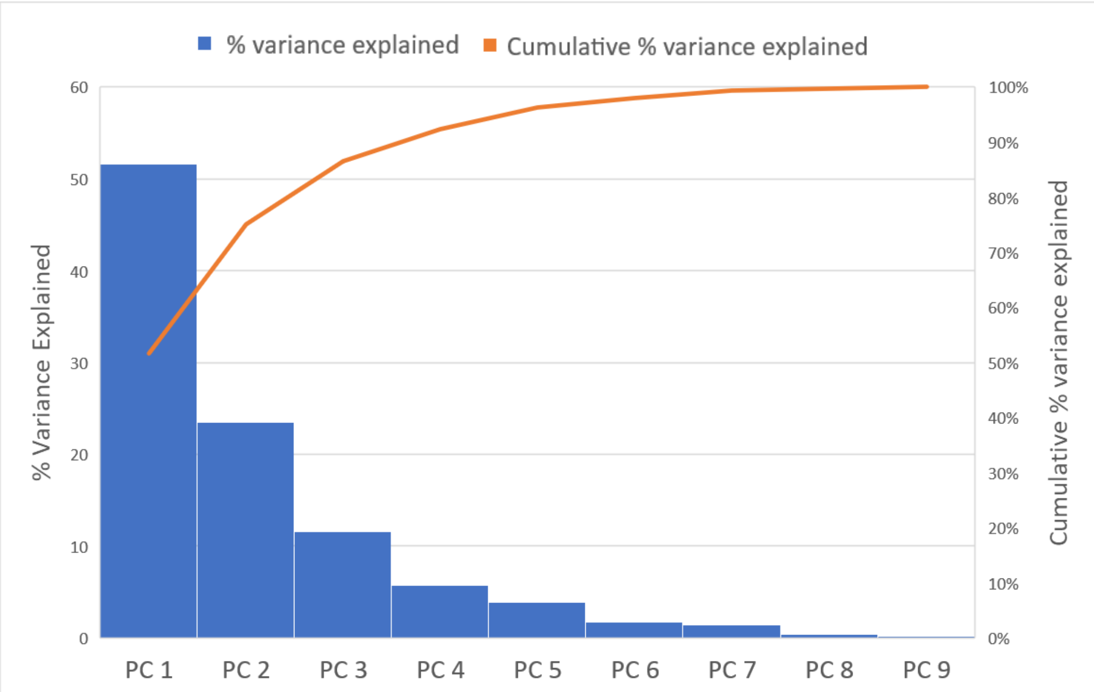

Figure 4.26: The percentage of variance explained by each PC of one of the subjects for Angle Pair A

Initially, a high degree of consistency in the waveform of the first three PCs for different angle pairs was observed across the participants, except for one case, that was not always associated with the same participant. However, it was noted that by interchanging the second and third PCs of that participant, the similarity of this participant's PCs to those of the other subjects improved significantly, as shown in Figure 4.27 (a). A similar level of consistency was also observed across the angle pairs, with the order of Angle Pair A interchanged, Figure 4.27 (b).

From the waveforms in Figure 4.27, one can observe that the first PC is characterized by the FLEX of the PIP joints of the index and the MRL finger, and to a lesser extent, the FLEX of the corresponding MCP joints and the FLEX of the thumb IP joint. This can be seen as the opening and closing of the hand, as in other studies found in the

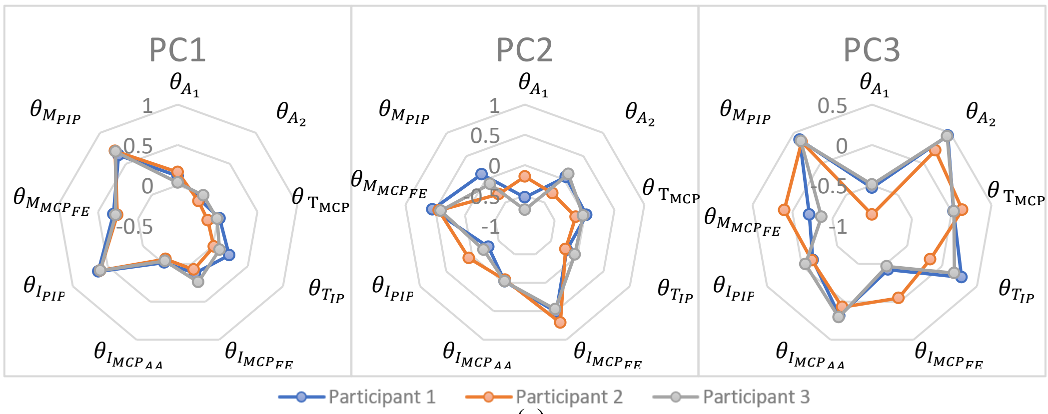

(a)

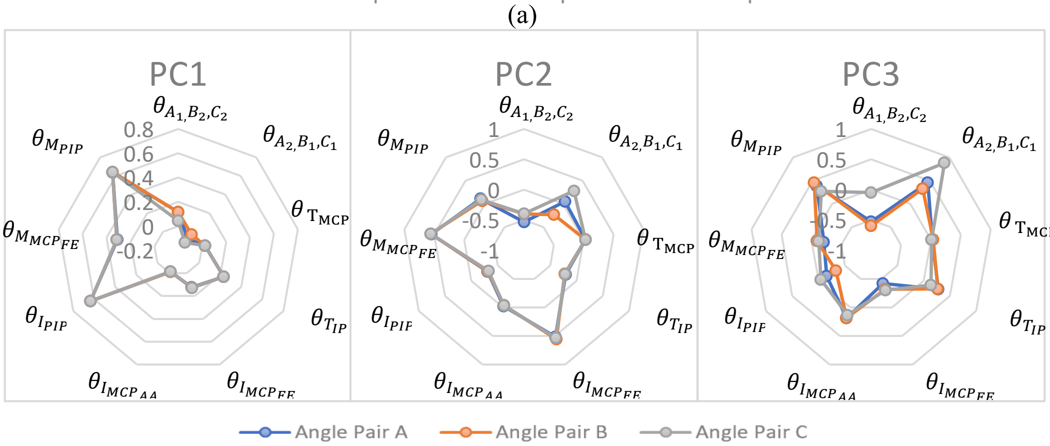

(b)

Figure 4.27: The waveforms of the first three PCs of: (a) all the participants for Angle Pair A were the second and third PCs of participant 2 where interchanged and (b) the three angle pairs for participant 1 where the order of Angle Pair A was interchanged

literature, such as the first synergy observed by Santello et al. [103]. However, in the latter study the first synergy was also characterized by the ADD between the fingers and the thumb ADD and external rotation, as shown in Figure 2.22 (on p.33). PC2 was characterised by the ADD of the thumb, by the FLEX of the MCP joints of the index and MRL finger, and to a lesser degree by the EXT of the thumb PIP joint and the EXT of the index PIP joint. Meanwhile, PC3 involved the ADD and FLEX of the thumb and the FLEX of the index PIP, as well as the ADD between the fingers and the EXT of the MRL PIP joint.

The PCs obtained here could not be compared easily with the PCs obtained from other studies, since this project does not take into account all the DOFs considered in the literature. However, similarity in the coordination of some of the joints could be noted, such as the coordination of all of the MCP joints as in [187]. The three postural synergies obtained for one of the participants are depicted in Figure 4.28, where the extreme hand postures correspond to the maximum and minimum value of each PC, while the middle hand posture represents the average of all twenty-seven postures.

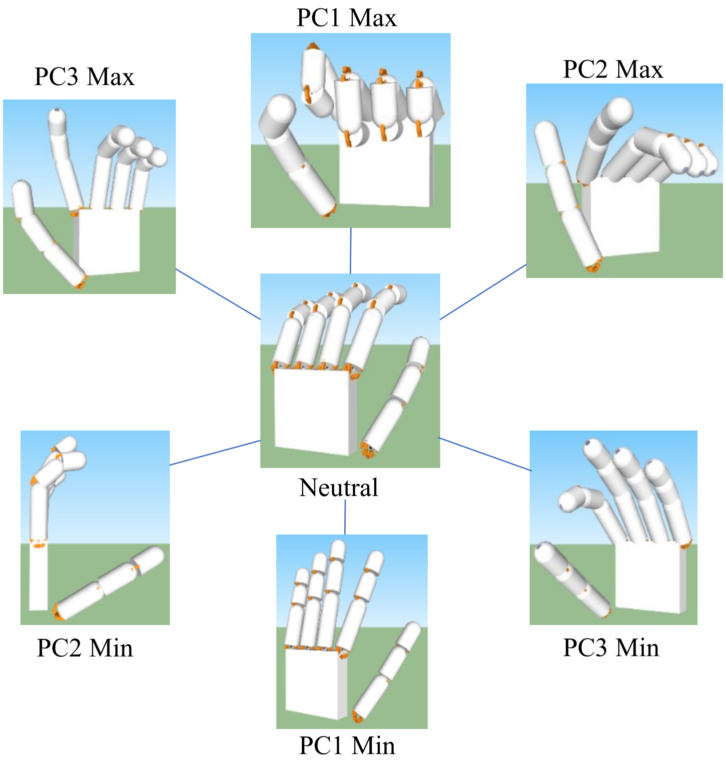

Figure 4.28: Visualization of the first three PCs

By combining the three synergies of one of the participants in different weightings, the original hand postures executed by the same participant could be reconstructed in the reduced dimension with a good level of accuracy regardless of the participant and angle pair considered. Taking Angle Pair A as an example, most of the joint angles in the reconstructed hand posture varied from the actual hand postures by less than 10°, as shown in Figure 4.29. Meanwhile, the average angular difference for each joint across the different participants is shown in Figure 4.30, for Angle Pair A.

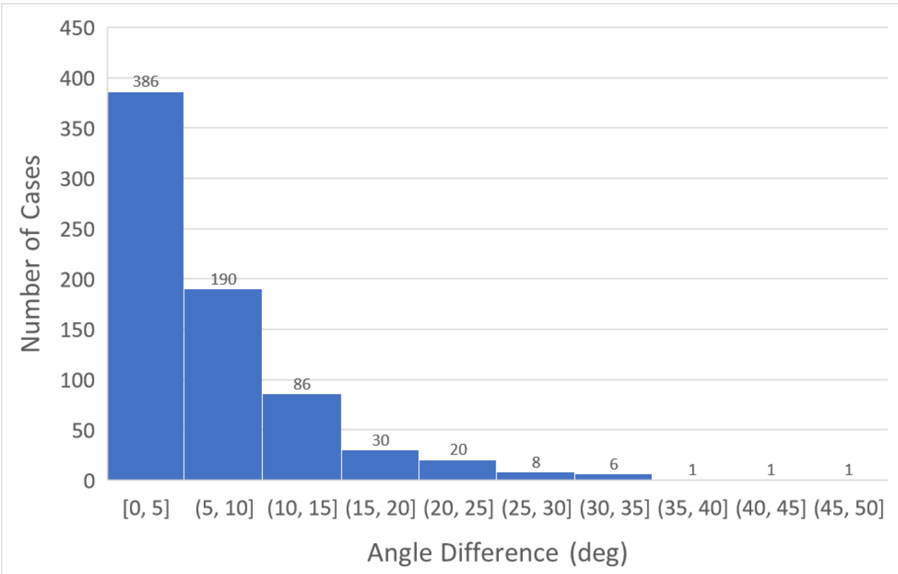

Figure 4.29: The distribution of the absolute difference in joint angles between the actual hand postures of all the participants and the postures reconstructed with Angle Pair A from the first three PCs corresponding to each participant

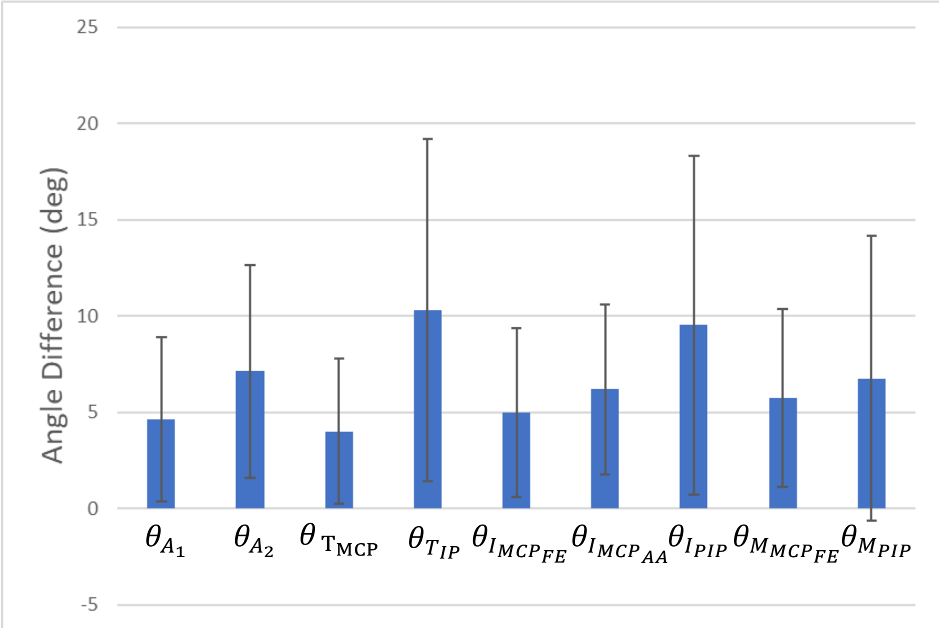

Figure 4.30: The absolute difference at each of the joint angles between the actual hand postures of all the participants and the postures reconstructed with Angle Pair A from the first three PCs corresponding to each participant

From Figure 4.29 and Figure 4.30, one can note that while higher-order PCs explain only a small percentage of the overall variance, they still transmit substantial information about the different joints, especially joints which had a larger SD. However, considering that nine PCs are required to accurately reconstruct the several representative hand postures in the PC space, fairly good results were obtained with just these three PCs. The movement of the hand along these PCs then defines basic motions necessary for a medium-sized prosthetic hand to provide sufficient dexterity as applicable for bimanual activities.

Ultimately, in order to keep the different strategies for the different participants separate, only the PCs of one of the participants, which were considered a good representation of the synergies obtained from the other participants, were selected for further analysis. This was repeated for each angle pair. The selection of the representative participant was carried out using a systematic approach, that is, clustering the first three subject-specific synergies of the different participants using a Hierarchical Cluster Analysis (HCA) [188] similar to the approach taken in [186]. HCA is an algorithm which successively groups small clusters together according to their similarity, as shown in Figure 4.31. In this project, the similarity between two clusters is defined by the absolute of the cosine of the angle between the two farthest synergies present in these clusters (i.e., the grouping measure used is the absolute value of cosine, while the clustering method used is complete linkage, also known as the farthest neighbouring distance). The number of clusters extracted was then determined by the minimum number that ensured that each cluster contained only one synergy from the same participant. For each angle pair, the HCA yielded three different clusters (i.e., the PCs of each participant were in each cluster). This analysis further confirmed the fact that the order of the PCs of each participant does not necessarily imply that they are similar, as they were grouped in different clusters.

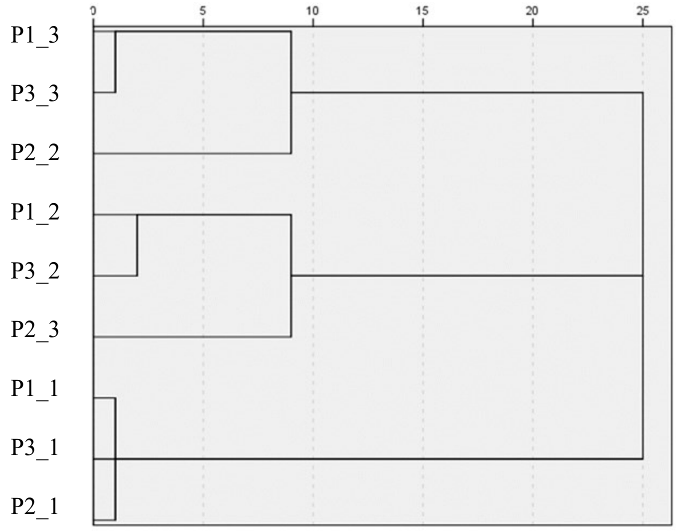

Figure 4.31: A graphical representation of the results of the HCA for Angle Pair A, where the similarity between two clusters is defined by the absolute of the cosine of the angle between the two farthest synergies present in these clusters

A good level of intra-cluster similarity was observed, especially for Cluster 1, where all the synergies across the different angle pairs were approximately 9º away from the core synergy (i.e., the average of all the synergies in that cluster). The participant whose synergies were on average closest to the core synergy was then chosen. On average, the PCs of the representative participants across the three angle pairs, were approximately 13.27±4.43º from the core synergies of the different clusters. This is indicative of the effectiveness of the chosen PCs to reconstruct, in the reduced dimension, the hand postures performed by the other subjects with fairly good accuracy. In fact, taking as an example Angle Pair A, Figure 4.32, shows that in most cases, the absolute angular difference in joint angles between the actual hand postures and the reconstructed postures of all the participants is less than 15º. The average absolute angular difference is slightly higher than what was observed in Figure 4.29, which is to be expected, since the PCs of the different participants were not an exact match.

This approach yielded three sets of PCs (i.e., one for each angle pair) on which the design of a dexterous prosthetic hand which is at the same time relatively simple and easy to use could be based. Given that the difference in the joint angles of the

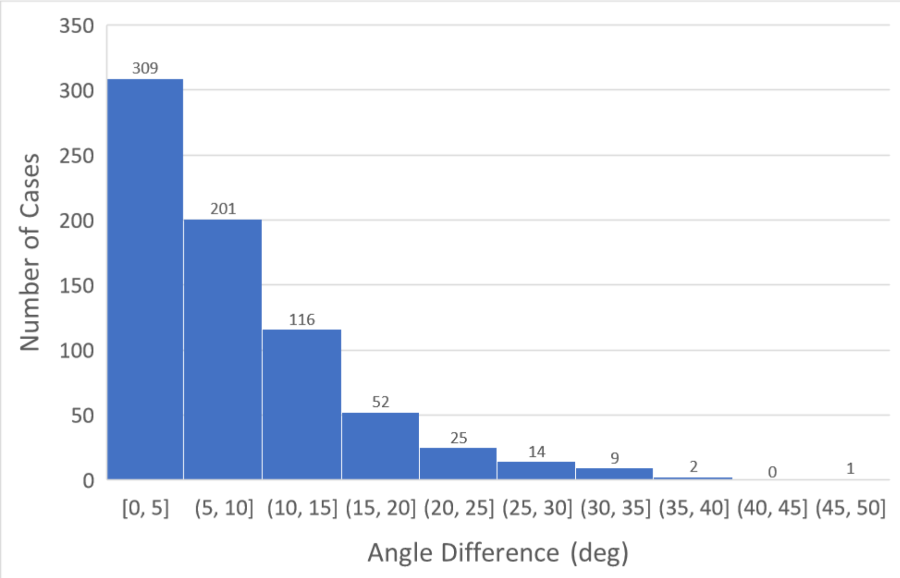

Figure 4.32: The distribution of the absolute difference in joint angles between the actual hand postures of all the participants and the postures reconstructed with Angle Pair A from the first three PCs of the representative participant

representative grasps was similar across the three angle pairs, any one of the sets of PCs identified in this work could be exploited. Thus, further analysis was carried out, using the three sets of PCs, since the slight difference present in one of the sets could prove more beneficial to this application.

4.6 ENHANCING THE USABILITY OF THE PROSTHETIC HAND THROUGH THE IDENTIFIED POSTURAL SYNERGIES

If a prosthetic hand is to exploit these PCs, it must not only be able to implement these motions; it also requires six intuitive and reliable sEMG signals to operate the prosthetic hand from one end of each PC to the other. For an intuitive sEMG signal, the signal for the movement that closely resembles the PCs should be chosen. However, most of the hand configurations at the extremes of the PCs, Figure 4.28 (on p.81), do not represent commonly used everyday grasps. This does not only imply that the actual input signals are not that intuitive, but also that during actual use, the amputee needs to combine the different synergies to reconstruct the required grasps in the reduced dimension. This will constitute a very complex, if not impossible, demand on the user and on the sEMG control system, unless significant compliance is implemented in the prosthetic hand to compensate for this inability to combine these PCs. Either way it will reduce drastically the usability of the system, or significantly increase the complexity of the mechanical system, as discussed in Section 2.8.3.5 (on p.37).

Hence, to reduce/eliminate the need to combine these PCs, for each PC, two commonly used hand postures in the 9D PC space close to the positive and negative extremes of the PC were selected from among the different grasps executed by the three participants. This results in the identification of six readily available proto-grasps (three pairs of representative grasps) for the amputee to use, which are natural and intuitive, since the accurate definition of the hand postures in the 9D PC space is considered. It is to be noted that the consideration of all of the participants' grasps does not constitute a mix-up of grasping strategies in this case; it only allows different grasps, which may be closer to the axes, to be considered in the analysis. The movements of the hand between the two proto-grasps of each PC (in both directions) constitute the six proto-gestures (PGs) for the hand, forming three axes that are still reasonably close to being orthogonal, and which enable the amputee to execute several distinct, usable grasps without the need to combine the PCs.

Some of the proto-grasps that emerged for the different angle pairs were the same, even if they were not necessarily performed by the same participant. These were the grasps used to hold a tablet, open a body cream container and cut a paper with scissors. Other proto-grasps, although not corresponding to the same task object, had similar hand configurations, as was the case with opening a water bottle and holding a medium-sized cup. Despite the similarity between the proto-grasps, there were still some differences in the set of proto-grasps defined by each angle pair. Hence, the angle pair that provided the most distinct and versatile proto-grasps was chosen. This was Angle Pair A, where the grasps chosen for the proto-grasps are listed in Table 4.8.

Table 4.8: The proto-grasps chosen for Angle Pair A and the angle created by each proto-grasp, with the corresponding PC

	PC 1 +	***PC 1 -***	***PC 2 +***	***PC 2 -***	***PC 3+***	***PC 3-***
Grasp Type	SpP	NonP	Pinch	LatP	SpP	Pinch
Task Object	Toothpaste cap	Tablet	Medium Sized Cup	Paper	Body Cream Container	Sewing Pin
Abbreviation	C-grasp	T-grasp	M-grasp	P-grasp	B-grasp	SP-grasp
Level of similarity in angle (°)	23	15	24	27	35	35

From Table 4.8, one can observe that the angle between the proto-grasp and the corresponding PC tends to increase with the order of the PC. This is due to the fact that higher-order PCs tend to account for less of the variance, meaning that the other PCs usually also transmit substantial information for the accurate reconstruction of that particular proto-grasp. The proximity of the proto-grasps and the PGs to the PCs, in 3D space, is shown in Figure 4.33.

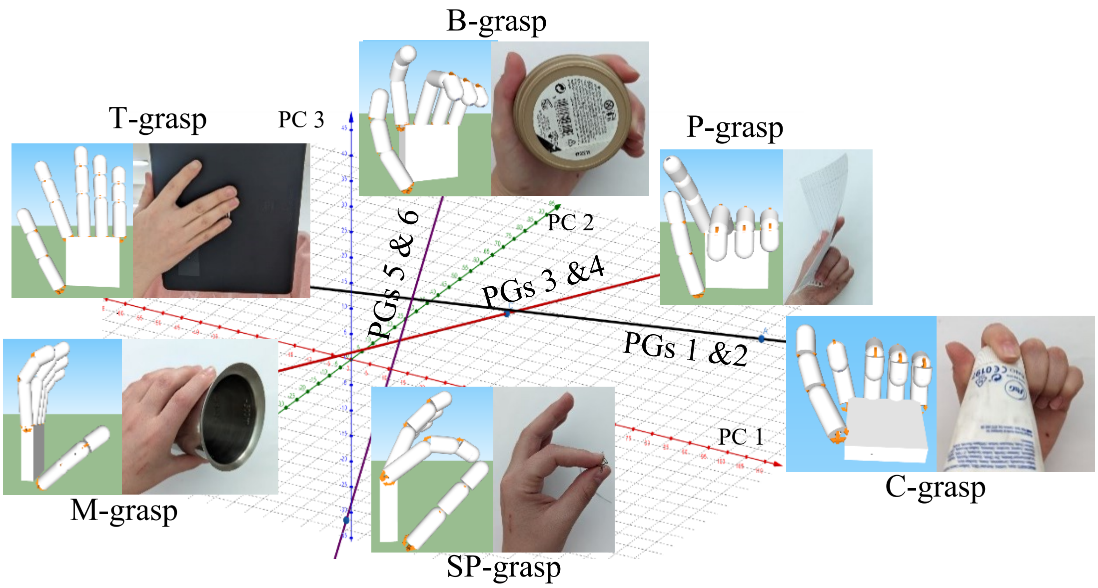

Figure 4.33: Visualisation of the proximity of the proto-grasps and the PGs to the PCs in 3D Space

Although the eventual sEMG control system of the prosthetic hand would be intuitive, in light of the above configuration, its reliability would be expected to be higher if the demand placed on it was lowered. Thus, it was prudent to try to reduce further the number of unique control commands required for operation of the hand.

If a prosthetic hand starts from the fully-open configuration (the O-grasp, which is the open-joint extrapolation beyond the T-grasp), it can only grasp objects when moving towards (not away from) three of the proto-grasps (namely the C-grasp, P-grasp and SP-grasp). Hence, the six PGs were reduced to three hand-closing Proto-Motions (PMs), and a fourth generic hand-opening PM which involved movement of the hand from any starting configuration to the O-grasp. The related study on sEMG signals [9] demonstrated that the motions from an open hand directly to these three proto-grasps and a generic "opening" motion (from any of these grasps) could be distinguished very reliably through appropriate signal processing.

In this manner, five of the six original proto-grasps are achievable through the following three closing PMs: (i) movement from the O-grasp, a variant of the T-grasp, towards the C-grasp (O-C); (ii) movement from the O-grasp towards the P-grasp (O-P); and (iii) movement from the O-grasp towards the M-grasp and then towards S-grasp, a variation of the SP-grasp in which the MRL finger is closed instead, (O-M-S). The introduction of the M-grasp as an intermediate grasp towards S-grasp increases the workspace of the prosthetic hand, such that larger objects could be grasped with a power grasp without affecting the functionality of the S-grasp itself, while the P-grasp (i.e., the proto-grasp which the M-grasp was associated with in Figure 4.33) could be utilised to grasp objects with a lateral pinch. The B-grasp is the only proto-grasp that is omitted in the above movement protocol. However, simulations have shown that this grasp can be replaced by intermediate hand configurations achieved during the selected PMs during ADL execution, for example during the movement of the prosthetic hand from the O-grasp to the P-grasp.

The prosthetic hand was also envisaged to have the capability of a fifth motion, involving hand movement from the O-grasp to a neutral position, N-grasp, representing the default pose of the hand when it is not in use. Motion to the N-grasp can take place autonomously after the hand has been in the open state for a pre-determined period of time, and therefore does not require a separate control signal to be sent by the user.

In conclusion, a small number of important and natural grasping motions/postures, together with the corresponding intuitive and reliable sEMG signals, have been identified for the development of a dexterous yet usable non-dominant, medium-sized prosthetic hand as applicable to bimanual activities. This also paves the way for a simple design, but it greatly depends on the approach taken to implement these grasping motions/postures. In this work, this is attained by optimizing the KHS of the prosthetic hand, as will be discussed in the next chapter.

CHAPTER 5: DEVELOPMENT OF A DEXTEROUS LOW-DEGREE-OF-FREEDOM KINEMATIC HAND STRUCTURE

5.1 INTRODUCTION

This chapter centres on optimizing the kinematic structure of the prosthetic hand. The goal is to identify the optimal KHS that enables the execution of the motions and grasps outlined in the previous chapter with maximum effectiveness and a natural appearance. Emphasis is placed on achieving these functionalities while maintaining the simplicity within the mechanical system, achieved through strategic minimization of the employed motors. By delving into the details of this optimization process, this chapter aims to explain the strategy adopted to achieve this balance between simplicity and dexterity.

5.2 THE PARAMETERS TO BE OPTIMISED FOR A DEXTEROUS LOW-DEGREE-OF-FREEDOM KINEMATIC HAND STRUCTURE

Ideally, each of the three PMs would be actuated by one motor, resulting in a requirement of just three motors. However, due to the different contributions of each joint to each PM, the design of such a system (in particular the transmission systems) could potentially be extremely complex, as discussed in Section 2.8.3.5 (on p.37), and would work against one of the key parameters of this project, namely, simplicity. Hence, the approach taken instead was to assign one motor to each active digit (therefore there would still be three motors in all) and to optimise the architecture of each digit to remain as close as possible to the original proto-grasps within the 9D space, while taking into account the gripping force required for the held object to be able to withstand the external loads present during daily activities.

The possibilities are endless, thus, a rigorous iterative process was required to determine the optimal mechanical actuation/coupling system for each digit, as well as the optimal values for the geometrical parameters of the hand, defined in Section 4.3.2 (on p.54), such as the length of the phalangeal bones, whose value, so far, had been previously set on the basis of observation or the literature. The only parameters which were not optimized were the inclination of the phalangeal joints (i.e., the rotation of the $(i+1)^{th}$ frame about the y_i-axis), which completes the definition of the bone orientation in 3D-space. This is due to the fact that preliminary simulations showed that these parameters negatively impacted the aesthetics of the overall hand, which is another important aspect, as mentioned in the Product Design Specifications in Chapter 3 (on p.44). Other requirements, such as the overall dimensions of the prosthetic hand, must also be taken into consideration during this optimization process.

5.3 SETTING UP A FRAMEWORK FOR THE OPTIMISATION OF THE KINEMATIC HAND STRUCTURE

To guide the fine adjustments of the design, a framework was required to evaluate the performance of each iterative design in achieving natural-looking PMs that allow the KHS to effectively attain the representative set of grasps for the successful execution of daily bimanual activities in addition to some other useful grasps.

Hence, the resulting PMs of each iterative design must not only look natural, but also be able to achieve grasps that constrain the motion of the task objects through the application of reasonable forces and torques at a set of contact points which define the interaction between the hand and the object. Considering a local reference frame defined at the point of contact (with the positive z-axis pointing along the surface normal into the object), the force applied at each contact point, $\vec{f_i}$, can be written as in Equation 5.1 [189]:

$$\vec{f_i} = \vec{f}_{n_i} + \vec{f}_{t_i} \tag{5.1}$$

Where,

- i, refers to one of the contact points that make up the grasp;
- $\vec{f}_{n_i}$, is the vector component along the normal direction with a magnitude of f_z, which is greater than 0, N;
- $\vec{f}_{t_i}$, is the vector component along the surface of the object with a magnitude of f_x and f_y along the x and y direction, respectively, N.

The set $\mathcal{F}_i$ of admissible forces that can be transmitted through a particular contact point depends on the interaction present between the hand and the object, such as the area of surface friction. The types of contact models commonly used in grasp analysis are the following [190], [191]:

- *Frictionless Point Contact*, a contact where only a force along the surface normal can be applied on the object (i.e., $\vec{f}_{t_i} = 0$);

- *Point Contact with Friction* (also known as hard finger model), which is able to transmit a normal force as well as a force along the tangent plane. Using Coulomb's law of friction [192], the admissible set of forces is given by Equation 5.2, which defines the friction cone in Figure 5.1(a)

$$\mathcal{F}_i = \{\vec{f}_i \mid \|\vec{f}_{t_i}\| \leq \mu_s \|\vec{f}_{n_i}\|, \qquad f_z > 0\} \tag{5.2}$$

Where,

- μ_s, is the static coefficient of friction associated with the surface at the point of contact.

However, for computational purposes, a pyramidal, inner approximation of the friction cone is more useful, since the friction cone is defined by a finite set of vectors, as shown in Figure 5.1(b). Hence, for a contact point, i, the friction cone $\mathcal{F}_i$ can be defined by the following set of u forces [189], [193]:

$$\{\vec{f}_{i,1}, \vec{f}_{i,2}, \dots, \vec{f}_{i,u}\} \tag{5.3}$$

such that $\vec{f}_i$ can be written as follows, where $\alpha_{i,j}$ defines the weighting of each of these forces:

$$\vec{f}_i = \sum_{j=1}^{u} \alpha_{i,j}\, \vec{f}_{i,j}, \qquad \sum_{j=1}^{u} \alpha_{i,j} \leq 1, \qquad \alpha_{i,j} \geq 0 \tag{5.4}$$

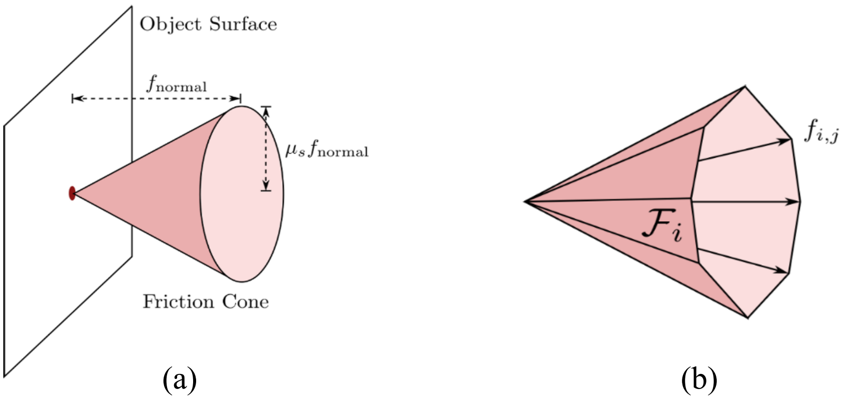

(a) (b)

Figure 5.1: (a) The friction cone associated with a point contact with friction and (b) a pyramidal, inner approximation of the friction cone [189]

- *Soft-finger Contact Model*, in addition to the friction cone present in the previous model, can apply a torque around the normal axis, τ_{normal}, which is also constrained by friction.

In this work, it is expected that while the friction between the hand and the object will be significant, the area of contact will not be large enough for the phalanges to apply a torque. Hence, the contact points were modelled as point contact with friction, where a conservative μ_s of 0.5 was considered since high frictional material, such as rubber, should be utilised for the surface of the prosthetic hand.

The force transmitted through one of these contact points then applies a wrench, $\vec{w}_i$ on the object (i.e., a vector which quantifies the forces and torques applied with respect to a global reference frame fixed on the object, usually the object's centre of mass), which is given by Equation 5.5 [189], [193],

$$\vec{w}_i = \begin{bmatrix} \vec{f}_i \\ \vec{d}_i \times \vec{f}_i \end{bmatrix}, \quad \begin{matrix} \vec{w}_i \in \mathrm{R}^3 \; for \; 2D \; objects \\ \vec{w}_i \in \mathrm{R}^6 \; for \; 3D \; objects \end{matrix} \tag{5.5}$$

where,

- $\vec{d}_i$, is the vector quantifying the position of the i^{th} contact point with respect to the fixed frame, m.

A grasp can then be defined as the combination of all the wrenches applied by each contact point, where the total wrench applied on the object by a grasp of p contact points is given by Equation 5.6,

$$\vec{w} = G \begin{bmatrix} f_1 \\ \vdots \\ f_p \end{bmatrix} \tag{5.6}$$

where,

- G, is the grasp map which defines the linear mapping of $\vec{f}_i$ to the corresponding w_i, together with the transformation from the local-contact reference frame to the object-defined fixed frame.

Using this definition of a grasp, a *grasp wrench space*, W_g, which defines the set of all the possible $\vec{w}$ that can be applied on the object through the admissible forces of each contact point, can be computed. In the case of point contact with friction, the W_g for a grasp with p contact points can be written as shown in Equation 5.7. A simple 2D example of the W_g associated with a grasp consisting of two contact points with friction is shown in Figure 5.2 [189], [193].

$$\begin{gathered} W_g = \{\vec{w} \mid \vec{w} = \sum_{i=1}^{p} \vec{w}_i \,, \qquad \vec{w}_i = \sum_{i=1}^{p} \alpha_{i,j} \, \vec{w}_{i,j} \,, \qquad \vec{w}_{i,j} = \begin{bmatrix} \vec{f}_{i,j} \\ \vec{d}_i \times \vec{f}_{i,j} \end{bmatrix} \\ \sum_{j=1}^{u} \alpha_{i,j} \leq 1, \qquad \alpha_{i,j} \geq 0 \; \} \end{gathered} \tag{5.7}$$

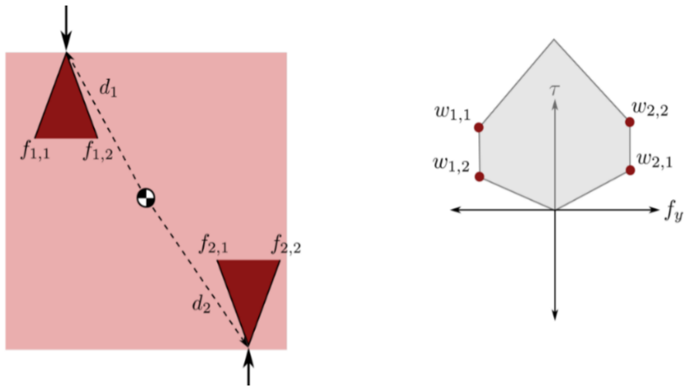

Figure 5.2: The W_g of a simple 2D grasp consisting of two contact points with friction [189]

However, computing all the possible $\vec{w}$ that a grasp can apply on an object can be quite cumbersome. Hence, a more efficient approach for the characterisation of a grasp is the *grasp wrench hull*, W_{gh}, which is similar to W_g, except that it is the convex hull of all the $\vec{w}_{i,j}$, making it easier to compute [189], [193].

A grasp that can maintain every possible disturbance load that might be present is referred to as *grasp closure*. This means that for any $\vec{w}_e$ there exists a set of contact forces, $\{\vec{f}_i\}_{i=1}^{p}$, such that $-\vec{w}_e \in W_{gh}$. However, this assumes that the magnitude of the contact forces can be infinite, which is not reasonable given that the hardware utilised has its limitations. Hence, a more practical definition of grasp closure is that for a n-dimensional vector space, the W_{gh} being based on at least $n+1$ wrenches, n of which are linearly independent. Also, the grasp must also be able to apply a zero wrench even when the contact forces are non-zero. This is equivalent to the origin of the axis being contained inside W_{gh} [189], [193].

There are two types of grasp closure, which are *form closure* and *force closure*, Figure 5.3. Form closure refers to the type of grasp where the object is geometrically constrained in all directions, using frictionless point contact forces. If, on the other hand, only a subset of the possible DOFs are constrained geometrically, the object is

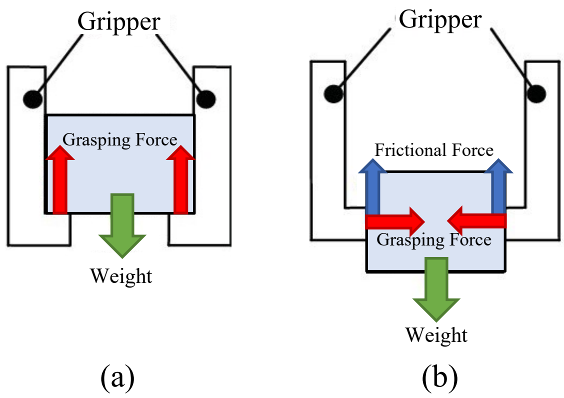

Figure 5.3: (a) Form Closure and (b) Force Closure [193]

said to be grasped with a *partial-form closure*. Form-closure grasps usually occur when the palm and the joint angles of the fingers lock around the object, with no room for any slight movements. Using the definition of grasp closure, for a grasp to provide form closure to a 3D object in six dimensions, at least seven contact points are required. Meanwhile, force closure relies on the force and the friction applied at each contact point to resist $\vec{w}_e$. Therefore, fewer contact points are required, which makes them more common in artificial hands [191], [194].

However, for the artificial hand to achieve force closure, it must be able to control the force applied at each contact point, such that the wrench applied on the object by the grasp, Equation 5.6, is equal to the external disturbance (i.e., knowledge on G and $\vec{w}_e$ is required). Given that these parameters depend on the grasped object and its intended use, it is difficult for the force control system of the prosthetic hand to determine the contact forces required for the different task objects. To overcome this problem, concepts which exploit the postural synergies, such as soft synergies or adaptive synergies [48], [139], have been referred to in the literature, as discussed in Section 2.8.3.5 (on p.37).

However, given the approach used in this work to actuate the different PMs, the grasping force control system was simplified by varying only the force applied by the thumb in the direction of the PM, which is usually in opposition to the other digit. Meanwhile, the other digits are non-backdriveable so that they can provide a reactive force (this implies that the actuators of these two digits do not need to be as powerful as that of the thumb, thus simplifying the mechanical design of the prosthetic hand even further while minimizing power consumption and heat generation). The amputee can then select the force applied by the thumb from four different force levels, namely, no-, low-, medium- and high-force, by varying the intensity with which the muscles are recruited in the forearm; this has been shown to be related to the amplitude of the sEMG signals [9].

The ability of the grasp to constrain a specific object can be characterised and compared to other possible grasps, including grasps attained by a different KHS. In the literature, there are several grasp quality metrics available for different types of artificial hands [195], [196]. These metrics quantify the ability of a grasp to resist external loads for a given bound on the magnitude of the contact forces. Examples of such quality metrics include the volume of the W_{gh} and the maximum wrench that can be resisted. However, given the force control system utilised in this work, it was considered more appropriate to determine whether there exist a set of force vectors $\{\vec{f_i}\}_{i=1}^{p}$, that are able to resist a desired $\vec{w}_e$, while still satisfying the friction-cone constraints in Equation 5.2 (on p. 90) and any other kinematic constraints, C, (e.g., the thumb is in contact with the object at multiple points, and thus, the forces that can be applied at the contact points are a function of each other; this is simplified by defining this function according to their position relative to the active joint), and if so, to optimise their magnitude, if possible, to reduce the demand on the actuation system. This problem can be written as follows [189], [197]:

$$minimize_{\vec{f}_i,\ i\in\{1,\dots p\}}\ J(f_1 \dots f_p) \tag{5.8}$$

Such that

$$\vec{f_i} \in \mathcal{F}_i, \qquad i = 1, \dots, p$$
$$\vec{f_i} \in C, \qquad i = 1, \dots, p$$
$$\vec{w}_e - G[f_1 \dots f_p]^T = 0$$

Assuming the weight of the phalanges is negligible and the joints are frictionless, the torque required at each of the corresponding active joints, $\vec{T}_D$, can be determined using Equation 5.9 [198].

$$\vec{T}_D = \sum J_{C_i}^T . \vec{f_i} , \quad i \in D \tag{5.9}$$

Where,

- $J_{C_i}^T$, is the transpose of the hand Jacobian matrix, which relates the torque required at the active joint of digit D to the i^{th} contact force, with reference to the local-contact frame.
- D, as previously defined, indicates the digit being considered, with T, I, and M referring to the Thumb, the Index and the Middle finger, respectively.

Utilising this approach requires not only knowledge on the position and orientation of the contact forces relative to the object's centre of mass and the active joint, but also information on the $\vec{w}_e$ present during different daily bimanual activities. This work focuses on the ability of the prosthetic hand to execute the representative set of daily bimanual activities listed in Table 4.1 (on p.52), and three additional activities for a more complete force representation (excluding activities which are difficult even for an average person, such as the use of a manual can opener, since specific tools, such as an electric can opener in this example, are usually available for the amputee to use).

These additional activities were opening a hand-tightened jar, opening a can of beverage and cutting food with a knife (even though a knife is not typically held by the left-hand, this would be required for the mirrored version). They were chosen from functional hand assessments, as in [199],[200], and based on the magnitude of the loads that would be expected to be present to execute that particular activity. However, literature on the magnitude of the $\vec{w}_e$ present during these activities was limited. Thus, the magnitude of these loads was determined by a series of experiments discussed in Appendix C (on p.220) [201]. From these experiments, it was observed that the maximum force that the hand would need to apply was around $25N$ when opening a large drawer, and the highest torque was $2.96Nm$ to open a hand-tightened cap with a diameter of $0.072m$. Nevertheless, the set of force vectors required and the corresponding torque at each of the active joints had to be determined for each activity, since they not only depend on the magnitude and direction of the external loads, but also on the prevailing configuration of the fingers.

This could be determined, using software such as Opengrasp [202], Graspit![203] and SynGrasp [204], which are tools commonly used in grasp analysis to predict and visualise the behaviour of a grasp in the face of external disturbances. However, the software chosen must also allow the parameters of the KHS to be varied with ease, while facilitating the actuation of the KHS along the resulting PMs, not only for the grasp analysis, but also for the members of the research team to scrutinise the aesthetics of the PMs, which is possibly somewhat subjective but still an important requirement for the prosthetic hand. For these reasons, a simulation of each candidate KHS grasping the different task objects in Unity (version 2020.2.0b14) [205], which is a game engine commonly used in a variety of fields, such as gaming, augmented reality, animation in the film industry and engineering systems simulations, was preferred. Unity includes a physics engine (Nvidia PhysX [206]) which allows the development of realistic projects, with objects responding correctly to gravity, collisions and forces; it also provides easy access to raw data on the direction and position of the force applied at each contact point relative to both the object's centre of mass and the corresponding active joint. Extensive documentation, resources and an exceptionally large active community are also present; these facilitate the development process when using Unity.

Hence, a model of the kinematic hand architecture, discussed in Section 4.3.2 (on p.54), was first set up in Unity using articulation bodies (i.e., a component that defines the physical behaviour of a body) arranged in a logical tree, in which constrained relative motion takes place between the child and the parent. This facilitates the simulation of objects that involve joints, which is why it is typically used to simulate multi-DOF robotic arms. Currently, four different joint types are supported, namely, fixed, prismatic, revolute and spherical, but for this application, only the revolute and the fixed joints were necessary [207].

Each phalanx was then modelled with a simple cylindrical mesh, while a 3D mesh model of the palm was imported from Inventor. A collider defined the boundary of the phalanges and the palm, which ensured a more realistic collision between the hand itself and the environment, as it prevented the different aspects of the simulation from passing through each other.

Any changes made to the KHS during the iterative process could be implemented automatically via two C# scripts (a program written in C# that allows the user to trigger game events, respond to user input and modify the properties of the objects over time) that run before the start of the simulation. These scripts modify the parameters in the simulation that define the physical length, position and orientation of each phalanx, as well as the allowable motion relative to the parent body according to the values inputted by the user for each of these optimised parameters, as shown in Figure 5.4.

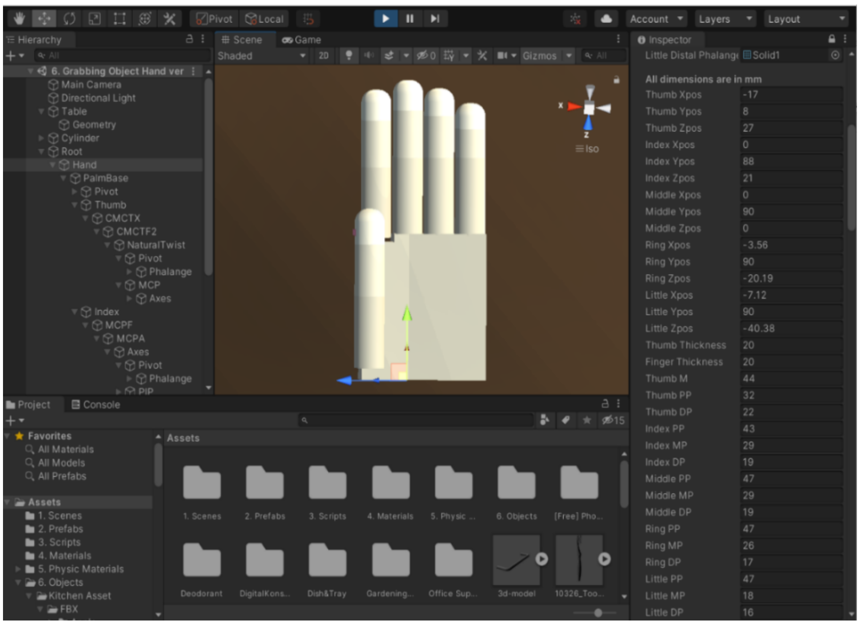

Figure 5.4: The graphical user interface which allows the user to vary the different design parameters of the hand with ease.

The resulting PMs could then be invoked by the user through several keyboard commands, where each command was associated with a specific proto-grasp. This was achieved through another script that ran in the background, where in each frame, the position of the phalanges was updated according to the user input and the current joint angles, such that all joints would reach their final position at the same time. However, if during this motion, a model of an everyday object (which can be either imported from Unity Asset Store [208], a library of different objects that one can use in one's project, or approximated using basic 3D shapes available in Unity) was present within the hand workspace, the digit(s) whose movement was first constrained would be stopped, while allowing the PM to continue operating through the remaining free joints. This exploits the independent actuation of each digit to introduce a limited form of compliance in the active digits without any complex sub-systems.

The ability of the resulting grasp to constrain the motion of the object, either through partial form closure or force closure, was then determined using a static force analysis, since the friction model used by Nvidia PhysX did not necessarily present a close approximation of real-world physics as it is tuned for the stability and the performance of the simulation [206]. This involved solving Equation 5.8 (on p.94) for each activity to determine whether there exists $\{\vec{f}_i\}_{i=1}^{p}$ that is able to resist the $\vec{w}_e$ corresponding to that activity, while taking into consideration additional support from the environment and the intact hand (i.e., neglecting the resultant load in certain directions since the environment or the intact hand will be able to counteract such loads, as long as they are reasonable), as well as a SF of 1.5, as discussed in Chapter 3 (on p.44).

For this reason, information on the number of contact points, and the position and direction of the contact forces relative to both the centre of mass of the object and the corresponding active joint, was extracted from Unity. This meant that the computation of the G and the J_C to determine the grasping forces and the torques required at the corresponding active joints was not necessary, as they were taken care of by Unity. In the case of force closure, the allowable friction present between the hand and the object had to be also taken into consideration. However, due to the force control system adopted in this work, the admissible forces at each of the contact points could not be

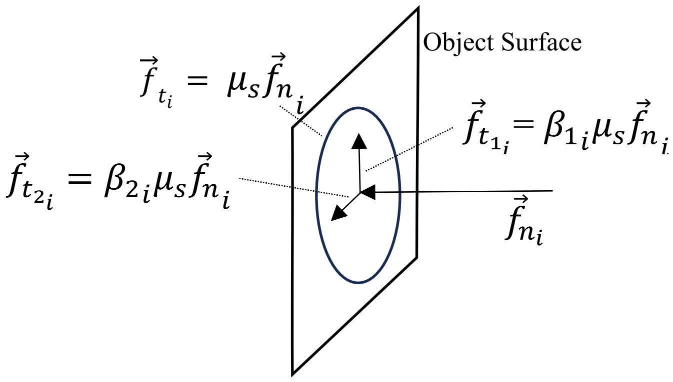

Figure 5.5: The frictional model used in this work

approximated using Equation 5.4 (on p.90), since the normal force applied by the fingers is a function of the thumb. Instead, the normal component, $\vec{f}_{n_i}$, and the frictional component, $\vec{f}_{t_i}$, were considered separately, where $\vec{f}_{t_i}$ was resolved along two perpendicular axes that lie on a plane tangent to the normal, $\vec{f}_{t_{1_i}}$ and $\vec{f}_{t_{2_i}}$, as shown in Figure 5.5. The magnitude of $\vec{f}_{t_{1_i}}$ and $\vec{f}_{t_{2_i}}$ was then determined by scaling the maximum allowable friction present between the hand and the object given by Equation 5.2 (on p.88), such that the condition in Equation 5.10 is satisfied

$$\sqrt{\beta_{1_i}^2 + \beta_{2_i}^2} \leq 1, \; |\beta_{1_i}| \leq 1 \; \& \; |\beta_{2_i}| \leq 1 \tag{5.10}$$

where,

- β_{1_i}, β_{2_i} are the frictional weightings for $\vec{f}_{t_{1_i}}$ and $\vec{f}_{t_{2_i}}$, respectively.

The frictional weights of each contact point can be varied to determine whether there exists $\{\vec{f}_i\}_{i=1}^{p}$ that can resist $\vec{w}_e$, and if so, their optimal value, such that the maximum force applied by the contact points is reduced as much as possible.

This necessitates the use of an optimization tool to determine the optimal solution. Optimization tools are algorithms used to determine the set of inputs that maximises or minimizes the objective function based on a set of constraints. There are several optimization tools available that can solve from simple, linear problems to more complex, problems with multiple objectives. In this case, the problem which is defined in Equation 5.8 (on p.93) is smooth but nonlinear due to the nature of the frictional force that can be applied at each of the contact points. Example of smooth nonlinear optimization tools are Sequential Quadratic Programming and Generalised Reduced Gradient (GRG) [209]. These tools usually exploit information obtained from first and/or second-order derivatives carried out at various trial solutions to follow the curvature of the problem as well as its direction. This is repeated until there is no improvement in the solution. The GRG nonlinear tool was chosen for this project since it is available in Microsoft Excel which facilitates the computation of the objective function. However, if the problem is non-convex, GRG nonlinear can only find the local minimum that is closest to the starting point.

Therefore, to see if a better solution could be found, the solution obtained from GRG nonlinear served as the initial solution for the evolutionary algorithm [210] which is available in Microsoft Excel. This is because the evolutionary algorithm is not as susceptible to local minima as the GRG nonlinear since it does not rely on information from the derivative of the objective function to determine the optimal solution but rather utilises several Genetic Algorithms (GA) and local search methods. Evolutionary algorithms are based on the idea of natural selection, where mutations of the optimal solution from a random population are used to create offspring (also known as chromosomes) for the next generation, while taking into consideration the constraints imposed by the user on all the parameters. This is repeated until there is no improvement in the objective function from one population to the next during a defined period of time. The process can be time-consuming, but parameters such as the mutation rate (i.e., the frequency of the population that will be altered to create a new solution) and the population size (i.e., the number of solutions the algorithm considers at any given time) can be varied to limit its duration. However, these parameters might negatively impact the algorithm if they are not carefully adjusted, since changing the mutation rate significantly may lead to a random search, while a small population size limits the search space available [211]. The solution from the Evolutionary algorithm was fed back to the GRG nonlinear. This was repeated several times until there was no change in the initial solution, which confirms that the problem has converged.

Meanwhile, $\overrightarrow{T_D}$ required at each of the active joints can be determined using Equation 5.11.

$$\overrightarrow{T_D} = \sum \vec{d}_{c_i} \times \vec{F}_{c_i}, \; i \in D \tag{5.11}$$

Where,

- $\vec{F}_{c_i}$, refers to the contact-force vector corresponding to one of the phalanges of the digit, D, in terms of the coordinate system of the active joint, which was obtained from Unity, N;
- $\vec{d}_{c_i}$, is the positional vector between the active joint of digit, D, and the contact force, $\vec{F}_{c_i}$, in terms of the coordinate axes of the active joint, which was also obtained from Unity, m.

In the case of the fingers, the components of $\overrightarrow{T_D}$ along the primary axes of the joint coordinate system indicate the torque that must be sustained along each direction, with T_{D_z} (i.e., the component of $\overrightarrow{T_D}$ in the z-axis) supported by the actuation/transmission system, and the components in the other directions supported by the structure. For the thumb, the motor will need to provide sufficient torque, $\overrightarrow{T_{m_T}}$, to actively achieve the required contact forces applied by the corresponding phalanges. Hence, the minimum required magnitude for $\overrightarrow{T_{m_T}}$ is the magnitude that can provide the required torque $\overrightarrow{T_T}$

(i.e., the $\overrightarrow{T_D}$ calculated using Equation 5.11 for the thumb), when resolved along the direction of this torque and two other perpendicular directions, Figure 5.6. The torque applied along the latter two directions, $\overrightarrow{T_s}$, are "unnecessary" torques that are being applied at the thumb CMC joint against the structure of the finger, reducing the efficiency of the motor.

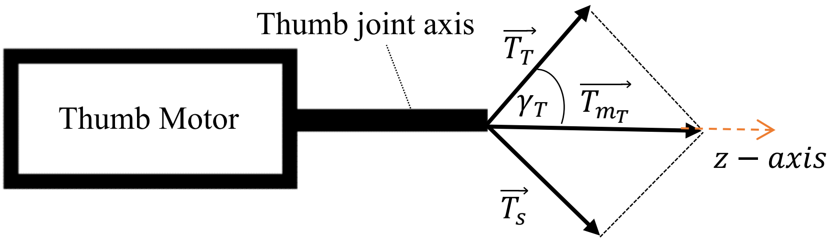

Figure 5.6: A 2D analogy of how the magnitude required for $\overrightarrow{T_{m_T}}$ was determined

The required magnitude of $\overrightarrow{T_{m_T}}$ was determined by first calculating the angle between $\vec{n}_{m_T}$ and $\vec{n}_T$ (i.e., the unit vectors of $\overrightarrow{T_{m_T}}$ and $\overrightarrow{T_T}$), γ_T, which was found using the cosine rule, Equation 5.12, where the unit vector of $\overrightarrow{T_{m_T}}$ acts along the z-axis:

This angle was then substituted in Equation 5.13.

$$cos\gamma_T = \vec{n}_T . \vec{n}_{m_T} = \frac{T_{T_z}}{\left\|\overrightarrow{T_T}\right\|} \quad 5.12$$

$$\left\|\overrightarrow{T_{m_T}}\right\| = \frac{\left\|\overrightarrow{T_T}\right\|}{cos\gamma_T} \quad 5.13$$

A typical example of this analysis can be found in Appendix D (on p.231). Using this framework, the parameters of the KHS can be optimised in a systematic manner.

5.4 OPTIMIZATION OF THE ARCHITECTURE AND THE GEOMETRIC PARAMETERS OF THE KINEMATIC HAND STRUCTURE

Building on the valuable insights gathered from the Unity framework regarding the functionality and aesthetic of a KHS, this section delves into the intricacies of the iterative process employed to optimize both the architecture and geometric parameters of the prosthetic hand.

5.4.1 Simplification of the Architecture of the Kinematic Hand Structure

In the approach taken in this work, the simplification of the KHS involves the optimisation of the mechanical architecture of each active digit to best utilise the three actuators while taking into consideration the simplicity of the design, as well as the aesthetics of the hand movements/grasps.

In this optimisation procedure, each of the nine joints were defined as one of three types: actuated; coupled to another DOF; or fixed at a specific angle. In the case of coupling one-DOF joints (e.g., the PIP and the DIP joints), the relationship between the position of the coupled joint (CJ) and of the driving joint (DJ) is given by Equation 5.14.

$$CJ = [DJ * CR] - FA \qquad 5.14$$

Where,

- CR, is the coupling ratio.
- FA, is a fixed angle, °.

Meanwhile, the coupling of two-DOF joints (i.e., the thumb CMC joint and the index MCP joint, which are both located at the proximal end) can be obtained by optimizing the D-H parameter, α_{D_2}, of the corresponding digit; this was first mentioned in Section 4.3.2 (on p.54). The axis of rotation of the motor can then be either perpendicular to the proximal phalanx (i.e., θ_{D_3} is fixed, while θ_{D_4} is actuated), Figure 5.7(a), or at an angle to the proximal phalange (i.e., θ_{D_3} is actuated, while θ_{D_4} is fixed), Figure 5.7(b). The resulting position of the proximal phalanx in 3D space can be expressed in terms of the original joints angles as shown in Appendix E (on p.236).

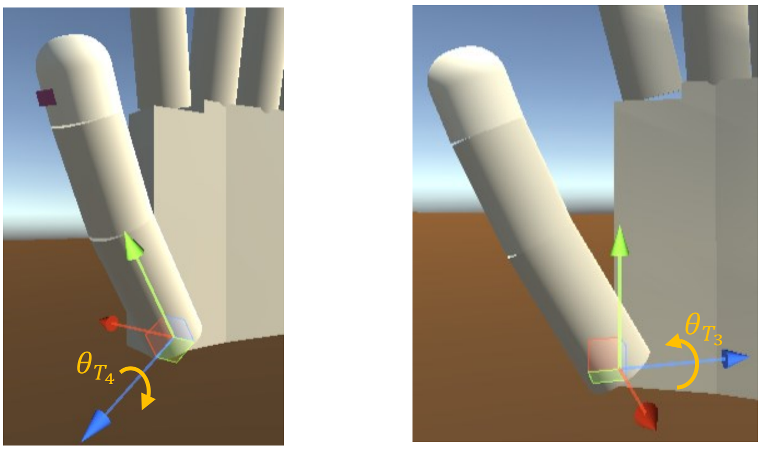

(a) (b)

Figure 5.7: The different coupling methods considered for two DOF joints, taking the thumb CMC joint as an example, where the blue line indicates the axis of rotation of the motor (note: Unity uses a left-hand coordinate system)

Given that each finger will only be actuated by one motor, one of the proximal DOFs should be actuated to keep the centre of mass of the prosthetic hand towards the wrist. Meanwhile, the other joints should be fixed, wherever possible, for a simple design. Otherwise, the joint should be coupled to the previous actuated joint, ideally the DOF parallel to it, to keep the complexity of the design to a minimum by avoiding linkages across the different joints/digits.

The resulting proto-grasps can then be expressed in terms of the nine PCs chosen in Section 4.6 (on p.84), using Equation 2.1 (on p. 32). However, a consequence of reducing the number of motors (from the theoretical nine, to three) and coupling or fixing some of the joints is that the proto-grasps, as well as the neutral position, would shift in the 9D PC space, as illustrated in Figure 5.8. As a result, the directions of the new PMs would vary from the original directions, affecting the ROM of each of the joint angles.

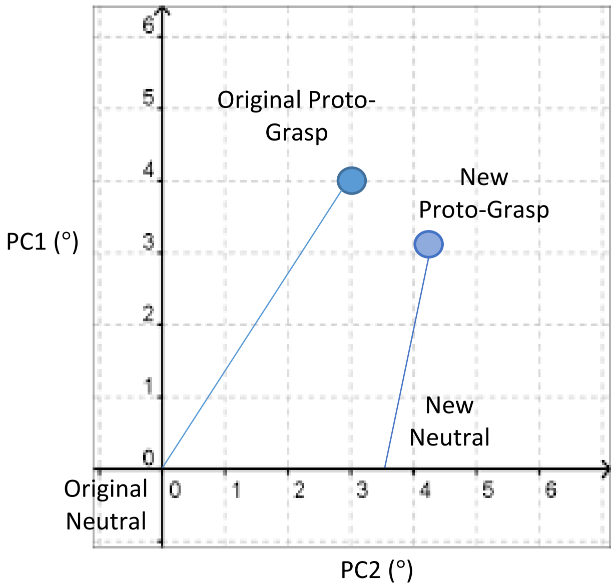

Figure 5.8: A simplification of the effect that reducing the number of motors, and coupling or fixing some of the joints has on the proto-gestures

The difference between the original and the new proto-grasps can be measured by the *Shift of the Proto-Grasps* (SPG), in °, which is calculated through the weighted average of the following objectives:

- *Similarity of the proto-grasps, (°)*: This measures the similarity between the original proto-grasps and the new ones. It is quantified by computing the average of the angles between the original six proto-grasps and the corresponding new ones, from the new neutral. Equal weighting was given to all six proto-grasps to increase the probability that the B-grasp can still be attained during the execution of day-to-day activities.
- *Similarity of the direction (°)*: This measures the similarity in the ROM of the joints when moving from one grasp to another. It is quantified by averaging the angle difference between the vector from the original neutral point to the original grasp point in the 9D space, and between the vector from the new neutral point to the corresponding new grasp point. Although the PMs start from the open hand position, it was the neutral position that was considered as the reference point, since

the six vectors of the proto-grasps relative to the neutral position were found to be more distinct than the corresponding ones from the open hand position. This ensures a better representation of the ROM of the different joints.

- *Similarity of the PCs (°)*: This measures the angle between the new proto-grasps and the corresponding PCs. This aspect of the measurement was included to give greater weight to solutions which are closer to the PCs in order to promote more distinct proto-grasps and proto-motions.

In weighting the above three measurements, priority was given to the first two objectives, with an equal weight of 0.4, while the third one was given a weighting of 0.2.

For the optimal mechanical joint couplings/fixed angles, the SPG should be reduced as much as possible to achieve a three-motor hand that can attain with high similarity the proto-grasps and the corresponding motions of the original PMs. The SPG is non-linear, and thus, the Evolutionary algorithm and the GRG Nonlinear method in Microsoft Excel, which were discussed in the previous section, were used to determine the optimal solution for multiple configurations of the KHS.

However, the SPG function takes into consideration neither the *aesthetics* of the hand (i.e., how natural it looks and if the resulting new proto-grasps resemble in any way the original ones, since Microsoft Excel simply views the grasps as points in 9D space) nor the *simplicity* of the design (e.g., a fixed joint is better than a coupled joint in this regard), which are also important for the KHS. Hence, for each configuration considered, the members of the research team scrutinised the aesthetics of the new PMs in Unity. Unless the PMs looked completely unnatural (e.g., the index PIP joint is fixed at a certain angle), an attempt was made to improve the results obtained, where the constraints imposed on each of the parameters were modified as necessary, taking also into account the ability of the KHS to execute the bimanual activities considered in this work. For example, it was noted that the FA parameters, which characterised the coupling of the PIP joints of the index and the MRL finger to the corresponding MCP joint, were preventing the PIP joint from fully opening in the resulting O-grasp. This limited its usage in applications requiring non-prehensile grasps. Thus, a constraint on the FA parameter was introduced, which limited the MCP joint to an angle less than 20°, for when the PIP joint has reached its minimum limit so that the resulting O-grasp can still be considered acceptable for an open hand. On the other hand, even though the fingers were not necessarily closed in the original C-grasp, the versatility of the grasp would increase if the distance between the fingertips and the palm were to be minimised, as it would allow smaller objects (e.g., a toothbrush and a fork) to be grasped between the fingers and the palm. Hence, the constraints of CR and FA were adjusted accordingly.

During the fine-tuning process, the other parameters of the KHS modelled in Unity, which also play a crucial role in the aesthetics and the functionality of the hand, were continuously being updated on the basis of the optimisation process discussed in the next section.

5.4.2 Optimization of the Geometrical Parameters of the Kinematic Hand Structure

Thirty-one other kinematic parameters of this three-motor hand, including the dimensions of the phalanges, the nature of the DIP joints, and the exact positions and orientations of the different joints still had to be optimised, while taking into consideration the size of the prosthetic hand required, referred to in Chapter 3 (on p.44).

Anthropomorphic data of different populations, such as [212], [213], can be utilised to determine the optimal value of some of these parameters. However, apart from the fact that these studies tend to not include some of the required parameters (e.g., parameters which are more difficult to measure, such as the position of the thumb CMC joint and the twist of the different phalanges), this approach focuses mainly on the aesthetics of the prosthetic hand, rather than its overall performance. Thus, to maximise the space in the palm for the mechanical system and ensure a natural look relative to the overall height of the prosthetic hand, the anthropomorphic data in [147], [214] were used to determine the height of the palm (i.e., l_{M_x}), and consequently the length of the MRL finger. Meanwhile, a more systematic approach that can also evaluate the performance of the prosthetic hand was required to optimise the remaining parameters.

As discussed in Section 5.3 (on p.89), the performance of a prosthetic hand can be characterized by using grasp quality metrics. However, this requires initial grasp parameters, such as the geometry of the fingers, the shape of the object and the placement of the contact points, to be specified, which in turn limits its ability to act as a performance index. For this reason, Mouri et al. [215], who recognised the importance of thumb opposition to the other digits for the dexterity of the human hand, proposed the performance index: ‘opposability of thumb’. This performance index evaluates the grasping ability of a hand in terms of the workspace intersection volume between the thumb and each of the fingers, using only its kinematic structure, so that other important factors such as fingertip shape and material can be determined at a later stage. However, You et al. [216], [217] noted that parameters related to the fingers, such as their lengths, were not included in the performance index, which led to artificial hands with odd shapes, since the opposability of the thumb could be increased by simply increasing the length of the fingers. Hence, You et al. [216], [217] developed this idea even further, and proposed the Interactivity of Fingers (IF).

The performance index IF quantifies the capabilities of the artificial hand for multi-fingered precision grasping. The authors observed that the strategy used by the human hand for precision grip (i.e., two- or three-finger precision grips, typically used to manipulate objects in 3D space) is not based only on the performance of the thumb, but also on the interaction capability of each finger, including the thumb. In this light, this performance index quantifies the dexterity of the hand based on the workspace intersection volume between the thumb fingertip and each of the other fingertips, and the workspace intersection volume between the thumb fingertip and two neighbouring, alternative fingertips, Figure 5.9.

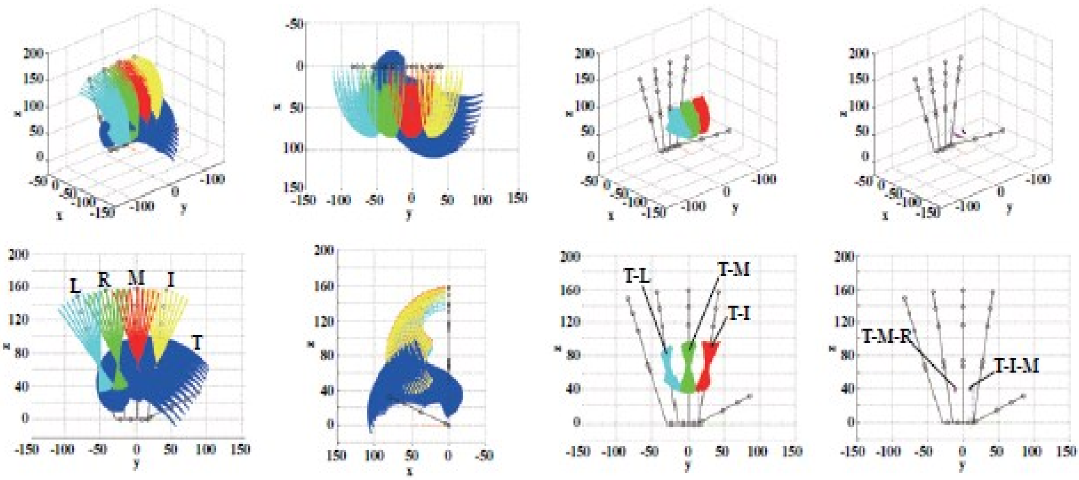

Figure 5.9: Workspace and Workspace intersection area of a mathematical model of a robotic hand [217]

The interaction between the digits, in particular, the thumb and the index, is essential in this work, since this three-motor hand must be able to achieve the S-grasp and the P-grasp. Thus, although the motion of the joints in the performance index is not constrained to occur in synergy, as in this application, the IF provides a good foundation for the optimisation of the parameters of the KHS, especially if it is slightly modified to take into consideration the overall function and appearance of the MRL finger (i.e., a distinction is made between the digits and the active digits). The modified

IF is defined as follows:

$$IF = \frac{\sum_{m_d=1}^{n_d-1} w_{m_d} h_{m_d}}{(N_a - 1)\theta_{total} L_t^2 L_f^2} \left(\sum_{m_d=1}^{n_d-1} w_{m_d} v_{m_d} + k \sum_{m_d=2}^{n_d-1} w_1 w_{m_d} v_{1m_d} \right) \quad 5.15$$

Where,

- m_d, can have a value from 1 to 4, representing the four fingers, from the index to the little finger.
- N_a, is the number of active digits, which will be three for this three-motor hand.
- n_d, is the number of digits, which in this case will be five.
- w_{m_d}, is a weighting factor which reflects the importance of each finger in the robot hand. You et al. [217] used the weighting factors 1, 1, 0.5 and 0.5 for the index, middle, ring and little finger, respectively. This weighting scheme was also adopted for this project since the thumb-index-middle fingers are primarily used for precision grasping. In fact, these three fingers were considered the most important fingers for the minimal anthropomorphic hand described in [8].
- h_{m_d}, is the distance between the position of the MCP of the m_d^{th} finger and the base of the thumb, mm.
- L_t, is the length of the thumb, mm.
- L_f, is the length of the fingers, mm. If the lengths of the four fingers (i.e., index to little) are different, the average value can be used for L_f.
- θ_{total}, is the sum of the ROM of all joints, °.
- v_{m_d}, is the volume of intersection between the workspace of the thumb fingertip and the fingertip of the m_d^{th} finger, mm^3.
- v_{1m_d}, is the volume of intersection between the thumb and index fingertips and each of the other fingertips, so as to maximise the functionality of the MRL finger, mm^3.
- k, is the compensation coefficient that keeps the effect of v_{m_d} and v_{1m_d} balanced; this was set to 3, and was based on the You et al. [217] recommendation.

The intersection volumes, v_{m_d} and v_{1m_d}, were calculated in Matlab [218] using the procedure described in Figure 5.10.

In this procedure, the forward kinematics of each digit, with joint angles ranging from the minimum to the maximum ROM in increments of Δθ, were used to collect the fingertip points of the thumb, p_t, and the other fingers, p_{m_d}. Depending on the DOA

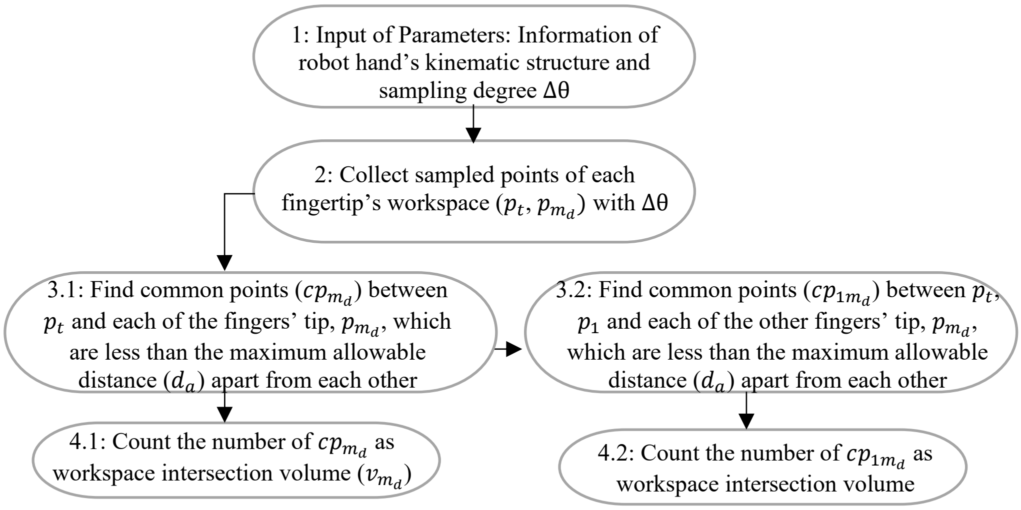

Figure 5.10: The procedure used to calculate the workspace intersection volumes, where the meaning of the parameter symbols is given in the text (adapted from [217])

and the value of Δθ, the calculation of the IF index might be time consuming due to the extensive number of points that the program would need to go through. As a compromise, You et al. suggest that Δθ is set to 5° and that the blanks in the workspace intersection volumes are filled in, using triangular pyramids. However, this was not considered necessary for this work since the developed KHS only has three DOAs, and thus, setting Δθ to 1° does not generate a significant number of points.

The next step involved finding the points where the artificial hand could attain two-finger pinch (cp_{m_d}) and three-finger pinch (cp_{1m_d}), by finding two or three sampled points from the different fingers involved in the pinch that were less than the maximum allowable distance away from each other, d_a. However, when You et al. suggest that d_a is set to $1mm$, the precision grips are limited to hand configurations where the two or three fingers involved must all be touching at the centre of each fingertip. On the other hand, precision grips where a fingertip is touching the side of the other digits can be just as useful, especially for KHS with low DOA, where the workspace of each digit is limited. Thus, d_a was increased to $15mm$, slightly smaller than the required thickness of the digits specified in Chapter 3 (on p.44), which was $20mm$. Each point was then considered as a $1mm^3$ volume, even if the fingertip points were slightly further away from each other, since it indicates the number of points where two- or three-pinch grasps can be achieved.

On the basis of this performance index, the geometric parameters of the hand model were then optimised, using the GA [219] available in Matlab, as recommended by the authors of this index. The idea of the GA is the same as the one implemented in Excel, but the approach used in Matlab is slightly different. In this approach, Matlab starts with a random initial population of size, Np, where crossovers between the different chromosomes and mutations take place to generate offspring for the next population. This process is governed by the following parameters, as discussed in Appendix F (on p.237) [220], [221]:

- Probability of Crossover, Pc – The probability that two chromosomes are combined, with 100% meaning that all the offspring are obtained by crossover;
- Distribution index for crossover, $etac$ – A non-negative number that governs the crossover between two chromosomes, with a higher value allowing the offspring to be closer to the parent chromosomes;
- Probability of Mutation, Pm – The probability that a chromosome is mutated, where 100% indicates that all the chromosomes in a generation are mutated;
- Distribution index for mutation, $etam$ – A non-negative number that governs the mutation of a chromosome, with a higher value resulting in an offspring further away from the parent.

This is repeated for a number of iterations before the GA algorithm is terminated. The solution with the highest IF is chosen as the optimal solution, but whether the result obtained is the optimal or near-optimal one depends on the GA parameters, since they can positively or negatively influence the results of the algorithm. Hence, the GA was run multiple times, each time varying the Pc, the $etac$, the Pm, and the $etam$ in a systematic manner while keeping Np and the number of iterations fixed. Each time the optimal solution of the previous run was included in the initial population of the next run. This was repeated until the change in the optimal solution was minimal, which confirms that the solution has converged.

The values that the GA could assign to each variable were limited to predetermined ranges so as to increase the performance of the prosthetic hand while ensuring that it is aesthetically pleasing, both in its stationary poses and in its motion. To determine these ranges, after each GA run, Unity was used to examine the ability of the resulting KHS to execute the bimanual activities considered in this work, as well as to scrutinise the aesthetics of the resulting grasps and PM. The limits of the variables were then adjusted accordingly, taking the anthropomorphic data in [147], [214] as reference. For example, the limits ensured that the proportions of the proximal and the middle phalanges relative to the distal phalanx were similar to the ones observed in [214]. This affected not only the aesthetics of the hand, but also the ability of the fingers to wrap around objects of various sizes successfully. Meanwhile, the height difference between the MCP joint of the index and the MRL finger was limited, as otherwise it would not be very natural and would affect the functionality of the hand when closed. The limits were also adjusted to avoid unwanted interactions between the fingers, such as overlap between the index and the MRL finger when in the C-grasp position. In certain cases, this type of interaction could not be avoided by simply adjusting the limits, so the KHS had to be adjusted (e.g., coupling one of the joints) and re-optimised accordingly, as discussed in the previous section.

However, regardless of the values of the parameters, the MRL finger did not intersect with the thumb. For this reason, MRL parameters, such as the nature of the DIP joint and the ratios of the different phalanges with respect to the distal phalanx, were based on those of the index finger, except for the lengths of the proximal phalanges of the ring and little fingers, which were constrained to equal that of the middle finger due to the shared MCP and PIP joints of these two minor fingers with the middle finger. Meanwhile, the other parameters of the MRL finger, such as the orientation of the MCP/PIP joint and the overall lengths of the ring and little fingers, were optimised along those of the other digits on the basis of the aesthetics of the proto-grasps and the PMs, as well as the hand configurations when grasping different objects in Unity.

5.5 THE OPTIMAL PARAMETERS FOR THE SIMPLIFIED KINEMATIC HAND STRUCTURE

Several KHSs with different geometrical parameters were considered during the iterative process discussed in the previous two sections. The simplest KHS, with natural-looking proto-grasps and PMs in Unity, and which had the potential to successfully grasp different everyday objects in an aesthetically acceptable manner, was chosen.

Different configurations with one DOA were considered for the thumb. The impact that each configuration had on the SPG while actuating the joints of the other digits was relatively similar, as can be seen in Figure 5.11. The configuration most suitable for the thumb was then chosen based on its mechanical simplicity, aesthetics and functionality when the configuration of the other digits, as well as the geometric parameters were optimised. The configuration that was finally chosen through this exercise is relatively simple, with the two DOFs of the thumb CMC joint actuated by one motor, whose axis of rotation is re-oriented in 3D space, perpendicular to the proximal phalanx, as shown in Figure 5.7(a) (on p.101), whilst both the MCP and IP joints are fixed.

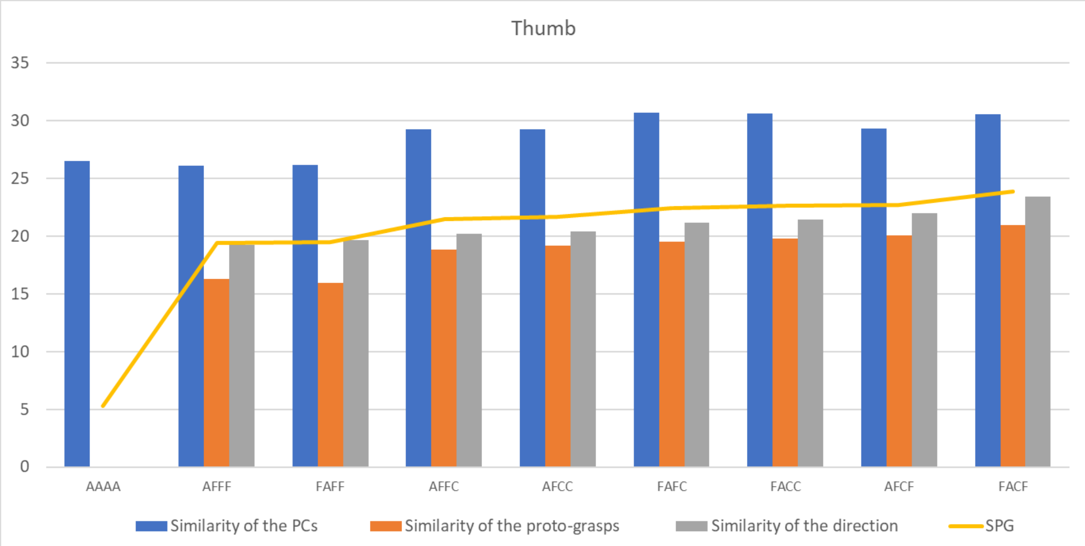

Error! Reference source not found.: The SPG and its breakdown for different thumb c onfigurations with one DOA; where A, C and F indicate that the joint is actuated, coupled or fixed, respectively, with the order from left to right referring to the two DOF of the CMC joint and the one DOF of both the MCP and IP joint.

Despite the mechanical simplicity of this configuration, the thumb can move in and out of the path of the index finger, making it possible for the thumb to make contact with the index finger at two distinct positions, which are required for the P-grasp and the S-grasp, while still maintaining an anthropomorphic look. Alternatively, the same effect could have been obtained by an equally simple configuration, in which the two DOFs of the thumb CMC joint are coupled as shown in Figure 5.7(b). However, in the previous case, the twist of the thumb as it was moving within Unity appeared more natural, which is why it was preferred. The ROM of the thumb was then extended at both ends, so long as the end grasps remained natural, in order to increase the workspace of the hand. This meant that larger objects, such as a two-litre water bottle, could be grasped by the hand; it also ensured that when the thumb is in the ADD position, an object can lie flat against the palm, allowing for a better contact between the object and the hand.

In the case of the index and the MRL finger, the impact on the SPG for different possible configurations with one DOA while actuating the joints of the other digits, is shown in Figure 5.12 and Figure 5.13. A significant difference in the SPG was observed between the two possible configurations for the MRL finger. Meanwhile, the effect on the SPG was relatively similar for the index finger. After scrutinizing the aesthetics of the hand when in motion and stationary, the configuration that was found to be the most suitable for both the index and the MRL finger is the PIP joint coupled to the actuated MCP joint, while the DIP joint is fixed at a specific angle.

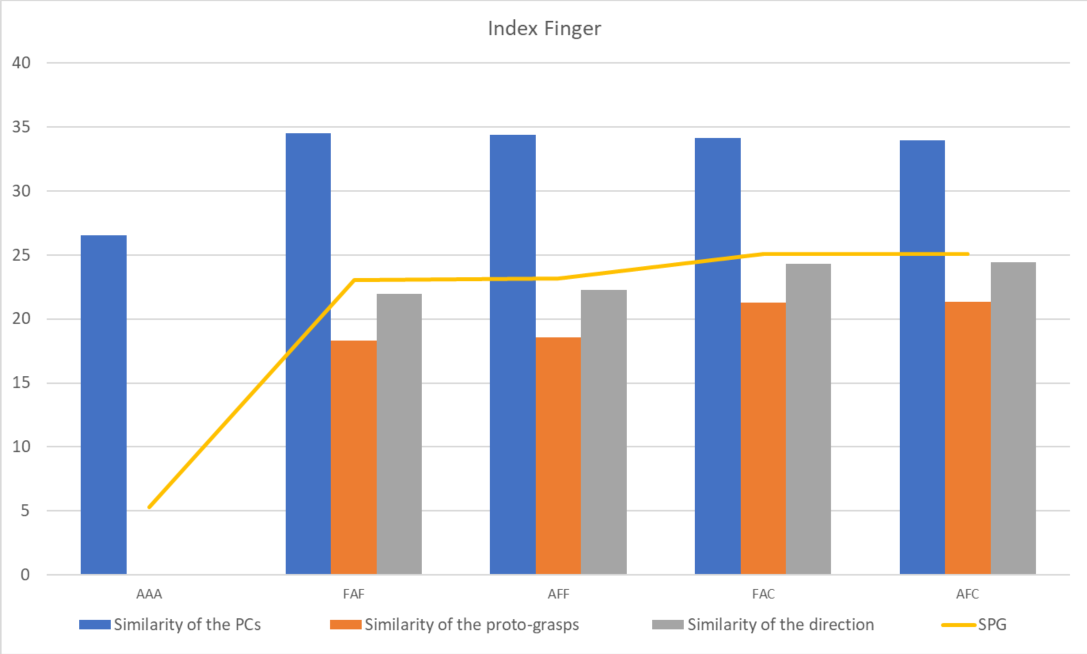

Figure 5.11: The SPG and its breakdown for different configurations with one DOA for the index finger; where A, C and F indicate that the joint is actuated, coupled or fixed, respectively, with the order from left to right referring to the two DOFs of the MCP joint and the one DOF of the PIP joint.

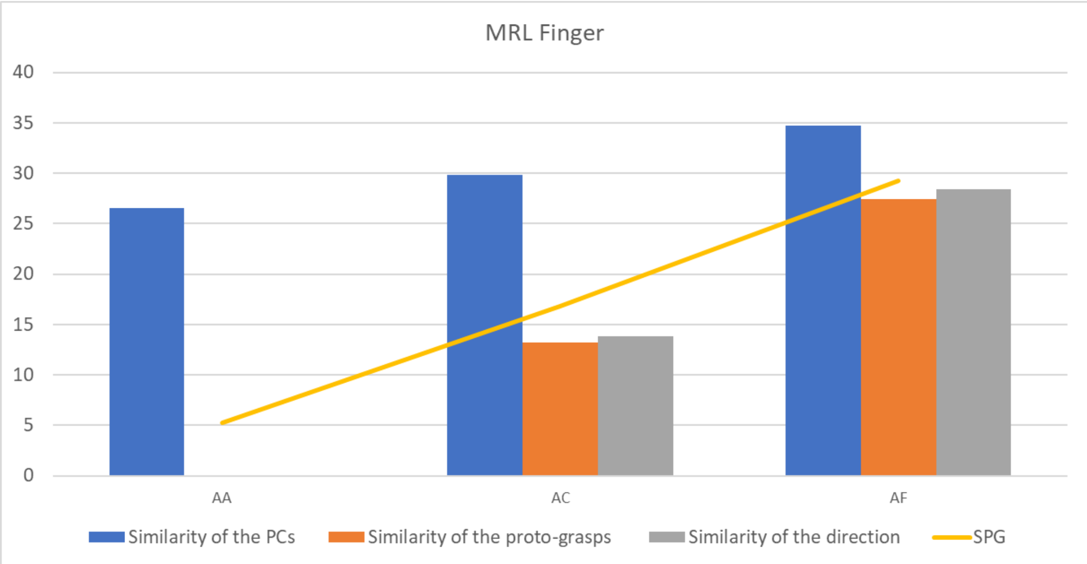

Figure 5.12: The SPG and its breakdown for different configurations with one DOA for the MRL finger; where A, C and F indicate that the joint is actuated, coupled or fixed, respectively, with the order from left to right referring to the one DOF of the MCP joint since the ADD/ABD angle was assumed to be zero and the one DOF of the PIP joint.

For the actuation of the MCP joints, several configurations were considered, as this significantly affected the aesthetics and the functionality of the hand. In the case of the MRL finger, the α_{M_2} parameter was slightly increased even though this was originally modelled as 0°. This caused the little finger to protrude slightly in the palmar direction,

Figure 5.14 and gave the palm a slightly raised edge that can provide grasped objects with added support; this is similar to the movement created by the limit mobility of the fourth and fifth CMC joints, which were not included in this work. An attempt was also made to include the misalignment in the MCP joints of the three fingers in the MRL digit by giving the motor a slight inclination, as shown in Figure 5.7(a) (on p.101), even if the ADD/ABD angle was originally set to 0°. However, this parameter remained unchanged due to the resulting motion of the MRL finger, where the little finger would usually be the one to first touch the object, which then constrained the motion of the other fingers.

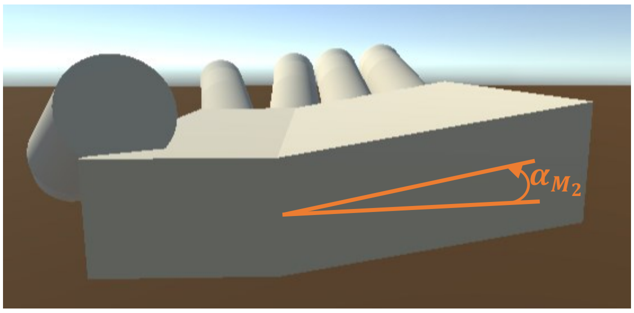

Figure 5.13: The effect varying α_{M_2} has on the orientation of the MRL finger

For the orientation of the index motor, both configurations shown in Figure 5.7 were considered, where the axis of rotation was mainly in the direction of the FLEX/EXT of the MCP joint. On one hand, the configuration in Figure 5.7(a) could facilitate the coupling of the PIP joint, since the axes of rotation of both joints were parallel, but the resulting motion was similar to that of the thumb, with the distal phalanx remaining at an angle to that of the MRL finger, as shown in Figure 5.15(a). Meanwhile, the ADD/ABD angle in Figure 5.7(b) was almost constant, which, depending on its angle, enabled the index finger to move in the direction of the thumb. However, it created an unnatural gap between the index and the MRL finger when the hand was closed, as shown in Figure 5.15(b). Thus, while for both configurations contact between the index finger and the thumb was possible, especially if some of the limits of geometrical parameters were modified (e.g., allowing the thumb to be placed closer to the centre of the palm), this was done at the expense of the aesthetics and/or functionality of the overall hand.

However, after further optimisation and manual fine-tuning, the configuration in Figure 5.7(a) was modified, where the PIP joint of the index finger was rotated, relative to the MCP joint, in the direction of the thumb. Even though this slightly increased the complexity of the coupling system, as the PIP joint was no longer aligned with the

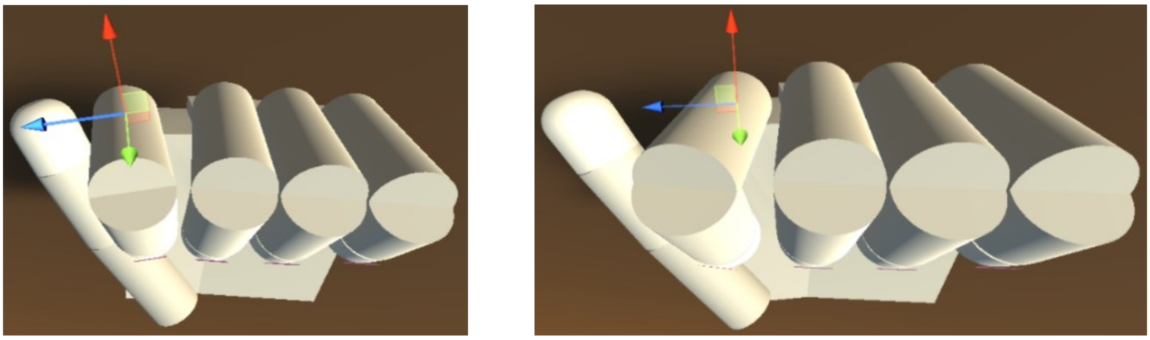

(a) (b)

Figure 5.14: Difference in the closed-hand position for the two configurations considered for the index MCP joint

MCP joint, it allowed a more natural interaction between the different fingers and improved the overall functionality of the hand. In fact, a consequence of these modifications was that the middle phalanx of the index finger exhibited a slight rotation towards the MRL finger as it closed, thus, allowing the thumb to be placed further away from the centre of the palm. This increased the FLEX angle of the thumb in the open hand position, and limited the interference between the thumb and the index finger when grasping smaller objects (e.g. a toothbrush) with a power grasp, while still being able to achieve natural-looking proto-grasps. An improvement in the overall functionality of the hand was also observed after modifying the coupling parameters of the MRL finger to equal those of the index finger; this also simplified the overall design of the hand.

Hence, the D-H parameters, (discussed in Section 4.3.2 (on p.54)), for a simplified, yet aesthetically pleasing KHS that can achieve a set of grasping motions relevant for a medium-sized, left, non-dominant prosthetic hand, were determined as shown in Table 5.1, with an SPG and IF value of 38.86° and $2.1983x10^{-8}mm^4$, respectively.

Table 5.1: The D-H parameters for the optimized KHS

	Joint Type	*Optimized Values*	*Lower Bound*	*Upper Bound*
		Thumb		
l_{T_x}		$8mm$	$0mm$	$10mm$
l_{T_y}		$-27mm$	$l_{I_y}mm$	l_{I_y}+$30mm$
l_{T_z}		$17mm$	$l_{I_z} + 15mm$	$l_{I_z} + 35mm$
α_{T_2}		$13.18°$	$-90°$	$90°$
θ_{T_3}	Fixed	$30.79°$	$-65°$	$65°$
θ_{T_4}	Actuated	$-25°$ to $73°$	/	/
$l_{T_{MC}}$		$44mm$	$2l_{T_{DP}}mm$	$2.5l_{T_{DP}}mm$
α_{T_4}		$65°$	$50°$	$65°$
$\theta_{T_{MCP}}$	Fixed	$7°$	$0°$	$25°$
$l_{T_{PP}}$		$32mm$	$l_{T_{DP}}mm$	$1.5l_{T_{DP}}mm$
α_{T_5}		$17°$	$-20°$	$20°$
$\theta_{T_{IP}}$	Fixed	$4°$	$0°$	$35°$
$l_{T_{DP}}$		$22mm$	$20mm$	$30mm$
α_{T_6}		$0°$	$0°$	$0°$
		Index		
l_{I_x}		$88mm$	$l_{M_x} - 5mm$	l_{M_x}
l_{I_y}		$-21mm$	$20mm$	$30mm$
l_{I_z}		$0mm$	$0mm$	$5mm$
α_{I_2}		$-10°$	$-90°$	$90°$
θ_{I_3}	Fixed	$10°$	$-20°$	$20°$
θ_{I_4}	Actuated	$13°$ to $90°$	/	/
$l_{I_{PP}}$		$43mm$	$2l_{I_{DP}}mm$	$2.5l_{I_{DP}}mm$
α_{I_4}		$-10°$	$-10°$	$0°$
$\theta_{I_{PIP}}$	Coupled to θ_{I_4}	$CR = 1.56$, $FA = 20.60°$	$CR = 1.33$ $FA = 0°$	$CR = 1.71$ $FA = 35°$
$l_{I_{MP}}$		$29mm$	$l_{I_{DP}}mm$	$1.5l_{I_{DP}}mm$
α_{I_5}		$0°$	$0°$	$0°$
$\theta_{I_{DIP}}$	Fixed	$7°$	$0°$	$20°$
$l_{I_{DP}}$		$19mm$	$15mm$	$22mm$
α_{I_6}		$0°$	$0°$	$0°$
		MRL		
l_{M_x}		$90mm$	/	/
l_{M_y}		$0mm$	/	/
l_{M_z}		$0mm$	/	/
α_{M_2}		$-10°$	$-10°$	$0°$
θ_{M_3}		$0°$	$-10°$	$0°$
$\theta_{M_{MCP_{FE}}}$	Actuated	$13°$ to $90°$	/	/
$l_{M_{PP}}$		$47mm$	$2l_{M_{DP}}mm$	$2.5l_{M_{DP}}mm$
α_{M_4}		$0°$	$0°$	$0°$
$\theta_{M_{PIP}}$	Coupled to $\theta_{M_{MCP}}$	$CR = 1.56, FA = 20.60°$	$CR = 1.33$ $FA = 0°$	$CR = 1.71$ $FA = 35°$
$l_{M_{MP}}$		$M = 29mm, R = 26mm,$ $L = 18mm$	$l_{M_{DP}}mm$	$1.5l_{M_{DP}}mm$
α_{M_5}		$0°$	$0°$	$0°$
$\theta_{M_{DIP}}$	Fixed	$7°$	$0°$	$20°$
$l_{M_{DP}}$		$M = 19mm, R = 17mm,$ $L = 16mm$	$15mm$	$22mm$
α_{M_6}		$0°$	$0°$	$0°$

5.6 EVALUATION OF THE SIMPLIFIED KINEMATIC HAND STRUCTURE

Even though the KHS has only three actuators, three active joints and two coupled joints, with the optimised geometrical parameters discussed in the previous section, it can still attain proto-grasps that are very similar to the original ones intended, as shown in Figure 5.16 (compare to Figure 4.33 (on p.86)).

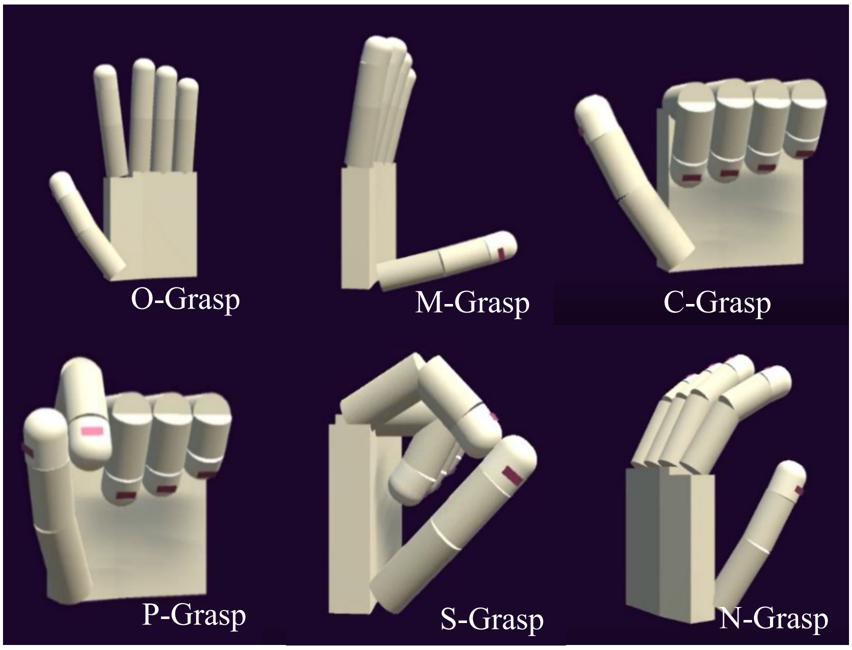

Figure 5.15: The proto-grasps, and the N-Grasp, with the developed KHS

The PMs are further exploited by the compliance modelled on the simulation environment, which involves having each individual finger stop when it encounters resistance to its motion due to the object being grasped, but maintaining the movement of the free joints. This allows all the fingers of the prosthetic hand to wrap around objects of arbitrary shapes and sizes such that the grasps are not restricted to only the end-state configurations. In fact, using only the available PMs, the KHS simulated in Unity could wrap its finger around the different representative objects in an aesthetically acceptable manner, as shown in Table 5.2.

The O-M-S PM was used to achieve 41% of the grasps shown in Table 5.2, closely followed by the O-P and O-C PMs with 33% and 22%, respectively. The fact that the O-C PM was the least common closing PM, even though it mainly correlated to the first PC extracted from the PCA, indicates that, while the set of chosen proto-grasps is sufficient for a non-dominant prosthetic hand, the coupling/fixing of the joints, meant that the KHS had to approach the objects in a slightly different way. In particular, the O-M-S PM was found to be very useful in allowing the KHS to grasp objects with a

Table 5.2: The KHS wrapping its finger around the twenty-seven representative objects, using only the four PMs

Sweeping	***Peeling a potato***	***Opening a hand-tightened bottle***
Broom	*Potato*	*Large Water Bottle*
N-O-C	O-M-S	O-M-S
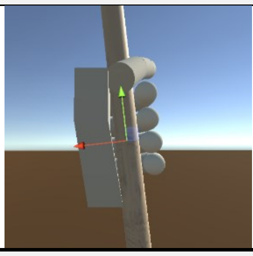	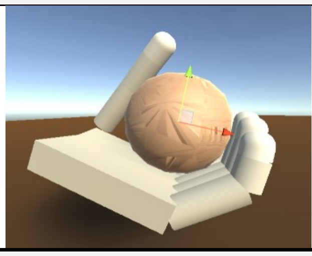	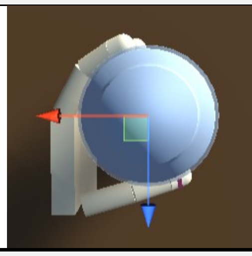
Putting toothpaste on a toothbrush	***Opening the zipper of a purse***	***Pouring from a frying pan***
Toothbrush	Purse	*Frying Pan Handle*
O-C	O-P	N-O-C
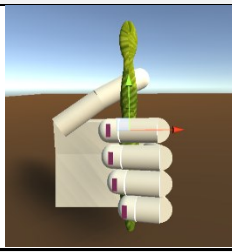		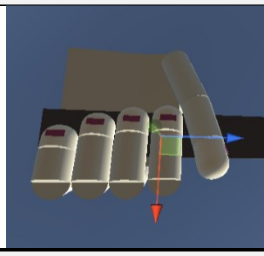
Passing a thread through a needle	***Opening a hand-tightened cap***	***Pouring water into a cup***
Sewing Pin	*Soap Bottle Cap*	*Medium-Sized Cup*
O-M-S	O-M-S	O-M-S
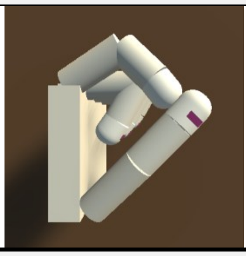	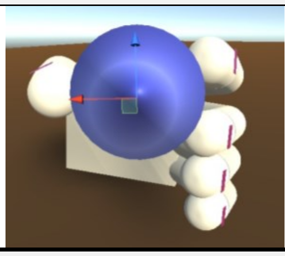	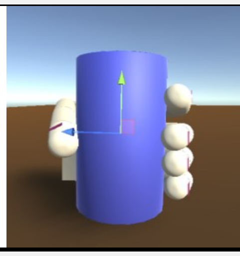
Playing Cards	***Carrying a tray***	***Opening a packaged-food box***
Cards	*Tray*	*Cracker box*
O-P	O-M-S	O-M-S
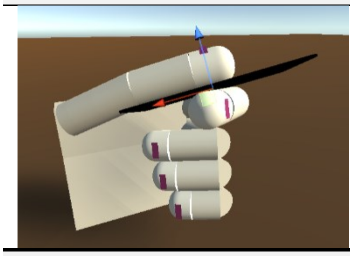	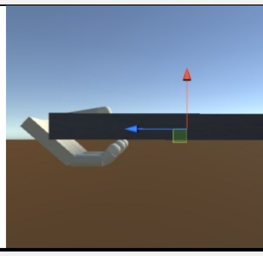	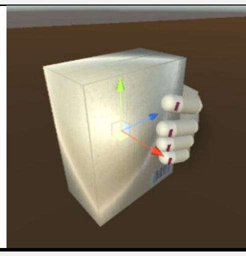
Carrying a shopping bag	***Pulling a drawer***	***Carrying a briefcase***
Shopping bag	*Cabinet handle*	*Briefcase*
O-N-C	N-O	O-M-S
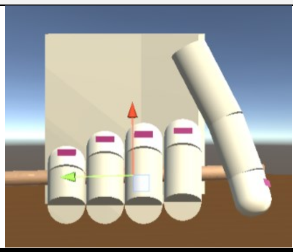	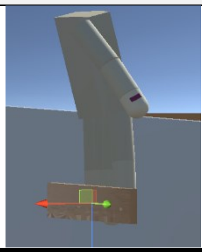	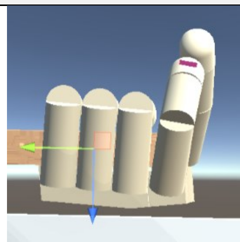

Table 5.2: The KHS wrapping its finger around the twenty-seven representative objects, using only the four PMs (cont.d)

Sharpening a pencil	***Opening a hand-tightened toothpaste cap***	***Opening a hand-tightened body cream cap***
Small Sharpener	*Toothpaste Cap*	*Body Cream Container*
O-P	O-P	O-P
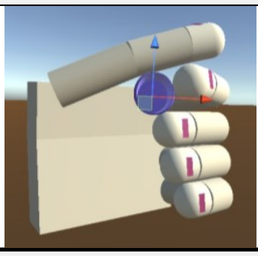	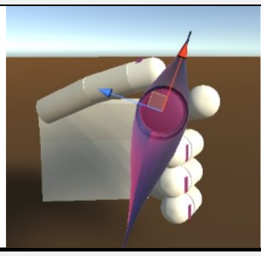	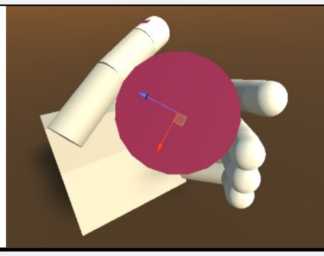
Putting glue on a paper	***Using a tablet***	***Throwing a ball***
Paper	*Tablet*	*Beach Ball*
N-O	N-O	N-O
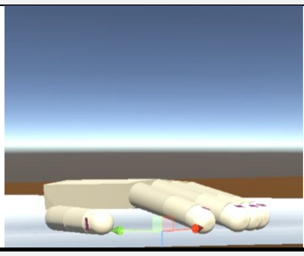	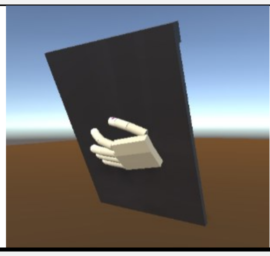	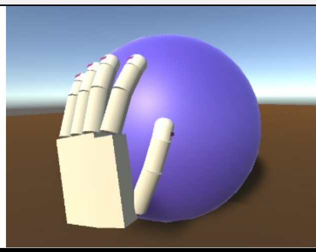
Eating with a fork and a knife	***Dialling a telephone number***	***Spraying a detergent while wiping a surface***
Fork	*Telephone*	*Spray bottle*
N-O-C	O-P	O-M-S
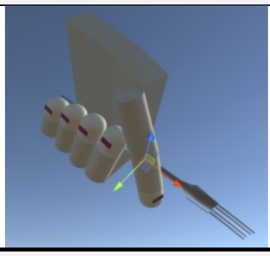	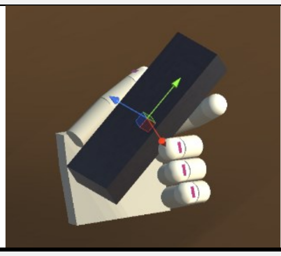	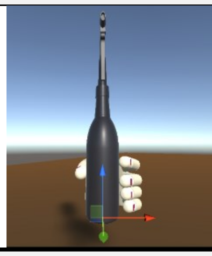
Cutting with scissors	***Opening a hand-tightened bottle Cap***	***Opening the flip top of a toothpaste tube***
Paper	*Water Bottle Cap*	*Toothpaste Cap*
O-P	O-P	O-P
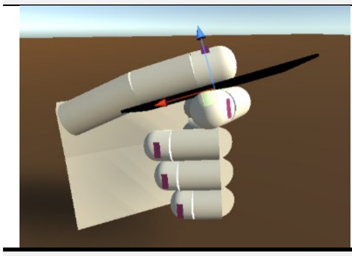	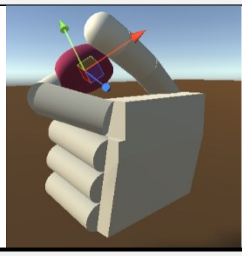	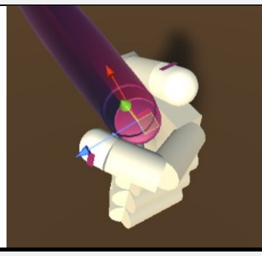
Opening a can of beverage	***Opening a hand-tightened jar***	***Eating with a fork and a knife***
Can of beverage	*Jar*	*Knife*
O-M-S	O-M-S	N-O-C
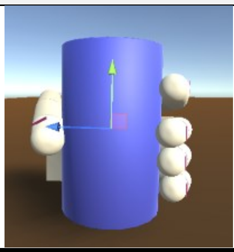	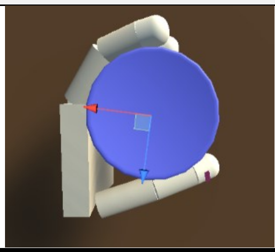	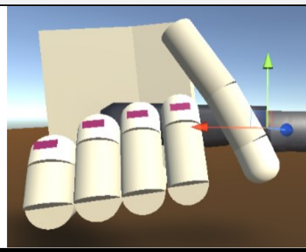

power grasp, but in the case of small objects the thumb and the index finger would touch before having the chance to grasp the object. In that case, the O-C PM was useful because the KHS would start from the N-grasp, where the object would be placed between the thumb and the palm, before giving the closing command. However, the force applied by the thumb would not be possibly varied as it would move in the opposite direction of the object. Furthermore, using the N-grasp during day-to-day activities can be time-consuming for the amputee since the motion to the N-grasp takes place automatically after the hand has been inactive for a period of time, as discussed in Section 4.6 (on p.84). Hence, given that the O-C PM was only used for the toothbrush, this PM was modified by introducing the N-grasp as an intermediary grasp between the O-grasp and the C-grasp, especially since the toothbrush could still be grasped. The O-P PM was especially useful in producing different grasp types, where the side of one or two fingers was required to stabilise the object, such as LatP and SpP. Meanwhile, the N-O PM was used for 15% of the objects, namely, the NonP grasps, although a subsequent closing command still needed to be given to ensure that all the fingers were in contact with the object.

Although a few of the hand configurations differed from the ones shown in Table 4.1 (on p.52), the KHS was able to grasp most of the representative objects, using the specified grasp types. The cases where this was not possible were mainly those where the KHS was not able to wrap its fingers around the object, as specified in the definition of the grasp type, due to the configuration of the PMs and/or the size of the object. Examples of such cases include holding playing cards, carrying a tray/briefcase, opening a drawer and eating with a fork. However, there were certain cases where, even though the KHS was able to produce the required grasp type, an alternative grasp type was considered more appropriate as it reduced the force required to keep the object from slipping during the intended task, such as when pouring from a frying pan. Meanwhile, although the spraying bottle could be grasped with the specified grasp type, the KHS does not have the ability to move the index independently to actuate the spraying head of the bottle (it is to be noted for this specific activity that, by interchanging the functions of the natural and prosthetic hands, such activity can still be performed successfully).

Spraying the detergent bottle was therefore the only activity considered that could not be carried out in the normal manner. Otherwise, using these grasps with some additional support from the environment and the intact hand, if applicable, the KHS should be able to hold these objects firmly during the intended task. A force closure grasp was used for most of these objects, except for specific cases, such as the shopping bag and the briefcase, where a form closure grasp was used instead. For force closure grasps, the frictional force required to keep the object from slipping can be guaranteed by varying the force applied by the thumb, which in turn varies the reactive forces built up at the palm and the other digits. For a μ_s of 0.5, the average contact forces that need to be applied or sustained by the digits and the palm across the different activities considered in this work are listed in Table 5.3.

Table 5.3: The contact forces that need to be applied or sustained by the digits and the palm averaged across the different bimanual activities

	Thumb	***Index***	***MRL***	***Palm***
Average (N)	35.28	25.82	21.08	25.42
SD (N)	38.98	31.36	28.45	44.92

These contact forces are higher than the forces that can be applied by most commercial prosthetic hands, as shown in [46]. This is mainly due to the reduction in dimensionality of the KHS, which results in fewer contact points. Whilst these forces are reasonable (the maximum force that a man can apply with the thumb is around $137N$ [222]) and will not damage the grasped object, they do increase the demands placed on the actuation/transmission system. However, due to the force control system adopted in this work, the actuation system of the index and the MRL finger does not need to attain such forces in an active manner. Hence, the higher contact forces were considered a reasonable compromise because of the simplicity of the three-motored KHS, but an effort still had to be made to increase the μ_s of the prosthetic hand in an attempt to reduce the required contact forces.

The T_{m_T} that is required for each of the bimanual activities, and which is calculated by using the approach described in Section 5.3 (on p.89), is shown in Figure 5.17. The first five activities on the left-hand side of the graph involve a form closure grasp. This means that the thumb motor will not need to apply any additional force; instead, it will have to only sustain the built-up torque. In this case, the maximum torque that the thumb motor needs to sustain was found to be $1.09Nm$, that is, for when an exaggerated force of $50N$ is applied with the open hand to hold a paper on a table or to throw a beach ball, which is still significantly less than $8.31Nm$, the maximum torque that the thumb motor would need to apply to open a hand-tightened cap. For some of the activities, T_{m_T} was even higher than T_{T_z}, since T_{m_T} does not only depend on the magnitude of the contact forces, but also on the position and orientation of the force relative to the active joint of the thumb. In fact, it was observed that the efficiency of the thumb in applying the contact forces was lower for grasp types which involved its side, such as LatP and SpP. This is to be expected since for these types of grasps, the contact force tends to have a larger component along the z-axis (i.e., the axis of the thumb CMC joint).

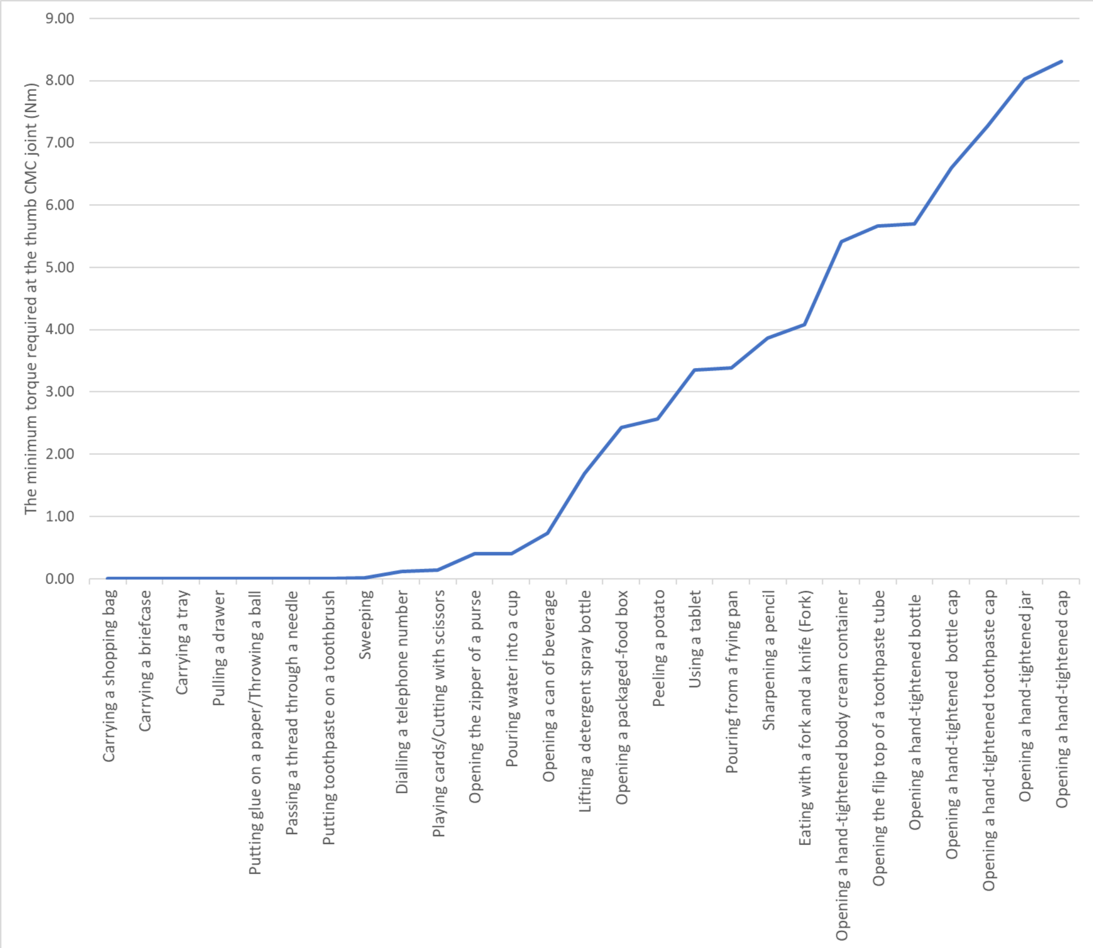

Figure 5.16: The minimum torque that needs to be applied at the thumb CMC joint, $\overrightarrow{T_{m_T}}$, for the different bimanual activities

On the other hand, the actuation/transmission system of the fingers will need to sustain a maximum torque of $4.68Nm$, while the structure of the fingers withstands a maximum bending moment of $3.28Nm$.

The feasibility of developing and constructing a prosthetic hand based on this KHS, which can apply and sustain these torques while resembling the human hand in terms of weight and size, still needs to be determined, and will be discussed in the next chapter.

CHAPTER 6: PRACTICAL DEMONSTRATION OF THE APPROACH THROUGH THE DEVELOPMENT OF MAPROHAND

6.1 INTRODUCTION

Following the identification of the optimal KHS in the previous chapter, the focus of this chapter now shifts to the development of a tangible prototype named MAProHand. Serving as a concrete manifestation of the identified KHS, this prototype enables the evaluation of the proposed PMs approach to grasping within a controlled laboratory setting. Throughout this chapter, the development process, ranging from the initial conceptual design to the construction, is discussed in significant detail. This aims to highlight the design principles, methodologies, and technologies employed in bringing the optimized KHS to life through the MAProHand prototype.

6.2 CONCEPTUAL DESIGN

One of the earliest phases of a design process, and arguably the most important one, is the conceptual design. It involves generating and evaluating different solutions for the problem at hand to narrow down the direction of the design, while taking into consideration the required specifications.

In the light of the analysis carried out in previous chapters, the developed design must be able to actuate the different digits according to the resulting PMs, as well as apply enough force to keep the object from slipping. Given the importance of sensory feedback when grasping these objects, the prosthesis must also provide some form of force feedback to the amputee.

Hence, during the conceptual design phase, the functions of each aspect of the design, namely, the actuation system, the transmission system, and the force feedback system, were clearly defined. Taking the actuation system as an example, it was decided very early on (Section 5.2 (on p.88) and Section 5.3 (on p.89)), that it must be able to move each digit separately in the required direction, and to stop its movement when it encounters an object or has reached the desired position. Once the object is grasped, it must also ensure that the thumb provides enough force to hold it securely during the bimanual activity. Depending on the control system of the prototype, which is being developed simultaneously in a separate study, the actuation system will also need to determine the current position of each digit. There are other aspects of the design of the prosthetic hand, such as the user interface and the charging method. However, while these aspects are important for the final product to be used by the amputees in their daily activities, they are beyond the scope of this prototype. Instead, the effect that the decisions taken during the design process have on these aspects should be considered, wherever possible.

Research was then carried out to generate several possible concepts for each function of the design. For example, the movement of the digits can be achieved with the use of several types of actuators, such as electric, hydraulic and pneumatic; their movement can then be stopped when either an increase in the current drawn is detected, or feedback on the torque applied by the thumb exceeds a set threshold, or feedback on the position of the digits varies from the one estimated by the controller of the actuator by a set amount.

Alternative solutions for the entire system can then be generated by choosing a concept for each function. The most suitable solution with respect to the product requirements can then be fed to the next phase of the design process, which is the embodiment design, so that it can be developed in more detail. However, as specified in Chapter 3 (on p.44), most of the components utilised in this project should ideally be readily available on the market. This means that the feasibility of a solution depends on whether the components that satisfy the required parameters, such as weight, size, and strength, are commercially available. Hence, a more appropriate approach is to choose the actuators first (since they dictate the transmission system required, as well as the remaining space available in the palm for the other components), and then develop the rest of the design around the chosen actuators, as will be discussed in the next section.

6.3 EMBODIMENT DESIGN

6.3.1 PROCURING THE REQUIRED ACTUATORS

6.3.1.1 Requirements for the Actuators

The actuators, like the muscles in our hand, are responsible for the movement of the various parts of the hand and the build up of the necessary forces, by converting energy, usually electrical, hydraulic or pneumatic, into mechanical force.

As discussed in Section 5.2 (on p.88), each digit will be actuated separately, thus, three actuators are required, which are able to move the digits at a speed between $90°/s$ (i.e., $15rpm$) and $230°/s$ (i.e., $38rpm$) as indicated in Chapter 3 (on p.44). Given that that the thumb is the only one that applies the required force on the object, while the necessary reactive forces build up at the other digits, two different actuators are required, one for the thumb and the other one for the fingers. In the case of the thumb actuator, it should be able to attain the maximum T_{m_T} observed when executing the representative set of bimanual activities, which was $8.31Nm$, as discussed in Section 5.6 (on p.5.6). For the fingers, only the torque necessary to move the fingers at the desired speed is required, as long as it is non-backdriveable, to build up the required reactive forces.

In general, these motors must also be compact and lightweight so that they can be embedded in the palm of an anthropomorphic prosthetic hand. Thus, the overall diameter of the motors should not exceed $20mm$, which is the maximum allowable thickness of the palm. The overall height of the actuators should be less than $65mm$, slightly less than the height of the palm to allow some space for other components that might be required. Meanwhile, the maximum allowable weight for the thumb motor was set to $200g$ (i.e., half the desired weight of the prosthetic hand), since powerful motors tend to be heavy. This is then compensated by the fact that the weight of the finger motors should not exceed $50g$.

There are different types of actuators that could potentially be used to satisfy these requirements, such as DC motors and ultrasonic motors, with unconventional solutions such as artificial muscles and soft actuators gaining more popularity in recent years for their strength to weight ratio [223]. However, this work focuses on conventional motors, namely, brushed DC motors and brushless DC motors, due to their ease of accessibility, low cost, and extensive knowledge and experience available in controlling these devices.

Brushed DC motors are the simplest type of motors, Figure 6.1(a) [224]; they consist of a coil wire (i.e. the rotor - the rotating part of the motor) arranged within a fixed magnetic field (i.e. the stator - the part of the motor that remains fixed). The coil, with a commutator attached to its end, is then connected to the electric supply through brushes. The current passing through these coils then generates a magnetic force on both sides, producing a torque which causes the coil to rotate, depending on the mechanical load. The magnitude of this torque depends on inherent properties of the motors, such as the number of windings, and also on the magnitude of the current, which can be varied through a technique known as Pulse Width Modulation (PWM), where the average power applied over time is varied by modifying the duty cycle of the applied voltage. Although the use of brushes creates noise, friction and reduces the service life of the motor, DC motors are typically used due to their low cost and ease of control [225]. In fact, prosthetic hands such as Vincent and the i-Limb are actuated by these types of motors [46].

On the other hand, brushless DC motors make use of the same working principle, but instead a fixed magnet is used as a rotor, whilst the stator consists of multiple coils, Figure 6.1(b) [224]. Controlling the magnitude and the direction of the current that passes through the coils through PWM adjusts the magnetic field generated by the stator, causing the rotor to rotate at various speeds. This eliminates the need for brushes, so, brushless DC motors offer high efficiency, high durability and low noise [226], [227]. Examples of artificial hands which have made use of brushless DC motors include the Michelangelo Hand [43] and the DRL-HIT Hand II [228]. Belter et al. [46] recommended the use of brushless DC motors for a prosthetic hand, as discussed in Section 2.6 (on p.21), but given their similar characteristics, both types of motors were considered for this prototype so as to widen the number of possible candidates while focusing mainly on rotary motion.

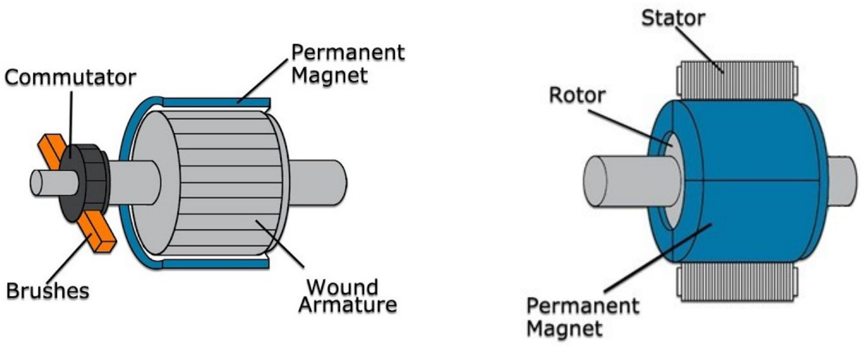

(a) (b)

Figure 6.1: (a) Brushed DC motors and (b) Brushless DC motor [222]

Nevertheless, these types of motors are typically used to continuously rotate a load at a rated speed. However, in this application, the digits are required to close on an object and apply/sustain the necessary forces. This means that the motors are going to be stalled (i.e., the torque required to continue moving the digits is greater than the maximum torque that can be applied by the motor, and thus, a force proportional to the maximum torque of the motor is applied on the object), so, operating the motor in this region for long periods of time could possibly damage the windings due to overheating, especially if operated at the rated voltage [229]. Hence, to make the best use of the chosen motors, the digits must be able to apply/sustain the necessary force in the absence of the power supply, which in turn also reduces the heat generated and the power consumed. Therefore, brakes or clutches can be used to prevent the load from driving the input shaft, but these types of devices tend to be bulky and add to the overall weight of the hand. Alternatively, as discussed in Section 2.4.3.2 (on p. 13), NBDMs, such as worm gears with a low lead angle, γ, can be incorporated in the gear transmission system. Despite the relatively high gear ratio and low efficiency of worm gears [230], they were preferred for their simple design, as it avoids the need for any additional components.

However, self-locking gears tend to tighten when high torques are applied, which may lead to the entire hand jamming when trying to open. Hence, given that the thumb still needs to apply the required contact forces (i.e., the gears in the entire transmission must still be able to sustain the required forces), the non-backdriveability of the thumb is achieved through a high gear reduction such that the torque applied on the output shaft is not sufficient to overcome the friction of the actuation system. Manufacturers do not guarantee the non-backdriveability of a gearhead, and thus, it has to be tested in the laboratory, but gearheads with four stages or more (i.e., a gear reduction of over 200) tend to be non-backdriveable [228]. Hence, the minimum gear reduction required for the thumb was set to 250. Alternatively, stepper motors, another type of electric motor which can maintain the motor shaft position in the presence of external loads, as well as provide open loop positional feedback could also have been used instead. However, they were not considered suitable for this application due to their low efficiency and high power consumption [231], [232]. In fact, the use of stepper motors in prosthetic hands, as in [233], is less common.

While the power consumed by the prosthetic hand during a typical day of sixteen hours is not that critical for this prototype, since a power supply will be used, taking into consideration the weight and size of the required battery is still important as it will eventually need to be placed inside the socket. The battery capacity of commercial prosthetic hands tends to range from $800mAh$ to $2200mAh$ [234], [235]. Taking the upper limit as the maximum allowable limit for the prosthetic hand, the energy consumption of the thumb motor should be less than $1500mAh$ since a more powerful motor will be required. Depending on the actual consumption of the thumb motor chosen, the remaining allowable capacity is then dedicated to the other two motors. Another parameter that also needs to be considered is the supply voltage required. DC motors with high nominal voltage tend to consume less energy, but as the supply voltage increases, the weight and size of the battery increases as well. Commercial prosthetic hands, such as the Michelangelo and the BeBionic, make use of supply voltages of $11.1V$ [43] and $7.4V$ [236], respectively. In light of industry norms, the motors should have the same nominal voltage, that is, $12V$ or less.

For precise movement control of the digits using DC motors, position sensors, such as encoders, could then be used to determine the current rotor position. However, since all the PMs start from the O-grasp, the relative speed of each digit can be predefined according to the required PM. Alternatively, for a more robust control system, the speed of each active digit can be set the same for all the PMs, and appropriate time constants (i.e., the motor operates for a fixed period of time) and delays can then be introduced during the actuation of each PM. While this approach implies that the digits do not reach their final position at the same time, it was still preferred as it simplifies the control system as well as avoids the need for additional components, which increase the weight and the overall length of the motor. In the case where the digit must be stopped prior to reaching its final position (e.g., the digit has encountered an object or reached the end of its allowable motion), the control system is used to detect an increase in the current drawn so that the corresponding motor can be powered OFF.

In the light of these requirements, an extensive search on the market was carried out to determine which two commercially available motors should be used for the thumb and the fingers. This will be discussed in the following sections.

6.3.1.2 Selection Process for the Thumb Actuator

The search for the thumb motor that best satisfied the required specifications began with the collection of relevant information on the brushed and brushless DC motors available on the market, such as the stall torque and the no-load speed, as well as information on the corresponding gearboxes recommended by the manufacturer, such as their efficiency.

Gearboxes tend to be available in different Gear Ratios (GRs). Given that the chosen motor must have an overall gear reduction of over 250, the gearbox with the highest GR possible that satisfies the required specifications without exceeding the maximum allowable intermittent output torque of the gearbox was chosen. This eliminates or reduces the need to implement a gear-down system after the gearbox (which will be referred to as an additional gear train), simplifying the design. Hence, the output torque of the gearbox, $T_{O_{gb_T}}$, was first calculated using Equation 6.1:

$$T_{O_{gb_T}} = T_{Stall_T} * GR_{gb_T} * \eta_{gb_T} \tag{6.1}$$

Where,

- T_{Stall_T} is the rated stall torque of the thumb motor, Nm.
- GR_{gb_T} is the gear reduction of the thumb gearbox.
- η_{gb_T} is the efficiency of the thumb gearbox, %.

$$GR_{AG_T} = \frac{T_{m_T}}{T_{O_{gb_T}} * \eta_{AG_T}} \tag{6.2}$$

If $T_{O_{gb_T}}$ was less than the torque required, T_{m_T}, the additional gear reduction that had to be implemented, GR_{AG_T}, would be determined using Equation 6.2, where the efficiency of the gear train, η_{AG_T}, was taken to be 73%, assuming that three sets of helical/spur gears, each with an efficiency of 90% [237], were used.

The feasibility of implementing any given gear reduction depends on the remaining space and the gears available on the market, but higher gear reductions tend to be bulkier and heavier, especially since the non-backdriveability of the thumb is not to be achieved with a worm and wheel, as discussed in the previous section. Thus, the maximum allowable limit for the GR_{AG_T} was set to five.

However, the increase in the output torque of the motor was achieved at the expense of the output angular speed. Hence, the resulting angular speed of the thumb, ω_T, due to the gearbox and the additional gear train was checked to determine whether it was within the required specifications. This was found using Equation 6.3, where the weight of the digit when rotating freely was assumed to be negligible compared to the high torque that the motor had to apply. Thus, the angular input speed of the thumb gearbox, $\omega_{gb_{In_T}}$, was assumed to be the same as the no-load speed, unless it exceeded the maximum recommended input speed of the gearbox, in which case $\omega_{gb_{In_T}}$ would then be limited to that value (i.e., the output speed of the motor would need to be lowered by varying its PWM) so as to ensure that the stress applied on the teeth of the gearbox during operation would not be excessive.

$$\omega_T = \frac{\omega_{gb_{In_T}}}{GR_{gb_T} * GR_{AG_T}} \tag{6.3}$$

The energy consumed by the thumb motor during a typical sixteen-hour day was approximated using Equation 6.4. In this equation, the number of grasps utilised during this period was estimated to be 1920 (i.e., an average of two objects per minute), which even though arbitrarily chosen, was based on the idea that an amputee with a prosthetic hand will most likely take longer to execute an activity, while for some of the time it will be idle. Each grasp was then split into three phases: the closing of the digit, the building up of the required force and the opening of the digit, where each phase was taken to last one second.

$$Energy\ Consumption\ (mAh) = 1920 * Energy\ Consumption\ of\ 1\ Grasp\ (mAh) = 1920 * \frac{I_{stall_T} + \left(2 * I_{Noload_T}\right)}{60 * 60} \quad 6.4$$

In such a situation,

- I_{stall_T} is the rated stall current of the thumb motor, mA.
- I_{Noload_T} is the rated no load current of the thumb motor, mA.

The actuators found on the market that satisfied the required specifications were then ranked according to the decision matrix in Table 6.1, where each parameter was given a score based on the scoring system shown in Table 6.2. The motor with the highest total score, which is the weighted sum of all the parameters scores, was then chosen.

Table 6.1: Decision Matrix used to evaluate and rank the different motors available for the thumb

Parameter	***Criteria***	***Absolute Allowable limit***	***Weighting***
Total Weight	Total weight of actuator/ Absolute Allowable Limit	200g	3
Additional Gear Reduction	Additional Gear Reduction/Absolute Allowable Limit	5	2
Overall Length	Overall Length of actuator/ Absolute Allowable Limit	65mm	2
Diameter	diameter of actuator/Absolute allowable diameter of actuator	20mm	1
Overall Gear Reduction	Absolute Allowable Limit/ overall gear reduction	250	1
Output Speed	Absolute Allowable/Output Speed	15rpm	1
Energy Consumption	Energy consumption of actuator/ Absolute Allowable Limit	1500mAh	1

Table 6.2: The scoring system used to evalute the different parameters of the actuator

Score	0	1	2	3	4	5
Criteria	>1	1-0.8	0.8-0.6	0.6-0.4	0.4-0.2	0.2-0

From Table 6.1 one can see that priority was given to the total weight of the actuator due to the importance of keeping the entire weight of the prosthetic hand to a minimum. While the overall weight of the prosthetic hand also depended on the required additional gear reduction, some form of a gear train still needed to be implemented to change the direction of the axis of rotation of the motor; consequently, it was given a slightly lower weighting. A similar weighting was also given to the overall length of the motor, while an even lower weighting was given to its diameter. The reason for this is because while the actuator must be compact to be able to fit the other components required in the palm, it is more likely that these motors will need to fit along the height or width of the palm, rather than along its thickness. Meanwhile, the output speed, the battery capacity, and the total gear reduction were given the lowest weighting, because even with the absolute allowable limit of these parameters, the prosthetic hand would still be able to complete its function.

However, it was observed early on that the motors available on the market were not able to achieve the required torque of $8.31Nm$ while satisfying all the required parameters. Hence, to have a better idea of the minimum increased torque capability needed by an eventual commercial product, without running the risk of over-design, the required T_{m_T} was reduced to $3.5Nm$, which was comparable to the force capabilities of existing commercial prosthetic hands [46]. Despite the reduction in force capability, a lot of the activities can still be done, as shown in Figure 5.17 (on p.120), especially if carried out at a lower SF and/or using materials with a higher friction coefficient. Any unsuccessful activities could then be attempted with slightly altered hand configurations.

The actuator that was eventually chosen was the 16DCT Athlonix, Figure 6.2(a) [238], from Portescap, a brushed DC motor with precious metal commutation, combined with the 88:1 R16 planetary gearhead, Figure 6.2(b) [239]. The general specifications of the chosen actuator are listed in Table 6.3.

(a) (b)

Figure 6.2: (a) 16DCT Althlonix [238], and (b) R16 planetary gearhead [239]

Table 6.3: List of specifications for the actuator chosen for the thumb

	16DCT PM + R16
Nominal Voltage	$6V$
Total Weight	$39g$
Diameter	$16mm$
Overall Length	$49.7mm$
Output Speed	$17.42rpm$
Additional Gear Reduction	4.89
Overall Gear Reduction	430.6
Energy Consumption	$1396.28mAh$

From Table 6.3, one can observe that whilst the motor chosen is on the slower side, with $17.42rpm$ (i.e., $104.52°/s$), it can reach the required torque of $3.5Nm$ in a light, compact and energy efficient mechanism, with an overall gear reduction of 430.6; still, only a gear reduction of 4.89 with a minimum efficiency of 73% is required.

6.3.1.3 Selection Process for the Finger Actuators

A similar procedure was then carried out to choose the motor that best satisfied the specifications required by the fingers. However, in this case, the required output torque, T_{m_f}, depended on the desired angular speed of the fingers, ω_F; in such a situation, the selection process was based on this parameter, while ensuring that the resulting T_{m_f}, as well as other parameters, were according to the required specifications.

In light of the control strategy used to actuate the PMs, which is discussed in Section 6.3.1.1 (on p.122), ω_F can be anywhere between $90°/s$ (i.e., $15rpm$) and $230°/s$ (i.e., $38rpm$). Ideally, it should be around $126°/s$ (i.e., $21rpm$), which is an adequate closing speed without being too excessive when compared to ω_T. This desired ω_F must be achieved through an additional gear train that incorporates a worm and wheel, as discussed in Section 6.3.1.1, to attain the required non-backdriveability of the fingers. Worm and wheels tend to have high gear reductions since for one or two revolutions of the worm, the gear wheel only rotates by one tooth. Thus, the gear reduction of the additional gear train, GR_{AG_F}, cannot be too small, but it still needs to be reasonable due the limited space available in the palm. Given that the GR_{AG_F} can be altered during the design of the transmission system by opting for the same gearbox with a different gear reduction, GR_{gb_F}, (other parameters of the actuators, such as weight and size, remain approximately the same), during the selection process, actuators with a lower GR_{AG_F}were prioritised, with the maximum allowable limit set to 60. Hence, the GR_{AG_F} required for a given $GR_{gb_F}$was then found, using Equation 6.5, where $\omega_{gb_{In_F}}$ is the angular input speed of the gearbox.

$$GR_{AG_F} = \frac{\omega_{gb_{In_F}}}{GR_{gb_F} * \omega_F} \tag{6.5}$$

However, $\omega_{gb_{In_F}}$ is a function of GR_{AG_F} since the load applied on the shaft of the motor when actuating the fingers at constant speed, T_{Load_F}, is not negligible for less powerful motors, especially when the motor has to work against the gravity of the fingers. Hence, GR_{AG_F} was found for when T_{Load_F} is negligible (i.e., $\omega_{gb_{In_F}}$ was equated to the no-load speed of the motor at nominal voltage, $\omega_{No_{Load_F}}$, unless it exceeded the maximum recommended input speed of the gearbox, in which case $\omega_{gb_{In_F}}$ would then be limited to that value), a situation similar to the assumption taken for the thumb. Given that the actual $\omega_{gb_{In_F}}$would then be less than the estimated value, the resulting angular speed of the finger, ω_{R_F}, was calculated to determine whether it was still acceptable. This was computed by first determining T_{Load_F} using Equation 6.6, where a SF of 3 was considered to compensate for any friction that might be present:

$$T_{Load_F} = \frac{m_{MRL} gr * SF}{(\eta_{gb_F} * GR_{gb_F}) * (\eta_{AG_F} * GR_{AG_F})} \tag{6.6}$$

Where,

- m_{MRL} is the mass of the MRL finger in kg, since it is heavier than the index finger, with each finger assumed to weigh 20g, such that the total weight of the fingers accounts for 1/4th of the overall allowable weight, which is $400g$.
- g is the gravitational pull, m/s^2.
- r is the radius between the point mass and the axis of rotation of the motor, m.
- η_{gb_F} is the efficiency of the finger gearbox %.
- η_{AG_F} is the efficiency of the additional gear train, which was estimated to be 23%, where the efficiency of the worm and wheel, η_{ww}, was determined to be 26%, using Equation 6.7 [240]. Also, a typical set of gears with an estimated efficiency of 90% [237]would also need to be used so as not to apply the axial load generated by the worm wheel on the shaft of the motor.

$$\eta_{ww} = \frac{tan\gamma(cos\phi - \mu_{ww} tan\gamma)}{cos\phi tan\gamma + \mu_{ww}} \tag{6.7}$$

Where,

- γ is the lead angle of the worm and wheel, °, which for self-locking gears is usually around 3°.
- ϕ is the pressure angle of the gear teeth, °, which is usually 20°.
- μ_{ww} is the static coefficient of friction between the worm and wheel, where different combinations of materials are used, with bronze and steel being the most common, having a static friction coefficient of 0.16 [241].

The speed of the motor, ω_{load_F}, when rotating the load, T_{Load_F}, was then estimated using Equation 6.8, where $\frac{\Delta\omega}{\Delta T}$ is the slope of the speed vs torque of the selected finger motor, rpm/Nm.

$$\omega_{load_F} = \omega_{No_{Load_F}} - \frac{\Delta\omega}{\Delta T} * T_{Load_F} \tag{6.8}$$

If ω_{load_F} was less than the maximum recommended input speed of the gearbox, ω_{R_F} was determined using Equation 6.9, otherwise it remained the same:

$$\omega_{R_F} = \frac{\omega_{load_F}}{GR_{gb_F} * GR_{AG_F}} \tag{6.9}$$

The GR_{AG_F} was then adjusted accordingly to minimise the difference between the actual and the desired speed of the finger. The maximum allowable difference between the two speeds should be less than $6rpm$, given that the desired speed is $21rpm$, while the minimum allowable speed is $15rpm$.

The resulting T_{m_f} due to the overall gear reduction was then determined using Equation 6.10, where T_{Stall_F} is the rated stall torque of the finger motor, Nm:

$$T_{m_f} = T_{Stall_F} * \left(GR_{gb_F} * \eta_{gb_F}\right) * \left(GR_{AG_F} * \eta_{AG_F}\right) \tag{6.10}$$

T_{m_f} should be sufficient to overcome the weight of the finger and accelerate it from 0 to $21rpm$ in $0.1s$ (which is considered to be more than enough and can later be adjusted as necessary), while also considering a SF of 3 to compensate for any friction that might be present, Equation 6.11.

$$T_{m_f} \geq (I_F\alpha + m_{MRL}gr) * SF \tag{6.11}$$

Where,

- α is the angular acceleration, which is equal to $21.99rad/s^2$.

- I_F is the moment of inertia of the system, m^4, which was calculated as follows, assuming the inertia of the transmission system was negligible, and each digit was a point mass located towards the middle of each digit:

$$I_F = m_{MRL} r^2 \tag{6.12}$$

The minimum T_{m_f} required for the motor to be able to rotate the MRL finger (i.e., the heavier digit) was found to be $92.8 mNm$.

Meanwhile, the energy consumed by one finger was approximated using Equation 6.13, which is similar to the equation used for the thumb (i.e., Equation 6.4 (on p.128)), except that the opening and closing of each grasp is defined by the acceleration/deceleration period and the constant velocity phase. During the acceleration/deceleration period, the maximum rated stall current, I_{stall_F}, was assumed to be drawn for its entire duration of $0.1s$. Meanwhile, depending on the desired angular speed, the constant speed phase was taken to last $0.6s$, during which the corresponding current, I_{Load_F}, was drawn.

$$\begin{aligned} Energy\ Consumption\ (mAh) &= 1920 * Energy\ Consumption\ of\ 1\ Grasp\ (mAh) \\ &= 1920 * \frac{2\left(\left(2 * I_{stall_F} * 0.1\right) + \left(I_{Load_F} * 0.6\right)\right)}{60 * 60} \end{aligned} \tag{6.13}$$

Where, I_{Load_F} was determined using the following equation:

$$I_{Load_F} = \frac{2\,\pi\,\omega_{R_F}\,T_{Load_F}}{60 * 1000\,\eta_{m_F}\,V_{sp}} \tag{6.14}$$

Where,

- η_{m_F} is the efficiency of the finger motor, %.
- V_{sp} is the supply voltage of the finger motor, V.

Given that the battery capacity required for the thumb was estimated to be $1396.28 mAh$, the maximum allowable limit for each finger motor was set to $401.86 mAh$, such that the total capacity of the battery required was less than $2200 mAh$, as mentioned in Section 6.3.1.1 (on p.122).

Based on the parameters discussed above, the decision matrix in Table 6.4 was used to evaluate and rank the motors found, where each parameter was given a score based on the scoring system shown in Table 6.2 (on p.128).

Table 6.4: Decision Matrix used to evaluate and rank the different motors available for the fingers

Parameter	***Criteria***	***Absolute Allowable limit***	***Weighting***
Additional Gear Reduction	Additional Gear Reduction/Absolute Allowable Limit	60	1
Output Torque	Minimum Output Torque/ Absolute Allowable Limit	$92.8mNm$	1
Total Weight	Total weight of actuator/ Absolute Allowable Limit	$65g$	3.5
Overall Length	Overall Length of actuator/ Absolute Allowable Limit	$65mm$	1.75
Diameter	Maximum diameter of actuator/ Absolute Allowable Limit	$20mm$	1.75
Energy Consumption	Energy Consumption of actuator/ Absolute Allowable Limit	$401.86mAh$	1
Difference in Output Speed of Finger	Difference in Output Speed/ Absolute Allowable Limit	$6rpm$	1.25

The highest priority was given to the overall weight of the actuator as it remains one of the important parameters of the prosthetic hand, closely followed by its size and the difference in the output speed of the finger. Meanwhile, a lower weighting was given to T_{m_f}, GR_{AG_F}, and the battery capacity required, since the absolute allowable limit of these parameters should be sufficient for the success of the prosthetic hand. In fact, T_{m_f} already takes into consideration a SF of 3, thus, whilst it should be maximised as much as possible, a motor should not be chosen only on the basis of this parameter. Similarly, the GR_{AG_F} can be easily adjusted during the design of the transmission system, as discussed previously. Meanwhile, the maximum allowable battery capacity of these motors should be more than enough, especially since it is greater than the battery capacity required for the thumb motor.

The actuator that was finally chosen was the 1024…SR model [242], Figure 6.3 a), a brushed DC motor from Faulhaber, combined with the 10/1 planetary gearbox [243], Figure 6.3(b), a configuration similar to the one used in the Bebionic hand for all of its digits [244]. During the design of the transmission system, which will be discussed later on in this chapter, the lowest gear reduction of 4:1 was considered the most suitable for our application, given that the next available model was 16:1. The general specifications of this actuator are listed in Table 6.5.

From Table 6.5, one can note that the actuator chosen is not only light and compact, but with an additional gear reduction of 59.51 and a minimum efficiency of 23%, it should also be able to attain sufficient torque to rotate the fingers at the desired speed of $21rpm$ with minimal power consumption.

(a) (b)

Figure 6.3: (a) 1024..SR [242] and (b) 10/ 1 planetary gearbox [243]

Table 6.5: List of specifications for the actuator chosen for the fingers

	1024…SR + 10/1
Nominal Voltage	6V
Total Weight	$16.8g$
Diameter	$10mm$
Overall Length	$33.6mm$
Output Speed	$21rpm$
Output Torque	$226.67Nm$
Additional Gear Reduction	59.51
Energy Consumption	$366.98mAh$

6.3.2 Product Architecture

The mechanical design of MAProHand was then developed around the selected motors, where a solution for each function of the prosthetic hand was chosen from among the different ideas generated during the conceptual design and combined, taking into consideration the overall size and weight of the prosthesis, as well as the ease of the manufacturing and assembly process.

This mechanical design was first developed in Autodesk Inventor [245], a Computer-Aided Design (CAD) software used for modelling 3D products so that their form and function can be validated before they are built. Hence, the KHS modelled in Unity was set up in Inventor to establish the optimal position and orientation of each joint. This model ensured the proportions of the human hand but was found wanting in the overall aesthetics, and consequently, a more realistic mesh was required. Several realistic 3D CAD models can be found in public repository, such as the one in [246]. However, the CAD model would need to be split into various parts, with each part scaled and re-oriented to fit the original KHS as much as possible. While this would undoubtedly affect the aesthetic of the hand negatively, it would provide a more realistic visualization of the space that would be available within the palm for the mechanical design. Hence, the CAD model in [247] was used as a foundation for the embodiment design until a more realistic mesh that best fit the needs of the design could be modelled from scratch, Figure 6.4.

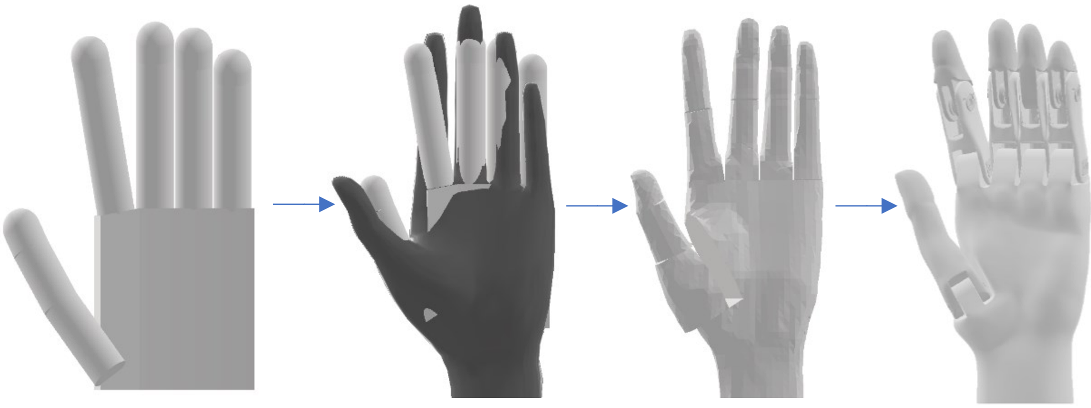

(a) (b) (c) (d)

Figure 6.4: Development of the hand model in Inventor: (a) a simple hand model based on the KHS developed in Unity, (b) a 3D hand model from a public repository superimposed on the simple model, (c) the different parts of the 3D hand model scaled and re-oriented to match the original KHS and serve as a foundation for the embodiment design and (d) a realistic hand model developed from scratch to fit the requirements of the embodiment design

The motors chosen were the first components to be fitted inside the palm, where the three motors were placed next to each other, along the width of the palm, as shown in Figure 6.5. This layout was considered the most suitable as it made the best use of the space available as well as allowed easy palmar access to each of the motors. By further placing the thumb motor between the two other motors, the weight of the prosthetic hand is more balanced around its centre, avoiding unnecessary strain on the amputee's stump. This also meant that the same kind of transmission system could be used for both the index and the MRL finger, as shown in Figure 6.5, with the orientation of each motor relative to one another optimised according to the transmission system of all the digits, further simplifying the overall design of the prosthetic hand.

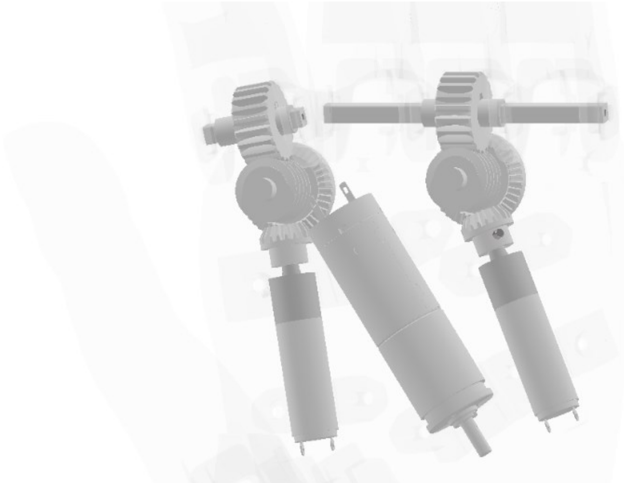

Figure 6.5: The layout of the three motors in the palm and the transmission system of the fingers

The transmission system of the fingers consisted of a worm and wheel, as discussed previously, to take advantage of its self-locking property. The wheel was placed towards the middle of the active joint to minimize the number of gears in the transmission system that would need to sustain the reactive forces, thus permitting the use of smaller and lighter gears, while the worm was placed directly beneath the wheel to minimise the protrusion of the worm from the palm. A simple 90° bevel gear was then used to change the axis of rotation of the motor. For an even more compact design, the bevel gears were placed at the back, so that they could have a larger diameter, allowing the pinion to fit exactly under the worm without interfering with the movement of the finger. Whilst this assembly may limit the palmar access of each individual component, it should be relatively easy to assemble, provided that the housing of the transmission system can ensure that the shaft of the worm remains in place during this process.

The finger motors were then rotated about the worm axis in such a way that the thumb motor could be oriented perpendicular to the active joint of the thumb. This enabled the thumb transmission system to be implemented with the least possible number of gears; in fact, only a 90° bevel gear and two sets of standard straight spur gears were required, as shown in Figure 6.6. Based on standard gear calculations [248], two sets of spur gears were necessary to achieve the required gear reduction in the limited space available, as well as to place the thumb motor closer to the proximal end of the hand. The position of each gear relative to one another and the length of each shaft were then adjusted as necessary to avoid interference between the different components.

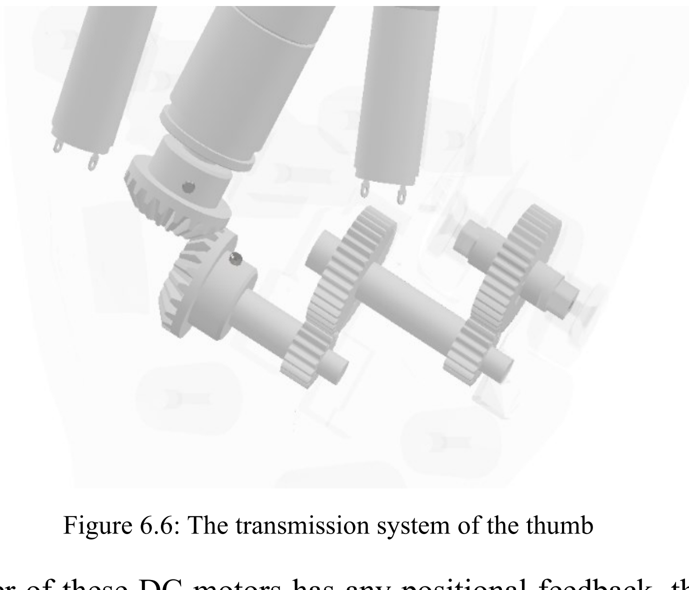

Figure 6.6: The transmission system of the thumb

Given that neither of these DC motors has any positional feedback, the two moving parts of each joint were designed to create a mechanical stop at each limit of the motion. This increases the current drawn by the motor, indicating to the control system to turn off the corresponding motor.

Meanwhile, the PIP joint of both the index and the MRL finger were coupled with the corresponding MCP joint. Given that the index PIP joint was deliberately not aligned with the MCP joint, as discussed in Section 5.5 (on p.109), the crossed pulley system shown in Figure 6.7 was used, as it allowed the two pulleys to be slightly misaligned. The same coupling mechanism was also used for the MRL finger, even if the PIP joint and MCP joint were aligned, to simplify the overall design of the prosthetic hand. However, due to the width of the MRL finger, two coupling mechanisms were installed, one in the "middle" finger and the other one in the "little" finger. This also avoids the misalignment of the two pulleys due to the gear wheel.

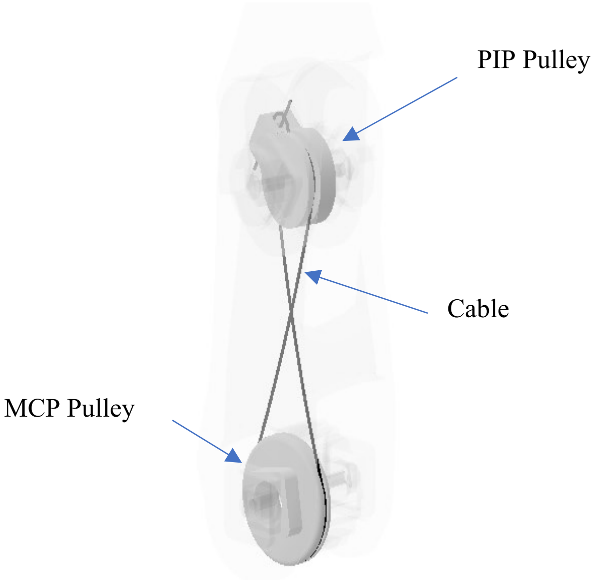

Figure 6.7: Schematic of a crossed-pulley system used to couple the PIP joint with the MCP joint

In this coupling mechanism, the MCP pulley remains stationary as the proximal phalange rotates. As a result, one of the cables tightens, causing the PIP pulley to rotate, relative to the proximal phalange, in a ratio based on the diameter of the two pulleys, which in return rotates the middle/distal phalange (this will be referred to as the distal phalange since the DIP joint is fixed). This means that while a clear path must be present between the two pulleys, the MCP pulley must remain stationary relative to the MCP shaft on which it is mounted. Thus, to simplify the design of the MCP pulley, a positive lock was created between the pulley and the palm support of the MCP shaft, which were both placed within the proximal phalange, Figure 6.8(a). A clearance hole then allowed the MCP shaft to rotate freely inside the corresponding pulley. Meanwhile, to increase the space available for the cable within the proximal phalange, the supports of the PIP shaft were placed on the outside of the distal phalange, as shown in Figure 6.8(b).

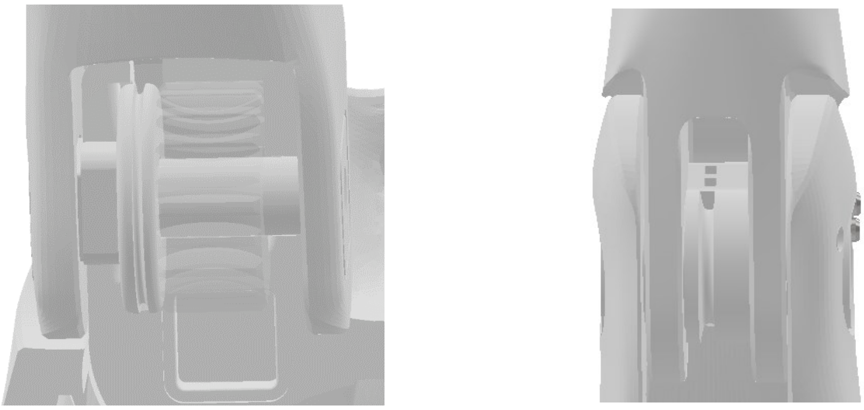

(a) (b)

Figure 6.8: Configuration of the (a) MCP shaft and (b) PIP shaft

Given the importance of the cable being taut and fixed, the MCP and PIP pulleys were custom designed, Figure 6.9, so that the cable could be tightened in place while grub screws secured the cable relative to the pulleys. However, the cable tends to loosen with time. Thus, the ends of the cable were passed through two different holes in the PIP pulley and secured in place with another grub screw, creating a 90° bend which minimises the loosening of the cable. To then facilitate the assembly process, as well as the re-tightening of the cable, necessary slots and holes were created in the prosthetic hand to allow easy access to both the cable and the grub screws.

(a) (b)

Figure 6.9: Cross section of (a) MCP pulley and (b) PIP pulley

For ease of assembly, the outer shell of the palm was then split along the axis of each active joint, with the front side serving as the housing for the actuation and the transmission system, while the back side was used as a lid. The two parts were then secured together through screws at different points. A similar approach could also be followed for the assembly of the MCP shaft and the PIP shaft, which simplifies the manufacturing and the assembly process. However, splitting each phalange into two parts would significantly weaken the part, especially since the number of screws that can be used to secure both sides is limited due to the size of the phalanges. Instead, holes, which are large enough for the shaft to pass through, were created on each side of the phalange, allowing each shaft to be assembled in place with relative ease. Depending on the type of interface required (i.e., a positive lock or a clearance hole), the hole was designed with either a square or a circular shape. To then interface the shaft with the corresponding phalange, as well as prohibit side-to-side movement, a part having the same shape as the hole (which will be referred to as an interface key) was mounted on the shaft through a positive lock, with end interface keys also secured in place with a screw, as shown in Figure 6.10.

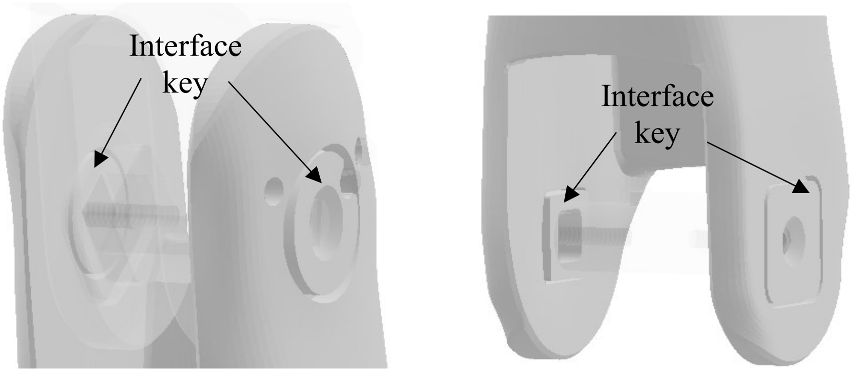

Figure 6.10: Examples of interface key

To then make the best use of the force applied by the thumb motor, wherever possible, the surface of the prosthetic hand was covered with a soft material that has a high friction coefficient, referred to as frictional covers. This maximises the frictional force present between the hand and the object, as well as distributes the contact force applied over a small area. Hence, dents as shown in Figure 6.11, were created on different parts of the hand, namely, the thumb, the distal phalange of the index and MRL finger, and the palmar side of the palm, to maintain the anthropomorphic look of the hand without weakening the parts. A glue could then be used to attach the material to the different parts.

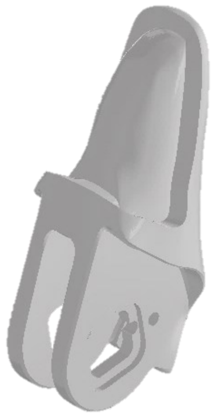

Figure 6.11: Dents to allow space for frictional covers to be placed on the surface

Feedback on the force applied by each finger was then provided to the amputee by measuring the axial reaction force, W_a, applied by one of the gears in the transmission system on the corresponding mounting shaft, Figure 6.12, and correlating it to the torque applied or sustained at the digit joint axis. While this approach only provides feedback on the force applied perpendicular to the active joint, the alternative is to mount a number of force sensors on the surface of the prosthetic hand, as in [249], [250]. The latter, in addition to being prone to missed or incorrect force readings, also complicates the integration of the sensors in the system. Thus, by measuring W_a instead, the number of sensors required is minimised and issues related to the wiring and the shape of the attachment surface are eliminated, while the force sensor embedded within each drive train can be easily accessed without affecting the coefficient of friction of the prosthetic hand. In the case of the thumb, which can apply a force in the direction of both the dorsal and palmar side, the W_a of the bevel gear mounted on the shaft was measured, since its direction is the same regardless of the rotation of the bevel gear. Meanwhile, for the fingers, only the W_a applied by the worm wheel on the mounting shaft could be measured, due to its self-locking property. Even though the configuration of the worm and wheel meant that the W_a in only one of the directions could be measured, it was considered sufficient since for all the activities, the fingers sustain the load towards the palmar side. The mounting of the force sensors then depends on the type of sensor used; this will be discussed in more detail in Section 6.3.3.4 (on p.152).

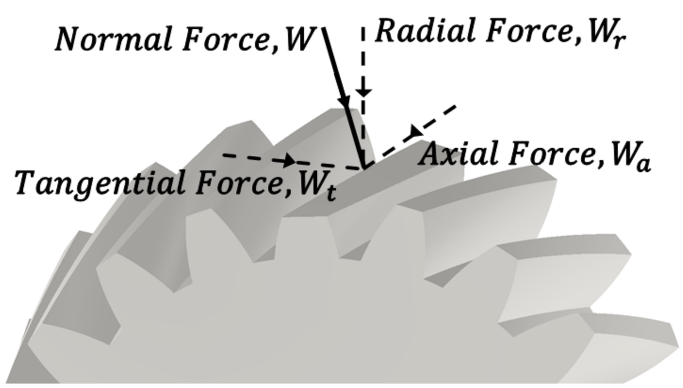

Figure 6.12: The typical forces acting on a gear teeth, where W_a is the axial force to be measured

To construct the prosthetic hand described in this section, several components were required, such as the gears and the force sensors. The sizing and the procuring of these parts will be discussed in the next section. Meanwhile, custom parts, such as the interface keys and the structure of the hand, were designed and manufactured to the required specifications, as will be discussed in Section 6.3.4 (on p.154).

6.3.3 Sizing and Procuring the parts required for the different systems

6.3.3.1 Thumb Transmission System

The thumb transmission system consists of a 90° bevel gear and two sets of straight spur gears, which together must achieve a gear reduction of 4.89 and sustain T_{m_T} of $3.5Nm$, as discussed in Section 6.3.3.1 (on p.142). Hence, a search on the market was carried out to identify the gears that best satisfy the specifications required for the gear train, while taking into consideration the weight and the space available within the palm.

Commercial gears are available in a wide range of GRs, where the GR of two gears is defined using Equation 6.15.

$$GR = \frac{z_2}{z_1} \tag{6.15}$$

Where,

- z_1 is the number of teeth on the driver gear.
- z_2 is the number of teeth on the driven gear.

Therefore, different GRs can be implemented at each stage of the gear train, yielding several possible combinations. However, a wider variety was observed regarding the spur gears available on the market, especially since the two meshing gears are sold separately, as long as the gear module, m_{gear}, (i.e., the ratio of the pitch circle diameter, p_d, divided by the number of teeth, indicating the size of the gear in mm) is the same for both gears. For this reason, a search was carried out for a 1:1 bevel gear (also known as a miter gear), since it is the most common GR available for bevel gears. Meanwhile, to simplify the search for the remaining gears, the same set of spur gears, with a reduction close to 2.21, was used at each stage of the gear train.

Apart from the GR, parameters such as the face width, b, and the p_d, Figure 6.13 [251], must also be taken into consideration during the selection process [252]. This is because the gears must fit within the space available, and if they are not properly sized, the load applied on the gear teeth may lead to premature wear or even breakage [253].

There are several equations that can be used to determine the maximum load that a gear can withstand [254]. For this prototype, the gears were sized solely according to the bending strength required to avoid breakage; the effect of dynamic loading was neglected since these gears will not operate for long periods of time, while the maximum load is applied when the motor is stalled or even turned OFF. The maximum

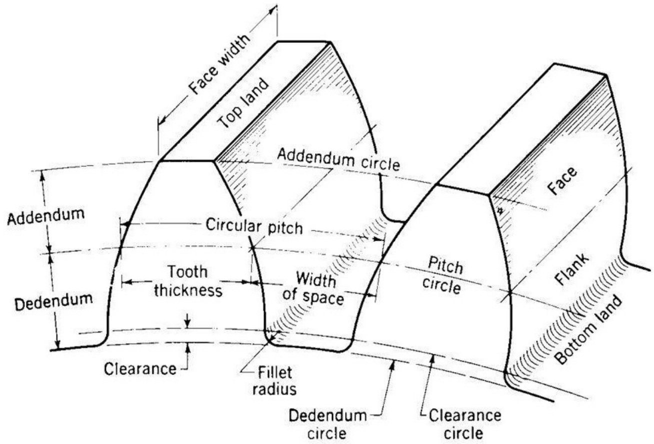

Figure 6.13: Parameters that define the shape and size of a gear, using a spur gear as an example [251]

bending stress present at the root of the spur gear tooth when the maximum load is applied statically was estimated using the Lewis formula [255], derived by Wilfred Lewis. In this formula, the gear tooth is treated as a simple fixed cantilever beam with a parabolic curve as the shape of the cross section. The full normal load, W, is then applied at the tip of a single tooth whose line of action is defined by the pressure angle, ϕ (it usually has a value of 20° for standard gears) and distributed uniformly across its entire face, as shown in Figure 6.14 [256].

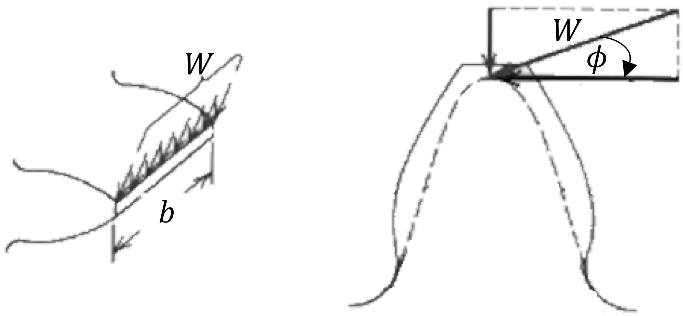

Figure 6.14: A gear tooth assumed as cantilever beam where the full normal load, W, is applied at the tip [251]

Taking into consideration only the tangential force, W_t, while assuming the stress concentrations at the tooth root fillet to be negligible, the standard bending equation leads to Equation 6.16.

$$W_{t_{LF}} = \frac{\sigma_y b m_{gear} Y}{1000\ SF} \tag{6.16}$$

Where,

- σ_y is the yield strength of the material from which the gears are manufactured; usually, it is steel, brass, aluminium, or nylon for commercial gears, MPa.
- SF is the safety factor, which was set to 1.5, as discussed in Chapter 3 (on p.44).
- $W_{t_{LF}}$ is the maximum allowable force that can be applied tangential to the tooth, N.

- Y is the Modified Lewis form factor. This is a dimensionless variable based on the number of gear teeth, z. For 20º full-depth involute gears, its value can be found using Equation 6.17 [257]:

$$Y = 0.484 - {}^{2.87}/_{z} \tag{6.17}$$

To ensure the safety of the design, the maximum W_t that is expected to be applied on the gear teeth must be less than $W_{t_{LF}}$. For a desired output torque, T_O, the magnitude of W_t applied on the gear tooth can be found using Equation 6.18.

$$W_t = \frac{2000T_O}{m_{gear}z} \tag{6.18}$$

Meanwhile, for the strength analysis of the bevel gears, the Lewis formula was slightly modified since the module and the thickness of these types of gears are not uniform. Hence, the Lewis formula was considered for a small element, dx, as shown in Figure 6.15, which was then integrated along b [258], which yielded Equation 6.1.

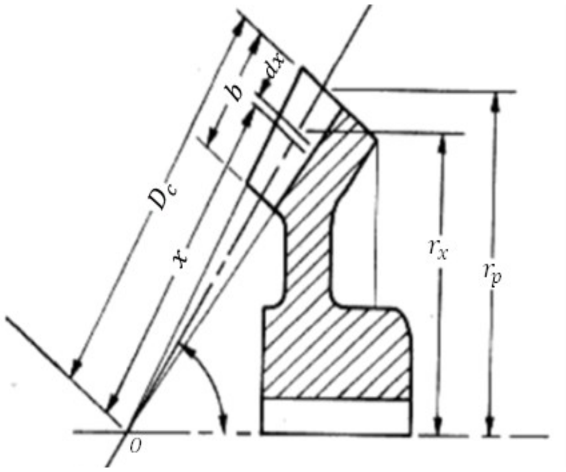

Figure 6.15: The small element considered for the bending strength analysis of bevel gears [253]

$$W_{t_{LF}} = \frac{\sigma_y Y m_{gear} b \left(1 - \frac{b}{L}\right)}{1000\,SF} \tag{6.19}$$

Where,

- D_c is the core distance in m, which is the distance measured along the face width of the tooth from the outside pitch circle diameter with a radius, r_P (this can be found using the m_{gear}), to the apex of the cone. This can be determined using Equation 6.21, where ε is the pitch cone angle, °, which is 45º for 90° bevel gears.

$$D_c = \frac{r_P}{\sin \varepsilon} \tag{6.20}$$

- Y can be calculated using Equation 6.17, except that the spur gear equivalent number of teeth z_{e_b} must be used instead of the actual number of teeth of the bevel gear. This can be found using Equation 6.21.

$$z_{e_b} = \frac{z}{\cos \varepsilon} \qquad 6.21$$

The obtained $W_{t_{LF}}$ must then exceed the expected W_t applied on the teeth of the bevel gear. This was found using Equation 6.22, where given that the pitch radius varies across the face width of the gear, the forces present between the gears were assumed to act at the centre of each tooth:

$$W_t = \frac{T_O}{r_{mean}} \qquad 6.22$$

Where,

- r_{mean} is the mean pitch radius of the gear being considered, m, which can be determined as follows:

$$r_{mean} = r_p - \frac{bsin(\varepsilon)}{2} \qquad 6.23$$

On the basis of this analysis and the space available, the steel miter gears from Reely [259], Figure 6.16(a), were chosen, with specifications listed in Table 6.6. The grade of steel from which these gears are manufactured was not specified by the suppliers, but if it is assumed to be medium carbon steel (i.e., a commonly used grade of steel for gears) with a yield strength of $343MPa$ [260], the gears should be able to withstand more than the required load. For the spur gears, the diameter of the driven gear that was to be mounted on the thumb active joint was increased, until it protruded from the thumb or the shaft of the driver gear interfered with the movement of the thumb as a result of the distance between the centres of the two gears being too small. This minimised the tangential load, reducing the required b of the spur gear. Given that the maximum allowable diameter of the driven gear was around 19mm, the spur gears, SS0.5-17A[261] and the SS0.5-36A [262], Figure 6.16(b), from KHK were chosen, with specifications listed in Table 6.6. The GR of these two medium carbon steel (S45C) gears is 2.12 (close to the one required), which yields an output torque of $3.21Nm$, taking the efficiency of each set of gear to be 90% [237]. While the output torque is slightly less than the required $\overrightarrow{T_{m_T}}$, it is the maximum load that the gears with a b of $5mm$, can sustain without any SF. Nevertheless, it was considered the best option given the space and the gears available on the market.

(a) (b)

Figure 6.16: The chosen: (a) Steel miter gears from Reely [259] and (b) Spur Gears from KHK [262]

Table 6.6: The specifications of the chosen miter gears and spur gears

	Miter Gears	***Driver Spur Gear***	***Driven Spur Gear***
Material	Steel	S45C	S45C
Module	$1mm$	$0.5mm$	$0.5mm$
Number of teeth	15	17	36
Outside diameter	$17.4mm$	$11.5mm$	$19mm$
Face width	$4mm$	$5mm$	$5mm$

From Figure 6.16, one can observe that the commercial gears come with hubs and specific bore diameters. Given the limited space, especially for the spur gears, the hubs take up unnecessary space. Hence, the parts were modified as necessary by a local manufacturing company, which involved the removal of the hub, the introduction of a positive lock and the widening of the hub diameter.

6.3.3.2 Finger Transmission System

Meanwhile, the transmission system of the fingers comprised of a worm and wheel, and a 90° bevel gear. Hence, as was the case with the thumb transmission system, a search on the market was carried out to find commercially available gears that best satisfy the required specifications.

In theory, for the worm and wheel to be non-backdriveable, the helix angle, γ, which is shown in Figure 6.17(a), must be less than the static friction angle, Figure 6.17(b), which is the angle of the slope at which the load starts to move [263]. This means that the maximum allowable γ for non-backdriveability depends on the friction coefficient, which is a factor of the combination of materials, the lubrication, and the roughness of the surface. Given that the non-backdriveability of a worm wheel is not guaranteed, a worm with the lowest γ possible should be chosen, even if it is less efficient, as indicated by Equation 6.7 (on p.131). These usually are worms with one thread, where the number of threads indicates the number of teeth of the worm.

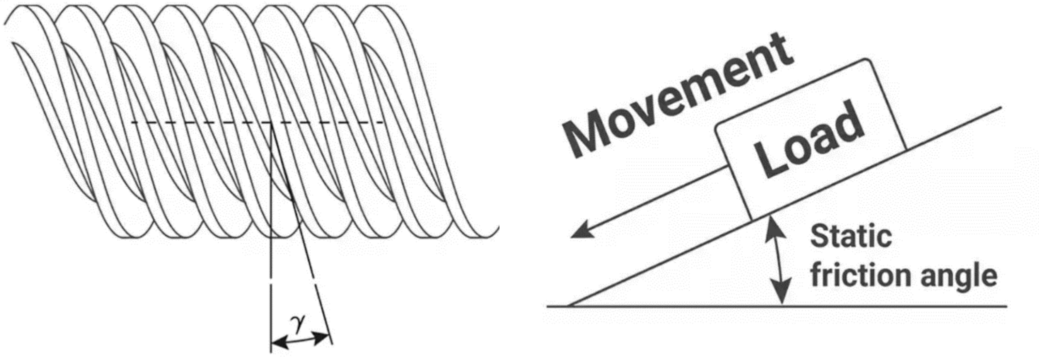

(a) (b)

Figure 6.17: (a) Worm Helix Angle and (b) the Static friction angle [263]

Apart from the γ, the wheel, which is usually made from a weaker material compared to the worm, should also be properly sized to withstand the reactive forces, as well as the force applied on the fingers due to the tension in the cable, as shown in Figure 6.18, while also taking into consideration the space available.

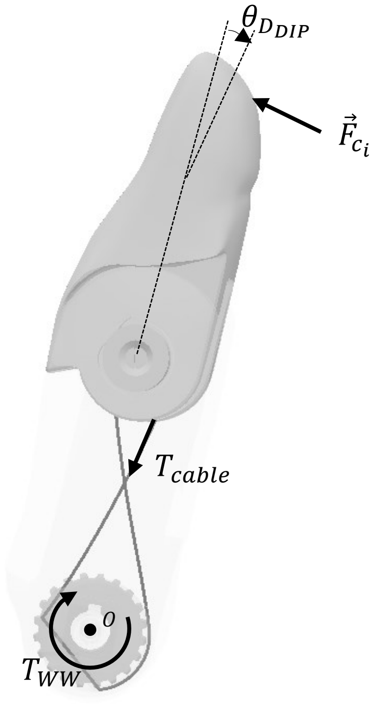

Figure 6.18: The forces that the worm wheel must be able to withstand

Hence, for each finger, the torque that the wheel would need to withstand, T_{WW}, when executing different activities was determined by considering the moments about O, which yields Equation 6.24.

$$T_{WW} = T_{D_{k_s}} + CR * T_{TC_{PIP}} \tag{6.24}$$

Where,

- $T_{D_{k_s}}$ is the torque applied by $\vec{F}_{c_i}$ about the fingers' active joint, which had been previously determined from Unity, as discussed in Section 5.3 (on p.89) but scaled according to the maximum torque that can be applied by the thumb, Nm.
- $T_{TC_{PIP}}$ is the torque created by the tension in the cable, T_{cable}, around the PIP joint, Nm. This was estimated using Equation 6.25, where the entire load, $\vec{F}_{c_i}$, was assumed to act at the end of the middle or distal phalange (depending on which phalange was in contact with the object), perpendicular to the axis of rotation of the PIP joint:

$$T_{TC_{PIP}} = (\left| \vec{F}_{c_i} \right| * l_{DP}) + (\left| \vec{F}_{c_i} \right| * cos\theta_{D_{DIP}} * l_{MP}) \quad 6.25$$

The T_{WW} that each wheel would need to sustain is shown in Figure 6.19, where one can observe that the load is usually borne by one of the fingers, with the maximum required torque being 7.80Nm.

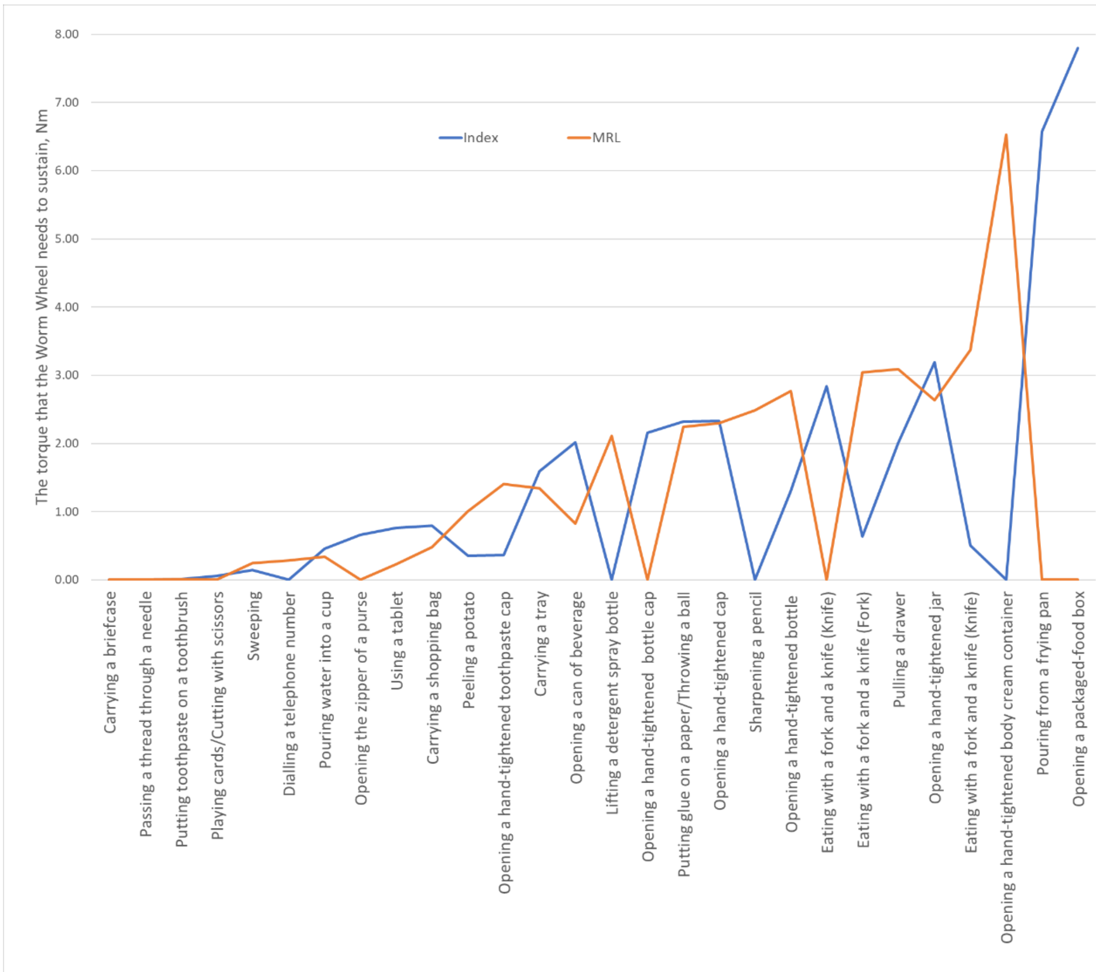

Figure 6.19: The torque that the wheel would need to withstand for each activity, distinguished by the finger

Hence, the wheel should be able to withstand a load that is more than $7.80Nm$; this can be determined using the Lewis formula for spur gears, Equation 6.16, except that Y is based on the spur gear equivalent number of teeth, z_{e_w}, which can be found using Equation 6.26 [264]:

$$z_{e_w} = \frac{z}{\sin\gamma} \tag{6.26}$$

Commercialised wheels tend to be manufactured from aluminium bronze, cast iron or nylon, which tend to have a lower σ_y when compared to other materials, such as steel. This means that larger gears are required to withstand the same load. For this reason, a search on the market was carried out to identify the wheel that could withstand the highest load given the space available and the corresponding worm. This was found to be the AG0.8-20R1[265] and the KWG0.8-R1[266], Figure 6.20, from KHK, with specifications listed in Table 6.7. Given that the wheel is manufactured from aluminium bronze, whose σ_y is $205MPa$ [267], the maximum load that it can withstand is $3.59Nm$, without any SF. While this is less than the required maximum load, a lot of the activities can still be completed, with the remaining activities being attempted with a lower grasping force and frictional covers with higher μ_s. As with the spur gears, the worm and wheel were modified by a local manufacturing company to ensure a better fit in the prosthetic hand.

(a) (b)

Figure 6.20: (a) the wheel and (b) the worm chosen [265] [266]

Table 6.7: List of specifications for the chosen worm and wheel

	Wheel	***Worm***
Model	AG0.8-20R1	KWG0.8-R1
Material	CAC702, Aluminium Bronze	SCM440, Medium Alloy Steel
Module	$0.8mm$	$0.8mm$
Number of teeth	20	1
Lead angle	86.51º	3.49º
Outside diameter	$17.63mm$	$13.6mm$
Face Width	$8mm$	/

On the other hand, the bevel gears only need to withstand the T_{Stall_F} of the motor. For a more compact design, as discussed in Section 6.3.2 (on p.135), the diameter of the bevel gear to be mounted on the worm shaft must be larger than the outside diameter of the worm. Meanwhile, the bevel gear mounted on the motor shaft must fit within the thickness of the palm. This implied that a gear down ratio was required for the bevel gears. For this reason, the gearbox of the fingers was chosen with a GR of 4 instead of 16, as the latter, in combination with the worm and wheel, which already had a GR of 20, would have required a gear up. Since the GR_{AG_F} required was then 59.51, a search on the market was carried out for a 3:1 bevel gear. However, the bevel gears available would interfere with the motion of the fingers. Hence, the required GR of the bevel gear was lowered to 2:1, since the resulting T_{m_f}, which was estimated to be $152.35mNm$, was still greater than the necessary T_{m_f} of $92.8mNm$. The resulting ω_{R_F} could then be adjusted through PWM. The bevel gears that were eventually chosen were the DB0.5-2040 [268] and DB0.5-4020 [269], a 2:1 Duracon (M90-44) bevel gear from KHK, Figure 6.21, with specifications listed in Table 6.8. Using the Lewis formula in Equation 6.1, where the tensile strength (as the σ_y was not available) was set to $62MPa$ [270], the maximum output torque that the bevel gears can withstand is $345mNm$, which yields a SF of 2.27.

Figure 6.21: The chosen bevel gears [263], [264]

Table 6.8: List of specifications for the chosen bevel gears

	DB0.5-2040	***DB0.5-4020***
Material	M90-44	M90-44
Module	$0.5mm$	$0.5mm$
Number of teeth	20	40
Face Width	$2.5mm$	$2.5mm$
Outside diameter	$11.2mm$	$20.29mm$

6.3.3.3 Finger Coupling System

A crossed-cable pulley system was used to couple the PIP joint of each finger with the corresponding MCP joint. This coupling mechanism consists of two pulleys, whose diametral ratio is defined by the CR of the two joints, and a cable, which couples the two pulleys. Given the required specifications, discussed in Section 6.3.2 (on p.135), the two pulleys were custom designed, while a search on the market was carried out to identify the cable that can withstand the required load.

The coupling mechanism must be as compact as possible. However, as the diameter of the pulleys decreases, thicker cables that can withstand higher loads will be required; these are more difficult to wrap around smaller pulleys. Hence, the diameter of the MCP pulley, $D_{MCP_{pulley}}$,which is the larger pulley, was made as large as possible by setting it to $16.6mm$, comparable to the outside diameter of the worm wheel while still allowing space for a cable of $0.5mm$ to wrap around the pulley. Consequently, the diameter of the PIP pulley, $D_{PIP_{pulley}}$, was set to $10.56mm$.

The magnitude of T_{cable} was then determined using Equation 6.27, where the $T_{TC_{PIP}}$ found in the previous section was scaled on the basis of the maximum load that the chosen worm and wheel can withstand (i.e., $3.59Nm$). In the case of the MRL finger, the T_{cable} was then assumed to be equally distributed between the two coupling mechanisms located within the finger. The T_{cable} required for each activity is shown in Figure 6.22, with the maximum tension that the cable would need to withstand being $280N$.

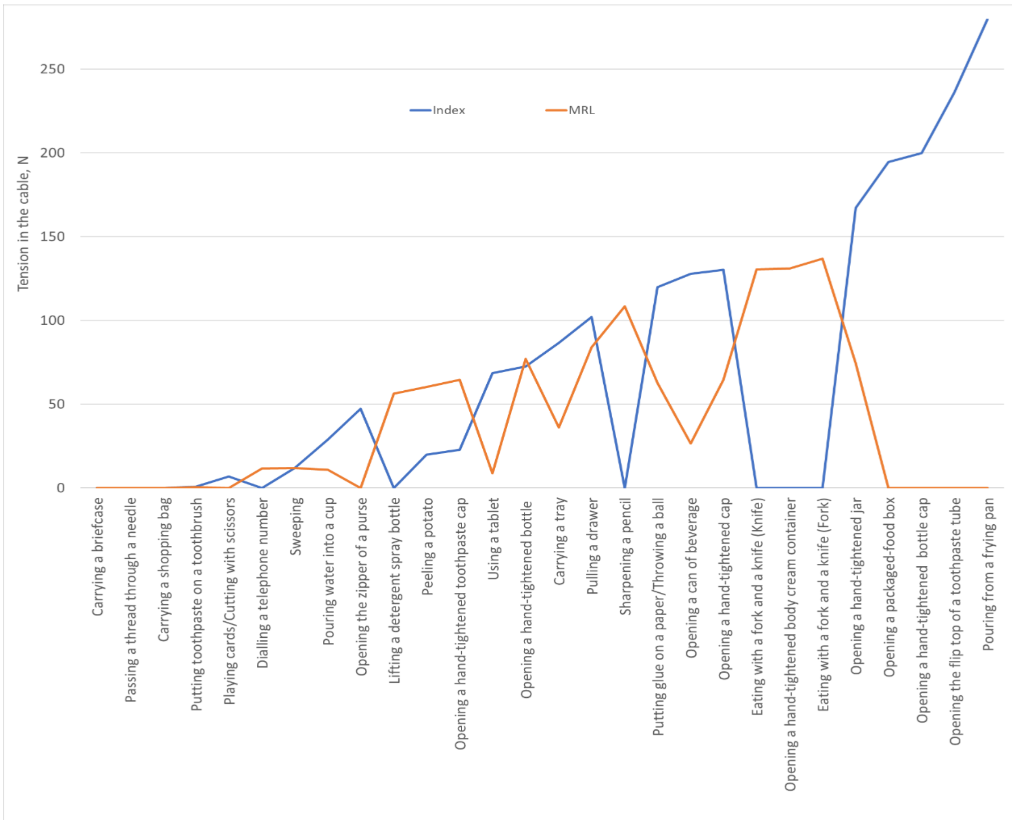

Figure 6.22: The tension in the cable for the index and the MRL finger across the different activities

$$T_{cable} = \frac{2T_{TC_{PIP}}}{D_{PIP_{pulley}}} \quad 6.27$$

The cable chosen must also be inelastic to retain the non-backdriveability of the fingers. Cables are available in different materials, such as steel and nylon, but given the high loads, Wire Leader, a steel cable typically used when fishing, was considered the most appropriate [271]. However, while there are steel Leader wires of $0.5mm$ that can withstand loads of $39kg$, such as [272], limited information is provided on their flexibility, which would dictate their ability to wrap around the pulley. For this reason, the Leader wire of $0.5mm$ was locally sourced despite it having a working load of only $22kg$. Even though this is slightly less than the required load, the cable was considered sufficient, since for most of the activities T_{cable} is less than $200N$, while in the remaining activities the loads are applied for short periods of time.

The part of the cable that does not move, relative to the pulley, during the entire motion of the finger, was then secured to the pulley through grub screws. The location of the grub screw was identified though Inventor, while also taking into consideration the accessibility of the grub screw when the prosthetic hand is assembled. The rest of the pulley, such as the clearance hole and the positive lock, was designed on the basis of the other components of the prosthetic hand. The manufacturing of these pulleys will be discussed in more detail in Section 6.4.1.1 (on p.155).

6.3.3.4 Force Feedback System

For feedback on the force applied/sustained by each digit, force sensors, placed in strategic locations within the gear trains of the thumb and the fingers, were used to measure the W_a applied by the bevel and the worm gears, respectively, on the mounting shaft. In a separate study, the varying output of the sensor is translated into different levels of vibrations in the forearm of the amputee. Hence, a search on the market was carried out for sensors that can measure the expected loads while being compact and light. High accuracy was not that critical in this application since the amputee is not able to detect small changes in the level of vibration.

There are several force sensors available on the market, with different working principles, such as optical, capacitive, and magnetic [273]. Each type of sensor has its own advantages and disadvantages, as discussed in [274]. However, for low-level force feedback, Force Resistive Sensors (FSRs) tend to be used due to their light weight, thin flexible profile, ease of use and low cost. FSRs are a piezoresistive sensing technology whose resistance varies as the force applied across it changes [275].

The maximum W_a that the FSR would need to measure was found to be $448N$ (i.e., the W_a applied by the worm when sustaining the maximum torque that it can withstand). On the basis of the required specifications, the FlexiForce ESS102 Sensor [276], Figure 6.24, from Tekscan, was chosen. This small sensor can measure a maximum force of $444.8N$; loads below $510N$ can still be applied without damaging it, even if the output sensor will be saturated.

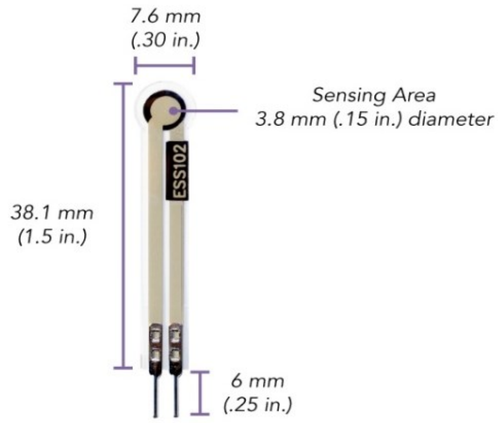

Figure 6.23:Tackscan FlexiForce ESS102 Sensor [276]

The FSRs were then placed within the gear trains, as shown in Figure 6.23, taking into consideration the direction of the W_a being measured. From this figure, one can observe that the FSR was kept in place by an FSR holder, while a shaft bearing surface was used as an interface between the shaft and the FSR. This not only prevented the shaft from rotating directly on the surface of the FSR, but also ensured that the force

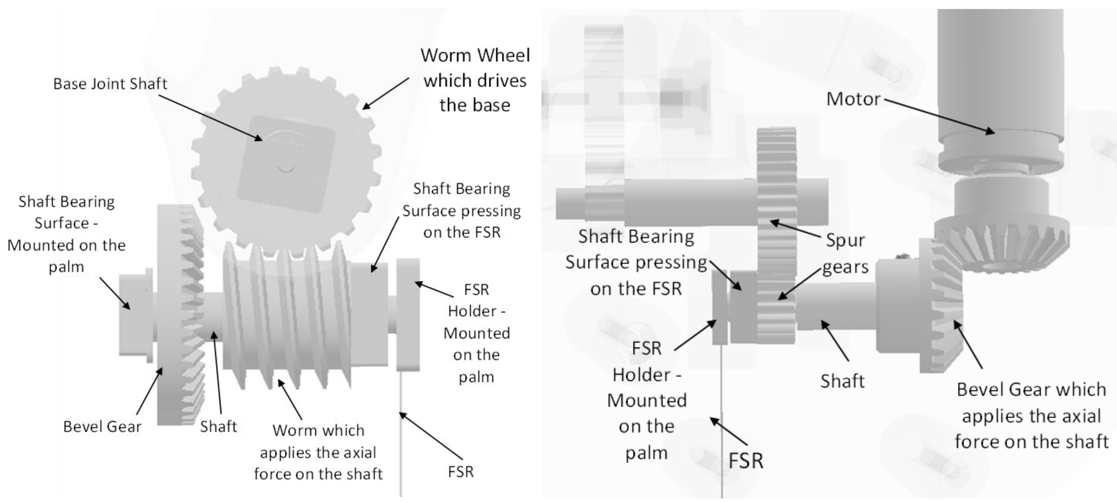

(a) (b)

Figure 6.24: The position of the force sensor within (a) the finger gear train and (b) the thumb gear train

is evenly distributed, especially for cases where the shaft diameter is larger than the sensing area. Both the FSR holder and the shaft bearing surface were custom designed to fit the required specifications. The manufacturing of these parts will be discussed in more detail in Section 6.4.1.1 (on p.155).

6.3.4 Developing a mesh model of an anthropomorphic hand

Once the embodiment design was finalised, a more realistic mesh of the hand, as discussed in Section 6.3.2 (on p.135), was developed.

This required modelling complex curvatures which were beyond the capabilities of Inventor. Thus, a more dedicated computer graphics software, such as Blender [277], which is typically used for animated films and art, was required. For this reason, th, which is typically used in animated films and art, was required. For this reason, the mesh model was developed in collaboration with Mr. Fabrizio Cali (a visiting lecturer from the Faculty of Media and Knowledge Sciences, specializing in Blender) on the basis of the required specifications. Boolean modifications to the mesh, such as adding supports for the different components and creating holes for the cable, were then implemented in Inventor. The developed hand model and the corresponding proto-grasps are shown in Figure 6.25.

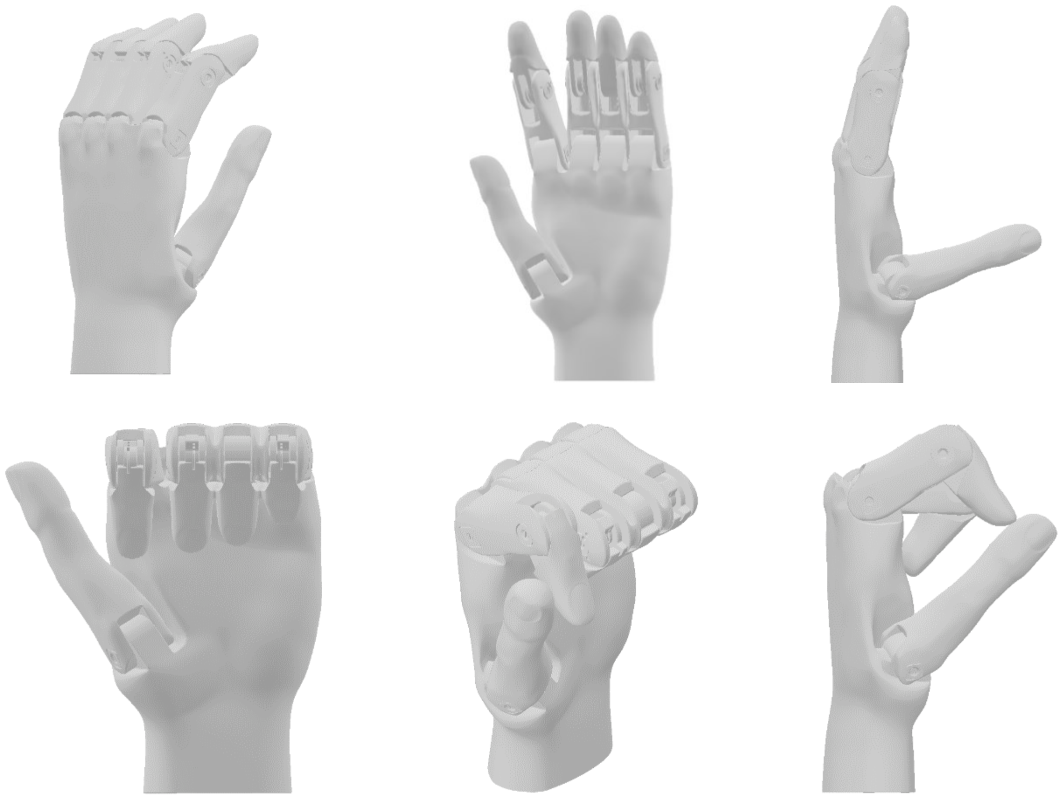

Figure 6.25: The developed mesh model actuating the different proto-grasps, excluding the indentations on the outside surface to cover the prosthetic hand with a material having a high friction coefficient

6.4 DETAILED DESIGN AND CONSTRUCTION

6.4.1 Selecting the material and the manufacturing process for the specific parts of MAProHand

6.4.1.1 Manufacturing the parts designed for MAProHand

While most of the hand components were readily available on the market, all custom-built parts, namely, the structure, the interface keys, the pulleys, the shafts, the FSR holder and the shaft bearing surface, obviously had to be manufactured. The manufacturing process, as well as the material chosen for each part depend on the required properties, taking into consideration the ease of manufacturing.

In general, the parts must be rigid and able to withstand the maximum loads applied on them, while also being lightweight, compact, and cost effective. Given the size and/or complexity of some of the custom-built parts, manufacturing these parts using subtractive processes, such as milling, can be time consuming and expensive. For this reason, all of the custom-built parts, except for the shafts, were 3D printed (based on the requirements discussed in Chapter 3 (on p.44)).

Understanding the stress present in each of the parts then allows the optimization of any unconstrained parameters of the part (e.g., its thickness), as well as the selection of an appropriate material to best satisfy the required properties. However, while the maximum bending/shear stress present can be easily determined for a simple part (e.g., a shaft, as discussed in Appendix G (on p.238)), the behaviour of complex parts under load will have to be simulated using a Finite Element Analysis (FEA) software, such as Ansys [278]. Even then, FEA models a part as a uniform homogeneous solid, which is not a realistic representation of the porosity, as well as the anisotropic property of 3D-printed parts [279]. In fact, a huge discrepancy was observed by Abbot et. al. [280] when comparing the simulated and the actual result in a series of compression tests. Consequently, the strength of the 3D-printed parts (which were designed to have a reasonable thickness of around $3mm$ all round) was made as high as possible, especially in areas which would need to withstand the highest loads, while keeping its weight to a minimum. Thus, wherever possible, small parts, namely, the FSR holders and shaft bearing surfaces, were integrated in the structure of the palm to strengthen the overall design.

The most common 3D printing process for quick and low-cost prototyping is Fusion Deposition Modelling (FDM), with a wide range of materials (also known as filaments) available, such as PLA and ABS, which are continually evolving to produce stronger and lighter parts. FDM is an additive manufacturing process in which a continuous thermoplastic or composite material is fed through a heated nozzle and extruded layer by layer onto the build platform in a predetermined automated path, Figure 6.26(a) [281]. This path, as well as the support necessary to print the part with a certain orientation, is generated in a slicer program, such as Cura [282] and Creality Slicer [283], which converts a 3D model file (e.g., STL) into a G-code script that can be interpreted by the firmware of the printer. The printed part consists of an infill surrounded by the walls and the top and bottom layer, Figure 6.26(b), with higher strength along the layers than across them [284]) [285]. This is because tension applied normally to the layers relies on the bonding strength between the layers rather than the strength of the printing material. Parts printed with FDM may also be susceptible to visible layer lines and/or blemishes on the surface, especially when nozzles with a larger diameter are used. However, given that the prosthetic hand does not have any fine and/or intricate details, the low resolution of the 3D-printed parts should not be an issue to its overall function [32], [33], [34].

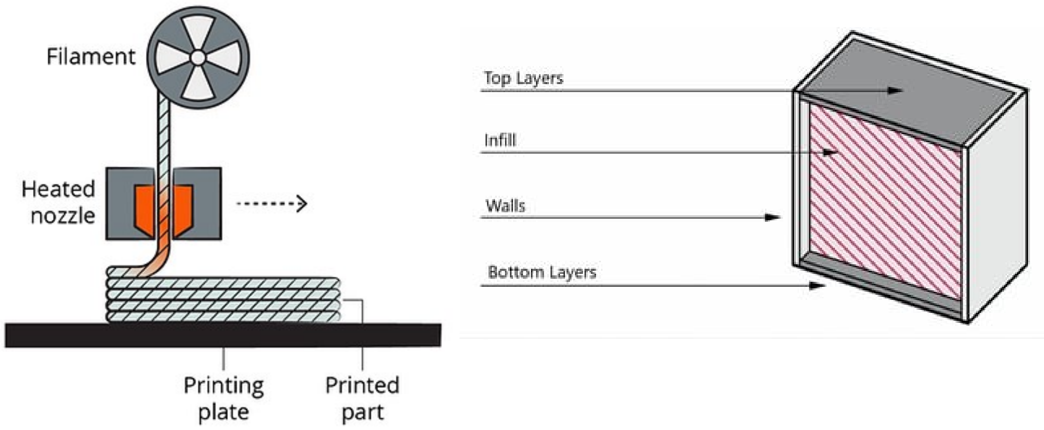

(a) (b)

Figure 6.26: (a) The working principle of FDM [281] and (b) a schematic of a 3D-printed part [284]

A search on the market was carried out to identify the filament with the highest strength, provided that the density of the different filaments was relatively similar. The filament that was chosen was Nylon Power Carbon Fiber from Prima Creator Select [289], based on a Nylon12 filament reinforced with 20% carbon fibre. It is an extremely tough filament suitable for parts used in remote control cars and the automotive industry [289]. However, a nozzle diameter of $0.6mm$ or higher is recommended with this filament to minimise the risk of clogging and nozzle wear due to the carbon fibre. While this is not an issue for larger parts, such as the phalanges, smaller details, such as the holes in the pulleys, become more challenging to print. Hence, the pulleys were instead printed from Polylactic Acid, PLA [290] (a common material typically used for prototyping that has adequate strength) with a nozzle diameter of $0.4mm$. The specifications for both Nylon Power Carbon Fiber and PLA are listed in Table 6.9.

Table 6.9: Specifications of Nylon Power Carbon Fiber [289] and PLA [290]

Property	***Nylon Power Carbon Fiber***	***PLA***
Printing temperature	$250 - 265°C$	$180\text{-}210°C$
Heated build platform	$60 - 70°C$	$60 - 70°C$
Density	$1.00g/cm^3$	$1.03g/cm^3$
Tensile Modulus	$6000MPa$	$2000MPa$
Tensile Strength	$100MPa$	$44MPa$
Heat Deflection Temp	$155°C$	/

Due to the inherent anisotropic property of FDM printed parts, the strength of the part, in the direction that will exhibit the highest stress, can be optimised by orienting that direction parallel to the printing bed, as shown in Figure 6.27 (a). However, printing in this orientation generates a lot of support, which can be challenging to remove from tighter areas, especially if the support is printed from the same material, which tends to form a stronger bond with the part. For this reason, the supports were instead printed from PrimaSelect PVA High Temperature [291], Figure 6.27(b), a material that dissolves in water.

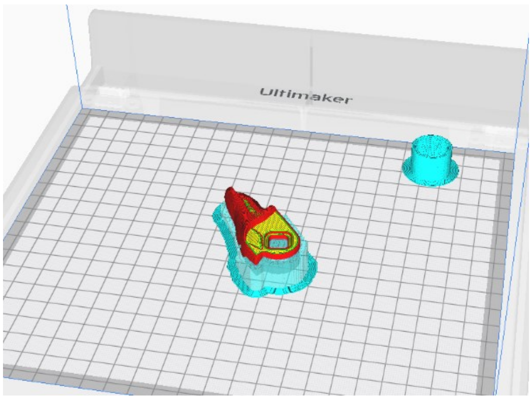

(a)

(b)

Figure 6.27: (a) Simulation in Creality Slicer of one of the 3D-printed parts printed with the shaft suppports oriented parallel to the printing bed and (b) the printing of a part with dissolvable supports

The printing of these parts was outsourced to a local 3D printing company with an FDM printer having two nozzles that can withstand the necessary printing temperatures. Given that Nylon Power Carbon Fiber tends to absorb moisture at room temperature, which may negatively influence the consistency and the accuracy of the

3D-printed part, the filament was dried before and during the printing process, which was also carried out in an enclosure.

Apart from the material and part orientation, there are other factors that play a role in the strength of the part, namely 3D printing settings. Thus, these settings were adjusted to optimise the strength-to-weight ratio of the parts, especially larger parts, such as the palm, which would significantly contribute to the overall weight of the prototype. Common slicer programs, such as Creality Slicer [283], allow the user to modify various printing settings, such as the infill density and the wall thickness. The following settings have the greatest impact on the strength and the weight of the parts:

- *Infill density*: This refers to the amount of material present on the inside of the part. It ranges from 0% to 100%, with 0% meaning the part is completely hollow and 100% meaning the part is solid, and thus, much stronger. However, depending on the size of the part, it is usually not recommended to increase the infill density beyond 70%, since the gain in strength does not outweigh the material usage, printing time and cost [292], [293]. For standard parts, the recommended infill density is 20-25% [294].
- *Infill pattern:* This refers to the shape and structure of the material inside the part. There are different infill patterns available, Figure 6.28, such as grid, tri-hexagon and cubic [295]. One of the strongest infill patterns is the cubic pattern. It consists of stacked cubes rotated by 45° in the plane of the printing bed, making it suitable for functional parts which require strength in all directions [296], [297].

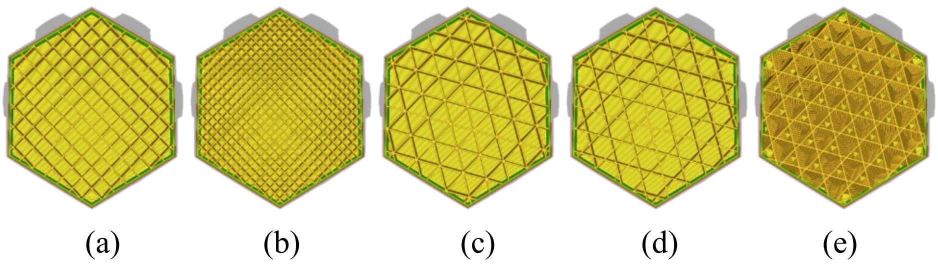

Figure 6.28: Some of the infill patterns available: (a) Grid, (b) Lines, (c) Triangle, (d) Tri-hexagonal and (e) Cubic [295]

- *Layer Height:* This refers to the height of each layer, with thinner layers usually yielding models with a smoother and finer surface finish. However, there are some opposing views on which parts are stronger. On one hand, thinner layers imply a shorter distance between the nozzle and the previous layer, which not only warms up the previous layers, but also squishes the filament on it, creating a better bond. Given that there is less gap between the layers, parts with thinner layers can also be denser. On the other hand, thicker layers imply that the strands have a larger cross-section [298], [299]. Furthermore, there is a lower risk of a defect in one of the layers which would lead to part failure [298], [299]. For this reason, an experiment was carried out in [300] which examined the strength of a part printed in various layer heights. It concluded that parts printed with thinner layers had a higher tensile strength.

- *Shell thickness*: This refers to the thickness of the exterior shell of the model, which consists of the walls and the top and bottom layers. For moderately strong parts, a wall thickness of 0.8-1.6mm, and a top-and-bottom layer of thickness 0.8-1.2mm, are recommended [284]. However, the wall thickness must be a multiple of the nozzle diameter, while the thickness of the top and bottom layers are a multiple of the layer height. Depending on the size of the part, a thicker shell can significantly contribute to its overall weight.

Given that each part could not be printed with different settings and tested, the settings that best optimise the strength-to-weight ratio of a part were based on the observations made in the literature, while using the weight estimated in Creality Slicer as guidance. Therefore, the thinnest recommended layer height for a nozzle diameter of $0.6mm$ was chosen, which is 25% of the nozzle diameter (i.e., $0.15mm$) [301], even if it increases the printing time. Given that parts experience higher strain on the outside surface compared to the inside, a thicker wall has a greater impact on the mechanical strength of the model than the infill density [302]. A thicker shell is also beneficial when filing the parts to the required tolerance, so as not to expose the infill. Hence, for larger parts, the walls were $1.2mm$, with the thickness of the top and bottom layers set to $0.9mm$. A 10% cubic infill was then used to keep the weight of the part to a minimum, with areas around the shaft, which are expected to withstand high stress concentrations, reinforced with an infill density of 50%. Meanwhile, smaller parts, such as the interface keys, were printed with 100% cubic infill since these parts consisted mainly of the shell.

A simple test was then carried out on the index finger, as discussed in Appendix H (on p.242), to verify whether it would be able to withstand the required loads. It revealed that while the structure could withstand the load applied on it, some deformation was observed in the interface keys. Alternatively, Direct Metal Laser Sintering, another form of additive manufacture for metal parts, could be used. However, the material is more expensive and like any other 3D printers, the tolerance of the parts would need to be finetuned. Therefore, for this prototype, FDM was still considered acceptable for the interface keys, especially since they can be easily replaced, if damaged.

Meanwhile, the shafts were manufactured by the Department of Industrial and Manufacturing Engineering at the University of Malta on the basis of the engineering drawing created for each part. An example of one of the engineering drawings is shown in Figure 6.29, which is the drawing for the MRL MCP shaft. The diameter of these shafts was highly dependent on the bore diameters of the purchased gears and the design of the positive lock, which meant that there was not a lot of room for optimisation. A material, well known for its high strength-to-weight ratio, that is readily available was then chosen; this was Aluminium 7075. It has a yield strength of $503 MPa$ and shear strength of $331 MPa$ [303], which exceeded the minimum strength required by the shafts. However, the MRL PIP shaft had to be manufactured from steel due to the difficulty encountered in manufacturing the part, given the tools available, the raw material, and the dimensions of the part.

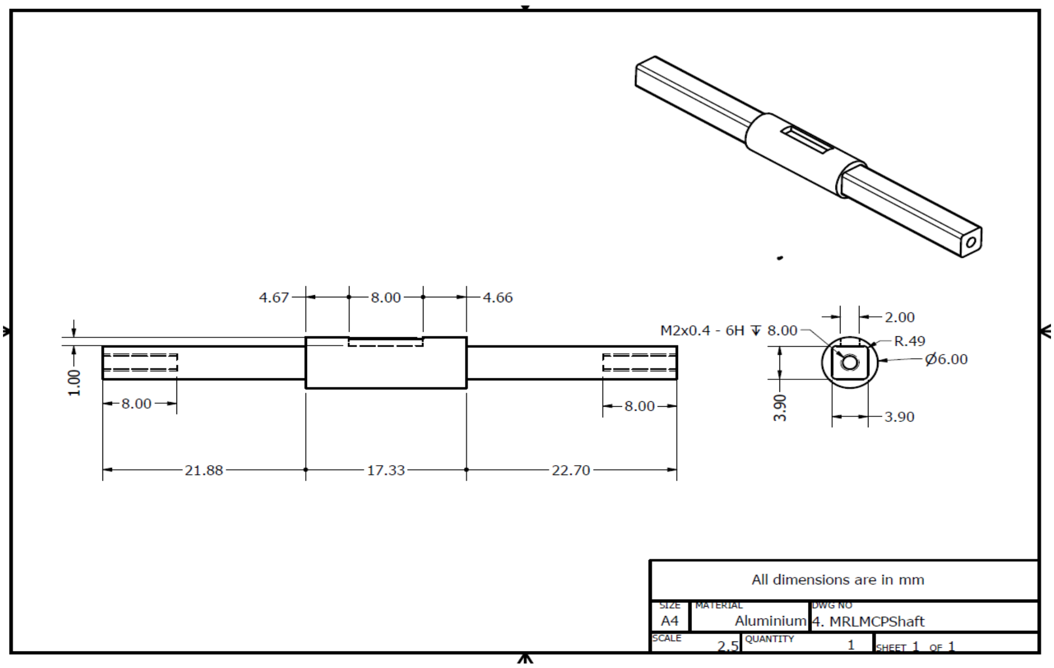

Figure 6.29: Engineering drawing of the MRL MCP shaft

6.4.1.2 Manufacturing the frictional covers

The purpose of the frictional covers was to increase the hand surface friction coefficient, as well as to increase the surface area in contact with the object. Hence, the material chosen for the frictional covers must not only have a high friction coefficient with different day-to-day materials, it must also be flexible, to conform to the shape of the phalange, and soft, to allow the contact area to slightly deform under the load.

Rubbers are typically used for such applications due to their high static friction coefficient with various other materials [304]. Different rubbery materials were considered, such as rubber foam sheets used for crafts, non-slip mats, latex gloves, and packaging rubber. The latter, with a thickness of $3mm$, Figure 6.30(a), was chosen as it deformed easily, without being too stiff, and had a good grip. In fact, the experiment discussed in Appendix H (on p.242), revealed that μ_{rubber}, the friction coefficient between this rubber and different materials used in everyday activities, such as wood, plastic and glass, ranged from 0.75 to 1.19. This is higher than the μ_s assumed during the force analysis discussed in Section 5.3 (on p.89), which was 0.5. Therefore, the frictional force present between the object and the hand would be higher than estimated. In fact, Figure 6.31 shows that considering only the lowest end of μ_{rubber}

(a) (b)

Figure 6.30: (a) Packaging rubber and (b) Moulds for the frictional covers

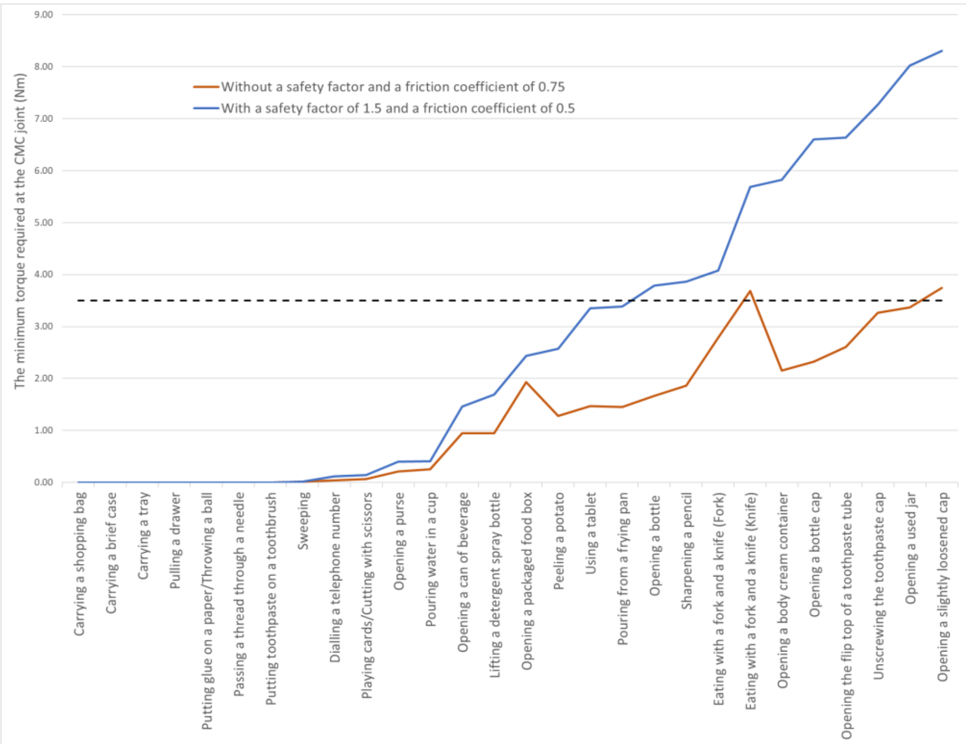

Figure 6.31: The effect that a higher μ_s and a lower SF has on the minimum torque required at the thumb CMC joint, $\overrightarrow{T_{m_T}}$, for the different bimanual activities

and a lower SF, most of the activities can still be executed, despite the reduction in T_{m_T}. However, while μ_s was a conservative value, not all the surface of the prosthetic hand could be covered in rubber, as discussed in Section 6.3.2 (on p.135); this is why the μ_s of 0.5 was a fair assumption.

The rubber was then cut into the required shapes using moulds of each dent, Figure 6.30(b), which were printed in PLA using FDM printer. The edges of the rubber were then chamfered using a pair of scissors to ensure that the covers were flush with the rest of the part.

6.4.2 Construction of the Prototype of the Prosthetic Hand

The next step was to assemble all the different components as shown in Figure 6.32 to Figure 6.35.

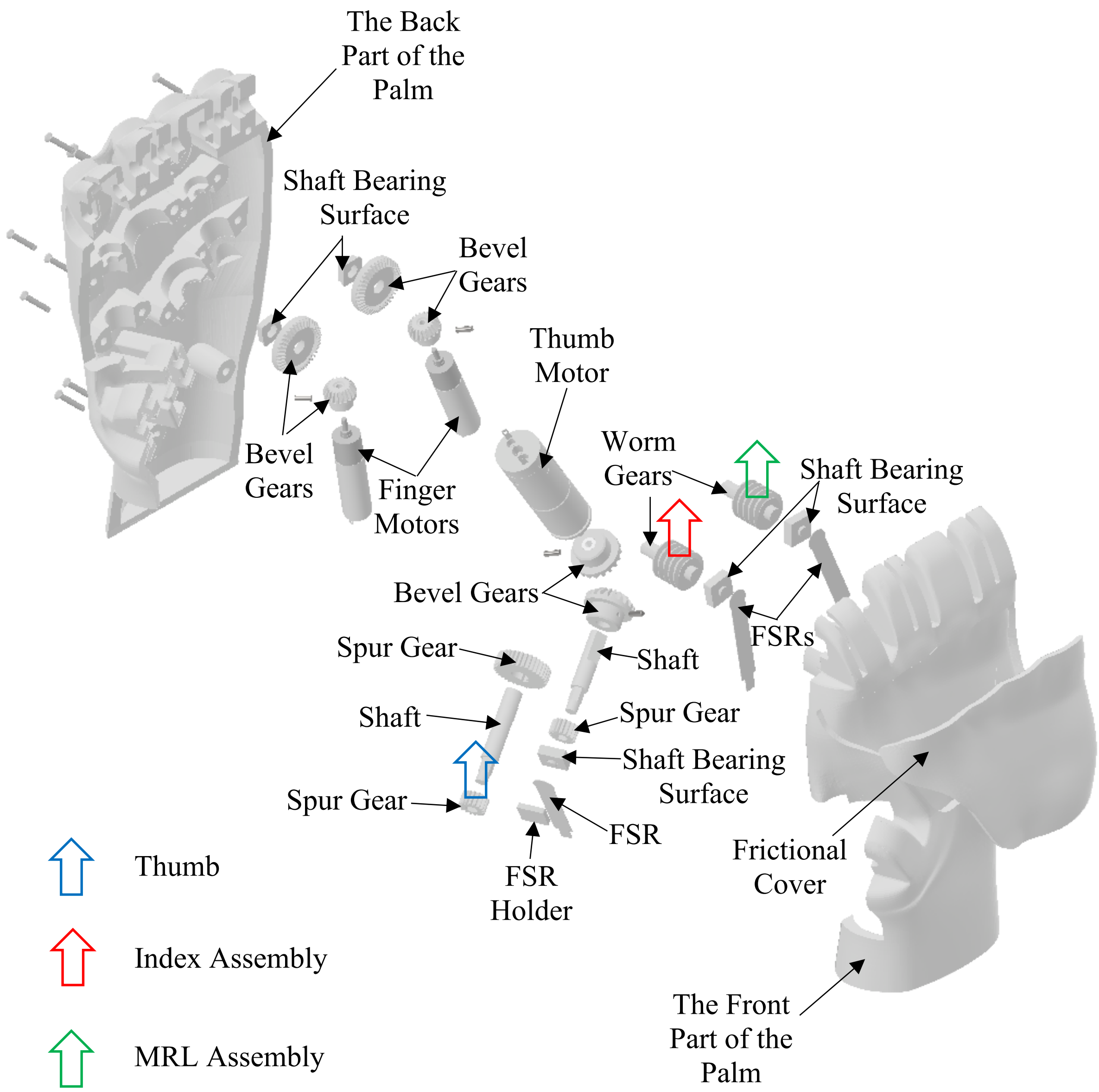

Figure 6.32: Exploded view of the palm

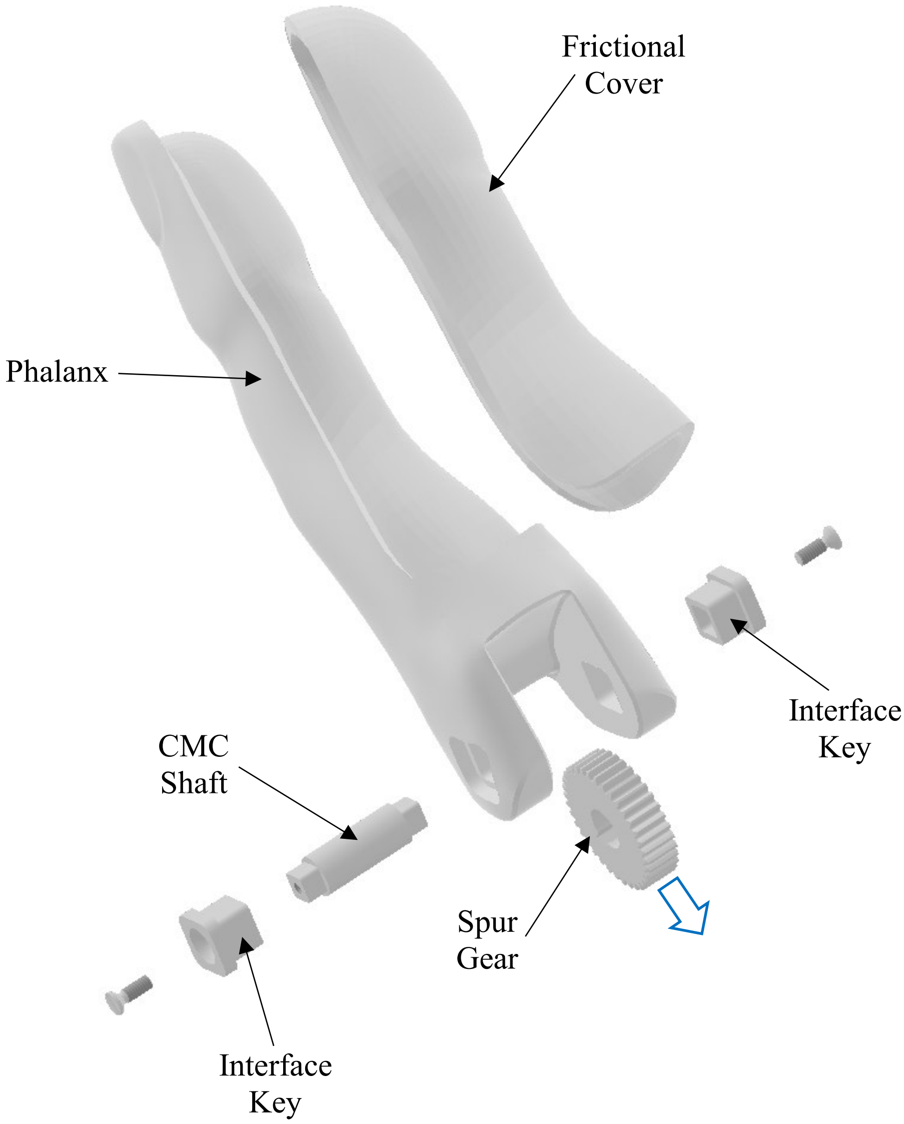

Figure 6.33: Exploded view of the thumb

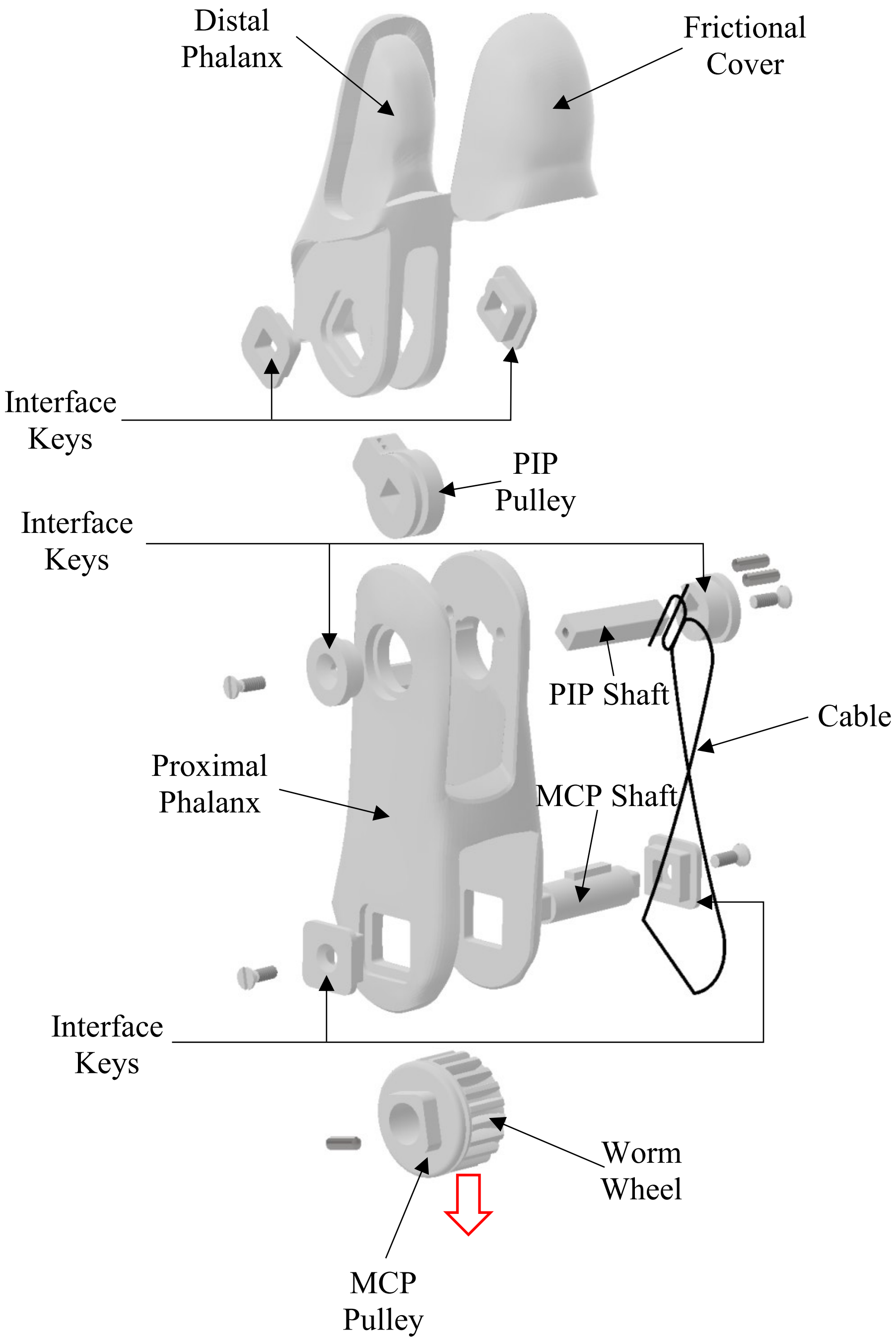

Figure 6.34: Exploded view of the index finger

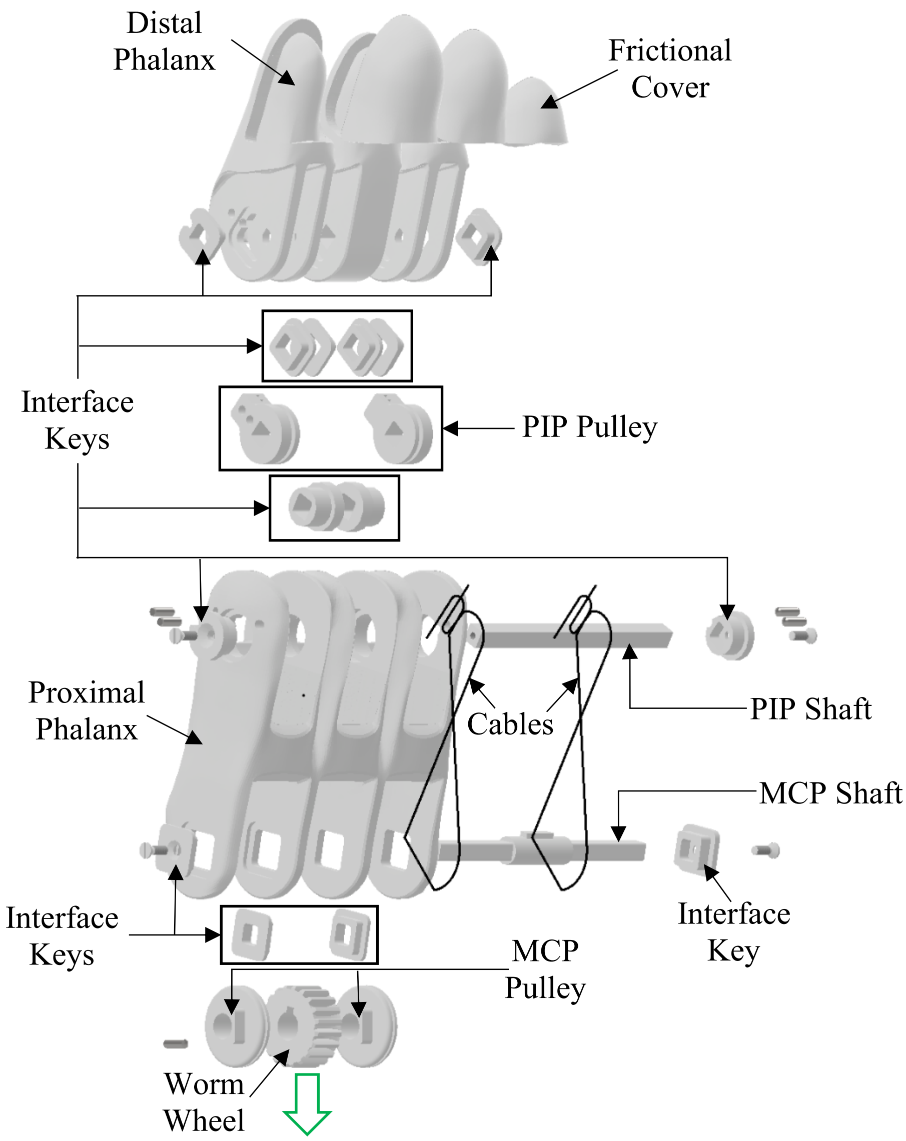

Figure 6.35: Exploded view of the MRL finger

While the necessary precautions were taken to ensure ease of assembly and overall performance of the prosthetic hand, challenges might still arise. Therefore, the prototype was first printed in the laboratory, using PLA, to identify these challenges and modify the design accordingly before printing the final parts. For example, it was noted that the original orientation of the index motor complicated the assembly of the palm, so, it was altered together with the split of the palm. Other changes included the addition of more screws on the palm that were closer to the joints of the fingers. This minimised the separation of the two halves of the palm due to the loads applied on the shaft. The clearance between two moving parts was also increased.

Once the design was finalised, the parts were 3D-printed as discussed in Section 6.4.1.1 (on p.155). However, before assembly, they had to be filed down to minimise the friction present between the different moving parts, since the accuracy of the parts varied from one printer to another. Friction also arose due to the screws pressing the two halves of the palm against the different components. This friction hindered the movement of some of the components, especially the worm shaft, which lies along the thickness of the palm without any axial bearings, but this friction was necessary to keep certain components in place, particularly with regards to the motors due to their circular shape. Hence, as a compromise, a thin layer of rubber was added to the surface of the motor supports to increase the friction present between the motors and the palm. Given that the screws of the prototype would then need to be screwed and unscrewed several times, which could potentially damage the 3D-printed threads, heat-threaded inserts were used to create the threads for the screws. Thus, the inserts were heated and gently pushed into the part where the thread had to be. This deformed the part around the thread, which created a strong bond with the 3D-printed part. The same approach was not applicable to the threads of the grub screws due to the size of the heat-threaded inserts; in that case helical threads were used to reinforce the 3D-printed threads. Meanwhile, the frictional covers were glued to the corresponding part using Pattax, a heavy-duty glue. The moulds shown in Figure 6.30(b) were then used to keep the rubber in place while the glue dried.

The gears, the motors and the digits were then placed in the palm in the correct order and the two halves of the palm screwed together, where each digit had been assembled prior to this process. In the case of the fingers, the jig in Figure 6.36 was then used to tighten the cables of the coupling mechanism. The jig consisted of a guitar-tuning chord attached to one of the ends of the cable which had only been passed through the lower hole of the PIP pulley (Figure 6.9(b) (on p.139)), while the cable was held in

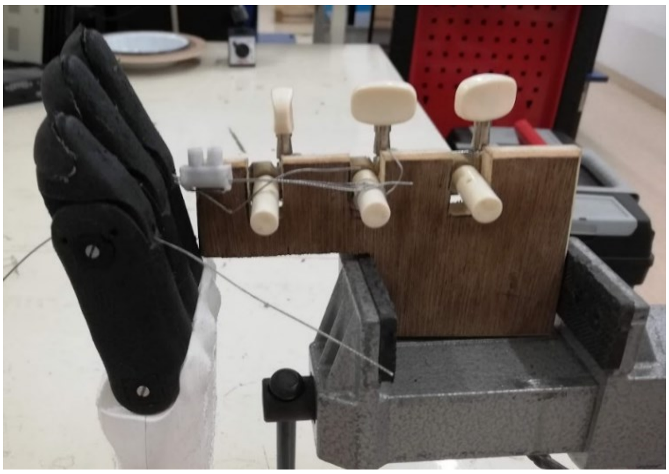

Figure 6.36: The set-up used to tighten the cables of the coupling mechanism

place with the grub screw located on the MCP pulley. This grub screw was kept in place during the entire retightening process to avoid weakening the cable due to the dents created by the grub screws. Hence, as the guitar-tuning chord was rotated, the cable was tightened on one side. Once the required tightness had been achieved, the end of the cable secured by the jig was passed through the top hole of the PIP pulley and secured in place with the grub screws. The entire process was then repeated with the other end of the cable.

The constructed prototype of MAProHand is shown in Figure 6.32 .

Figure 6.37: Assembly of MAProHand

CHAPTER 7: EVALUATION OF THE APPROACH AND THE PERFORMANCE OF MAPROHAND

7.1 INTRODUCTION

This chapter undertakes a detail examination of the approach and overall performance of MAProHand. The assessment delves into the general characteristics of MAProHand and the functionality of the PMs, exploring its effectiveness beyond the representative bimanual activities. A comparative study is also conducted to assess the performance of MAProHand in comparison to both the human hand and other prosthetic hands. The overall goal of this chapter is to provide a comprehensive understanding of the capability and performance of MAProHand within diverse contexts.

7.2 GENERAL CHARACTERISTICS OF MAPROHAND

MAProHand is a prototype of a medium-sized prosthetic hand that optimizes the balance regarding simplicity, dexterity, and usability by utilizing the postural synergies of the non-dominant hand in the minimal anthropomorphic condition as the foundation. The balance of these three attributes is discussed in this section with reference to the specifications mentioned in Chapter 3 (on p.44).

The developed prosthetic hand is relatively simple with only five joints, of which only three are independently actuated; the other two joints are coupled. Given the simplicity of the kinematic hand model, the number of actuators and gears required was minimal. This not only increased the reliability of the overall prosthetic hand (as there were fewer parts that could potentially fail) and kept its cost, heat and noise level to a minimum, but also facilitated the embedment of the actuation/transmission system and the coupling mechanism in a device of the same size and weight of the human hand. In fact, the developed prosthetic hand weighed $428g$, with an overall length of $195mm$, a width of $135mm$ (including thumb), and a maximum thickness of $35mm$, which was comparable to large/medium prostheses and human hands, as shown in Figure 7.1. Even though the prosthetic hand is slightly heavier than the desired weight of $400g$, the fact that it only has three motors allows room for a lighter version with further optimization, especially in the 3D-printed parts. The overall noise level generated by the prosthetic hand is $26dB$ with reference to the standard threshold hearing level for the human ear, equivalent to a whisper, the cost of its construction was 3,600Eur, well below the mentioned cost of 5,000Eur.

Figure 7.1: Size comparison between a human hand and MAProHand

Despite the significant reduction in dimensionality when compared to the twenty-one DOFs of the human hand and the nine DOFs of the minimal anthropomorphic hand, the prosthetic hand was able to execute four distinct PMs and the corresponding proto-grasps, as modelled in Unity, Figure 7.2, where each of the PMs can correspond to a reliable and intuitive sEMG signal, enhancing the usability of the device.

However, since the prosthetic hand had no positional feedback, achieving the same proto-grasps in various hand orientations was a challenging task, especially since the angular speed of the index and the MRL fingers was highly dependent on the orientation of the prosthetic hand, with the angular speed being lower in orientations where gravity works against the motors. In fact, while the desired angular speed of the fingers was $126°/s$, it varied from $175°/s$ to $203°/s$ for the index finger, and from $92°/s$ to $158°/s$ for the MRL finger, with the MRL motor not being able to close the fingers completely when the digits pointed vertically downwards (e.g., when grasping a shopping bag). One of the main contributing factors to this was the friction present between the moving parts despite the efforts taken to minimize it, such as filing the parts down, using lubrication and loosening the cables of the coupling mechanism.

This issue could be resolved in future improvements which tackle the friction present between the fingers. However, by exploiting the time constants and delays used during the actuation of each PM, which were mentioned in Section 6.3.1.1 (on p.122), the required interaction between the digits, especially in the S-grasp and the P-grasp, could

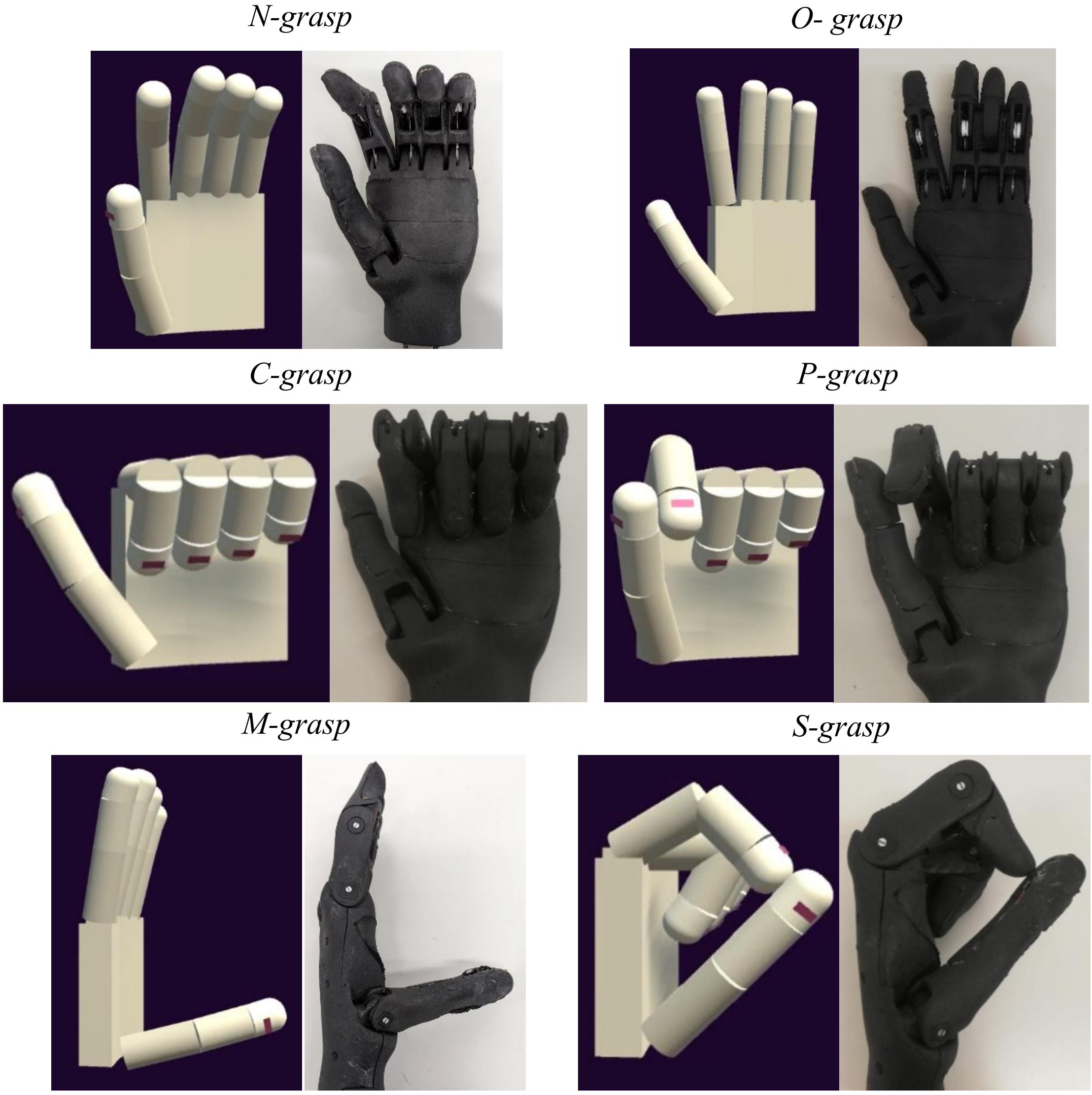

Figure 7.2: The proto-grasps

still be achieved regardless of the orientation of the prosthetic. For example, in the case of the O-M-S PM, the thumb, whose angular speed was more consistent in different orientations, was moved to the desired location first so as to be able to stop the motion of the fingers in the required position. If this was not possible, as in the case of the O-P PM, where the index finger had to move first to facilitate the approach of task objects, appropriate time constants were introduced to ensure that the index finger interacts with the thumb in all the different orientations. Meanwhile, the closing of the MRL finger when the digits are pointing vertically downwards was not that critical since this orientation is mainly used to carry objects, such as a briefcase. In that case, using the intact hand, the object can be grasped in an orientation more favourable for the prosthetic hand before orienting the same object in the vertical direction. The time taken to complete each of the PMs in the different orientations is averaged across three different times and listed in Table 7.1.

Table 7.1: The duration of each PM in different possible orientations

	O-N-C (s)	***O-P (s)***	***O-M-S (s)***
Palm facing up	3.76	3.72	4.40
Hand facing sideways	3.58	3.48	4.32
Palm facing down	3.59	3.47	4.23
Hand facing sideways with finger pointing up	3.56	3.62	4.20
Hand facing sideways with finger pointing down	/	/	/

On average it took around $3.8s$ for the prosthetic hand to complete the closing hand PMs. This was mainly dictated by the angular speed of the thumb, which was set to $43°/s$ (i.e., 50% of the maximum allowable PWM) to allow sufficient time for the amputee to place the task object within the workspace of the hand. As the amputee then gains experience using the prosthetic hand, with the digits moving first providing visual cues on where the object should be placed relative to the hand, the angular speed of the thumb can be modified according to the amputee's needs. During the execution of each of these PMs, the digit whose movement was constrained by the object was stopped, while the other digits kept on moving, permitting the hand to conform to objects of different shapes and sizes.

The force applied by the prosthetic hand on the gasped object is dictated by the amputee, on the basis of the intensity with which the muscles are recruited in the forearm. The user has four different levels to choose from, namely, no, low, medium, and high force. The force that is applied by the thumb on the object in the closing (i.e., when moving away from the O-grasp) and opening (i.e., when moving towards the O-grasp) directions was determined for when either one of these force levels is selected. The set-up in Figure 7.3 was used, where a spring balance, perpendicular to the joint axis at a distance of $70mm$, was used to measure the force required to stop the thumb.

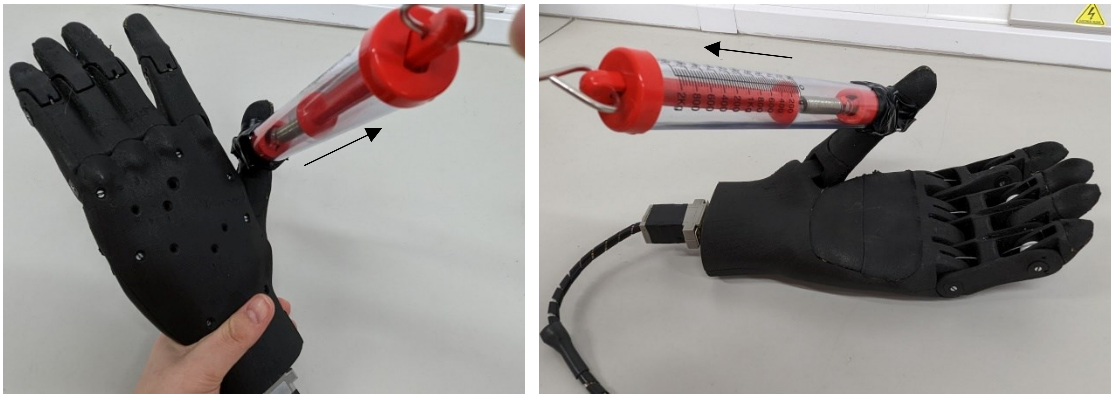

(a) (b)

Figure 7.3: The set-up used to determine the torque applied by the thumb in (a) closing and (b) opening direction

This was noted in Table 7.2. and compared with the theoretical output torque, assuming η_{AG_T} to be 73% as mentioned in Section 6.3.1.2 (on p.126).

Table 7.2: Comparison between the theoretical and measured torque applied by the thumb in the opening and closing directions for the different force levels available

Force Level	*PWM (%)*	*Measured Force (N)*	*Measured Torque (Nm)*	*Theoretical Torque Applied (Nm)*	*Percentage Error (%)*
			Closing Direction (e.g., O-P)		
Low	37.5	6.88	0.48	1.24	61
Medium	50	9.32	0.65	1.66	61
High	75	11.76	0.82	2.49	67
			Opening Direction (e.g., O-M-S)		
Low	37.5	6.52	0.46	1.24	63
Medium	50	9.46	0.66	1.66	60
High	62.5	11.84	0.83	2.07	60

From the above table, one can observe that the maximum force applied by the thumb in both directions was around $11.8N$, with the maximum output torque applied being around $0.83Nm$. This is less than the estimated torque of $3.21Nm$, which is due to several reasons.

First and foremost, one can observe, from Table 7.2, that the PWM for the highest force level did not correspond to 100% (i.e., the maximum allowable torque that can be applied by the thumb motor). This was because the resulting torque applied on the object caused the thumb mechanism not to perform as intended, with the two halves of the palm pulling away from one another, which was enough for the gears in the transmission system to pull apart and unmesh. Thus, future prototypes should have the two halves of the palm snap on top of each other instead of being tightened together with screws.

Still, the margin of error noted in Table 7.2 was still significant in both directions. Thus, while experimental errors might have been observed, such as human sensitivity and parallax errors, the discrepancy in the output torque applied is highly attributable to the inefficiencies of the circuitry and the mechanical design. In fact, when the motor was assembled, I_{stall_T} was observed to be significantly less than the one specified in the motor datasheet (later confirmed by connecting the motor directly to the power supply), indicating an increased resistance across the circuitry of the motor, which reduces its overall performance. The error due to the circuitry was calculated and noted in Table 7.3 by computing the percentage difference between the I_{stall_T} obtained from the datasheet and the one observed in the palm, and assuming that the relationship between I_{stall_T} and the output torque of the motor remains the same. This table shows that the circuitry contributed a significant part of the overall error, with higher resistance present in the closing direction and lower duty cycles. Meanwhile, the error due to the mechanical design, noted in Table 7.3, was calculated by computing the percentage difference between the measured torque and the theoretical torque applied on the basis of the observed I_{stall_T}. For most of the cases, the percentage error was observed to be around 41%, which indicates that the transmission system had an efficiency lower than 73% (i.e., the efficiency assumed during calculations). This was due to the friction and/or wear present. For the low and medium force levels in the closing direction, experimental errors may have played a more crucial role since the theoretical tangential force was going to be smaller.

Table 7.3: Breakdown of the overall percentage error for the thumb

Force Level	***Duty Cycle (%)***	***Circuitry Percentage Error (%)***	***Mechanical Percentage Error (%)***	***Overall Percentage Error (%)***
		Closing Direction (e.g., O-P)		
Low	37.5	70	-27	61
Medium	50	60	3	61
High	75	44	40	67
		Opening Direction (e.g., O-M-S)		
Low	37.5	41	38	63
Medium	50	30	43	60
High	62.5	27	46	60

As the thumb applied the required force on the object, it was observed that the position of the fingers was not retained, until the backlash (e.g., the play between the different gears) and elastic deformation present in the fingers was taken up and/or the movement of the thumb was constrained. During this process, the movement of the distal phalanx was not necessarily coupled with that of the proximal phalanx, mainly due to the cable not being tight enough. This introduced another form of compliance in the fingers, but there was also the risk that, depending on the shape of the object, the number of contact points would be reduced or moved to a less stable grasp. In that case, an alternative grasp, if possible, would have to be used.

However, as soon as the power supply was turned OFF, it was noted that regardless of the force applied, the grip on the object was loosened. This was mainly because, when the power supply is turned OFF, the force that separates the two halves of the palm as the thumb applies the required force, is removed. Hence, as the two halves of the palm return to the original position, the thumb is slightly rotated in the opposite direction reducing the built force between the object and the hand.

The gripping force was also reduced in the presence of certain external loads applied to the hand, which, depending on their direction, would cause one or more of the digits to lose contact with the object. In this case, the main contributing factor is the elastic deformation of the parts, and given that the power supply will be turned OFF, the thumb is not able to adjust the grasp to compensate for this deformation. Furthermore, if sufficient force is applied on the thumb, the load will be able to back-drive the shaft of the thumb motor (i.e., the thumb will become back-driveable). The maximum external torque that would need to be applied on each joint for the corresponding phalanx to move relative to the grasped object was then determined. In the case of the thumb, both the opening and closing directions were considered since the object can be grasped in either direction. A set-up similar to the one shown in Figure 7.4 was used, where a spring balance, perpendicular to the joint and at a known distance, was used to measure the force required for the corresponding phalanx to move relative to the object.

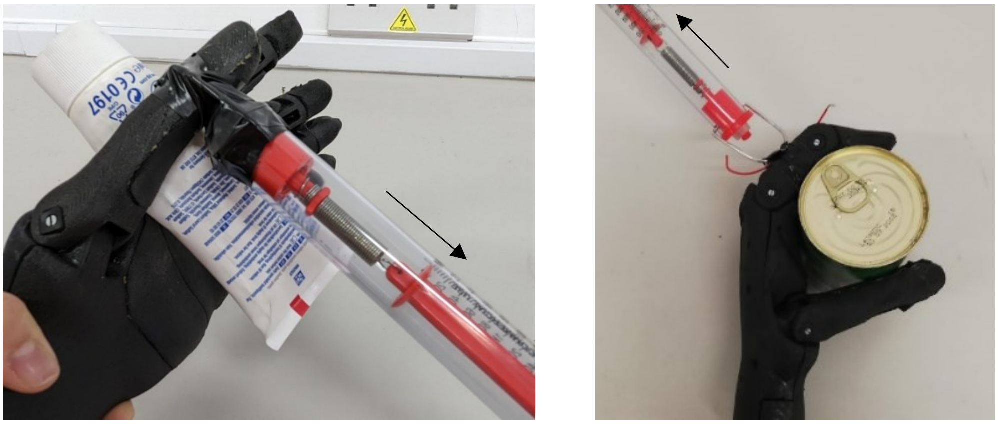

(a) (b)

Figure 7.4: The set-up used to measure the external torque that would need to be applied on (a) the thumb in the closing direction and (b) the proximal phalanx of the MRL finger after the motors are turned off

The torque required for each of the three digits, averaged across ten readings, is noted in Table 7.4. From this table one can observe that a torque less than $0.26Nm$ was required for the phalanges to move relative to the grasped object, with the distal phalanx exhibiting the least resistance to movement due to the cable not being tight enough. Thus, to ensure that for this prototype the grasped object does not slip, especially for force closure grasp, the external loads necessary to execute an activity will possibly be applied before the power supply is turned OFF (this way the thumb is able to compensate for the compliance of the fingers), and/or the demands on the grasp are reduced as much as possible by making more use of the environment or the remaining, intact, hand. Alternatively, the thumb motor can be kept ON for stall currents lower than the rated continuous current (i.e., the low-level force), even if the energy consumed is higher. However, future prototypes need to focus on solving this issue, for example, by having the interface keys made from a stronger material. Meanwhile, given the usefulness of the compliance added by the backlash/elastic deformation in the fingers, future improvements might opt for a coupling mechanism that makes use of stiff springs as a compromise between the added compliance in the finger and the lack of resistance in the movement of the distal phalanx in the presence of external loads.

Table 7.4: The external torque applied on each joint for the corresponding phalanx to lose contact with the object after the motors are turned OFF.

Thumb	
	External Torque Required (Nm)
Closing Direction	0.28±0.03
Opening Direction	0.26±0.04
Index	
	External Torque Required (Nm)
Proximal Phalanx	0.13±0.01
Distal Phalanx	0.06±0.01
MRL	
	External Torque Required (*Nm*)
Proximal Phalanx	0.21±0.03
Distal Phalanx	0.05±0.01

It is noted that none of the issues listed above are conceptual in nature, they are rather due to minor shortcomings in the detailed design of the prototype. The presence of such shortcomings is something to be expected in early prototypes, and these should all be rectifiable in future iterations of a similar prototype.

Even though the torque that can be retained by each digit is limited, MAProHand has the potential to provide the amputee with vibrational feedback related to its magnitude. In general, the amplitude of the vibrations, which correspond to the output voltage of each of the FSRs embedded in the transmission system, increases, as the torque sustained by each digit increases. Figure 7.5shows the relationship between the torque applied/sustained by the thumb in the opening and closing direction and the corresponding FSR output voltage. Even though the output voltage in the opening and closing directions was different, which could be due to misalignment of the FSR sensor relative to the shaft, the vibrations would allow the amputee to learn the force level required for certain objects with minimal visual feedback.

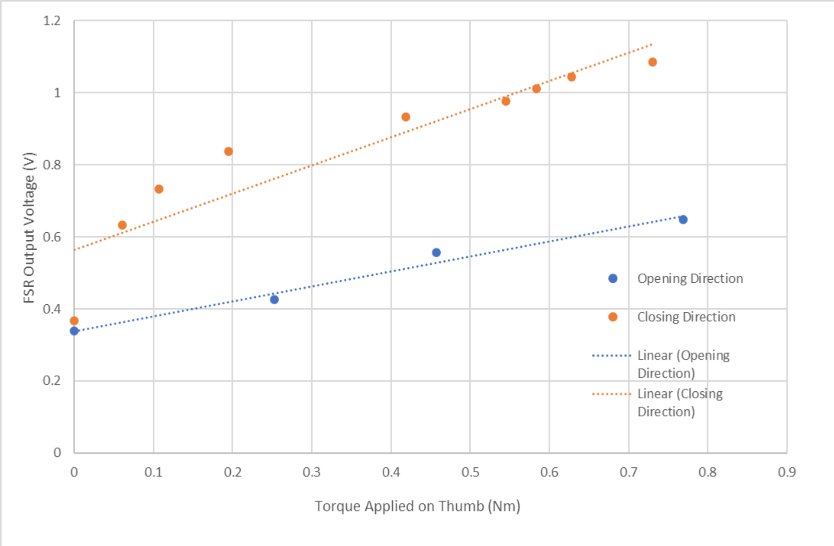

Figure 7.5: The graph of FSR output voltage against torque applied by the thumb

While there is still room for improvement, this first prototype has shown that with the developed KHS as the foundation for its design, MAProHand has the potential to be a lightweight prosthetic hand that can significantly improve the general daily functionality of the amputees with intuitive control, all at a price that is competitive when compared with that of other prostheses.

7.3 ASSESSMENT OF THE FUNCTIONALITY OF THE PROTO-MOTIONS

The objective of any prosthetic hand is to assist the amputee during their day-to-day activities. Therefore, the success of MAProHand depends on whether it can complete the representative bimanual activities together with the remaining intact hand, using just the four PMs.

The representative activities were carried out in a laboratory setting, where the prosthetic hand was held from the wrist by an able-bodied person. The PM specified in Table 5.2 (on p.116) for each activity was then used to replicate, as closely as possible, the hand configurations modelled in Unity. Each activity was then evaluated using the following criterion:

- Score 0, if the activity was not completed in the normal manner.
- Score 1, if the activity was completed with some modifications to the task object and/or additional assistance from the environment, which had not already been taken into consideration during the force analysis in Section 5.3 (on. p.89), such as reducing the external load.
- Score 2, if the activity was completed without any assistance, except for the use of a table and the intact hand, even if the objects needed to be grasped multiple times.

This criterion considers only the completion of the activity, regardless of the time taken to complete it. This is because while the duration of the activity is also important, each of the PMs only takes a few seconds to complete. Thus, with usage, the amputee should learn the best way to execute each activity in the least amount of time/attempts. The scores for the different activities were then normalized and added to express a percentage of the task completed.

The prevailing hand postures, Table 7.5, were relatively similar to the ones modelled in Unity, except for the fork and the briefcase, where an alternative grasp type was used for a better grip that also looked more natural. Using these postures and the above score method, MAProHand, together with the remaining intact hand, was able to complete 73% of the activities. Only peeling the potato required multiple attempts, the reason being that the force applied on the object was not retained, as discussed in Section 7.2 (on p.168), and thus, the potato would slip while it was being peeled. In fact, as expected in the previous section, the external loads had to be reduced for several activities, either by loosening the cap or by reducing the carrying capacity (e.g., the load placed on the tray). For activities where the external load could not be reduced or was not sufficient, the task object was modified accordingly. For instance, the utensils were covered in rubber, which increased their size and the friction present between the object and the hand. Alternatively, a smaller version of the object was used, as in the case of opening a jar, pouring from a frying pan and carrying a briefcase. While the number of modifications should be kept to a minimum so as to ensure that the amputee is still able to use the prosthetic hand in different environments, using adaptive equipment is a common approach used by people suffering from limited functionality in their hand [305]. It is noted that when the internal frictional and the other issues discussed in Section 7.2 are resolved in future prototypes, the need for these modifications will decrease or disappear. Meanwhile, the only activity which could not be completed in the normal manner was the spraying of a detergent, because as already indicated in Section 5.6 (on p.115), the spray lever could not be actuated by the PMs.

Thus, MAProHand, with just the four PMs, provided sufficient dexterity for a non-dominant hand in bimanual activities, whose success rate can be increased further with future improvements that tackle the retention of the force applied on the object.

Table 7.5: Hand Postures used to complete the different representative bimanual activities

Sweeping	***Peeling a potato***	***Opening a hand-tightened bottle***
Broom	*Potato*	*Large Water Bottle*
O-N-C	O-M-S	O-M-S
		
Putting toothpaste on a toothbrush	***Opening the zipper of a purse***	***Pouring from a frying pan***
Toothbrush	Purse	*Frying Pan Handle*
O-N-C	O-P	O-N-C
		
Passing a thread through a needle	***Opening a hand-tightened cap***	***Pouring water into a cup***
Sewing Pin	*Soap Bottle Cap*	*Medium-Sized Cup*
O-M-S	O-M-S	O-M-S
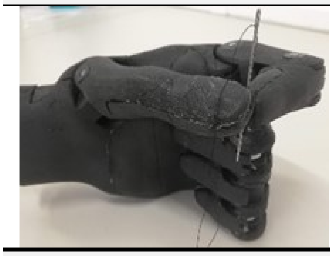		
Playing Cards	***Carrying a tray***	***Opening a packaged-food box***
Cards	*Tray*	*Cracker box*
O-M-S	O-M-S	O-M-S
	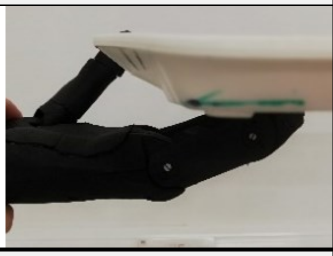	
Carrying a shopping bag	***Pulling a drawer***	***Carrying a briefcase***
Shopping bag	*Cabinet handle*	*Briefcase*
O-N-C	N-O	O-M-S
		

Table 7.5: Hand Postures used to complete the different representative bimanual activities (cont.d)

Sharpening a pencil	***Opening a hand-tightened toothpaste cap***	***Opening a hand-tightened body cream cap***
Small Sharpener	*Toothpaste Cap*	*Body Cream Container*
O-P	O-P	O-P
		
Putting glue on a paper	***Using a tablet***	***Throwing a ball***
Paper	*Tablet*	*Beach Ball*
N-O	N-O	N-O
		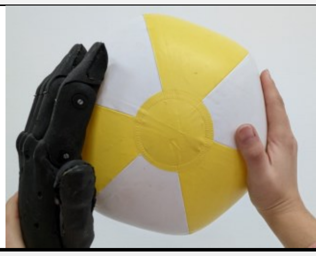
Eating with a fork and a knife	***Dialling a telephone number***	***Spraying a detergent while wiping a surface***
Fork	*Telephone*	*Spray bottle*
O-P	O-P	O-M-S
		
Cutting with scissors	***Opening a hand-tightened bottle Cap***	***Opening the flip top of a toothpaste tube***
Paper	*Water Bottle Cap*	*Toothpaste Cap*
O-P	O-P	O-P
		
Opening a can of beverage	***Opening a hand-tightened jar***	***Eating with a fork and a knife***
Can of beverage	*Jar*	*Knife*
O-M-S	O-M-S	O-N-C
		

7.4 COMPARISON OF MAPROHAND WITH THE HUMAN HAND AND OTHER PROSTHETIC HANDS

Understanding the effectiveness of the approach used in this work is important for the progress of research and development of the hand. Hence, the performance of MAProHand was compared with that of the human hand and other prosthetic devices.

Table 7.6 compares the general characteristics of MAProHand with the human hand and seven other medium/large prosthetic hands, three of which are commercially available (i.e., Michelangelo, i-Limb Quantum, and BeBionic v3), while the rest are 3D-printed prosthetic hands, with Limbitless, Dexterus v2.0 and InMooV being the three most common open source, transradial prosthetic hands, currently available online that have documented clinical usage. From this table, one can observe that all the prosthetic hands are underactuated, but compared to the other prosthesis, MaProHand is relatively simple in terms of mechanical design due to the balance between the number of joints and the number of actuators, resulting in a more reliable and cost-effective system. Although the higher number of joints and motors implies that the hand can attain a wider range of grasping hand postures, including the proto-grasps achieved by MAProHand, the four PMs developed in this work and actuated by three motors were sufficient for a non-dominant hand in bimanual activities, as

Table 7.6: Comparison of the general characteristics of MAProHand with other medium/large human and prosthetic hands (adapted from [46], [82], [147], [310])

Hand	*Weight (g)*	*Height (mm)*	*Width (excluding thumb) (mm)*	*Thickness (mm)*	*Number of Joints*	*Number of Actuators*	*Motor Location*
Human Hand	400	181	81	30	15	21	Palm/ Forearm
Michelangelo [43]	460	180	/	/	6	2	Palm
i-Limb Quantum [44]	488	182.5	80.5/ 85.7	35-41	11	6	Palm
BeBionic v3 [50]	588	188	85	50	11	5	Palm
The Hero Arm [63]	322/ 336	165/ 178	75/ 80	55	10	3-4	/
Kit prosthetic hand (female) [307]	377	194	77	28	10	2	Palm
Limbitless [64]	144.5	200	89	/	14	1	Forearm
Dextrus v2.0 [308]	131	185	87	/	15	5	Palm
InMooV [309]	201.5	194	95	/	17	5	Forearm
IMMA [310]	131.5	184	80	/	15	6	/
MAProHand	428	195	90	35	5	3	Palm

discussed in the previous section. This in turn allowed the development of a more reliable and intuitive control system, when compared to other prostheses, as only four EMG signals were required to operate MAProHand.

However, the overall weight of the prosthetic hand not only depends on the number of actuators, but also, on the strength of each actuator and the corresponding transmission system. In fact, while being lighter than commercial prosthetic hands of the same size (assuming that the weight and size of the control system, which have not yet been considered so far, can be reduced significantly such that they can fit in the forearm), MAProHand is heavier than the other 3D-printed prosthesis, which make use of nylon cables and weaker motors (except for the Hero Arm [63] and the KIT prosthetic hand [307]). This is also reflected in the overall cost of the prosthetic hand, with 3D-printed prosthesis typically costing less than 2,600Eur [150] and commercial prosthesis costing over 25,000Eur [62]. Hence, MAProHand achieves a balance between these two extremes when it comes to strength, weight, and cost, and still demonstrates an adequate level of dexterity and usability.

While this comparison provides some insight into various aspects of the hand with respect to the amputee's requirements, the performance of the different prosthetic hands in everyday use cannot be compared directly, and a more functional assessment is needed. In the literature, there is a lack of standardized performance testing or benchmarking which could be used to evaluate and compare the performance of different artificial hands. Protocols typically used in rehabilitation to measure hand function, such as SHAP [311], Sollerman Hand Function Test [199], and Box and Block test [312], have been used as in [313], [314]. However, these protocols are mainly intended for clinical evaluation, such as training of subjects wearing the prostheses, instead of experimental evaluation to identify areas for design improvement. In fact, these types of protocols tend to evaluate the performance of the prosthetic hand on the basis of the time taken to complete an activity, as opposed to its anthropomorphic grasping capabilities. Hence, Liop-Harillo et al. [315] recently developed the Anthropomorphic Hand Assessment Protocol (AHAP).

The aim of the AHAP protocol was to provide an experimental benchmark to evaluate the grasping ability of an anthropomorphic hand. The grasping ability is defined as the ability of the prosthetic hand to attain ten grasping/non-grasping postures for day-to-day activities, Figure 7.6, and to keep the grasped object under the motion of the arm without any external force being present. The ten grasping/non-grasping postures include hook, spherical grip, tripod pinch, extension grip, cylindrical grip, lateral pinch, pulp pinch, index pointing/pressing and platform, which are similar to the grasp types in Figure 4.1 (on p.49).

Figure 7.6: The ten grasping/non-grasping types of postures considered in the AHAP [315]

In the Liop-Harillo et al. protocol, the prosthetic hand, with the palm facing upwards, is used to grasp different objects for three seconds. For each hand posture, three objects of different shapes, sizes, weight, rigidity and texture were chosen from the publicly available Yale-CMU-Berkeley Object and Model Set [316], except for the index pointing/pressing and the platform, where only one object was considered. A grasping score is then given for each object, based on the following criterion developed by Liop-Harillo et al. in [315]:

- The score of 0 if the artificial hand could not hold the object;
- The score of 0.5 if the artificial hand used a grasping posture different from the one specified;
- The score of 1 if the artificial hand held the object with the correct grasp postures, which are defined in [315].

While still maintaining the grasp, the hand is rotated 180° in a natural way with low acceleration and held in that position for another three seconds. A maintaining score is then given for each object, based on the following criterion [315]:

- The score of 0 if the object falls;

- The score of 0.5 if the object moves within the artificial hand but is not dropped;
- The score of 1 if no motion between the object and the prosthetic is observed.

In the case of the index pointing/pressing, an additional score is given if the activity can be completed in less than three seconds. No additional scores were allocated for the platform. For each object, this procedure is repeated three times and the average grasping and maintaining score for these three trials is expressed as a percentage. The correctness of the different grasps (i.e., the overall grasping score) and the stability of the grasp under motion (i.e., the overall maintaining score) are then determined by averaging the corresponding percentages across the different objects. The average of the overall grasping score and the overall maintaining score then yield the Grasping Ability Score (GAS), which is a measure of the functionality and human-like grasping of artificial hands, with 100% corresponding to the human hand.

Hence, this protocol was used to compare the performance of MAProHand in everyday use to the human hand and other prostheses. However, some of the objects in the Yale-CMU-Berkeley Object and Model Set, which were used to determine this index, had been replaced. Hence, to replicate this protocol in the laboratory, similar objects in terms of both size and weight were used instead of the objects from the Yale-CMU-Berkeley Object and Model Set. Table 7.7 compares the objects utilized in Liop-Harillo et al.'s study [315] with those used in this work. Even though the objects were not the same, they were still sufficiently similar to allow for a reasonable, accurate comparison with other prosthetic hands that have been evaluated using this protocol.

The GAS for MAProHand was estimated to be 62%, where the grasping score and the maintaining score were 67% and 57%, respectively. Given that this prosthetic hand only has three DOFs, attaining 62% of the grasping ability of the human hand is quite an achievement. However, the effectiveness of the developed KHS and the PMs depends on how MAProHand fairs compared to other prosthetic hands evaluated using this protocol. Even though the number of prostheses evaluated using this protocol is limited, with the devices being open-source 3D-printed prosthetic hands, they still provide an indication of the effectiveness of the developed hand model and the approach. Table 7.8 lists the GAS and its breakdown for MAProHand and the 3D-printed prosthetic hand evaluated in [305], [310].

Table 7.7: Comparison between the object utilized in Liop-Harillo et al.'s study [315] and the objects used in this work

Liop-Harillo et al's work [315]			***This Work***		
Object	*Mass (g)*	*Dimensions (mm)*	*Object*	*Mass (g)*	*Dimensions (mm)*
Hook					
Skillet Lid	652	270x10x22	*Toolbox*	862	400x250x50
Pitcher Base	178	108x235	*Pitcher Base*	150	117x107
Wood Blocks with Rope	361.8	/	*Wooden Blocks with Rope*	368	/
Spherical Grip					
Plastic Apple	68	75	*Plastic Apple*	36	74x77x79
Softball	191	96	*Small Basketball*	178	120
Mini Soccer Ball	123	140	*Beach Volleyball*	179	150
Tripod Pinch					
Large Marker	15.8	18x121	*Large Marker*	20	16.9x139
Tuna Can	171	85x33	*Tuna Can*	193	85x38
Golf Ball	46	42.7	*Golf Ball*	46	42.6
Extension Grip					
Plate	279	258x24	*Plate*	285	188x18
Cracker Box	411	60x158x210	*Pasta Box*	537	62x139x196
Chocolate Pudding Box	187	35x110x89	*Corn Flour*	217	37x151x85
Cylindrical Grip					
Chips Can	205	75x250	*Chips Can*	220	75x233
Coffee Can	414	102x139	*Oats Can*	414	102x115
Power Drill	895	35x46x184	*Power Drill*	1092	200x45x185
Diagonal Volar Grip					
Phillips Screwdriver	97	31x215	Screwdriver	99	34.4x215
Spatula	51.5	35x83x350	Spatula	48	30x62x250
Skillet	950	270x25x30	Skillet	427	378x221x38
Lateral Pinch					
Bowl	147	159x53	*Bowl*	183	162x45
XS Clamp	19.2	85x65x10	*Clamp*	18	85x62x11.36
Key	10.1	23x43x2.2	*Key*	6	21x41x1.86
Pulp Pinch					
Small Marker	8.2	8x135	*Ballpen*	6	8.3x145
Plastic Pear	49	66.2x100	*Plastic Aubergine*	25	65.82x72.6x145
Washer 10mm	0.7	10	*Washer*	<1	12
Index pointing/pressing					
Timer	102	80x80x40	*AC Remote*	96	139x51x21
Platform					
Plate	279	258x24	*Plate*	285	188x18

Table 7.8: The GAS and its breakdown into the overall grasping and maintaining scroes for different prosthetic hands [310], [315]

Hand	*GAS (%)*	*Overall Grasping (%)*	*Overall Maintaining (%)*
The Kit prosthetic hand	79	68	91
IMMA	57	77	37
Limbitless	50	63	37
Dextrus v2.0	48	61	34
InMooV	49	57	40
MAProHand	62	67	57

From Table 7.8, one can observe that MAProHand had the second highest score, following the Kit prosthetic hand. The high score is mainly attributed to the maintaining score, which although less than the grasping score (a characteristic also observed with some of the other prosthetic hands), is significantly higher than with most other prosthetic hands. Therefore, while powerful motors increase the overall weight of the prosthetic hand, they are necessary to maintain the grasped object against its own weight, as this is more demanding than just grasping it. In fact, there were seven objects (i.e., the toolbox, the tuna can, the plate (extension grip), the pasta box, the oats can, the power drill and the skillet) which were all grasped, but when the hand was rotated by 180°, they were dropped in all trials. The main contributing factor was the back-driveability discussed in Section 7.2 (on p.168), which meant that the resulting grasping force in force closure grasps was not enough to withstand the weight of the object, while the position of the digits in form closure grasps was not maintained. However, with future improvements the maintaining score can be further increased in a very significant manner.

The grasping score of MAProHand was still competitive with the other prosthetic hands despite having only three DOFs with limited compliance. In fact, MAProHand was able to grasp all the objects, except for the small basketball and the beach volleyball, with the O-M-S PM accounting for 50% of the grasps, followed by the O-P PM with 30.77%. The reason for the low grasping score was that the prosthetic hand used a grasp posture different from the one specified in the protocol. This could simply be because the hand posture used did not classify as the correct one on the basis of the definition of the grasp types, which were more precise than the ones in Figure 4.1(a) (on p.49), as they even specified the number of phalanges and fingers that must be involved in the grasp. Otherwise, the digits were not able to wrap around the object properly due to the architecture of the kinematic hand model and/or the size of the grasped object. For example, the prosthetic hand can only grasp objects of a certain size with a tripod grasp, which depends on the gap present between the thumb and the MRL finger.

The effectiveness of the prosthetic hand in attaining specific grasp types was then quantified by the "partial GAS", where all the percentages pertaining to one of the grasps were averaged [315]. Similarly, the "partial grasping score" and the "partial maintaining score" were determined by averaging the corresponding percentages of a particular grasp type. Table 7.9 lists the "partial GAS" of the ten-hand postures and their breakdown for MAProHand and the Kit prosthetic hand (i.e., the prosthetic hand with the highest overall GAS).

Table 7.9: Comparison of the effectiveness of each grasp type for MAProHand and the KIT prosthetic hand [315]

	MAProHand			***The Kit prosthetic hand***		
	Partial GAS	*Partial Grasping*	*Partial Maintaining*	*Partial GAS*	*Partial Grasping*	*Partial Maintaining*
Hook	58	83	33	81	100	61
Spherical grip	25	17	33	81	62	100
Tripod pinch	67	67	67	87	74	100
Extension grip	50	67	33	72	53	90
Cylindrical grip	50	67	33	89	78	100
Diagonal volar grip	58	50	67	64	50	78
Lateral pinch	81	83	78	75	51	99
Pulp pinch	92	83	100	83	67	100
Index pointing/ pressing	100	100	100	100	100	100
Platform	100	100	/	50	50	/

From Table 7.9, one can observe that MAProHand was able to achieve the platform, index pointing/pressing and pulp pinch quite effectively, which is crucial, given that pulp pinch and platform are the two hand postures most relevant for a non-dominant hand in bimanual activities, as shown in Figure 4.2 (on p.50). The least effective grasp type was the spherical grip, since two of the corresponding objects (the small basketball and the beach volleyball) could not be grasped.

In general, the “partial GASs” of MAProHand for the different grasp types were lower than those of the Kit prosthetic hand, but this is mainly due to the maintaining score. Taking a closer look at the “partial grasping score”, one can further observe that MAProHand, with a one-DOF thumb without any compliant joints, as in the KIT prosthetic hand, was able to obtain higher scores in both the pulp pinch and the lateral pinch despite the circumduction rotation necessary to move from one grasp to another. This highlights the effectiveness of the optimised parameters of the developed KHS, especially since a study on the effect of the orientation and actuation of the thumb on the functionality of the hand, [317], demonstrated the importance of having a two-DOF thumb as a trade-off between the desired versatility and the complexity of the control system. In fact, commercial prosthetic hands which are able to achieve such grasps either opt for manual adjustments where the amputee rotate the thumb to the opposed position using external force, as in the BeBionic Hand, or make use of a complex cam system as in the Michelangelo Hand [46].

Therefore, the optimised KHS and the resulting PMs were effective in maintaining a sufficient level of dexterity comparable to other prosthetic hands, despite having fewer DOFs and grasp patterns available, while still keeping the mechanical design as simple as possible

7.5 ASSESSMENT OF MAPROHAND BEYOND THE REPRESENTATIVE BIMANUAL ACTIVITIES

MAProHand using just the four PMs has demonstrated the ability to achieve various hand postures. However, the versatility of these PMs when it came to the execution of daily important activities, other than the representative one was yet to be analysed.

Hence, an additional set of important day-to-day activities were chosen, such as folding a towel, tying a shoelace, and opening a zipper, activities pertaining to specific jobs and hobbies were excluded. These activities were mostly taken from functional assessments, such as SHAP [311] and the Chedoke Arm and Hand Activity [318], so as to ensure the relevance of each activity. However, given that the focus of these assessments is usually the dominant hand, unilateral activities, as well as activities which are predominantly carried out by the dominant hand, such as opening a door handle and writing, were also chosen to assess the limits of MAProHand.

The prosthetic hand was able to complete all the different activities (some of which are shown in Table 7.10), with some cases even requiring multiple PMs. These activities further highlighted the importance of the collaboration between the prosthetic hand and its surroundings, whether it is the environment or the remaining intact hand. This is intended not only to compensate for the backdriveability present in the digits, but also to orient the object in a more favourable position relative to the hand so that one of the closing hand PMs could be used, or to stop the digits at the required position. For instance, when picking up a coin from a flat surface, such as a table, the coin must be pushed towards the edge before it can be picked up with the O-P PM. Otherwise, the digits would collide with the table before being able to wrap around the coin. Another example would be the intact hand interfering with the motion of both the thumb and the index finger when actuating the O-P PM to achieve the pointing grasp required for typing. These are just a few examples and the amputee, with help from his/her occupational therapist, would need to learn how to take advantage of their surroundings so as to make the best use of MAProHand. Thus, as with any other prosthetic hand, prior training would be required to be able to grasp the object and to complete the activity successfully, especially if the hand posture used differed from what is commonly used.

This shows that the optimised KHS and the resulting PMs are not limited to the original representative activities; on the contrary, they are quite versatile, especially when the prosthetic hand exploits its surroundings. Thus, MAProHand has the potential to significantly improve the general daily functionality of the amputee while being intuitive and easy to use.

Table 7.10: The prosthetic hand executing various day-to-day activities

Tying a shoelace	***Closing a button on a skirt***	***Folding a facecloth***
Shoelace	*Skirt*	*Facecloth*
O-P	O-P	O-P/N-O
	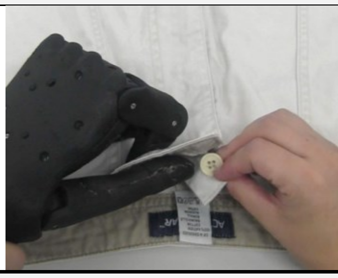	
Opening a coffee bottle	***Pouring from a measuring jug***	***Opening a packet***
Coffee Bottle	*Measuring jug*	*Packet*
O-M-S	O-N-C	O-P
		
Slicing a cucumber	***Pouring from a carton***	***Opening a door handle***
Cucumber	*Carton*	*Door handle*
O-P	O-M-S	O-P
		

.

Table 7.10: The prosthetic hand executing various day-to-day activities (cont.d)

Opening a clothing pin	***Collecting dirt from the floor***	***Typing***
Clothing pin	*Dustpan*	*Keyboard*
O-P	O-P	O-P
		
Solving a rubric cube	***Writing***	***Placing a folded paper inside an envelope***
Rubric cube	*Pencil*	*Envelope*
O-M-S	O-P	O-P
		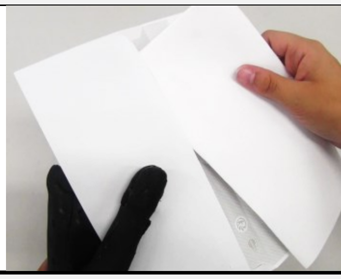
Turning a page	***Picking up a coin from a table***	***Holding an object while unscrewing a screw***
Book	*Coin*	*Object*
N-O	N-O/ O-P	O-M-S
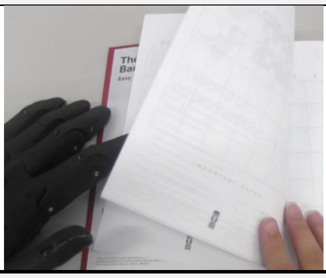	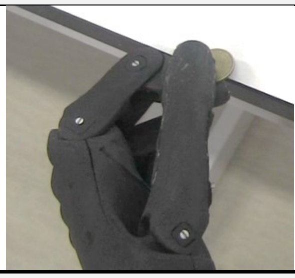	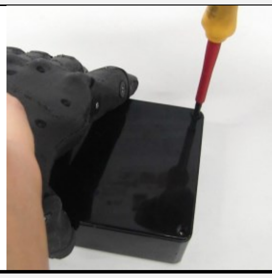
Rotating a key	***Opening a makeup palette***	***Opening a pocket***
Key	*Makeup palette*	*Pocket*
O-P	O-M-S	O-M-S
	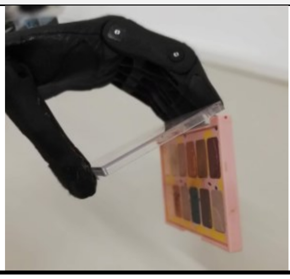	

CHAPTER 8: CONCLUSION AND FUTURE WORK

8.1 MAIN FINDINGS

Simplicity, dexterity, and usability are the three most important attributes of a prosthetic device; they play a crucial role concerning acceptance by the amputee. They ensure that while the prosthetic hand is highly functional for day-to-day activities, its design is lightweight, reliable and convenient to use. However, as evidenced by the prosthetic hands available on the market, designing an anthropomorphic hand that excels in all three of these attributes is a challenging task. Hence, the primary objective of this research was to carry out a systematic exercise and seek a practical solution for unilateral amputees that optimizes the trade-off involving these three different attributes. The various goals that constituted this primary objective, which were listed at the end of Chapter 1 (on p. 1), have been achieved, as summarized in the remainder of this section and in the next section.

Following a thorough literature review in Chapter 2 (on p.4), on the challenges encountered and the approach taken to overcome such challenges, it was noted that most of the variance in the patterns of the human hand configurations and movements can be described by a few parameters, giving rise to postural synergies. Depending on the number of synergies required, effective coupling of joints can simplify the control system and the mechanical design while maintaining relatively high dexterity; this makes sures that the requirements noted in Chapter 3 (on p.44) are met. However, while Santello et al. [103] observed that most of the variance can be accounted for by just two postural synergies, other researchers, as in [118], [127], noted that significantly more synergies were in fact necessary to express the same level of variance. This highlights the dependence of the postural synergies on the size and the variability of the hand movements analysed.

Given that postural synergies can only simplify the control strategy if the set of synergies is small and task-independent, the variance in the data must be minimized while still capturing the frequency and the full range of daily movements. So, while most of the above studies focus on replicating the function of the dominant hand, which involves more individuated movements as it tends to be used for unimanual activities and in-hand manipulation, this work focuses on the non-dominant hand in the minimal anthropomorphic condition, a novel approach that builds on the previous work carried out at the University of Malta. This approach is validated by the fact that studies as in [28], [29] have shown that unilateral amputees tend to rely heavily on their intact hand, even if the amputated side used to be the dominant side.

Thus, in Chapter 4 (on p.48), a data glove was developed to measure the non-dominant hand of right-handed human volunteers with medium-sized hands executing grasps commonly used during bimanual ADLs, with their ring and little fingers constrained to move with the middle finger. The corresponding postural synergies were then determined through a PCA of these new experimental data. From this analysis, it was found that the first three PCs for each participant accounted for a mean variance of 85.5±1.8%. This implied that very good dexterity could be achieved with just three DOFs instead of the original twenty-one of the human hand. On the bases of these synergies, six important hand postures that a left, non-dominant, medium-sized prosthetic hand must be able to execute for it to be useful in several bimanual activities, were identified. Most of these postures were then incorporated into four PMs, further enhancing the usability of the device, as it ensured more reliable and intuitive sEMG signals to detect the amputee's intent.

8.2 ACHIEVEMENTS

On the basis of these findings, a medium-sized KHS that optimised the balance between simplicity and dexterity could then be achieved. This involved a rigorous iterative process, as discussed in Chapter 5 (on p.88), to determine optimal values for all the critical functional/aesthetic parameters of the hand, using the framework set-up in Unity as a guide.

The final KHS, which achieved an acceptable and optimised level of dexterity in the simulation environment, comprised of five joints, with the corresponding PMs realized using only three actuators driving respectively the thumb, the index, and the MRL digit. Given that many of the leading commercial multiarticulating hands currently on the market incorporate about eleven joints and five actuators, the potential saving in complexity, weight, and cost, as well as the potential alleviation in space constraints is evident with this approach.

To evaluate its effectiveness, a physical prototype based on this structure was then designed and constructed, as discussed in Chapter 6 (on p.121), where different joints were actuated through simple transmission drive trains and coupling mechanisms. The simplicity of the overall device allowed the developed prosthetic hand to be lighter and less expensive than other commercial devices of the same size. While the number of different hand postures that can be achieved is smaller, this prototype, has demonstrated in Chapter 7 (on p.168), that the resulting PMs were sufficient to achieve most of the grasp postures required by the non-dominant hand during the normal bimanual activities of daily living, as well as certain unimanual activities, and to do so in an aesthetically acceptable manner. In particular, it has been shown that within this approach a simple, one-DOF thumb can attain a LatP and a Pinch in a manner that is sufficient for bimanual activities. This is an important achievement, considering that other commercial prosthetic hands use either multi-DOF thumbs, or complex transmission systems, or even external forces to move the thumb into position prior to the execution of specific grasp types.

The new, minimal kinematic structure and PM approach taken in this work, in conjunction with the intuitive sEMG control system that accompanies it, can potentially define a new paradigm for the development of prosthetic hands for unilateral upper limb amputees, resulting in lightweight, relatively simple, but sufficiently dexterous devices that can be worn and used for long periods, and that can be controlled by the amputee in a manner that is similar to how s/he would control her/his natural hand.

8.3 FUTURE WORK

While substantial work has been done in this project, further work is still necessary for the developed prosthetic hand to be used in the real world by unilateral amputees.

Future models should first focus on tackling the issues observed in Chapter 7 (on p.168), mainly the friction, the attachment design of the two halves of the palm, and the back-driveability of the digits, accompanied by further reduction in the overall weight of the device. This should lead to an even lighter, and more reliable prosthetic hand with more functionality. Hence, the balance regarding simplicity, dexterity and usability would be optimised even more.

For the amputee to be able to make use of this device, a socket, which incorporates all the electronics components, with a wrist attachment that can be easily integrated with it, would need to be designed and constructed. During the design phase of the wrist attachment, the same three attributes of the prosthetic hand must be taken into consideration to ensure that it complements the developed device in terms of weight, size, cost, and usability. Thus, while a wrist attachment with multi-DOFs provides higher functionality, the weight, and the size penalty, as well as the added complexity concerning its usability would need to be analysed thoroughly. Otherwise, several models would need to be developed to cater for the different needs of the amputees, an approach commonly followed by larger companies.

However, the present prototype of this prosthetic hand is only suitable for amputees with medium to large hand size that had their left hand amputated. Naturally, the next step should be to investigate the effectiveness of this approach in developing the corresponding right-hand model, as well as a smaller model. In the case of the right-hand model, this is the mirrored version of the current prosthetic hand. Thus, one will need to investigate whether there are any issues that arise when mirroring the design. Meanwhile, for the smaller model, the parameters of the KHS may need to be scaled and/or re-optimised. For this model, the main challenge would be to fit the different components in an even smaller palm while maintaining the same level of functionality. Thus, despite the simplicity of the mechanical design, the use of custom-built components, such as gears, becomes crucial for the prosthetic hand to satisfy the amputees' requirements.

REFERENCES

[1] J. Wald and R. Alvaro, “Psychological Factors in Work-Related Amputation: Considerations for Rehabilitation Counselors,” *J. Rehabil. Alex.*, vol. 70, no. 4, pp. 6–15, Dec. 2004.

[2] “Product Narrative prostheses | AT2030 Programme.” Accessed: Sep. 29, 2023. [Online]. Available: https://at2030.org/product-narrative-prostheses/

[3] K. Ziegler-Graham, E. J. MacKenzie, P. L. Ephraim, T. G. Travison, and R. Brookmeyer, “Estimating the prevalence of limb loss in the United States: 2005 to 2050,” *Arch. Phys. Med. Rehabil.*, vol. 89, no. 3, pp. 422–429, Mar. 2008, doi: 10.1016/j.apmr.2007.11.005.

[4] W. R. Frontera, J. K. Silver, and T. D. Rizzo, *Essentials of Physical Medicine and Rehabilitation E-Book*. Elsevier Health Sciences, 2014.

[5] “Google Scholar Search: ‘Hand Prosthesis’ OR ‘Prosthetic Hand’ 2022.” [Online]. Available: https://scholar.google.com/scholar?hl=en&as_sdt=0%2C5&as_vis=1&q=%E2%80%9Chand+prosthesis%E2%80%9D+OR+%E2%80%9Cprosthetic+hand%E2%80%9D&btnG=

[6] D. Piscitelli *et al.*, “Prosthesis rejection in individuals with limb amputation: a narrative review with respect to rehabilitation,” *Riv. Psichiatr.*, vol. 56, no. 4, pp. 175–181, Jul. 2021.

[7] D. Dalli and M. A. Saliba, “Addressing simplicity, dexterity and usability of compact, multi-degree-of-freedom mechatronic devices,” in *2016 IEEE International Conference on Advanced Intelligent Mechatronics (AIM)*, Banff, AB, Canada: IEEE, Jul. 2016, pp. 1357–1362. doi: 10.1109/AIM.2016.7576959.

[8] M. A. Saliba, A. Chetcuti, and M. J. Farrugia, “Towards the Rationalization of anthropomorphic Robot Hand Design: Extracting Knowledge from Constrained Human Manual Dexterity Testing,” *J Humanoid Robot.*, vol. 10, 2013, doi: 10.1142/S0219843613500011.

[9] R. Cauchi, K. P. Camilleri, M. A. Saliba, and J. Attard, “Development of an Electromyogram-based Intent Interpretation System for a Minimal Anthropomorphic Prosthetic Hand”, unpublished.

[10] M. A. Saliba, “MAProHand Project Proposal.” University of Malta, 2018.

[11] “Orthopaedic Centre Malta | Orthopaedic supply store Gela,” Centro Ortopedico Aliotta. Accessed: Jun. 28, 2023. [Online]. Available: https://www.orthopaedicentremalta.com/

[12] B. León, A. Morales, and J. Sancho-Bru, *From Robot to Human Grasping Simulation*. Springer Science & Business Media, 2013.

[13] A. Freivalds, *Biomechanics of the Upper Limbs: Mechanics, Modeling and Musculoskeletal Injuries, Second Edition*. CRC Press, 2011.

[14] “9.4 Synovial Joints – Anatomy and Physiology.” Accessed: Jul. 18, 2019. [Online]. Available: https://opentextbc.ca/anatomyandphysiology/chapter/9-4-synovial-joints/

[15] R. Drake, A. W. Vogl, and A. W. M. Mitchell, *Gray’s Anatomy for Students E-Book*. Elsevier Health Sciences, 2009.

[16] "Carpometacarpal joint - OrthopaedicsOne Articles - OrthopaedicsOne." Accessed: Oct. 06, 2022. [Online]. Available: https://www.orthopaedicsone.com/display/Main/Carpometacarpal+joint

[17] W. P. Cooney, M. J. Lucca, E. Y. Chao, and R. L. Linscheid, "The kinesiology of the thumb trapeziometacarpal joint.:," *J. Bone Jt. Surg.*, vol. 63, no. 9, pp. 1371–1381, Dec. 1981, doi: 10.2106/00004623-198163090-00002.

[18] A. Hollister, W. L. Buford, L. M. Myers, D. J. Giurintano, and A. Novick, "The axes of rotation of the thumb carpometacarpal joint," *J. Orthop. Res.*, vol. 10, no. 3, pp. 454–460, 1992, doi: 10.1002/jor.1100100319.

[19] S. Sandra, H. Peggy, and P. David, *Examination of Musculoskeletal Injuries With Web Resource-4th Edition*. Human Kinetics, 2015.

[20] "Chapter 18. The Forearm, Wrist, and Hand | Dutton's Orthopaedic Examination, Evaluation, and Intervention, 3e | AccessPhysiotherapy | McGraw-Hill Medical." Accessed: Aug. 30, 2019. [Online]. Available: https://accessphysiotherapy.mhmedical.com/content.aspx?bookid=475&sectionid=40791214

[21] *The Promise of Assistive Technology to Enhance Activity and Work Participation*. doi: 10.17226/24740.

[22] C. L. Shehan, *The Wiley Blackwell Encyclopedia of Family Studies, 4 Volume Set*. John Wiley & Sons, 2016.

[23] C. H. Jang *et al.*, "A Survey on Activities of Daily Living and Occupations of Upper Extremity Amputees," *Ann. Rehabil. Med.*, vol. 35, no. 6, pp. 907–921, Dec. 2011, doi: 10.5535/arm.2011.35.6.907.

[24] I. Dudkiewicz, R. Gabrielov, I. Seiv-Ner, G. Zelig, and M. Heim, "Evaluation of prosthetic usage in upper limb amputees," *Disabil. Rehabil.*, vol. 26, no. 1, pp. 60–63, Jan. 2004, doi: 10.1080/09638280410001645094.

[25] M. H. Mohd Zaini, S. A. Ahmad, M. H. Marhaban, and W. Z. Wan Hasan, "UPM prosthetic hand system design - preliminary results," in *2011 IEEE Student Conference on Research and Development*, Dec. 2011, pp. 174–177. doi: 10.1109/SCOReD.2011.6148730.

[26] R. W. Beasley, "General considerations in managing upper limb amputations," *Orthop. Clin. North Am.*, vol. 12, no. 4, pp. 743–749, Oct. 1981.

[27] F. Cordella *et al.*, "Literature Review on Needs of Upper Limb Prosthesis Users," *Front. Neurosci.*, vol. 10, 2016, Accessed: Sep. 29, 2023. [Online]. Available: https://www.frontiersin.org/articles/10.3389/fnins.2016.00209/full

[28] A. Chadwell, L. Kenney, M. H. Granat, S. Thies, J. Head, A. Galpin, R. Baker and J. Kulkarni, "Upper limb activity in myoelectric prosthesis users is biased towards the intact limb and appears unrelated to goal-directed task performance," *Sci. Rep.*, vol. 8, no. 1, pp. 1–12, Jul. 2018, doi: 10.1038/s41598-018-29503-6.

[29] A. J. Spiers, J. Cochran, L. Resnik, and A. M. Dollar, "Quantifying Prosthetic and Intact Limb Use in Upper Limb Amputees via Egocentric Video: An Unsupervised, At-Home Study," *IEEE Trans. Med. Robot. Bionics*, vol. 3, no. 2, pp. 463–484, May 2021, doi: 10.1109/TMRB.2021.3072253.

[30] B. A. Philip and S. H. Frey, "Compensatory Changes Accompanying Chronic Forced Use of the Nondominant Hand by Unilateral Amputees," *J. Neurosci.*,

vol. 34, no. 10, pp. 3622–3631, Mar. 2014, doi: 10.1523/JNEUROSCI.3770-13.2014.

[31] “Some Problems in the Management of Upper Extremity Amputees | O&P Virtual Library.” Accessed: Jul. 17, 2019. [Online]. Available: http://www.oandplibrary.org/al/1955_02_036.asp

[32] K. Østlie, I. M. Lesjø, R. J. Franklin, B. Garfelt, O. H. Skjeldal, and P. Magnus, “Prosthesis use in adult acquired major upper-limb amputees: patterns of wear, prosthetic skills and the actual use of prostheses in activities of daily life,” *Disabil. Rehabil. Assist. Technol.*, vol. 7, no. 6, pp. 479–493, Nov. 2012, doi: 10.3109/17483107.2011.653296.

[33] “Synergy Prosthetics - A Short History of Prosthetics.” Accessed: Jun. 28, 2023. [Online]. Available: https://synergypo.com/blog/a-short-history-of-prosthetics/, https://synergypo.com/blog/a-short-history-of-prosthetics/

[34] “Upper Limb Prosthetics,” PM&R KnowledgeNow. Accessed: Oct. 10, 2022. [Online]. Available: https://now.aapmr.org/upper-limb-prosthetics/

[35] A. Saikia, S. Mazumdar, N. Sahai, and S. Paul, “Below Elbow Prosthetic: A Path to Independent Era,” *Int. J. Adv. Inf. Sci. Technol.*, vol. 34, pp. 9–14, Feb. 2015.

[36] B. Maat, G. Smit, D. Plettenburg, and P. Breedveld, “Passive prosthetic hands and tools: A literature review,” *Prosthet. Orthot. Int.*, vol. 42, no. 1, pp. 66–74, Feb. 2018, doi: 10.1177/0309364617691622.

[37] “Cosmetic upper limb solutions | Ottobock US.” Accessed: Sep. 02, 2019. [Online]. Available: https://www.ottobockus.com/prosthetics/upper-limb-prosthetics/solution-overview/cosmetic-solutions/

[38] R. Radocy, “Chapter 24 Upper Limb Prosthetics for Sports and Recreation,” 2010.

[39] K. Berning, S. Cohick, R. Johnson, L. A. Miller, CP, and J. W. Sensinger, “Comparison of body-powered voluntary opening and voluntary closing prehensor for activities of daily life,” *J. Rehabil. Res. Dev.*, vol. 51, no. 2, pp. 253–262, 2014, doi: 10.1682/JRRD.2013.05.0123.

[40] R. Ayub, D. J. Villarreal, R. D. Gregg, and F. Gao, “Evaluation of transradial body-powered prostheses using a robotic simulator.,” *Prosthet. Orthot. Int.*, vol. 41, no. 2, pp. 194–200, 2017, doi: 10.1177/0309364616650077.

[41] Yumpu.com, “VASI Electric Hands for Children,” yumpu.com. Accessed: Jun. 29, 2023. [Online]. Available: https://www.yumpu.com/en/document/view/12032736/vasi-electric-hands-for-children

[42] “SensorHand Speed | Myo Terminal Devices | Myo Hands and Components | Upper Limb Prosthetics | Prosthetics | Ottobock US B2B Site.” Accessed: Jan. 19, 2023. [Online]. Available: https://shop.ottobock.us/Prosthetics/Upper-Limb-Prosthetics/Myo-Hands-and-Components/Myo-Terminal-Devices/SensorHand-Speed/p/8E38~58

[43] “Michelangelo prosthetic hand.” Accessed: Sep. 02, 2019. [Online]. Available: https://www.ottobockus.com/prosthetics/upper-limb-prosthetics/solution-overview/michelangelo-prosthetic-hand/

[44] “Prosthetics_Master_Catalog_en-us.pdf.” Accessed: Sep. 13, 2023. [Online]. Available: https://media.ossur.com/ossur-

dam/image/upload/v1691688605/product-documents-global/Prosthetics_Master_Catalog_en-us.pdf

[45] "Bebionic Hand." Accessed: Jan. 19, 2023. [Online]. Available: https://www.ottobockus.com/prosthetics/upper-limb-prosthetics/solution-overview/bebionic-hand/

[46] J. T. Belter, J. L. Segil, A. M. Dollar, and R. F. Weir, "Mechanical design and performance specifications of anthropomorphic prosthetic hands: A review," *J. Rehabil. Res. Dev.*, vol. 50, no. 5, p. 599, 2013, doi: 10.1682/JRRD.2011.10.0188.

[47] C. Piazza, G. Grioli, M. G. Catalano, and A. Bicchi, "A Century of Robotic Hands," *Annu. Rev. Control Robot. Auton. Syst.*, vol. 2, no. 1, pp. 1–32, 2019, doi: 10.1146/annurev-control-060117-105003.

[48] M. G. Catalano, G. Grioli, E. Farnioli, A. Serio, C. Piazza, and A. Bicchi, "Adaptive synergies for the design and control of the Pisa/IIT SoftHand," *J Robot. Res*, vol. 33, pp. 768–782, 2014, doi: 10.1177/0278364913518998.

[49] G. Cerruti, D. Chablat, D. Gouaillier, and S. Sakka, "ALPHA: A hybrid self-adaptable hand for a social humanoid robot," in *2016 IEEE/RSJ International Conference on Intelligent Robots and Systems (IROS)*, Oct. 2016, pp. 900–906. doi: 10.1109/IROS.2016.7759157.

[50] "bebionic Hand EQD | The most lifelike prosthetic hand." Accessed: Nov. 04, 2022. [Online]. Available: https://www.ottobock.com/en-us/product/8E70

[51] "TrueLimb Full Arm Solution Demonstration - Unlimited Tomorrow," Calendly. Accessed: Oct. 12, 2022. [Online]. Available: https://calendly.com/sean-j/truelimb-full-arm-solution-demonstration

[52] W. Williams, "Ottobock Michelangelo Hand," Bionics For Everyone. Accessed: Oct. 11, 2022. [Online]. Available: https://bionicsforeveryone.com/ottobock-michelangelo-hand/

[53] T. A. Kuiken *et al.*, "Targeted muscle reinnervation for real-time myoelectric control of multifunction artificial arms," *JAMA*, vol. 301, no. 6, pp. 619–628, Feb. 2009, doi: 10.1001/jama.2009.116.

[54] R. F. ff Weir, P. R. Troyk, G. A. DeMichele, D. A. Kerns, J. F. Schorsch, and H. Maas, "Implantable myoelectric sensors (IMESs) for intramuscular electromyogram recording," *IEEE Trans. Biomed. Eng.*, vol. 56, no. 1, pp. 159–171, Jan. 2009, doi: 10.1109/TBME.2008.2005942.

[55] M. Atzori and H. Müller, "Control Capabilities of Myoelectric Robotic Prostheses by Hand Amputees: A Scientific Research and Market Overview," *Front. Syst. Neurosci.*, vol. 9, 2015, Accessed: Oct. 12, 2022. [Online]. Available: https://www.frontiersin.org/articles/10.3389/fnsys.2015.00162

[56] A. Dwivedi, Y. Kwon, A. J. McDaid, and M. Liarokapis, "EMG Based Decoding of Object Motion in Dexterous, In-Hand Manipulation Tasks," in *2018 7th IEEE International Conference on Biomedical Robotics and Biomechatronics (Biorob)*, Aug. 2018, pp. 1025–1031. doi: 10.1109/BIOROB.2018.8487222.

[57] C. Piazza *et al.*, "The SoftHand Pro-H: A Hybrid Body-Controlled, Electrically Powered Hand Prosthesis for Daily Living and Working," *IEEE Robot. Autom. Mag.*, vol. 24, no. 4, pp. 87–101, Dec. 2017, doi: 10.1109/MRA.2017.2751662.

[58] “Coapt - Myoelectric Pattern Recognition for Upper Limb Prostheses,” Coapt Myo Pattern Recognition. Accessed: Oct. 12, 2022. [Online]. Available: https://coaptengineering.com

[59] “Myo Plus pattern recognition.” Accessed: May 14, 2021. [Online]. Available: https://www.ottobockus.com/prosthetics/upper-limb-prosthetics/solution-overview/myo-plus/myo-plus.html

[60] “The Complete Guide To Arm & Hand Amputations and Prosthetics | MCOP,” MCOP Prosthetics. Accessed: Oct. 12, 2022. [Online]. Available: https://mcopro.com/blog/resources/arm-hand-prosthetics/

[61] Engr. P. Ezigbo, F. Kelechi, N. Opara, and N. Chukwuchekwa, “Development Of 3D Printable Prosthetic Arm For Amputees Using Computer Aided Design And Fused Deposition Modelling,” Jul. 2019.

[62] J. ten Kate, G. Smit, and P. Breedveld, “3D-printed upper limb prostheses: a review,” *Disabil. Rehabil. Assist. Technol.*, vol. 12, no. 3, pp. 300–314, Apr. 2017, doi: 10.1080/17483107.2016.1253117.

[63] “Hero Arm - an affordable, advanced and intuitive bionic arm.” Accessed: Jul. 21, 2020. [Online]. Available: https://openbionics.com/hero-arm/

[64] “Creative, Expressive, Personalized Prosthetics | Limbitless Solutions.” Accessed: Sep. 06, 2022. [Online]. Available: https://limbitless-solutions.org/

[65] S. Salminger *et al.*, “Current rates of prosthetic usage in upper-limb amputees – have innovations had an impact on device acceptance?,” *Disabil. Rehabil.*, vol. 44, no. 14, pp. 3708–3713, Jul. 2022, doi: 10.1080/09638288.2020.1866684.

[66] E. Biddiss and T. Chau, “Upper-Limb Prosthetics: Critical Factors in Device Abandonment,” *Am. J. Phys. Med. Rehabil.*, vol. 86, no. 12, pp. 977–987, Dec. 2007, doi: 10.1097/PHM.0b013e3181587f6c.

[67] E. Biddiss and T. Chau, “The roles of predisposing characteristics, established need, and enabling resources on upper extremity prosthesis use and abandonment,” *Disabil. Rehabil. Assist. Technol.*, vol. 2, no. 2, pp. 71–84, Jan. 2007, doi: 10.1080/17483100601138959.

[68] C. Widehammar, I. Pettersson, G. Janeslätt, and L. Hermansson, “The influence of environment: Experiences of users of myoelectric arm prosthesis—a qualitative study,” *Prosthet. Orthot. Int.*, vol. 42, no. 1, pp. 28–36, Feb. 2018, doi: 10.1177/0309364617704801.

[69] L. A. Wheaton, “Neurorehabilitation in upper limb amputation: understanding how neurophysiological changes can affect functional rehabilitation,” *J. NeuroEngineering Rehabil.*, vol. 14, p. 41, May 2017, doi: 10.1186/s12984-017-0256-8.

[70] E. Biddiss, D. Beaton, and T. Chau, “Consumer design priorities for upper limb prosthetics,” *Disabil. Rehabil. Assist. Technol.*, vol. 2, no. 6, pp. 346–357, Jan. 2007, doi: 10.1080/17483100701714733.

[71] N. Ju, K.-H. Lee, M.-O. Kim, and Y. Choi, “A User-Driven Approach to Prosthetic Upper Limb Development in Korea,” *Healthcare*, vol. 9, no. 7, Art. no. 7, Jul. 2021, doi: 10.3390/healthcare9070839.

[72] L. C. Smail, C. Neal, C. Wilkins, and T. L. Packham, “Comfort and function remain key factors in upper limb prosthetic abandonment: findings of a scoping review,” *Disabil. Rehabil. Assist. Technol.*, vol. 16, no. 8, pp. 821–830, Nov. 2021, doi: 10.1080/17483107.2020.1738567.

[73] G. H. Kejlaa, “Consumer concerns and the functional value of prostheses to upper limb amputees,” *Prosthet. Orthot. Int.*, vol. 17, no. 3, pp. 157–163, Dec. 1993, doi: 10.3109/03093649309164376.

[74] D. J. Atkins, D. C. Y. Heard, and W. H. Donovan, “Epidemiologic Overview of Individuals with Upper-Limb Loss and Their Reported Research Priorities,” *JPO J. Prosthet. Orthot.*, vol. 8, no. 1, p. 2, Winter 1996.

[75] J. R. Napier, “The prehensile movements of the human hand.,” *J. Bone Joint Surg. Br.*, vol. 38-B, no. 4, pp. 902–913, 1956, doi: 10.1302/0301-620X.38B4.902.

[76] M. R. Cutkosky, “On grasp choice, grasp models, and the design of hands for manufacturing tasks,” *IEEE Trans. Robot. Autom.*, vol. 5, no. 3, pp. 269–279, Jun. 1989, doi: 10.1109/70.34763.

[77] T. Feix, J. Romero, H.-B. Schmiedmayer, A. M. Dollar, and D. Kragic, “The GRASP Taxonomy of Human Grasp Types,” *IEEE Trans. Hum.-Mach. Syst.*, vol. 46, no. 1, pp. 66–77, Feb. 2016, doi: 10.1109/THMS.2015.2470657.

[78] I. M. Bullock, J. Z. Zheng, S. D. L. Rosa, C. Guertler, and A. M. Dollar, “Grasp Frequency and Usage in Daily Household and Machine Shop Tasks,” *IEEE Trans. Haptics*, vol. 6, no. 3, pp. 296–308, Jul. 2013, doi: 10.1109/TOH.2013.6.

[79] A. Saudabayev, Z. Rysbek, R. Khassenova, and H. A. Varol, “Human grasping database for activities of daily living with depth, color and kinematic data streams,” *Sci. Data*, vol. 5, May 2018, doi: 10.1038/sdata.2018.101.

[80] S. Edwards, D. Buckland, and J. McCoy-Powlen, “Developmental and Functional Hand Grasps,” *Books Monogr. WMU Authors*, Nov. 2002, [Online]. Available: https://scholarworks.wmich.edu/books/483

[81] V. Gracia-Ibáñez, J. L. Sancho-Bru, and M. Vergara, “Relevance of grasp types to assess functionality for personal autonomy,” *J. Hand Ther. Off. J. Am. Soc. Hand Ther.*, vol. 31, no. 1, pp. 102–110, Mar. 2018, doi: 10.1016/j.jht.2017.02.003.

[82] J. T. Belter and A. M. Dollar, “Performance characteristics of anthropomorphic prosthetic hands,” in *2011 IEEE International Conference on Rehabilitation Robotics*, Zurich: IEEE, Jun. 2011, pp. 1–7. doi: 10.1109/ICORR.2011.5975476.

[83] F. Buccino, A. Bunt, A. Lazell, and L. M. Vergani, “Mechanical Design Optimization of Prosthetic Hand’s Fingers: Novel Solutions towards Weight Reduction,” *Materials*, vol. 15, no. 7, p. 2456, Mar. 2022, doi: 10.3390/ma15072456.

[84] A. Arabian, D. Varotsis, C. McDonnell, and E. Meeks, “Global social acceptance of prosthetic devices,” in *2016 IEEE Global Humanitarian Technology Conference (GHTC)*, Oct. 2016, pp. 563–568. doi: 10.1109/GHTC.2016.7857336.

[85] M. S. Trachtenberg, G. Singhal, R. Kaliki, R. J. Smith, and N. V. Thakor, “Radio frequency identification — An innovative solution to guide dexterous prosthetic hands,” in *2011 Annual International Conference of the IEEE Engineering in Medicine and Biology Society*, Aug. 2011, pp. 3511–3514. doi: 10.1109/IEMBS.2011.6090948.

[86] A. W. Franzke *et al.*, “Users’ and therapists’ perceptions of myoelectric multi-function upper limb prostheses with conventional and pattern recognition

control," *PLOS ONE*, vol. 14, no. 8, p. e0220899, Aug. 2019, doi: 10.1371/journal.pone.0220899.

[87] L. J. Resnik *et al.*, "EMG pattern recognition compared to foot control of the DEKA Arm," *PLOS ONE*, vol. 13, no. 10, p. e0204854, Oct. 2018, doi: 10.1371/journal.pone.0204854.

[88] E. Cho, R. Chen, L.-K. Merhi, Z. Xiao, B. Pousett, and C. Menon, "Force Myography to Control Robotic Upper Extremity Prostheses: A Feasibility Study," *Front. Bioeng. Biotechnol.*, vol. 4, Mar. 2016, doi: 10.3389/fbioe.2016.00018.

[89] D. Dalli and M. A. Saliba, "Towards the development of a minimal anthropomorphic robot hand," in *2014 IEEE-RAS International Conference on Humanoid Robots*, Nov. 2014, pp. 413–418. doi: 10.1109/HUMANOIDS.2014.7041393.

[90] D. Dalli and M. A. Saliba, "The university of Malta minimal anthropomorphic robot (UM-MAR) Hand II," in *2016 IEEE International Conference on Advanced Intelligent Mechatronics (AIM)*, Banff, AB, Canada: IEEE, Jul. 2016, pp. 371–376. doi: 10.1109/AIM.2016.7576795.

[91] F. Sun *et al.*, "Robotic Grasping and Manipulation Competition @IROS2016: Team Tsinghua: First Robotic Grasping and Manipulation Challenge, RGMC 2016, Held in Conjunction with IROS 2016, Daejeon, South Korea, October 10–12, 2016, Revised Papers," 2018, pp. 161–171. doi: 10.1007/978-3-319-94568-2_10.

[92] B. Massa, S. Roccella, M. C. Carrozza, and P. Dario, *Design and Development of an Underactuated Prosthetic Hand.*, vol. 4. 2002, p. 3379. doi: 10.1109/ROBOT.2002.1014232.

[93] L. Birglen, T. Laliberté, and C. M. Gosselin, *Underactuated Robotic Hands*. Springer, 2007.

[94] C. Gosselin, F. Pelletier, and T. Laliberte, "An anthropomorphic underactuated robotic hand with 15 dofs and a single actuator," in *2008 IEEE International Conference on Robotics and Automation*, May 2008, pp. 749–754. doi: 10.1109/ROBOT.2008.4543295.

[95] M. Santello, G. Baud-Bovy, and H. Jörntell, "Neural bases of hand synergies," *Front. Comput. Neurosci.*, vol. 7, Apr. 2013, doi: 10.3389/fncom.2013.00023.

[96] C. R. Mason, J. E. Gomez, and T. J. Ebner, "Hand synergies during reach-to-grasp.," *J. Neurophysiol.*, vol. 86, no. 6, pp. 2896–2910, 2001, doi: 10.1152/jn.2001.86.6.2896.

[97] N. A. Bernshteĭn, *The co-ordination and regulation of movements,* [1st English ed.]. Oxford,: Pergamon Press, 1967.

[98] R. N. Lemon, "Neural control of dexterity: what has been achieved?," *Exp. Brain Res.*, vol. 128, no. 1–2, pp. 6–12, Sep. 1999, doi: 10.1007/s002210050811.

[99] R. Vinjamuri, M. Sun, D. Crammond, R. Sclabassi, and Z.-H. Mao, "Inherent Bimanual Postural Synergies in Hands," *Conf. Proc. Annu. Int. Conf. IEEE Eng. Med. Biol. Soc. IEEE Eng. Med. Biol. Soc. Conf.*, vol. 2008, pp. 5093–6, Feb. 2008, doi: 10.1109/IEMBS.2008.4650359.

[100] C. Häger-Ross and M. H. Schieber, "Quantifying the Independence of Human Finger Movements: Comparisons of Digits, Hands, and Movement

Frequencies," *J. Neurosci.*, vol. 20, no. 22, pp. 8542–8550, Nov. 2000, doi: 10.1523/JNEUROSCI.20-22-08542.2000.

[101] J. Starke, M. Keller, and A. Asfour, "Temporal Force Synergies in Human Grasping," in *2021 IEEE/RSJ International Conference on Intelligent Robots and Systems (IROS)*, Sep. 2021, pp. 3963–3970. doi: 10.1109/IROS51168.2021.9636223.

[102] D. Liang *et al.*, "Synergistic Activation Patterns of Hand Muscles in Left-and Right-Hand Dominant Individuals," *J. Hum. Kinet.*, vol. 76, no. 1, pp. 89–100, Jan. 2021, doi: 10.2478/hukin-2021-0002.

[103] M. Santello, M. Flanders, and J. F. Soechting, "Postural hand synergies for tool use," *J. Neurosci. Off. J. Soc. Neurosci.*, vol. 18, no. 23, pp. 10105–10115, Dec. 1998.

[104] Q. Liu *et al.*, "CNN-Based Hand Grasping Prediction and Control via Postural Synergy Basis Extraction," *Sensors*, vol. 22, no. 3, Art. no. 3, Jan. 2022, doi: 10.3390/s22030831.

[105] T. Proietti, E. Guigon, A. Roby-Brami, and N. Jarrassé, "Modifying upper-limb inter-joint coordination in healthy subjects by training with a robotic exoskeleton," *J. Neuroengineering Rehabil.*, vol. 14, no. 1, p. 55, 12 2017, doi: 10.1186/s12984-017-0254-x.

[106] "Flexion hyperextension finger goniometer large," Stockx Medical. Accessed: Dec. 16, 2019. [Online]. Available: https://www.stockxmedical.com/en/flexion-hyperextension-finger-goniometer-large.html?source=facebook

[107] "Goniometers | BIOPAC," BIOPAC Systems, Inc. Accessed: Nov. 14, 2022. [Online]. Available: https://www.biopac.com/product-category/research/transducers/goniometers/

[108] Y. Liu, L. Jiang, D. Yang, and H. Liu, "Analysis of Hand and Wrist Postural Synergies in Tolerance Grasping of Various Objects," *PLOS ONE*, vol. 11, no. 8, p. e0161772, Aug. 2016, doi: 10.1371/journal.pone.0161772.

[109] N. Oess, J. Wanek, and A. Curt, "Design and evaluation of a low-cost instrumented glove for hand function assessment," *J. Neuroengineering Rehabil.*, vol. 9, p. 2, Jan. 2012, doi: 10.1186/1743-0003-9-2.

[110] "CyberGlove III," CyberGlove Systems LLC. Accessed: Nov. 14, 2022. [Online]. Available: http://www.cyberglovesystems.com/cyberglove-iii

[111] "5TH Dimension Technologies." Accessed: Dec. 18, 2019. [Online]. Available: https://www.5thdt.com/

[112] L. K. Simone, N. Sundarrajan, X. Luo, Y. Jia, and D. G. Kamper, "A low cost instrumented glove for extended monitoring and functional hand assessment," *J. Neurosci. Methods*, vol. 160, no. 2, pp. 335–348, Mar. 2007, doi: 10.1016/j.jneumeth.2006.09.021.

[113] K. T. Manal and T. S. Buchanan, "Biomechanics of human movements," in *Standard Handbook of Biomedical Engineering & Design*, Revised Edition., M. Kutz, Ed., McGraw-Hill Education, 2003. Accessed: Jul. 24, 2023. [Online]. Available: https://www.accessengineeringlibrary.com/content/book/9780071356374/chapter/chapter5

[114] N. J. Jarque-Bou, M. Atzori, and H. Müller, "A large calibrated database of hand movements and grasps kinematics," *Sci. Data*, vol. 7, no. 1, Art. no. 1, Jan. 2020, doi: 10.1038/s41597-019-0349-2.

[115] J. Romero, T. Feix, C. H. Ek, H. Kjellström, and D. Kragic, "Extracting Postural Synergies for Robotic Grasping," *IEEE Trans. Robot.*, vol. 29, no. 6, pp. 1342–1352, Dec. 2013, doi: 10.1109/TRO.2013.2272249.

[116] V. Patel and M. Burns, "Linear and Nonlinear Kinematic Synergies in the Grasping Hand," *J. Bioeng. Biomed. Sci.*, vol. 05, no. 02, 2015, doi: 10.4172/2155-9538.1000163.

[117] R. Vinjamuri, V. Patel, M. Powell, Z.-H. Mao, and N. Crone, "Candidates for Synergies: Linear Discriminants versus Principal Components," *Comput. Intell. Neurosci.*, vol. 2014, p. 373957, 2014, doi: 10.1155/2014/373957.

[118] N. J. Jarque-Bou, A. Scano, M. Atzori, and H. Müller, "Kinematic synergies of hand grasps: a comprehensive study on a large publicly available dataset," *J. NeuroEngineering Rehabil.*, vol. 16, no. 1, p. 63, May 2019, doi: 10.1186/s12984-019-0536-6.

[119] K. Pearson, "LIII.On lines and planes of closest fit to systems of points in space," *Philos. Mag. Ser. 6*, Nov. 1901, doi: 10.1080/14786440109462720.

[120] H. Hotelling, "Analysis of a complex of statistical variables into principal components.," *J. Educ. Psychol.*, Jan. 1933, doi: 10.1037/h0071325.

[121] "Lesson 6: Principal Component Analysis." Accessed: Nov. 26, 2019. [Online]. Available: https://onlinecourses.science.psu.edu/stat508/book/export/html/639

[122] I. T. Jolliffe, *Principal Component Analysis*. Springer Science & Business Media, 2013.

[123] N. Jarrassé, A. T. Ribeiro, A. Sahbani, W. Bachta, and A. Roby-Brami, "Analysis of hand synergies in healthy subjects during bimanual manipulation of various objects," *J. NeuroEngineering Rehabil.*, vol. 11, p. 113, Jul. 2014, doi: 10.1186/1743-0003-11-113.

[124] F. Touvet, A. Roby-Brami, M. A. Maier, and S. Eskiizmirliler, "Grasp: combined contribution of object properties and task constraints on hand and finger posture," *Exp. Brain Res.*, vol. 232, no. 10, pp. 3055–3067, Oct. 2014, doi: 10.1007/s00221-014-3990-1.

[125] E. Todorov and Z. Ghahramani, "Analysis of the synergies underlying complex hand manipulation," in *26th Annual International Conference of the IEEE Engineering in Medicine and Biology Society*, 2004, pp. 4637–4640.

[126] B. Liu, L. Jiang, and S. Fan, "Hand Posture Reconstruction Through Task-Dependent Hand Synergies," in *Intelligent Robotics and Applications*, X.-J. Liu, Z. Nie, J. Yu, F. Xie, and R. Song, Eds., in Lecture Notes in Computer Science. Cham: Springer International Publishing, 2021, pp. 14–24. doi: 10.1007/978-3-030-89095-7_2.

[127] P. H. Thakur, A. J. Bastian, and S. S. Hsiao, "Multidigit movement synergies of the human hand in an unconstrained haptic exploration task.," *J. Neurosci. Off. J. Soc. Neurosci.*, vol. 28, no. 6, pp. 1271–1281, 2008, doi: 10.1523/jneurosci.4512-07.2008.

[128] J. N. Ingram, K. P. Körding, I. S. Howard, and D. M. Wolpert, “The statistics of natural hand movements,” *Exp. Brain Res.*, vol. 188, no. 2, pp. 223–236, Jun. 2008, doi: 10.1007/s00221-008-1355-3.

[129] M. Atzori and H. Muller, “The Ninapro database: A resource for sEMG naturally controlled robotic hand prosthetics,” in *2015 37th Annual International Conference of the IEEE Engineering in Medicine and Biology Society (EMBC)*, Milan: IEEE, Aug. 2015, pp. 7151–7154. doi: 10.1109/EMBC.2015.7320041.

[130] M. Grebenstein *et al.*, “The DLR hand arm system,” in *2011 IEEE International Conference on Robotics and Automation*, May 2011, pp. 3175–3182. doi: 10.1109/ICRA.2011.5980371.

[131] G. Palli *et al.*, “The DEXMART hand: Mechatronic design and experimental evaluation of synergy-based control for human-like grasping,” *Int. J. Robot. Res.*, vol. 33, no. 5, pp. 799–824, Apr. 2014, doi: 10.1177/0278364913519897.

[132] M. Ciocarlie, C. Goldfeder, and P. Allen, “Dimensionality reduction for hand-independent dexterous robotic grasping,” in *2007 IEEE/RSJ International Conference on Intelligent Robots and Systems*, San Diego, CA, USA: IEEE, Oct. 2007, pp. 3270–3275. doi: 10.1109/IROS.2007.4399227.

[133] K. Xu, Z. Liu, B. Zhao, H. Liu, and X. Zhu, “Composed continuum mechanism for compliant mechanical postural synergy: An anthropomorphic hand design example,” *Mech. Mach. Theory*, vol. 132, pp. 108–122, Feb. 2019, doi: 10.1016/j.mechmachtheory.2018.08.015.

[134] K. Xu, H. Liu, Y. Du, and X. Zhu, “Design of an underactuated anthropomorphic hand with mechanically implemented postural synergies,” *Adv. Robot.*, vol. 28, no. 21, pp. 1459–1474, Nov. 2014, doi: 10.1080/01691864.2014.958534.

[135] C. Y. Brown and H. H. Asada, “Inter-Finger Coordination and Postural Synergies in Robot Hands Via Mechanical Implementation of Principal Components Analysis,” in *2007 IEEE/RSJ International Conference on Intelligent Robots and Systems*, Oct. 2007, pp. 2877–2882. doi: 10.1109/IROS.2007.4399547.

[136] C.-H. Xiong, W.-R. Chen, B.-Y. Sun, M.-J. Liu, S. Yue, and W.-B. Chen, “Design and implementation of an anthropomorphic hand for replicating human grasping functions,” *IEEE Trans. Robot.*, vol. 32, no. 3, Art. no. 3, Jun. 2016, doi: 10.1109/TRO.2016.2558193.

[137] W. Chen, C. Xiong, and Y. Wang, “Analysis and Synthesis of Underactuated Compliant Mechanisms Based on Transmission Properties of Motion and Force,” *IEEE Trans. Robot.*, vol. 36, no. 3, pp. 773–788, Jun. 2020, doi: 10.1109/TRO.2019.2963650.

[138] Y. Liu, L. Jiang, H. Liu, and D. Ming, “A straightforward and miniature implementation method of postural synergies to replicate human grasp characteristics accurately and intuitively,” *Bioinspir. Biomim.*, vol. 17, no. 2, p. 026012, Feb. 2022, doi: 10.1088/1748-3190/ac3f7f.

[139] A. Bicchi, M. Gabiccini, and M. Santello, “Modelling natural and artificial hands with synergies,” *Philos. Trans. R. Soc. Lond. B. Biol. Sci.*, vol. 366, pp. 3153–61, Nov. 2011, doi: 10.1098/rstb.2011.0152.

[140] G. Grioli, M. Catalano, E. Silvestro, S. Tono, and A. Bicchi, “Adaptive synergies: An approach to the design of under-actuated robotic hands,” in *2012*

IEEE/RSJ International Conference on Intelligent Robots and Systems, Oct. 2012, pp. 1251–1256. doi: 10.1109/IROS.2012.6385881.

[141] C. Della Santina, C. Piazza, G. Grioli, M. Catalano, and A. Bicchi, “Toward Dexterous Manipulation With Augmented Adaptive Synergies: The Pisa/IIT SoftHand 2,” *IEEE Trans. Robot.*, vol. PP, Apr. 2018, doi: 10.1109/TRO.2018.2830407.

[142] H. Li, C. J. Ford, M. Bianchi, M. G. Catalano, E. Psomopoulou, and N. F. Lepora, “BRL/Pisa/IIT SoftHand: A Low-Cost, 3D-Printed, Underactuated, Tendon-Driven Hand With Soft and Adaptive Synergies,” *IEEE Robot. Autom. Lett.*, vol. 7, no. 4, pp. 8745–8751, Oct. 2022, doi: 10.1109/LRA.2022.3187876.

[143] M. Laffranchi *et al.*, “The Hannes hand prosthesis replicates the key biological properties of the human hand,” *Sci. Robot.*, vol. 5, no. 46, p. eabb0467, Sep. 2020, doi: 10.1126/scirobotics.abb0467.

[144] M. Rossi, C. Della Santina, C. Piazza, G. Grioli, M. Catalano, and A. Bicchi, “Preliminary results toward a naturally controlled multi-synergistic prosthetic hand,” in *2017 International Conference on Rehabilitation Robotics (ICORR)*, Jul. 2017, pp. 1356–1363. doi: 10.1109/ICORR.2017.8009437.

[145] “Myo Armband.” Accessed: Nov. 04, 2022. [Online]. Available: https://www.myo.com/

[146] K. Yancosek, “Injury-induced hand dominance transfer,” *Univ. Ky. Dr. Diss.*, Jan. 2010, [Online]. Available: https://uknowledge.uky.edu/gradschool_diss/18

[147] S. Pheasant, *Bodyspace: Anthropometry, Ergonomics And The Design Of Work: Anthropometry, Ergonomics And The Design Of Work*. CRC Press, 1996.

[148] “Prosthetic leg in India, Artificial limbs in India, Artificial limb supplier, Prosthetic support, Orthotic support.” Accessed: Mar. 13, 2023. [Online]. Available: https://www.karepoindia.com/wrist-disarticulation.html

[149] “Factors of Safety.” Accessed: Jul. 21, 2020. [Online]. Available: https://www.engineeringtoolbox.com/factors-safety-fos-d_1624.html

[150] “Open Bionics’ 3D-printed ‘Hero Arm’ is now available in the US,” TechSpot. Accessed: Jul. 21, 2020. [Online]. Available: https://www.techspot.com/news/79515-open-bionics-3d-printed-hero-arm-now-available.html

[151] M. Vergara, J. L. Sancho-Bru, V. Gracia-Ibáñez, and A. Pérez-González, “An introductory study of common grasps used by adults during performance of activities of daily living,” *J. Hand Ther.*, vol. 27, no. 3, pp. 225–234, Jul. 2014, doi: 10.1016/j.jht.2014.04.002.

[152] M. Querejeta González, *Discapacidad/dependencia: unificación de criterios de valoración y clasificación*. Madrid: IMSERSO, 2004.

[153] “Barthel Index for Activities of Daily Living (ADL),” MDCalc. Accessed: Mar. 05, 2020. [Online]. Available: https://www.mdcalc.com/barthel-index-activities-daily-living-adl

[154] D. McCabe, “Katz Index of Independence in Activities of Daily Living (ADL),” p. 2.

[155] J. DENAVIT, “A kinematic notation for lower-pair mechanisms based on matrices.,” *Trans ASME J. Appl. Mech.*, vol. 22, pp. 215–221, 1955.

[156] C. Li, A. Fahmy, and J. Sienz, “Development of a Neural Network-Based Control System for the DLR-HIT II Robot Hand Using Leap Motion,” *IEEE Access*, vol. 7, pp. 136914–136923, Sep. 2019, doi: 10.1109/ACCESS.2019.2942648.

[157] I. M. Bullock, J. Borràs, and A. M. Dollar, “Assessing assumptions in kinematic hand models: A review,” in *2012 4th IEEE RAS EMBS International Conference on Biomedical Robotics and Biomechatronics (BioRob)*, Jun. 2012, pp. 139–146. doi: 10.1109/BioRob.2012.6290879.

[158] F. Chen, S. Appendino, A. Battezzato, A. Favetto, M. Mousavi, and F. Pescarmona, “Constraint Study for a Hand Exoskeleton: Human Hand Kinematics and Dynamics,” *J. Robot.*, vol. 2013, Sep. 2013, doi: 10.1155/2013/910961.

[159] M. Gabiccini, G. Stillfried, H. Marino, and M. Bianchi, “A data-driven kinematic model of the human hand with soft-tissue artifact compensation mechanism for grasp synergy analysis,” presented at the IEEE International Conference on Intelligent Robots and Systems, Nov. 2013. doi: 10.1109/IROS.2013.6696890.

[160] “Human Hand: Kinematics, Statics, and Dynamics | International Conference on Environmental Systems (ICES).” Accessed: Nov. 17, 2022. [Online]. Available: https://arc.aiaa.org/doi/10.2514/6.2011-5249

[161] K. Kim, Y. Youm, and W. K. Chung, “Human kinematic factor for haptic manipulation : the wrist to thumb,” in *Proceedings 10th Symposium on Haptic Interfaces for Virtual Environment and Teleoperator Systems. HAPTICS 2002*, Mar. 2002, pp. 319–326. doi: 10.1109/HAPTIC.2002.998975.

[162] John Lin, Ying Wu, and T. S. Huang, “Modeling the constraints of human hand motion,” in *Proceedings Workshop on Human Motion*, Dec. 2000, pp. 121–126. doi: 10.1109/HUMO.2000.897381.

[163] “CaptoGlove - Virtual reality wearable gaming motion controller,” CaptoGlove®. Accessed: Nov. 16, 2022. [Online]. Available: https://www.captoglove.com/

[164] admin_Hendri, “5DT Data Glove Ultra,” 5DT. Accessed: Nov. 16, 2022. [Online]. Available: https://5dt.com/5dt-data-glove-ultra/

[165] L. Dipietro, A. M. Sabatini, and P. Dario, “A Survey of Glove-Based Systems and Their Applications,” *IEEE Trans. Syst. Man Cybern. Part C Appl. Rev.*, vol. 38, no. 4, pp. 461–482, Jul. 2008, doi: 10.1109/TSMCC.2008.923862.

[166] R. Gentner and J. Classen, “Development and evaluation of a low-cost sensor glove for assessment of human finger movements in neurophysiological settings,” *J. Neurosci. Methods*, vol. 178, no. 1, pp. 138–147, Mar. 2009, doi: 10.1016/j.jneumeth.2008.11.005.

[167] S. Zhu, A. Stuttaford-Fowler, A. Fahmy, C. Li, and J. Sienz, “Development of a Low-cost Data Glove using Flex Sensors for the Robot Hand Teleoperation,” in *2021 3rd International Symposium on Robotics & Intelligent Manufacturing Technology (ISRIMT)*, Sep. 2021, pp. 47–51. doi: 10.1109/ISRIMT53730.2021.9596972.

[168] G. Saggio, F. Riillo, L. Sbernini, and L. R. Quitadamo, “Resistive flex sensors: a survey,” *Smart Mater. Struct.*, vol. 25, no. 1, p. 013001, Dec. 2015, doi: 10.1088/0964-1726/25/1/013001.

[169] "Bend Sensor | Flexpoint Sensor Systems | United States," Flexpoint. Accessed: Feb. 26, 2020. [Online]. Available: https://www.flexpoint.com

[170] "Custom Linear Potentiometer Manufacturer | Spectra Symbol." Accessed: Dec. 18, 2019. [Online]. Available: https://www.spectrasymbol.com/

[171] G. Saggio, A. Pallotti, L. Sbernini, V. Errico, and F. Di Paolo, "Feasibility of Commercial Resistive Flex Sensors for Hand Tracking Applications," *Sens. Transducers*, vol. 201, pp. 17–26, Jun. 2016.

[172] G. Saggio, "Electrical Resistance Profiling of Bend Sensors Adopted to Measure Spatial Arrangement of the Human Body," in *Proceedings of the 4th International Symposium on Applied Sciences in Biomedical and Communication Technologies*, in ISABEL '11. New York, NY, USA: ACM, 2011, p. 5:1-5:5. doi: 10.1145/2093698.2093703.

[173] G. D. Kessler, L. F. Hodges, and N. Walker, *Kessler, Hodges, Walker: Evaluation of the CyberGloveTM as a Whole Hand Input Device 1 Evaluation of the CyberGlove TM as a Whole Hand Input Device*.

[174] F. Kahlesz, G. Zachmann, and R. Klein, "'Visual-fidelity' dataglove calibration," in *Proceedings Computer Graphics International, 2004.*, Jun. 2004, pp. 403–410. doi: 10.1109/CGI.2004.1309241.

[175] L. K. Simone and D. G. Kamper, "Design considerations for a wearable monitor to measure finger posture," *J. NeuroEngineering Rehabil.*, vol. 2, p. 5, Mar. 2005, doi: 10.1186/1743-0003-2-5.

[176] S. Wise *et al.*, "Evaluation of a fiber optic glove for semi-automated goniometric measurements," *J. Rehabil. Res. Dev.*, vol. 27, no. 4, p. 411, 1990, doi: 10.1682/JRRD.1990.10.0411.

[177] L. Dipietro, A. M. Sabatini, and P. Dario, "Evaluation of an instrumented glove for hand-movement acquisition.," *J. Rehabil. Res. Dev.*, vol. 40, no. 2, pp. 179–189, 2003, doi: 10.1682/JRRD.2003.03.0181.

[178] D. E. Nathan, M. J. Johnson, and J. R. McGuire, "Design and validation of low-cost assistive glove for hand assessment and therapy during activity of daily living-focused robotic stroke therapy," *J. Rehabil. Res. Dev.*, vol. 46, no. 5, pp. 587–602, 2009, doi: 10.1682/jrrd.2008.04.0052.

[179] G. Saggio, A. Lagati, and G. Orengo, "Shaping Resistive Bend Sensors to Enhance Readout Linearity," *ISRN Electron.*, vol. 2012, Nov. 2012, doi: 10.5402/2012/359759.

[180] "U6 | LabJack." Accessed: Jan. 19, 2023. [Online]. Available: https://labjack.com/products/u6

[181] "CB37 Terminal Board | LabJack." Accessed: Jan. 19, 2023. [Online]. Available: https://labjack.com/accessories/cb37-terminal-board

[182] "DAQFactory." Azeotech. Accessed: Jan. 19, 2023. [Online]. Available: https://www.azeotech.com/j/

[183] "SketchUp Software." Trimble, 2017. Accessed: Sep. 29, 2023. [Online]. Available: www.sketchup.com

[184] "IBM SPSS Statistics." IBM Corp., Armonk, NY, 2019. Accessed: Sep. 29, 2023. [Windows]. Available: https://www.ibm.com/spss

[185] L. S. Meyers, G. Gamst, and A. J. Guarino, *Applied Multivariate Research: Design and Interpretation*. SAGE, 2006.

[186] V. Gracia-Ibáñez, J. L. Sancho-Bru, M. Vergara, N. J. Jarque-Bou, and A. Roda-Sales, "Sharing of hand kinematic synergies across subjects in daily living activities," *Sci. Rep.*, vol. 10, no. 1, Art. no. 1, Apr. 2020, doi: 10.1038/s41598-020-63092-7.

[187] N. Jarrassé, A. T. Ribeiro, A. Sahbani, W. Bachta, and A. Roby-Brami, "Analysis of hand synergies in healthy subjects during bimanual manipulation of various objects," *J. NeuroEngineering Rehabil.*, vol. 11, no. 1, p. 113, Jul. 2014, doi: 10.1186/1743-0003-11-113.

[188] V. Serdarushich, *Vectors and Coordinate Geometry*. CreateSpace Independent Publishing Platform, 2016.

[189] "Fundamentals of grasping - stanford university, https://web.stanford.edu/class/cs237b/pdfs/lecture/lecture_567.pdf (accessed Jul. 5, 2023)."

[190] D. Prattichizzo and J. C. (Jeff) Trinkle, "Grasping," 2008, pp. 671–700. doi: 10.1007/978-3-540-30301-5_29.

[191] "Grasping | SpringerLink." Accessed: Jul. 11, 2023. [Online]. Available: https://link.springer.com/referenceworkentry/10.1007/978-3-540-30301-5_29

[192] V. L. Popov, "Coulomb's Law of Friction," in *Contact Mechanics and Friction: Physical Principles and Applications*, V. L. Popov, Ed., Berlin, Heidelberg: Springer, 2010, pp. 133–154. doi: 10.1007/978-3-642-10803-7_10.

[193] S. Carpin, S. Liu, J. Falco, and K. Van Wyk, "Multi-Fingered Robotic Grasping: A Primer," Jul. 2016.

[194] C. Ferraresi, D. Maffiodo, F. Pescarmona, O. Bounous, L. Bonaria, and M. Straiotto, "Low-Shock Manipulation and Testing of Micro Electro-Mechanical Systems (MEMS)," 2010. doi: 10.5772/10429.

[195] B. León, J. L. Sancho-Bru, N. J. Jarque-Bou, A. Morales, and M. A. Roa, "Evaluation of Human Prehension Using Grasp Quality Measures," *Int. J. Adv. Robot. Syst.*, vol. 9, no. 4, p. 112, Oct. 2012, doi: 10.5772/51907.

[196] M. Pozzi, M. Malvezzi, and D. Prattichizzo, "On Grasp Quality Measures: Grasp Robustness and Contact Force Distribution in Underactuated and Compliant Robotic Hands," *IEEE Robot. Autom. Lett.*, vol. 2, no. 1, pp. 329–336, Jan. 2017, doi: 10.1109/LRA.2016.2612304.

[197] S. Boyd and B. Wegbreit, "Fast Computation of Optimal Contact Forces," *Robot. IEEE Trans. On*, vol. 23, pp. 1117–1132, Jan. 2008, doi: 10.1109/TRO.2007.910774.

[198] H. Asada and J.-J. E. Slotine, *Robot Analysis and Control*. John Wiley & Sons, 1991.

[199] "Sollerman Hand Function Test: A Standardised Method and its Use in Tetraplegic Patients: Scandinavian Journal of Plastic and Reconstructive Surgery and Hand Surgery: Vol 29, No 2." Accessed: Sep. 05, 2022. [Online]. Available: https://www.tandfonline.com/doi/abs/10.3109/02844319509034334?journalCode=iphs19

[200] S. K. Coates, L. A. Harvey, S. A. Dunlop, and G. T. Allison, "The AuSpinal: a test of hand function for people with tetraplegia," *Spinal Cord*, vol. 49, no. 2, Art. no. 2, Feb. 2011, doi: 10.1038/sc.2010.86.

[201] Y. Aquilina, M. A. Saliba, J. Attard, and A. Dingli, “Typical External Loads that Require to be Resisted by a Non-dominant Prosthetic Hand,” in *2022 IEEE 21st Mediterranean Electrotechnical Conference (MELECON)*, Jun. 2022, pp. 142–147. doi: 10.1109/MELECON53508.2022.9843002.

[202] B. León *et al.*, “OpenGRASP: A Toolkit for Robot Grasping Simulation,” in *Simulation, Modeling, and Programming for Autonomous Robots*, vol. 6472, N. Ando, S. Balakirsky, T. Hemker, M. Reggiani, and O. Von Stryk, Eds., in Lecture Notes in Computer Science, vol. 6472. , Berlin, Heidelberg: Springer Berlin Heidelberg, 2010, pp. 109–120. doi: 10.1007/978-3-642-17319-6_13.

[203] A. T. Miller and P. K. Allen, “Graspit! A versatile simulator for robotic grasping,” *IEEE Robot. Autom. Mag.*, vol. 11, no. 4, pp. 110–122, Dec. 2004, doi: 10.1109/MRA.2004.1371616.

[204] M. Malvezzi, G. Gioioso, G. Salvietti, and D. Prattichizzo, “SynGrasp: A MATLAB Toolbox for Underactuated and Compliant Hands,” *IEEE Robot. Autom. Mag.*, vol. 22, no. 4, pp. 52–68, Dec. 2015, doi: 10.1109/MRA.2015.2408772.

[205] “Unity.” Unity Technologies. Accessed: Jan. 19, 2023. [Online]. Available: https://unity.com/

[206] U. Technologies, “Unity - Manual: Physics.” Accessed: Jan. 19, 2023. [Online]. Available: https://docs.unity3d.com/Manual/PhysicsSection.html

[207] U. Technologies, “Unity - Manual: Introduction to physics articulations.” Accessed: Jan. 05, 2023. [Online]. Available: https://docs.unity3d.com/Manual/physics-articulations.html

[208] “Unity Asset Store - The Best Assets for Game Making.” Accessed: Jan. 05, 2023. [Online]. Available: https://assetstore.unity.com/

[209] “Optimization Problem Types - Smooth Nonlinear Optimization,” solver. Accessed: Jan. 20, 2024. [Online]. Available: https://www.solver.com/smooth-nonlinear-optimization

[210] “Excel Solver - Algorithms and Methods Used,” solver. Accessed: Jan. 11, 2023. [Online]. Available: https://www.solver.com/excel-solver-algorithms-and-methods-used

[211] “Excel Solver - Evolutionary Solving Method Stopping Conditions,” solver. Accessed: Jan. 11, 2023. [Online]. Available: https://www.solver.com/excel-solver-evolutionary-solving-method-stopping-conditions

[212] M. Bures, T. Gorner, and B. Sediva, “Hand anthropometry of Czech population,” in *2015 IEEE International Conference on Industrial Engineering and Engineering Management (IEEM)*, Dec. 2015, pp. 1077–1082. doi: 10.1109/IEEM.2015.7385814.

[213] S. Jee and M. H. Yun, “An anthropometric survey of Korean hand and hand shape types,” *Int. J. Ind. Ergon.*, vol. 53, pp. 10–18, May 2016, doi: 10.1016/j.ergon.2015.10.004.

[214] A. Buryanov and V. Kotiuk, “Proportions of Hand Segments,” *Int. J. Morphol.*, vol. 28, no. 3, Sep. 2010, doi: 10.4067/S0717-95022010000300015.

[215] T. Mouri, “Anthropomorphic Robot Hand : Gifu Hand III,” 2002. Accessed: Jan. 18, 2023. [Online]. Available: https://www.semanticscholar.org/paper/Anthropomorphic-Robot-Hand-%3A-Gifu-Hand-III-Mouri/c09601e65dfaa49bea4e26718a8b556e930a8eda

[216] W. S. You, Y. H. Lee, G. Kang, H. S. Oh, J. K. Seo, and H. R. Choi, “Kinematic design optimization of anthropomorphic robot hand using a new performance index,” in *2017 14th International Conference on Ubiquitous Robots and Ambient Intelligence (URAI)*, Jun. 2017, pp. 20–25. doi: 10.1109/URAI.2017.7992878.

[217] W. S. You, Y. H. Lee, G. Kang, H. S. Oh, J. K. Seo, and H. R. Choi, “Kinematic design optimization for anthropomorphic robot hand based on interactivity of fingers,” *Intell. Serv. Robot.*, vol. 12, no. 2, pp. 197–208, Apr. 2019, doi: 10.1007/s11370-019-00274-x.

[218] “MATLAB.” TheMathWorks, Inc., 2020. Accessed: Jan. 19, 2023. [Online]. Available: https://uk.mathworks.com/products/matlab.html

[219] “Genetic Algorithm.” Accessed: Jan. 16, 2023. [Online]. Available: https://www.mathworks.com/matlabcentral/fileexchange/74132-genetic-algorithm

[220] A. Hassanat, K. Almohammadi, E. Alkafaween, E. Abunawas, A. Hammouri, and V. B. S. Prasath, “Choosing Mutation and Crossover Ratios for Genetic Algorithms—A Review with a New Dynamic Approach,” *Information*, vol. 10, no. 12, Art. no. 12, Dec. 2019, doi: 10.3390/info10120390.

[221] K. Deb and S. Agrawal, “A Niched-Penalty Approach for Constraint Handling in Genetic Algorithms,” in *Artificial Neural Nets and Genetic Algorithms*, A. Dobnikar, N. C. Steele, D. W. Pearson, and R. F. Albrecht, Eds., Vienna: Springer, 1999, pp. 235–243. doi: 10.1007/978-3-7091-6384-9_40.

[222] K.-H. Choi, J.-K. Kim, H.-H. Shim, and Y.-K. Kong, “Gender-Based Differences in Actual Thumb Force Exertions at Various Target Force Levels,” *Appl. Sci.*, vol. 10, no. 1, Art. no. 1, Jan. 2020, doi: 10.3390/app10010194.

[223] J. Szkopek and G. Redlarski, “Artificial-Hand Technology—Current State of Knowledge in Designing and Forecasting Changes,” *Appl. Sci.*, vol. 9, no. 19, Art. no. 19, Jan. 2019, doi: 10.3390/app9194090.

[224] “Brushless vs Brushed DC Motor | What`s Difference? | ELTRA TRADE.” Accessed: Feb. 08, 2023. [Online]. Available: https://eltra-trade.com/blog/brushless-vs-brushed-motor

[225] A. Hughes, *Electric Motors and Drives: Fundamentals, Types and Applications*. Elsevier, 2005.

[226] “Brushless Vs Brushed DC Motors: When and Why to Choose One Over the Other | Article | MPS.” Accessed: Jul. 29, 2021. [Online]. Available: https://www.monolithicpower.com/en/brushless-vs-brushed-dc-motors

[227] “What are Brushless DC Motors | Renesas.” Accessed: Jul. 29, 2021. [Online]. Available: https://www.renesas.com/us/en/support/engineer-school/brushless-dc-motor-01-overview

[228] H. Liu *et al.*, “A dexterous humanoid five-fingered robotic hand,” Sep. 2008, pp. 371–376. doi: 10.1109/ROMAN.2008.4600694.

[229] “What is Motor Stall - Stall Current and Stall Torque – Wira Electrical.” Accessed: May 10, 2023. [Online]. Available: https://wiraelectrical.com/what-is-motor-stall/

[230] “Gears: Self-locking or Back-drivability,” maxon Support. Accessed: Feb. 08, 2023. [Online]. Available: https://support.maxongroup.com/hc/en-us/articles/5881942527132-Gears-Self-locking-or-Back-drivability

[231] "All About Stepper Motors - What They Are and How They Work." Accessed: Jul. 29, 2021. [Online]. Available: https://www.thomasnet.com/articles/machinery-tools-supplies/stepper-motors

[232] "Stepper Motors vs. DC Motors - What's the Difference?" Accessed: Jul. 29, 2021. [Online]. Available: https://www.thomasnet.com/articles/machinery-tools-supplies/stepper-motors-vs-dc-motors

[233] L. Dunai, M. Novak, and C. Espert, "Human Hand Anatomy-Based Prosthetic Hand," *Sensors*, vol. 21, p. 137, Dec. 2020, doi: 10.3390/s21010137.

[234] "EnergyPack | Batteries | Myo Batteries / Chargers | Myo Hands and Components | Upper Limb Prosthetics | Prosthetics | Ottobock US Shop." Accessed: Feb. 10, 2023. [Online]. Available: https://shop.ottobock.us/Prosthetics/Upper-Limb-Prosthetics/Myo-Hands-and-Components/Myo-Batteries-Chargers/Batteries/EnergyPack/p/757B20

[235] Yumpu.com, "technical information - BeBionic," yumpu.com. Accessed: Feb. 10, 2023. [Online]. Available: https://www.yumpu.com/en/document/view/38440333/technical-information-bebionic

[236] "bebionicTechManualSmall.pdf." Accessed: Aug. 07, 2021. [Online]. Available: https://shop.ottobock.us/media/pdf/bebionicTechManualSmall.pdf

[237] "Comparison of Gear Efficiencies - Spur, Helical, Bevel, Worm, Hypoid, Cycloid." Accessed: Sep. 05, 2021. [Online]. Available: https://www.meadinfo.org/2008/11/gear-efficiency-spur-helical-bevel-worm.html

[238] "16DCT Athlonix - Precious Metal Brush DC Motor | Portescap." Accessed: Feb. 10, 2023. [Online]. Available: https://www.portescap.com/en/products/brush-dc-motors/athlonix-motors/16dct-athlonix-precious-metal-brush-dc-motor

[239] "R16 Mini Motor Gearhead | Portescap." Accessed: Feb. 10, 2023. [Online]. Available: https://www.portescap.com/en/products/accessories/gearheads/r16-ball-bearing-mini-motor-gearhead

[240] M. Controzzi, C. Cipriani, and M. C. Carrozza, "Miniaturized non-back-drivable mechanism for robotic applications," *Mech. Mach. Theory*, vol. 10, pp. 1395–1406, Oct. 2010, doi: 10.1016/j.mechmachtheory.2010.05.008.

[241] "Coefficients Of Friction - Roy Mech." Accessed: Feb. 18, 2023. [Online]. Available: https://roymech.org/Useful_Tables/Tribology/co_of_frict.html

[242] "Series 1024 ... SR," Dr. Fritz Faulhaber GmbH & Co. KG. Accessed: Feb. 13, 2023. [Online]. Available: https://www.faulhaber.com/en/products/series/1024sr/

[243] "Series 10/1," Dr. Fritz Faulhaber GmbH & Co. KG. Accessed: Feb. 13, 2023. [Online]. Available: https://www.faulhaber.com/en/products/series/101/

[244] "Small dc motors for Myoelectric prosthesis." Accessed: Sep. 04, 2021. [Online]. Available: https://www.faulhaber.com/en/markets/medical-laboratory-equipment/small-dc-motors-for-myoelectric-prosthesis/

[245] "Autodesk Inventor Professional." Autodesk, 2017. Accessed: Sep. 29, 2023. [Online]. Available: https://www.autodesk.com/products/inventor/free-trial

[246] "human hand - Recent models | 3D CAD Model Collection | GrabCAD Community Library." Accessed: Feb. 13, 2023. [Online]. Available:

https://grabcad.com/library?page=1&time=all_time&sort=recent&query=human%20hand

[247] "free human hands feet foot 3d model." Accessed: Jul. 10, 2022. [Online]. Available: https://www.turbosquid.com/3d-models/free-human-hands-feet-foot-3d-model/587188

[248] admin, "Gear Train : Gear Ratio, Torque and Speed Calculations," SMLease Design. Accessed: Feb. 15, 2023. [Online]. Available: https://www.smlease.com/entries/mechanism/gear-train-gear-ratio-torque-and-speed-calculation/

[249] M. Nabeel, K. Aqeel, M. N. Ashraf, M. Awan, and M. Khurram, *Vibrotactile stimulation for 3D printed prosthetic hand*. 2016, p. 207. doi: 10.1109/ICRAI.2016.7791254.

[250] A. Prakash and S. Sharma, "A low-cost system to control prehension force of a custom-made myoelectric hand prosthesis," *Res. Biomed. Eng.*, vol. 36, no. 3, pp. 237–247, Sep. 2020, doi: 10.1007/s42600-020-00064-w.

[251] "Gear nomenclature. - ppt video online download." Accessed: Feb. 15, 2023. [Online]. Available: https://slideplayer.com/slide/1701535/

[252] S. P. Radzevich, *Dudley's Handbook of Practical Gear Design and Manufacture, Second Edition*. CRC Press, 2012.

[253] "Damage to Gears | KHK Gear Manufacturer." Accessed: Feb. 15, 2023. [Online]. Available: https://khkgears.net/new/gear_knowledge/gear_technical_reference/damage_to_gears.html

[254] "Gear Strength and Gear Durability | KHK." Accessed: Jul. 10, 2022. [Online]. Available: https://khkgears.net/new/gear_knowledge/gear_technical_reference/gear-strength-and-gear-durability.html

[255] "Lewis Factor Equation for Gear Tooth Calculations." Accessed: Feb. 15, 2023. [Online]. Available: https://www.engineersedge.com/gears/lewis-factor.htm

[256] M. Ibrahim and M. Prem, "Implications of Static and Dynamic Analysis of Bevel Gear," *J. Adv. Res. Dyn. Control Syst.*, vol. 12, p. 2020, Feb. 2020.

[257] P. S. Sunil, "How to design spur gear effects of various parameters on strength of spur gear," vol. 3, no. 7, p. 3.

[258] "Bevel Gears," Roymech. Accessed: Jul. 10, 2022. [Online]. Available: https://www.roymech.co.uk/Useful_Tables/Drive/Bevel_Gears.html

[259] (C) 2020 Conrad Electronic, "Reely Steel bevel gear wheel Module Type: 1.0 No. of teeth: 16, 16 1 Pair | Conrad.com." Accessed: Jul. 10, 2022. [Online]. Available: https://www.conrad.com/p/reely-steel-bevel-gear-wheel-module-type-10-no-of-teeth-16-16-1-pair-237271

[260] J. He, "S45C Steel For Machine Structural Use JIS G4051 - Special Steel," Otai Special Steel. Accessed: May 11, 2023. [Online]. Available: https://www.astmsteel.com/product/jis-s45c-steel-machine-structural/

[261] "Buy KHK SS0.5-17A, 0.5, 17 Tooth, Carbon Steel Spur Gears Online at desertcart Malta." Accessed: Jul. 10, 2022. [Online]. Available: https://malta.desertcart.com/products/409979432-khk-ss-0-5-17-a-0-5-17-tooth-carbon-steel-spur-gears

[262] "Buy KHK SS0.5-36A, 0.5, 36 Tooth, Carbon Steel Spur Gears Online at desertcart Malta." Accessed: Jul. 10, 2022. [Online]. Available: https://malta.desertcart.com/products/409981218-khk-ss-0-5-36-a-0-5-36-tooth-carbon-steel-spur-gears

[263] "How to interpret the self-locking mechanism of worm gearboxes." Accessed: Feb. 17, 2023. [Online]. Available: https://www.bj-gear.com/about-bj-gear/information-centre/technical-knowledge-base/how-to-interpret-the-self-locking-mechanism-of-worm-gearboxes

[264] P. C. GOPE, *Machine Design: Fundamentals and Applications*. PHI Learning Pvt. Ltd., 2012.

[265] "KHK - Worm Gear Selector." Accessed: Jul. 10, 2022. [Online]. Available: https://khkgears2.net/catalog5/AG0.8-20R1

[266] "KHK - Worm Gear Selector." Accessed: Jul. 10, 2022. [Online]. Available: https://khkgears2.net/catalog5/KWG0.8-R1

[267] "Aluminium Bronze UNS C95400 – Copper Alloy," AZoM.com. Accessed: Feb. 17, 2023. [Online]. Available: https://www.azom.com/article.aspx?ArticleID=6291

[268] "KHK - Bevel Gear (or Miter Gear) Selector." Accessed: Jul. 10, 2022. [Online]. Available: https://khkgears2.net/catalog6/DB0.5-2040

[269] "KHK - Bevel Gear (or Miter Gear) Selector." Accessed: Jul. 10, 2022. [Online]. Available: https://khkgears2.net/catalog6/DB0.5-4020

[270] "Polyplastics Duracon® M90-44/M90S Acetal Co-polymer (POM), Standard, General." Accessed: Feb. 18, 2023. [Online]. Available: https://www.matweb.com/search/datasheet.aspx?matguid=3801a82d61974e15b563d86e41de45e4

[271] M. Loesche, "When to Use Wire Leaders for Fishing?," Strike and Catch. Accessed: Jul. 16, 2022. [Online]. Available: https://strikeandcatch.com/when-to-use-wire-leaders-for-fishing/

[272] "#8 ToothProof Stainless Steel Single Strand Leader, 86 lb (39 kg) test, .020 in (0.51 mm) dia, Camo, 1 lb (454 g)." Accessed: Feb. 20, 2023. [Online]. Available: https://www.afwfishing.com/afw_products/S08C-01.asp

[273] R. S. Dahiya, G. Metta, M. Valle, and G. Sandini, "Tactile Sensing—From Humans to Humanoids," *IEEE Trans. Robot.*, vol. 26, no. 1, pp. 1–20, Feb. 2010, doi: 10.1109/TRO.2009.2033627.

[274] Z. Kappassov, J.-A. Corrales, and V. Perdereau, "Tactile sensing in dexterous robot hands — Review," *Robot. Auton. Syst.*, vol. 74, pp. 195–220, Dec. 2015, doi: 10.1016/j.robot.2015.07.015.

[275] "How Does a Force Sensing Resistor (FSR) Work? | Tekscan." Accessed: Feb. 20, 2023. [Online]. Available: https://www.tekscan.com/blog/flexiforce/how-does-force-sensing-resistor-fsr-work

[276] "FlexiForce ESS102 Sensor," Tekscan. Accessed: Jul. 16, 2022. [Online]. Available: https://tekscan.com/products-solutions/force-sensors/ess102

[277] "blender.org." Blender Foundation. Accessed: Sep. 29, 2023. [Online]. Available: https://www.blender.org/

[278] "Ansys | Engineering Simulation Software." Accessed: Sep. 29, 2023. [Online]. Available: https://www.ansys.com/

[279] “FEA and 3D Printing - Challenges and Potential Workarounds,” GrabCAD Blog. Accessed: Feb. 27, 2023. [Online]. Available: https://blog.grabcad.com/blog/2016/04/27/fea-and-3d-printing-challenges/

[280] D. Abbot, D. Kallon, C. Anghel, and P. Dube, “Finite Element Analysis of 3D Printed Model via Compression Tests,” *Procedia Manuf.*, vol. 35, pp. 164–173, Jan. 2019, doi: 10.1016/j.promfg.2019.06.001.

[281] “Fused Deposition Modeling (FDM),” MakerVerse. Accessed: Mar. 01, 2023. [Online]. Available: https://www.makerverse.ai/technologies-fdm

[282] “Ultimaker Cura: Powerful, easy-to-use 3D printing software,” https://ultimaker.com. Accessed: Jul. 16, 2022. [Online]. Available: https://ultimaker.com/software/ultimaker-cura

[283] “3D printing software of Creality Cloud,” 3D printing software of Creality Cloud. Accessed: Jul. 19, 2023. [Online]. Available: https://www.crealitycloud.com

[284] J. O’Connell, “Wall Thickness (3D Printing): How to Make It Perfect,” All3DP. Accessed: Jul. 16, 2022. [Online]. Available: https://all3dp.com/2/3d-printing-wall-thickness-tutorial/

[285] M. Somireddy and A. Czekanski, “Anisotropic material behavior of 3D printed composite structures – Material extrusion additive manufacturing,” *Mater. Des.*, vol. 195, p. 108953, Oct. 2020, doi: 10.1016/j.matdes.2020.108953.

[286] “FDM vs SLA 3D Printer: The Best Pick for Your Application?” Accessed: Jul. 16, 2022. [Online]. Available: https://bigrep.com/posts/fdm-vs-sla-3d-printer/

[287] “3D Printing Technology Comparison: FDM vs. SLA vs. SLS,” Formlabs. Accessed: Jul. 16, 2022. [Online]. Available: https://formlabs.com/eu/blog/fdm-vs-sla-vs-sls-how-to-choose-the-right-3d-printing-technology/

[288] “FDM vs SLA - 3D Printing Process Breakdown.” Accessed: Jul. 16, 2022. [Online]. Available: https://markforged.com/resources/blog/fdm-vs-sla

[289] PrimaCreator, “PrimaCreator SELECT™ NylonPower Carbon Fiber,” PrimaCreator. Accessed: Jul. 16, 2022. [Online]. Available: https://primacreator.com/products/select%e2%84%a2-nylon-power-carbon-fiber

[290] PrimaCreator, “PrimaValue™ PLA,” PrimaCreator. Accessed: Apr. 04, 2023. [Online]. Available: https://primacreator.com/products/primavalue%e2%84%a2-pla

[291] PrimaCreator, “PrimaCreator™ Select PVA HT (High Temperature),” PrimaCreator. Accessed: Mar. 03, 2023. [Online]. Available: https://primacreator.com/products/primacreator%e2%84%a2-select-pva-ht-high-temperature

[292] “How to Make Strong 3D Prints: 5 Tips to Strengthen 3D Printed Parts,” Rapid Direct. Accessed: Jul. 16, 2022. [Online]. Available: https://www.rapiddirect.com/blog/how-to-make-strong-3d-prints/

[293] “3D Printing Part Strength · superjamie/lazyweb Wiki,” GitHub. Accessed: Jul. 16, 2022. [Online]. Available: https://github.com/superjamie/lazyweb

[294] Martin, “3D Printing Infill | Patterns, Density, Strength, Stability,” The 3D Printer Bee. Accessed: Jul. 16, 2022. [Online]. Available: https://the3dprinterbee.com/3d-printing-infill/

[295] “Infill settings,” Ultimaker Support. Accessed: Jul. 16, 2022. [Online]. Available: https://support.ultimaker.com/hc/en-us/articles/360012607079-Infill-settings

[296] “Cura infill patterns: What they are and when to use them,” Wevolver. Accessed: Jul. 16, 2022. [Online]. Available: https://www.wevolver.com/article/cura-infill-patterns-what-they-are-and-when-to-use-them

[297] F. Arceo, “Infill Patterns; Which is the Strongest one for 3D printing? – 3D Solved.” Accessed: Jul. 16, 2022. [Online]. Available: https://3dsolved.com/infill-patterns-which-is-the-strongest-one-for-3d-printing/

[298] “The influence of layer height on the strength of FDM 3D prints,” CNC Kitchen. Accessed: Jul. 16, 2022. [Online]. Available: https://www.cnckitchen.com/blog/the-influence-of-layer-height-on-the-strength-of-fdm-3d-prints

[299] “3D Printing Settings Impacting Part Strength.” Accessed: Jul. 16, 2022. [Online]. Available: https://markforged.com/resources/learn/design-for-additive-manufacturing-plastics-composites/understanding-3d-printing-strength/3d-printing-settings-impacting-part-strength

[300] J. R. Stojković *et al.*, “An Experimental Study on the Impact of Layer Height and Annealing Parameters on the Tensile Strength and Dimensional Accuracy of FDM 3D Printed Parts,” *Materials*, vol. 16, no. 13, Art. no. 13, Jan. 2023, doi: 10.3390/ma16134574.

[301] “7.2. Nozzle Sizes — Bob’s Project Notebook.” Accessed: Sep. 29, 2023. [Online]. Available: https://muppetlabs.co/3dprinting_nozzle_sizes.html

[302] C. Naramore, “How to Get Stronger FDM 3D Prints,” 3D Printing. Accessed: Jul. 16, 2022. [Online]. Available: https://3dprinting.com/how-to/how-to-get-stronger-fdm-3d-prints/

[303] “7075-T6 Aluminium: Overview & Properties - Matmatch.” Accessed: Jul. 16, 2022. [Online]. Available: https://matmatch.com/learn/material/7075-t6-aluminium

[304] “Coefficient of Friction Equation and Table Chart.” Accessed: Jul. 16, 2022. [Online]. Available: https://www.engineersedge.com/coeffients_of_friction.htm

[305] “The Active Hands Company | Limited Mobility Gripping Aids,” The Active Hands Company. Accessed: Mar. 16, 2023. [Online]. Available: https://www.activehands.com/

[306] Össur. Life Without Limitations., “i-limb hand user manual.” Accessed: Mar. 17, 2023. [Online]. Available: chrome-extension://efaidnbmnnnibpcajpcglclefindmkaj/https://training.touchbionics.com/pdfs/MA01382_i-limb_hand_user_manual_Sept18.pdf

[307] P. Weiner, J. Starke, F. Hundhausen, J. Beil, and T. Asfour, “The KIT Prosthetic Hand: Design and Control,” in *2018 IEEE/RSJ International Conference on Intelligent Robots and Systems (IROS)*, Oct. 2018, pp. 3328–3334. doi: 10.1109/IROS.2018.8593851.

[308] "3ders.org - Wounded war hero gets a 3D printed Dextrus bionic hand | 3D Printer News & 3D Printing News." Accessed: Mar. 17, 2023. [Online]. Available: https://www.3ders.org/articles/20150411-wounded-war-hero-has-been-provided-with-a-3d-printed-dextrus-bionic-hand.html

[309] "Hand and Forarm – InMoov," InMoov. Accessed: Mar. 17, 2023. [Online]. Available: https://inmoov.fr/hand-and-forarm/

[310] I. Llop-Harillo, A. Pérez-González, and J. Andrés-Esperanza, "Grasping Ability and Motion Synergies in Affordable Tendon-Driven Prosthetic Hands Controlled by Able-Bodied Subjects," *Front. Neurorobotics*, vol. 14, 2020, Accessed: Aug. 17, 2022. [Online]. Available: https://www.frontiersin.org/articles/10.3389/fnbot.2020.00057

[311] "Establishing a standardized clinical assessment tool of pathologic and prosthetic hand function: Normative data, reliability, and validity - Archives of Physical Medicine and Rehabilitation." Accessed: Sep. 05, 2022. [Online]. Available: https://www.archives-pmr.org/article/S0003-9993(02)09579-5/fulltext

[312] V. Mathiowetz, G. Volland, N. Kashman, and K. Weber, "Adult norms for the Box and Block Test of manual dexterity," *Am. J. Occup. Ther. Off. Publ. Am. Occup. Ther. Assoc.*, vol. 39, no. 6, pp. 386–391, Jun. 1985, doi: 10.5014/ajot.39.6.386.

[313] T. Duong *et al.*, "Comparative Study of Functional Grasp and Efficiency Between a 3D-Printed and Commercial Myoelectric Transradial Prosthesis Using Able-Bodied Subjects: A Pilot Study," *JPO J. Prosthet. Orthot.*, vol. 29, no. 3, pp. 112–118, Jul. 2017, doi: 10.1097/JPO.0000000000000130.

[314] J. T. Belter, M. T. Leddy, K. D. Gemmell, and A. M. Dollar, "Comparative clinical evaluation of the Yale Multigrasp Hand," in *2016 6th IEEE International Conference on Biomedical Robotics and Biomechatronics (BioRob)*, Jun. 2016, pp. 528–535. doi: 10.1109/BIOROB.2016.7523680.

[315] I. Llop-Harillo, A. Pérez-González, J. Starke, and T. Asfour, "The Anthropomorphic Hand Assessment Protocol (AHAP)," *Robot. Auton. Syst.*, vol. 121, p. 103259, Nov. 2019, doi: 10.1016/j.robot.2019.103259.

[316] B. Calli, A. Walsman, A. Singh, S. Srinivasa, P. Abbeel, and A. M. Dollar, "Benchmarking in Manipulation Research: Using the Yale-CMU-Berkeley Object and Model Set," *IEEE Robot. Autom. Mag.*, vol. 22, no. 3, pp. 36–52, Sep. 2015, doi: 10.1109/MRA.2015.2448951.

[317] J. Andrés-Esperanza, J. L. Iserte-Vilar, I. Llop-Harillo, and A. Pérez-González, "Effect of the Thumb Orientation and Actuation on the Functionality and Performance of Affordable Prosthetic Hands: Obtaining Design Criteria," *Biomimetics*, vol. 7, no. 4, Art. no. 4, Dec. 2022, doi: 10.3390/biomimetics7040233.

[318] "Chedoke Arm and Hand Activity Inventory (CAHAI) – Strokengine." Accessed: Sep. 07, 2022. [Online]. Available: https://strokengine.ca/en/assessments/chedoke-arm-and-hand-activity-inventory-cahai/

[319] A. Jain, H. Nguyen, M. Rath, J. Okerman, and C. Kemp, *The complex structure of simple devices: A survey of trajectories and forces that open doors and drawers*. 2010, p. 190. doi: 10.1109/BIOROB.2010.5626754.

[320] V. Singh, M. Das, and S. K. Das, “Effect of varying knife speed and contact area on peak cutting force during slicing of peeled potato (Solanum tuberosum),” vol. 23, pp. 2513–2518, Jan. 2016.

[321] T. Brown, S. J. James, and G. L. Purnell, “Cutting forces in foods: experimental measurements,” *J. Food Eng.*, vol. 70, no. 2, pp. 165–170, Sep. 2005, doi: 10.1016/j.jfoodeng.2004.09.022.

[322] R. C. Hibbeler, *Mechanics of Materials*. Pearson Education Limited, 2018.

APPENDIX A: CONVERTING THE TWO MEASURED THUMB CMC JOINT ANGLES TO THE THREE ANGLE PAIRS

The two angles measured for the thumb CMC joint are θ_{B_1} and θ_{C_2}; they need to be converted into each of the three angle pairs shown in Figure 4.5 (on p.57), to be able to model and analyse the different hand postures measured. This meant that a relationship between the three angle pairs was required.

Hence, for each angle pair, the orientation of the frame that comes after the CMC joint (i.e., the 4th frame) is defined relative to the coordinate system of the 1st frame, which is common for all the three cases. The transformation from the 1st to the 4th frame, $T_{T_4}^{1}$, is composed of the following transformations:

$$T_{T_4}^{1} = T_{T_2}^{1} T_{T_3}^{2} T_{T_4}^{3} \quad \text{A.1}$$

Using the D-H parameters, the transformation from the $i-1^{th}$ to the i^{th} frame, T_i^{i-1}, is determined by the following matrix:

$$T_i^{i-1} = \begin{bmatrix} c\theta_i & -s\theta_i c\alpha_i & s\theta_i s\alpha_i & a_i c\theta_i \\ s\theta_i & c\theta_i c\alpha_i & -c\theta_i s\alpha_i & a_i s\theta_i \\ 0 & s\alpha_i & c\alpha_i & d_i \\ 0 & 0 & 0 & 1 \end{bmatrix} \quad \text{A.2}$$

Where,

- c refers to the cosine function.
- s refers to the sine function.

The first three columns of $T_{T_4}^{1}$ represent the unit vectors along the x_{T_4}, y_{T_4} and z_{T_4} axis, relative to the coordinate system of the 1st frame. However, only the unit vector along x_{T_4} (i.e., the first column) is interchangeable across the three angle pairs, since x_{T_4} is defined along the metacarpal bone of the thumb whose position in 3D-space is independent of the angle pair being considered. This means that only the expressions related to unit vector along x_{T_4} can be utilised to define the relationship between the different angle pairs. Hence, for Angle Pair A, whose D-H parameters are defined in Table 4.3 (on p.58), the orientation of the unit vector along x_{T_4} is expressed as follows:

$$x_{T_1} = c\theta_{A_1} c\theta_{A_2} \quad \text{A.3}$$

$$y_{T_1} = s\theta_{A_2} \quad \text{A.4}$$

$$z_{T_1} = s\theta_{A_1} c\theta_{A_2} \quad \text{A.5}$$

Similarly, the $T_{T_4}^1$ for Angle Pair B and C were also determined, using the D-H parameters in Table A.1 and Table A.2, respectively.

Table A.1: The D-H Parameters of the thumb for Angle Pair B

Transformation	i_T	$\theta_{T_{i_T}}$	$d_{T_{i_T}}$	$a_{T_{i_T}}$	$\alpha_{T_{i_T}}$
$T_{T_2}^1$	2	0	0	0	0
$T_{T_3}^2$	3	θ_{B_1}	0	0	$\pi/2$
$T_{T_4}^3$	4	θ_{B_2}	0	$l_{T_{PP}}$	$\pi/2$

Table A.2: The D-H Parameters of the thumb for Angle Pair C

Transformation	i_T	$\theta_{T_{i_T}}$	$d_{T_{i_T}}$	$a_{T_{i_T}}$	$\alpha_{T_{i_T}}$
$T_{T_2}^1$	*2*	$-\pi/2$	0	0	$\pi/2$
$T_{T_3}^2$	3	$\theta_{C_1} + \pi/2$	0	0	$\pi/2$
$T_{T_4}^3$	4	$\theta_{C_2} - \pi/2$	0	$l_{T_{PP}}$	$\pi/2$

Thus, the orientation of the unit vector along x_{T_4} relative to the 1st frame can also be defined in terms of Angle Pair B and C as follows:

In terms of Angle Pair B:

$$x_{T_1} = c\theta_{B_1} c\theta_{B_2} \quad \text{A.6}$$

$$y_{T_1} = s\theta_{B_1} c\theta_{B_2} \quad \text{A.8}$$

$$z_{T_1} = s\theta_{B_2} \quad \text{A.10}$$

In terms of Angle Pair C:

$$x_{T_1} = c\theta_{C_2} \quad \text{A.7}$$

$$y_{T_1} = s\theta_{C_1} s\theta_{C_2} \quad \text{A.9}$$

$$z_{T_1} = c\theta_{C_1} s\theta_{C_2} \quad \text{A.11}$$

The measured angles can then be converted to each of the angle pairs by solving the above equations simultaneously, unless the thumb is in the open hand position, in which case the measured angles can be easily converted using Figure 4.5 (on p.57). Taking Angle Pair, A, as an example, θ_{A_2} is found by equating A.4 to A.8, as follows:

$$s\theta_{A_2} = s\theta_{B1} c\theta_{B_2} \quad \text{A.12}$$

Where θ_{B_2} is determined by equating A.6 to A.7, which yields the following equation:

$$c\theta_{B_2} = \frac{c\theta_{C_2}}{c\theta_{B_1}} \quad \text{A.13}$$

θ_{A_1} is then found by equating A.5 to A.10, which gives rise to the following equation:

$$s\theta_{A_1} = \frac{s\theta_{B_2}}{c\theta_{A_2}} \quad \text{A.14}$$

APPENDIX B: CONSENT FORM

Project: Development of the Mechanical Framework for a Minimal Anthropomorphic Prosthetic Hand

Experiment: Kinematic Analysis of Finger Joints Motion during Everyday Tasks

The purpose of this experimental procedure is to measure and investigate finger joint motion under both normal and minimal anthropomorphic conditions (i.e. through using only the thumb together with the index and middle finger) during everyday tasks.

Finger joint motion will be analysed through data gloves worn by each participant whilst performing the stated experimental day-to-day tasks. The various tasks to be conducted will be thoroughly explained by the test administrator and will consist of a series of grasping techniques. The gathered relative angles of the finger joints will then be analysed using a statistical method known as Principal Component Analysis.

<u>Consent</u>

- I confirm that I understand the nature and objectives of the experimental procedure which have been explained to me by the test administrator.
- I understand that the data gathered will be analysed statistically and in an anonymous manner.
- I also understand that I have the right to withdraw from participation in this research at any time during the experiment.

I hereby give my consent to participate in this experimental procedure.

___________________________	_________________	________________
Name	I.D. card number	Date

APPENDIX C: EXTERNAL LOADS PRESENT DURING TYPICAL DAILY BIMANUAL ACTIVITIES

To determine the ability of a prosthetic hand to successfully execute the set of activities listed in Table 4.1 (on p. 52), as well as three additional activities, namely opening a hand-tightened jar, opening a can of beverage and cutting food with a knife, data on the external loads applied on the task object during these activities are required.

Literature on the external loads present during the selected activities was limited, except for Jain et al.'s study [319], which determined the maximum force required to start opening the different drawers considered in their dataset to be $20N$. Otherwise, the literature found was mainly related to determining the forces required to perform a specific task in a manufacturing setting, as in [320], [321], which was not a good representation of the daily activity. Hence, a series of experiments were carried out to quantify the magnitude of the external loads present during these tasks.

The weight of the task object is usually one of the external loads present, unless the purpose of the prosthetic hand is to manipulate the object without supporting its weight (e.g. when opening a drawer). Its magnitude could be easily determined with an electronic weighing scale. Table C.1 lists the weight of the relevant task objects. However, other external loads are present during the following activities, and thus, specific experiments were designed and carried out to determine their magnitude, which will be discussed in the following sections [201]:

- Peeling a potato
- Opening a hand-tightened cap
- Opening and closing the zipper of a purse
- Opening a can of beverage
- Opening a packaged-food box
- Opening a drawer
- Dialling a telephone number
- Sharpening a pencil
- Spraying a detergent
- Eating with a fork and a knife

For some of these activities, various techniques or tools could be used to execute the activity. For example, a packaged-food item can be opened in different ways, depending on the person and the type of seal (e.g., whether the cardboard is perforated or whether there is some glue towards the end of the lid). However, this work focuses on just one technique/tool that is commonly used for each activity, since the main priority is to examine typical forces present in that activity rather than to compare the effect that such techniques/tools may have on the external forces. Experiments that were simple and reliable were repeated five times, while those that were more complex were repeated ten times, as indicated in the appropriate sections below.

Table C.1: The weight of the task objects for the bimanual activities considered, in which the weight of the object is one of the external loads present

Bimanual activity	***Task Object***	***Weight (kg)***
Sweeping	Broom	0.400
Peeling a potato	Potato	0.190
Opening a hand-tightened bottle	Large water bottle	2.000
Putting toothpaste on a toothbrush	Toothbrush	0.014
Opening the zipper of a purse	Purse	0.450
Pouring from a frying pan	Frying pan handle	0.800
Passing a thread through a needle	Sewing pin	/
Opening a hand-tightened cap	Cap	
Pouring water into a cup	Medium-sized cup	0.500
Playing Cards	Cards	/
Carrying a tray	Tray	3.000
Opening a packaged-food box	Cracker box	0.095
Carrying a shopping bag	Shopping bag	5.000
Carrying a briefcase	Briefcase	5.000
Sharpening a pencil	Small sharpener	0.018
Opening a hand-tightened toothpaste cap	Toothpaste cap	0.004
Opening a hand-tightened body cream cap	Body cream cap	0.115
Using a tablet	Tablet	0.800
Eating with a fork and a knife	Fork/Knife	0.032
Dialling a telephone number	Telephone	0.121
Spraying a detergent while wiping a surface	Spray bottle	0.680
Cutting with scissors	Paper	/
Opening a hand-tightened bottle cap	Bottle cap	0.002
Opening a can of beverage	Can of beverage	0.350
Opening a hand-tightened jar	Jar	0.850

C.1 Peeling a potato

There are two external forces present when peeling a potato with a peeler; one is along the perimeter of the potato, F_{A_1}, and the other one is pushing on the potato, F_2. The set-up used to measure these two forces is shown in Figure C.1. The experimenter, using only the dominant hand, manually peeled the potato, which was secured to a wooden wheeled cart with two nails. The force F_{A_2} was measured using the electronic weighing scale, and the maximum value recorded by the scale as the experimenter peeled the potato was noted. Meanwhile, the force F_{A_1} was the sum of the maximum force recorded on the spring balance, F_{SB}, and the force required for the cart to overcome the static friction and start to move, F_f. The latter was then found, using Coulomb's law of friction [192], which is given by Equation C.1:

$$F_f = \mu_{s1} * N \qquad \text{C.1}$$

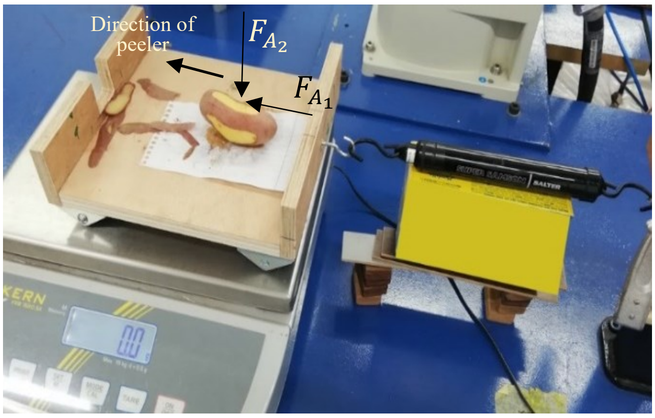

Figure C.1: The set-up used to determine the forces required to peel a potato

Here, μ_{s1} is the static coefficient of rolling friction between the cart and the scale, which was found experimentally to be 0.0675. Meanwhile, N is the normal force, which in this case was F_{A_2} plus the weight of the cart with the potato.

This experiment was repeated ten times for the two different types of potato, namely, a white and a red potato. Necessary precautions were taken during the experiment, such as making sure that both scales were zeroed before starting. The average results together with the SDs are shown in Table C.2. The large SD observed could be because it is exceedingly difficult for a person to apply just enough force to peel the potato. However, a limitation of this experiment is that the position of the peeler when the maximum forces were observed was not known. Hence, the worst-case scenario should be considered when determining the forces that the prosthetic hand must apply.

Table C.2: The average external loads applied to peel a potato

	Red Potato	***White Potato***
$\boldsymbol{F_{A_1}}$ $(\boldsymbol{N})$	8.4(1.13)	11.95(2.75)
$\boldsymbol{F_{A_2}}$ $(\boldsymbol{N})$	8.31(2.25)	9.18(1.8)

C.2 Opening a hand-tightened cap

The torque required to open a container may vary, depending on the size of the cap. Hence, ten different household containers having caps of different radii were chosen, ranging from a large water bottle to a toothpaste tube. Each container was then secured on the worktop and the cap was grasped with a G-clamp, creating a lever about its centre, as shown in Figure C.2(a). Weights were then added on the G-clamp in small increments until the cap opened. The torque required to open the cap was then found by determining the torque created by the weight of the G-clamp and the weights that were hanging on the G-clamp when the cap opened. This experiment was repeated five times for each container. Figure C.2 (b) shows the torque required to open the cap versus the diameter of the cap. One can observe that a torque of less than $3Nm$ is sufficient to open all the different containers considered in this experiment.

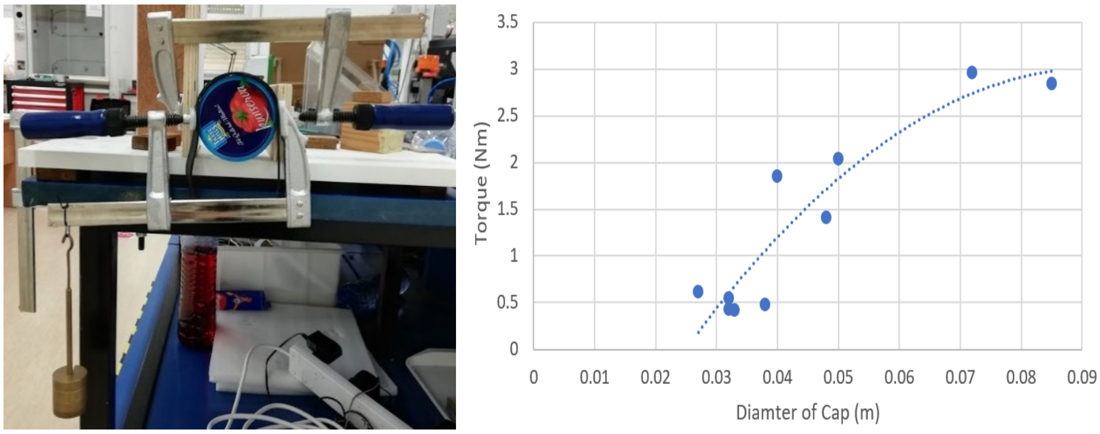

(a) (b)

Figure C.2: The set-up used to determine the torque required to open a container

C.3 Opening and closing the zipper of a purse

For this task zippers of five different pouches/purses typically used in ADLs, with different teeth dimensions, were considered. All the zippers used in the experiment were new and undamaged. Each pouch or purse was secured to the worktop as shown in Figure C.3. Weights were then added to the hanger in small increments until the zipper was fully opened or closed. The weight at which the zipper opened or closed was then noted. This experiment was repeated five times for opening and for closing each zipper.

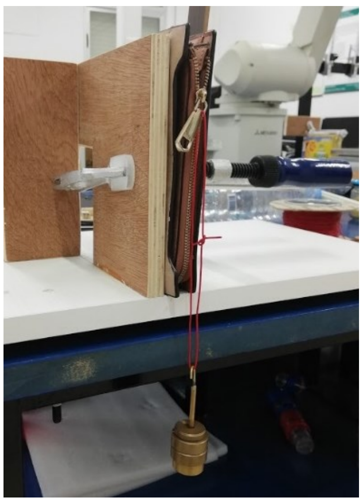

Figure C.3: The set-up used to determine the force required to open/close a zipper

The force required to open/close a zipper ranged from $0.81N$ to $2.73N$, with the opening and closing forces of each pouch/purse being relatively similar to each other.

C.4 Opening a can of Beverage

In this experiment the torque required to open ten cans of beverages of various sizes and brands was determined. The can of beverage was opened using a spring balance as shown in Figure C.4(a). A piece of wire was used to hang the pull tab of the can on the spring balance because it could fit between the can and the pull tab with minimal force, even when the can was closed.

The can was first pulled straight downwards until the seal was broken, then the experimenter pulled the can downwards while tilting it, such that the spring balance was kept perpendicular to the pull tab as much as possible. Even where the spring balance may not have been exactly perpendicular to the pull tab, the force observed on the spring balance would be a conservative one since only a component of that force would actually be used to open the can. The maximum value observed on the spring balance was then noted. This force was then used to determine the torque required to open the cap by multiplying it with the length of the lever shown in Figure C.4(b). From this experiment it was observed that the maximum force applied on the cans ranged from $15.5N$ to $20N$, with the torque varying between $0.28Nm$ and $0.36Nm$.

(a) (b)

Figure C.4: (a) The set-up used to determine the torque required to open a beverage can, and (b) the lever distance at the tab

C.5 Opening a packaged-food box

This experiment focused on a technique that could be used to open ten boxes of varied sizes, seals and brands. This technique involves first pushing a knife between the two cardboard flaps of the lid to slightly break the seal and create a gap, following which the person can use their fingers to grab the top cardboard flap and create a lever about the edge of the box to open it. Therefore, there were two parts to this experiment.

The first part addressed the forces required to push the thickness of the knife between the two sealed cardboard flaps. Here, the set-up shown in Figure C.5 was used to measure the force along the direction of the knife, F_{B_1}, and the force pushing on the surface of the cardboard, F_{B_2}. The maximum force downwards, F_{B_1}, was then read from the weighing scale. Meanwhile, the force F_{B_2} was measured by adding the maximum force observed on the spring balance, F_{SB}, to the force required to move the cart on the scale, F_f. As with the potato peeling experiment, F_f was determined using Coulomb's law of static friction, where the coefficient of friction between the cart and the weighing scale was already found to be 0.0675, and the normal force was the sum of F_{B_1} and the weight of the cart and the box.

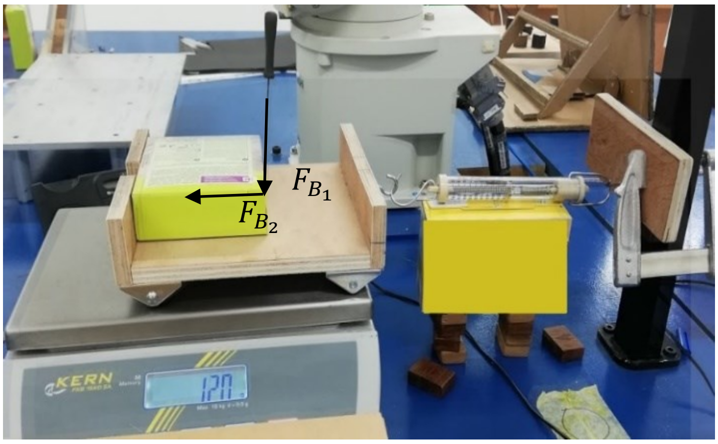

Figure C.5: The set-up used to determine the forces required to push the knife between the two cardboards of the sealed box

The set-up shown in Figure C.6(a) was used to determine the force required to break the seal completely, F_{B_3}. In this set-up, the knife was pushed through a pre-cut slot on the other side of the box, Figure C.6(b). This, together with the fact that the box was secured upside down, created a pivot for the knife at edge A, Figure C.6(b), which was realistic in light of what happens. Weights were then added in small increments to the

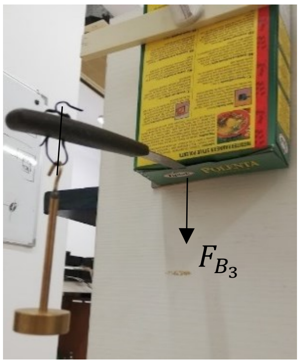

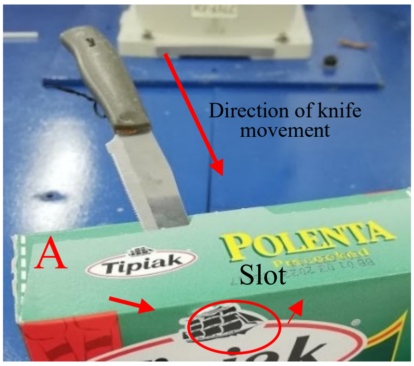

(a) (b)

Figure C.6: (a) The set-up used to determine the forces required to open the box and (b) the pre-cut hole on the other side of the box and the pivot of the knife hanger tied to the knife until the box opened. The force F_{B_3} was then found by considering the moments created by the weights about edge A.

For all the boxes, F_{B_2} was small, with the highest value observed being that of $2.5N$, but the same cannot be said for F_{B_1}. A large variation was observed for F_{B_1}, with the maximum force being $21.5N$ to open a chicken finger box. This variation is mainly due to the type of seal used to close the box, with boxes having glue all the way across the lid requiring higher forces. A similar variation was also observed for F_{B_3}, with the maximum force required to open the same box being $18.71N$.

C.6 Opening a drawer

There exist several types of drawers, such as push-to-open, traditional rails with a handle and electric drawers. However, in this experiment, the focus was on traditional rails since these are the types of drawers that are commonly found in homes and workplaces. Although the force required to open a drawer had already been established by Jain et al. [319], due to the simplicity of the experiment, the force required to open different drawers found in our lab was still determined to check whether similar forces would be required. Five different drawers found in our laboratory, having different widths, depths, and weights but similar rails as the drawers found in the typical home, were considered. For this experiment, a person opened the drawers with a spring balance, as shown in Figure C.7, while making an effort to keep the spring balance straight and in line with the drawer to avoid creating sideway forces. The maximum force observed on the spring balance was then noted. This was repeated five times for each drawer.

Figure C.7: The set-up used to determine the force required to open a drawer

The maximum force observed was $24.8N$ to open a drawer that weighed $14.7kg$, which is in line with the observations of Jain et al. [319].

C.7 Dialling a telephone number

The force applied on a telephone when dialling was measured. For this experiment, the telephone was placed on a weighing scale with the buttons parallel to the scale, as shown in Figure C.8. The experimenter then pressed one of the buttons at random and noted the maximum value observed, excluding the weight of the set-up. Effort was made to stop pressing the button once it had been pressed since the force recorded on the scale would then increase. This was repeated for ten times. On average the force required to press a button on a telephone was found to be $0.57 \pm 0.12N$.

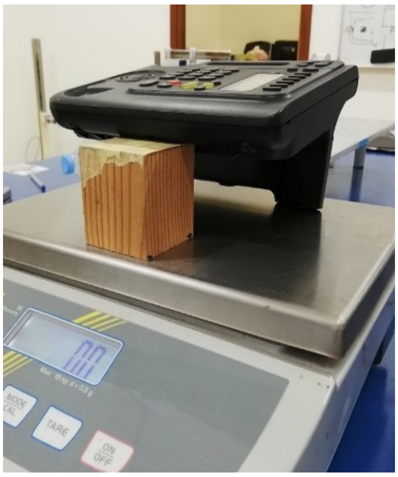

Figure C.8: The set-up used to measure the force applied on the telephone when dialling a number.

C.8 Sharpening a pencil

There are two external loads acting on the non-dominant hand when sharpening a pencil: (i) the force applied axially by the pencil against the sharpener, $F_{Sharpener}$; (ii) the torque applied by the pencil against the blade, T_{Sh}. In this experiment, these two loads were measured separately.

To measure F_{Sh}, the experimenter sharpened a pencil vertically downwards with the sharpener secured to the weighing scale to prevent it from rotating. The force applied on the sharpener could then be read directly off the scale. This experiment was repeated five times, and each time the maximum force observed on the scale was noted. Effort was made not to press down on the sharpener more than was necessary to sharpen the pencil.

Meanwhile, T_{Sh} was measured by winding a piece of wire around a pencil, and weights were added to the hanger in small increments, as shown in Figure C.9, until the pencil started to rotate while being pressed into the sharpener. The weight that was hanging on the wire when the pencil started to rotate, $m_{weights}$, was then noted. To ensure that the pencil was in fact sharpened during the experiment, a person applied a force along the pencil. Effort was made not to press the pencil more than necessary to minimise the friction between the hand and the pencil which would in turn increase the required weight. This part of the experiment was also repeated five times. Each time the torque, T_{Sh}, was found by determining the torque created by $m_{weights}$ about the centre of the pencil.

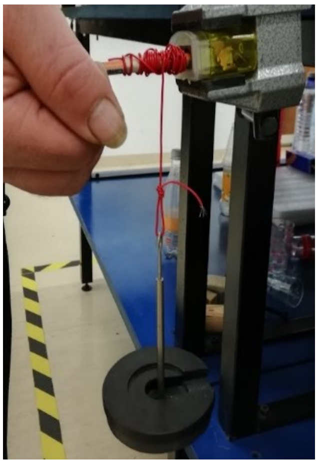

Figure C.9: The set-up used to determine the torque required to sharpen a pencil

An average force of $4.89 \pm 0.94N$ was applied along the pencil, while the average torque required to sharpen it was $0.02 \pm 0.001Nm$. Although the relationship between the two external loads was not examined, this experiment demonstrated that to sharpen a pencil one does not need to apply high loads.

C.9 Spraying a detergent

To trigger a detergent spray bottle, the force must be applied at a certain speed. Hence, the trigger of the spray bottle was placed parallel to one of the sides of a piece of wood, as shown in Figure C.10. The experimenter then pushed the trigger down at the required speed for an effective spray to be emitted from the nozzle. The force applied

Figure C.10: The set-up used to measure the force required to trigger a spray bottle downwards was then measured and noted using the weighing scale. Effort was made not to continue pushing down once the spray bottle had been triggered since this would increase the force applied on the scale. This was repeated five time for five different spray bottles since the stiffness of the trigger may vary from one bottle to another. The maximum force required to trigger a spray bottle in our dataset was found to be less than $13.6N$.

C.10 Eating food with a fork and a knife

This experiment examined the forces applied by the fork when cutting various types of food, namely, slices of cheddar cheese (width of $3cm$ and thickness $1cm$), cooked sausages (diameter $2cm$), and chicken fingers (of a thickness of $1cm$) with a knife. During this activity, the fork holds the food in place while the knife is used to cut the food. Hence, there is a force acting along the tines of the fork, F_{fk}. Meanwhile, the knife applies a force on the food to cut through it, F_k, (Figure C.11) and, depending on the distance of the knife from the fork and orientation of the knife, this force may also create an external moment on the fork, T_k.

To determine F_k, a piece of food was secured on the wooden cart as shown in Figure C.11, as with the set-up used to peel the potatoes, and the experimenter cut the food in half while keeping the knife at an angle typically used when cutting on a plate. Then, the force applied downwards, F_{k_1}, was measured using the weighing scale. Meanwhile, the force applied sideways, F_{k_2}, was found by adding the maximum force observed on the spring balance to the force required to move the cart when F_{k_1} was applied on the cart. The force F_k was then calculated by adding $F_{k_1}$and F_{k_2} vectorially. In this experiment, a more conservative approach was considered because each food item was cut in half in one go. This was then repeated ten times for each type of food.

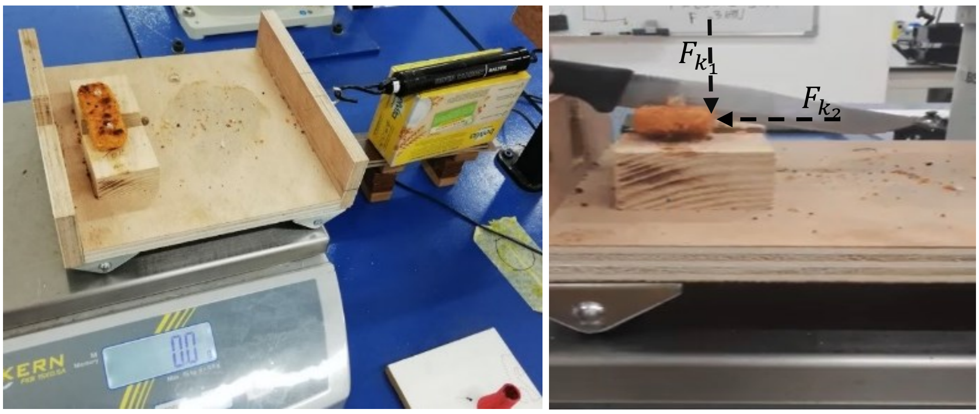

(a) (b)

Figure C.11: (a) The set-up used to measure the forces present when cutting with a knife, and (b) the forces applied by the knife on the piece of food

The torque T_k was then found by calculating the moment created by F_{k_2} around the tines of the fork, assuming that during cutting the knife is placed at an adequate distance of $3cm$ from the fork.

The force F_{fk} was then determined by cutting each food item on a scale, using both the fork and the knife. Since the scale measured the total force of F_{fk} and F_{k_1}, the motion of the knife was kept similar to that in the previous experiment as much as possible, so that the average F_{k_1} for each food item could be subtracted from the maximum value observed on the scale. This was repeated ten times for each food item.

From the foods considered in this experiment, it was observed that the highest forces were required when cutting a piece of meat, closely followed by chicken fingers. Lower forces were then required for the slices of cheese and sausages. The average force required to cut a piece of meat was $9.51N$ and $17.45N$ for F_k and F_{fk}, respectively. Meanwhile, for all the food items, F_k was less than $0.21Nm$.

In conclusion, these experiments provided a better understanding of the typical loads a non-dominant hand in bimanual activity would need to apply/sustain. Numerically, the maximum force that the non-dominant hand would need to apply was observed to be around $25N$ when opening one of the larger drawers, while the highest torque was $2.96Nm$ to open a hand-tightened cap with a diameter of $0.072m$.

APPENDIX D: DETERMINING THE ABILITY OF THE GRASP TO RESIST AN EXTERNAL WRENCH

This appendix describes the approach taken to determine if the prosthetic hand is able to secure a large water bottle weighing $2kg$ (i.e., including SF of 1.5, and weight, $\overrightarrow{W}_{bt}$ = $29.43jN$), that is resting on a table, while the intact hand opens the cap of radius $14mm$, with a torque, $\vec{T}_c$, of $0.93j\ Nm$ (derived from experiment C.2 (on p.222), and which includes a SF of 1.5). It would also determine the grasping force required and the torques that need to be sustained/applied at each of the active joints.

First, the KHS was simulated in Unity, wrapping its fingers around the modelled water bottle, Figure D.1. Information on the number of contact points and the position and orientation of each of the contact forces relative to the object's coordinate system, shown in Figure D.1 (where the red arrow is the x-axis, while the blue arrow is the z-axis in the opposite direction, as Unity uses the left-hand rule), was then extracted from Unity and noted in Table D.1

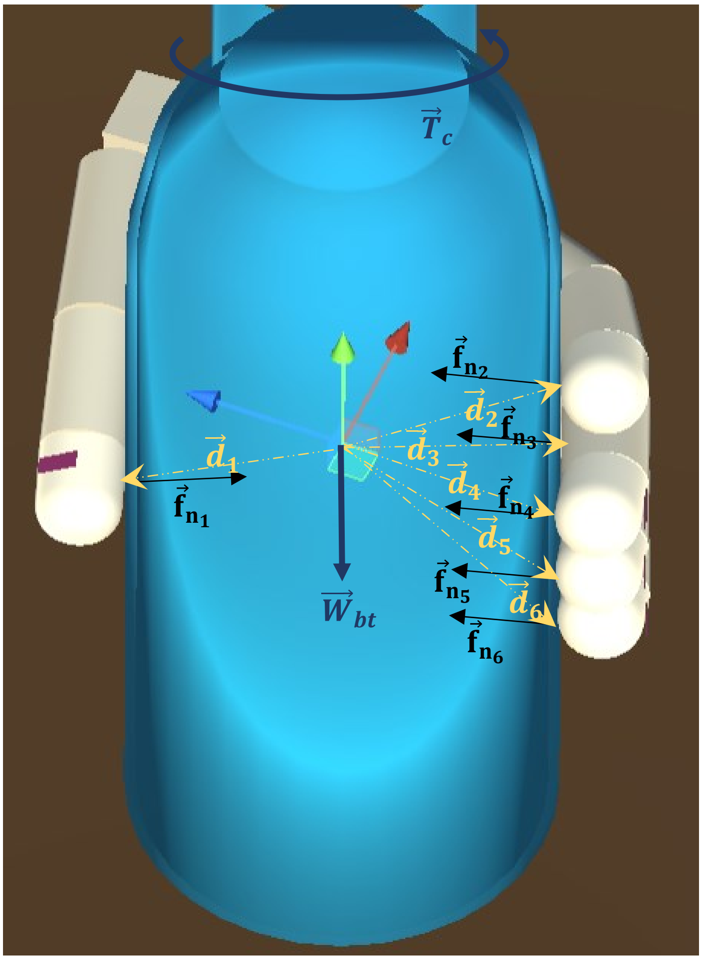

Figure D.1: The forces/torques acting on the water bottle when opening its cap with the intact hand, excluding the forces between the bottle and the table

Table D.2: The vectors of the position of the contact point and the contact forces applied on the water bottle in terms of the object's coordinate system

i	$\vec{d}_i$ (m)	$\vec{f}_{n_i}$ (N)
1	$(-0.02i - 0.01j - 0.05k)$	$(0.31i + 0.00j + 0.95k)f_1$
2	$(0.02i + 0.02j + 0.05k)$	$(-0.38i + 0.00j - 0.93k)f_2$
3	$(0.02i - 0.01j + 0.05k)$	$(-0.38i + 0.00j - 0.93k)f_3$
4	$(0.01i - 0.01j + 0.05k)$	$(-0.26i + 0.00j - 0.96k)f_4$
5	$(0.01i - 0.03j + 0.05k)$	$(-0.26i + 0.00j - 0.97k)f_5$
6	$(0.01i - 0.05j + 0.05k)$	$(-0.27i + 0.00j - 0.96k)f_6$

From Figure D.1, one can deduce that the water bottle is grasped through a force closure, meaning that the friction present between the hand and the object will play a crucial role in resisting the external loads. Hence, using the frictional model in Figure 5.5 (on p.97), two orthogonal frictional forces, at a tangent to the normal force, were considered for each contact point, i. The direction of each of these frictional forces was determined by exploiting the simple shape of the modelled object. In this case, all the contact points have a frictional force acting along the y-direction, $\vec{f}_{t_{1_i}}$, and another frictional force, $\vec{f}_{t_{2_i}}$, acting in the xz-plane, perpendicular to $\vec{f}_{n_i}$ (i.e., the x- and z-components of $\vec{f}_{n_i}$ are interchanged, while the sign of each component can be varied as necessary), as shown in Figure D.2, for contact point 1. The vectors of both $\vec{f}_{t_{1_i}}$ and $\vec{f}_{t_{2_i}}$ are listed in Table D.2, where μ_s was assumed to be 0.5.

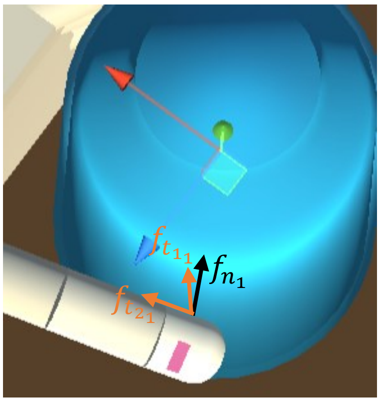

Figure D.2: The frictional forces present between the thumb and the water bottle

Table D.1: The vectors of the frictional forces with respect to the object's coordinate system

i	$\vec{f}_{t_{1_i}}$ (N).	$\vec{f}_{t_{2_i}}$(N)
1	$(0.00i + 1.00j + 0.00k)\beta_{1_1}\mu_s f_1$	$(-0.95i + 0.00j - 0.31k)\beta_{2_1}\mu_s f_1$
2	$(0.00i + 1.00j + 0.00k)\beta_{1_2}\mu_s f_2$	$(-0.93i + 0.00j - 0.38k)\beta_{2_2}\mu_s f_2$
3	$(0.00i + 1.00j + 0.00k)\beta_{1_3}\mu_s f_3$	$(-0.93i + 0.00j - 0.38k)\beta_{2_3}\mu_s f_3$
4	$(0.00i + 1.00j + 0.00k)\beta_{1_4}\mu_s f_4$	$(-0.96i + 0.00j - 0.26k)\beta_{2_4}\mu_s f_4$
5	$(0.00i + 1.00j + 0.00k)\beta_{1_5}\mu_s f_5$	$(-0.97i + 0.00j - 0.26k)\beta_{2_5}\mu_s f_5$
6	$(0.00i + 1.00j + 0.00k)\beta_{1_6}\mu_s f_6$	$(-0.96i + 0.00j - 0.27k)\beta_{2_6}\mu_s f_6$

Force closure is then achieved if there is a set of forces that constrain the motion of the water bottle, at least in the xz-plane, since the object is assumed to be placed on a table, which will be able to resist motion in the other directions. Therefore, in Equation 5.8 (on p.94), it is sufficient for the wrench applied by the contact points on the object to just counteract the forces in the x- and z-direction, as well as the moments about y. This implies that only three contact forces are necessary, and thus, this problem is indeterminant (i.e., there may be more than one set of forces that are able to resist $\vec{w}_e$). However, the forces applied at each contact point cannot be varied independently, since in the final prototype, the amputee will only be able to adjust the force applied by the thumb, $\vec{f}_1$, while a reactive force builds up at the other contact points. For this reason, the solution is found by varying the magnitude of $\vec{f}_1$ systematically, while for each iteration the moments about x and z were used so that all the reactive forces built up at the other contact points would be a function of $\vec{f}_1$. Note that the forces in the y-direction could have been used instead of the moments about either x or z, but since the weight of the object also acts in this direction, the grasping force required would have been even higher, which goes against the main objective of this analysis, namely, that of reducing the maximum grasping force as much as possible. Therefore, for this activity, Equation 5.8 can be written as follows, where the x, y, and z subscript indicates the component of the vector considered:

$$\begin{bmatrix} f_1 \\ \sum f_x \\ \sum f_z \\ \sum M_x \\ \sum M_y \\ \sum M_z \end{bmatrix} = \begin{bmatrix} f_1 \\ \sum_{i=1}^{i=6} f_{n_{i_x}} + f_{t_{1_{i_x}}} + f_{t_{2_{i_x}}} \\ \sum_{i=1}^{i=6} f_{n_{i_z}} + f_{t_{1_{i_z}}} + f_{t_{2_{i_z}}} \\ \sum_{i=1}^{i=6} (f_{n_{i_z}} * d_{i_y}) - (f_{t_{1_{i_y}}} * d_{i_z}) + (f_{t_{2_{i_z}}} * d_{i_y}) \\ \sum_{i=1}^{i=6} (f_{n_{i_x}} * d_{i_z}) - (f_{n_{i_z}} * d_{i_x}) + (f_{t_{2_{i_x}}} +* d_{i_z}) - (f_{t_{2_{i_z}}} * d_{i_x}) \\ \sum_{i=1}^{i=6} -(f_{n_{i_x}} * d_{i_y}) + (f_{t_{1_{i_y}}} * d_{i_x}) - (f_{t_{2_{i_x}}} * d_{i_y}) \end{bmatrix} = \begin{bmatrix} f_1 \\ 0 \\ 0 \\ 0 \\ -T_c \\ 0 \end{bmatrix} \qquad \text{D.1}$$

The above equations were solved simultaneously using Microsoft Excel, where the values of f_1, β_{1_i} and β_{2_i} were optimized using the evolutionary algorithm and the GRG nonlinear method so as to minimize the maximum contact force applied on the object, while satisfying the following conditions:

$$\|\vec{f}_i\| \geq 0 \qquad \sqrt{\beta_{1_i}^2 + \beta_{2_i}^2} \leq 1, \; |\beta_i| \leq 1$$

The GAs in Excel were able to satisfy all these conditions, where the optimal value of f_1 was found to be $37.15N$, while the values of β_{1_i} and β_{2_i} are noted in Table D.3. This table also lists the force that builds up at each contact point based on the equations in D1. Meanwhile, the component of these forces in the y-direction, which adds up to $1.66N$ in addition to the weight of the bottle, would then need to be supported by the table. This means that the resulting grasp, together with the table, is able to provide force closure of the water bottle, while the intact hand opens the cap.

Table D.3: The optimal values for f_1, β_{1_i} and β_{2_i} obtained from the GA and the corresponding values for the remaining f_i

i	β_{1_i}	β_{2_i}	$\lVert\vec{f_i}\rVert$ (N)
1	-0.11	-0.99	37.15
2	0.00	1.00	11.93
3	-0.74	-0.21	0.00
4	0.00	1.00	0.00
5	0.00	1.00	25.34
6	-0.42	0.91	0.00

The torque that would need to be applied or sustained at each active joint to actively achieve these contact forces, $\overrightarrow{T_D}$, was then determined. First, Unity was used to express the position and orientation of each contact force (considering only the contact forces whose magnitude is greater than zero) in terms of the coordinate system of the corresponding active joint, Table D.4.

Table D.4: The position and orientation of the contact forces applied on the water bottle in terms of the coordinate system of the corresponding active joint

i	D	$\vec{d}_{c_i}$ (m)	$\vec{F}_{c_i}$ (N)
1	T	$(0.01i + 0.08j + 0.01k)$	$(-0.80i + 0.04j - 0.60k)f_1$
2	M	$(-0.03i + 0.07j + 0.00k)$	$(0.80i + 0.58j + 0.18k)f_4$
5	M	$(-0.03i + 0.07j + 0.00k)$	$(0.77i + 0.64j + 0.02k)f_5$

The magnitude of $\overrightarrow{T_D}$ was then determined using the cross product in Equation 5.11 (on p.99). Taking the thumb as an example, $\overrightarrow{T_T}$ was calculated by substituting the known values in Equation D.2:

$$\overrightarrow{T_T} = \sum \vec{d}_{c_i} \text{ x } \vec{F}_{c_i}\,,\ i \in T$$

$$\overrightarrow{T_T} = \Big[\Big(d_{c_{1_y}}F_{c_{1_z}} - d_{c_{1_z}}F_{c_{1_y}}\Big)\,i + \Big(r_{c_{1_z}}F_{c_{1_x}} - r_{c_{1_x}}F_{c_{1_z}}\Big)\,j + \Big(r_{c_{1_x}}F_{c_{1_y}} - r_{c_{1_y}}F_{c_{1_x}}\Big)\,k\Big]\,f_1 \qquad \text{D.2}$$

This was repeated for the other digits and the results are noted in Table D.5.

Table D.5: The torque that needs to be applied or sustained at each active joint

Digit, D	$\overrightarrow{T_D}$ ***(Nm)***
T	$-1.82i - 0.14j + 2.39k$
I	$0.18i + 0.01j - 0.83k$
M	$0.04i + 0.00j - 1.76k$

In the case of the index and the MRL finger, the torque that needs to be supported by the actuation/transmission system is $0.83Nm$ and $1.76Nm$ respectively. Meanwhile, the torque along the other primary axes indicates the torque that needs to be supported by the structure of each finger. For the thumb, the component of the torque applied by the actuation/transmission system, $\overrightarrow{T_{m_T}}$, in the direction of $\overrightarrow{T_T}$ must at least be equal to the magnitude of $\overrightarrow{T_T}$. The cosine of the angle between the unit vectors of $\overrightarrow{T_{m_T}}$ and $\overrightarrow{T_T}$, γ_T, was found using the following equation:

$$cos\gamma_T = \frac{T_{T_z}}{\left\|\overrightarrow{T_T}\right\|}$$

$$cos\gamma_T = \frac{T_{T_z}}{\sqrt{\left(T_{T_x}\right)^2 + \left(T_{T_y}\right)^2 + \left(T_{T_z}\right)^2}} \qquad \text{D.3}$$

Substituting the known values, $cos\gamma_T$ was found to be 0.79. The magnitude of $\overrightarrow{T_{m_T}}$ was then determined using the following equation:

$$\left\|\overrightarrow{T_{m_T}}\right\| = \frac{\sqrt{\left(T_{T_x}\right)^2 + \left(T_{T_y}\right)^2 + \left(T_{T_z}\right)^2}}{cos\gamma_T} \qquad \text{D.4}$$

After substituting the known values, the torque that the thumb actuation/transmission system would need to apply was found to be $3.79Nm$. One can note that $\overrightarrow{T_{m_T}}$ is slightly higher than T_{T_z} in Table D.5, indicating that the thumb actuator is not 100% efficient in achieving the required contact force.

APPENDIX E: EXPRESSING THE COUPLING OF TWO DEGREES OF FREEDOM JOINTS IN TERMS OF THE ORIGINAL JOINT ANGLES

The coupling of two DOF joints is implemented by optimizing the D-H parameter, α_{D_2}, of the corresponding digit. This means that the two DOFs of the resulting joint have been rotated from the original ones. This appendix describes how the new position of the proximal phalanx can be expressed in terms of the original joint angles.

As with the approach considered in Appendix A (on p.217), the transformation matrix from the 1st to the 4th frame for the corresponding digit, $T_{D}{}_4^1$, was defined in terms of the original and the new joint angles so as to compare the orientation of the unit vector along x_{D_4}. The T_4^1 D-H parameters for the new joint angles are shown in Table E.1 in general terms. Here, α_{D_2} can have a value between $-\pi/2$ ° and $\pi/2$ °, while, depending on the orientation of the rotation axis of the motor, θ_{D_3} or θ_{D_4} is fixed at a specific angle, taking into consideration the limits of the smallest ROM among the two DOFs of the joint being considered (i.e., $\pm$ 65° for the thumb and $\pm$20° for the index finger). The negative range was also included to ensure that for any value of α_{D_2}, the actuated angle does not need to be negative.

Table E.1: The general D-H Parameters for the new joint angles

Transformation	i_D	$\theta_{D_{i_D}}$	$d_{D_{i_D}}$	$a_{D_{i_D}}$	$\alpha_{D_{i_D}}$
T_2^1	2	0	0	0	α_{D_2}
T_3^2	3	θ_{D_3}	0	0	$\pi/2$
T_4^3	4	θ_{D_4}	0	l_{D_4}	α_{D_4}

Taking the thumb CMC joint as an example, equations A.3 to A.5 (which are repeated below) define the orientation of the unit vector along x_{T_4}, relative to the 1st frame, in terms of the original joint angles. The equations from E.1 to E.3 define the orientation of the same vector in terms of the new joint angles.

original joint Angles:		*new joint angles:*	
$x_{T_1} = c\theta_{A_1} c\theta_{A_2}$	A.3	$x_{T_1} = c\theta_{T_3} c\theta_{T_4}$	E.1
$y_{T_1} = s\theta_{A_2}$	A.4	$y_{T_1} = c\alpha_{T_2} s\theta_{T_3} c\theta_{T_4} - s\alpha_{T_2} s\theta_{T_4}$	E.2
$z_{T_1} = s\theta_{A_1} c\theta_{A_2}$	A.5	$z_{T_1} = s\alpha_{T_2} s\theta_{T_3} c\theta_{T_4} + c\alpha_{T_2} s\theta_{T_4}$	E.3

Given the values of the new joint angles, θ_{A_2} is determined by equating A.4 to E.2. Meanwhile, θ_{A_1} is calculated by substituting the known value for θ_{A_2} in A.5 and equating it to E.3, which maintains the direction of the angle.

APPENDIX F: MUTATION AND CROSSOVER PROCESS IN MATLAB GENETIC ALGORITHM

The GA run in Matlab generates offspring for the next generation by combining two chromosomes together and/or mutating them. There are several ways of how this can be achieved. For example, typical methods used for the crossover operation include single-point crossover, multi-point crossover and simulated-binary crossover [220], [221]. This section discusses the process utilized in Matlab [219].

The crossover operation only takes place if a randomly selected number between 0% and 100% is less than Pc. In that case, the simulated-binary crossover is used, where a blending operation is carried out on each of the parameters of two parent chromosomes, x_1^p and x_2^p, to create two offspring solutions, x_1^c and x_2^c. The procedure involves first generating a random number, r_n, between 0 and 1. On the basis of the value of r_n, a parameter, β, is calculated using the following equations:

$$\beta = \begin{cases} (2r)^{\frac{1}{etac+1}} & if\ r_n < 0.5, \\ \left(\frac{1}{2(1-r)}\right)^{\frac{1}{etac+1}} & otherwise \end{cases} \tag{F.1}$$

The offspring solutions are then calculated as follows:

$$x_1^c = 0.5\left[(1+\beta)x_1^p + (1-\beta)x_2^p\right] \tag{F.2}$$

$$x_2^c = 0.5\left[(1-\beta)x_1^p + (1+\beta)x_2^p\right] \tag{F.3}$$

A similar approach is considered for the mutation process, where a parameter is only mutated if a random number generated between 0% and 100% is less than Pm. A polynomial mutation process is then used in which another random number, r_n, between 0 and 1, is generated. On the basis of this number, a parameter, δ, is computed using the following equations:

$$\delta = \begin{cases} (2r)^{\frac{1}{etam+1}} & if\ r_n < 0.5, \\ 1 - \left(2*(1-r)\right)^{\frac{1}{etam+1}} & otherwise \end{cases} \tag{F.4}$$

The mutated parameter is then calculated as follows:

$$x_1^c = x_1^p + [upper\ limit - lower\ limit] * \delta \tag{F.5}$$

Offspring which violate the upper or lower limits are then bound to the nearest limit. This is then repeated for all the parameters in each chromosome

APPENDIX G: STRESS ANALYSIS ON SIMPLE PARTS

Understanding the stress present in a part allows the optimization of any unconstrained parameters, as well as ensures that the material from which the part is manufactured has sufficient strength to withstand the loads present during the operation of the hand. Hence, this appendix describes the stress analysis carried out on simple, solid parts, taking the thumb CMC shaft as an example, to determine the minimum allowable yield/shear strength of the material as a function of the shaft radius, R_{shaft}.

The maximum stress that the thumb CMC shaft would need to withstand depends on the force that the thumb would need to apply/sustain, with higher loads applied/sustained closer to the joint axis. Given that objects are typically held by the proximal/distal phalange, the maximum perpendicular force that the thumb could apply/sustain by the centre of the proximal phalange (i.e., $\vec{F}_{c_1}$ has a magnitude of $53.5N$ and acts $60mm$ away from the joint axis, such that the moment applied by $\vec{F}_{c_1}$ around the joint axis, T_p, is equal to the maximum allowable output torque of the thumb transmission system (i.e., $T_p = 3.21Nm$), as shown in Figure G.1(a), was considered. On the basis of this load, the magnitude of the forces acting on the thumb CMC shaft, Figure G.1(b), was determined.

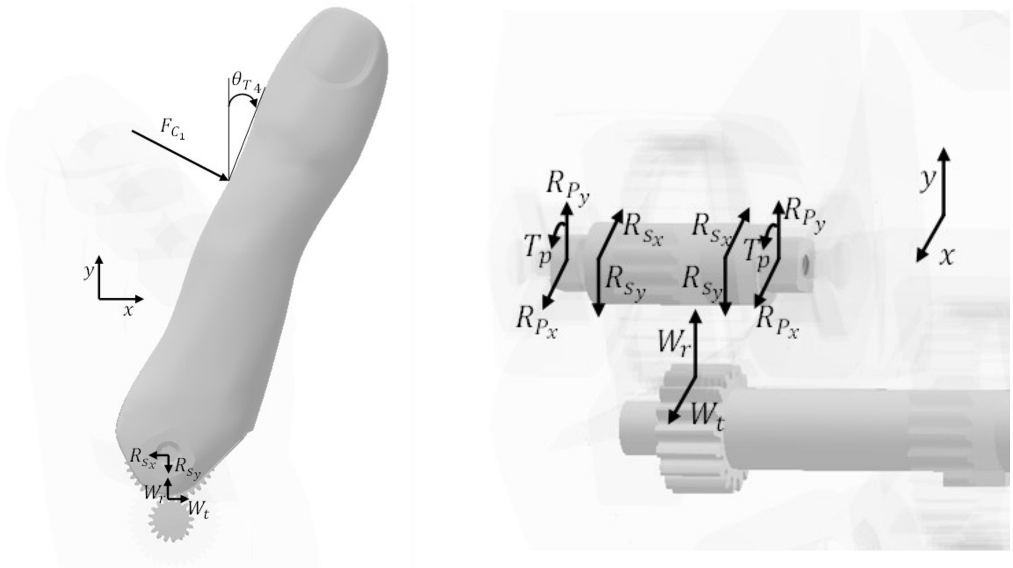

(a) (b)

Figure G.1: Forces acting on the thumb

The magnitude of the reaction force acting on the shaft due to the structure, R_s, was calculated, using the equations of equilibrium of the entire structure and taking into consideration the symmetry of the loads and knowledge on spur gears, which are given by Equations G.1 and G.2.

$$\sum F_x = 0 \qquad R_{s_x} = F_2 cos\, \theta_{T_4} + W_t \qquad \text{G.1}$$

$$\sum F_y = 0 \qquad R_{s_y} = F_2 sin\, \theta_{T_4} + W_r \qquad \text{G.2}$$

Using Equation 6.18 (on p.144), W_t was found to be 356.67N, where T_o is 3.21Nm. On the other hand, the radial force, W_r, which is also acting on the spur gear, was determined using Equation G.3:

$$W_r = W_t \tan \emptyset \qquad \text{G.3}$$

The reaction force between the shaft and the phalange, R_p, was determined by considering the equilibrium of the forces on the shaft in the x- and y-direction, as well as the moment about the z-axis, which are given by Equations G.4-G.6. It is to be noted that due to the symmetry of the loading, the reaction loads are equally distributed between the two supports.

$$\sum F_x = 0 \qquad R_{p_x} = R_{s_x} - W_t \qquad \text{G.4}$$

$$\sum F_y = 0 \qquad R_{p_y} = R_{s_y} - W_r \qquad \text{G.5}$$

$$\sum M_z = 0 \qquad T_p = W_t\, P_d = 3.21Nm \qquad \text{G.6}$$

As a result of these loads acting on the shaft, internal loads, such as bending moment, M_b, shear force, V, and torsion, T, are present at every point withing the shaft, as shown in Figure G.2, and occur in equal-and-opposite pairs.

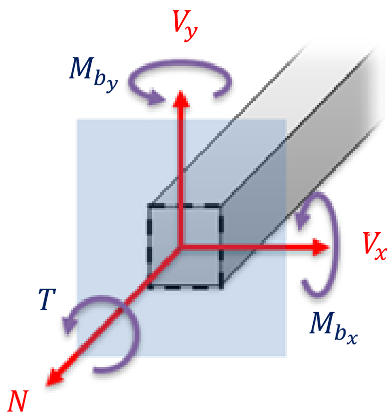

Figure G.2: The internal loadings acting on a cross-section of a beam [322]

The variation of these internal loads along the length of the shaft was then plotted, noting that their value may vary depending on θ_{T_4}. Figure G.3 shows the bending moment diagram for both the x- and y-direction, when θ_{T_4} is -25°

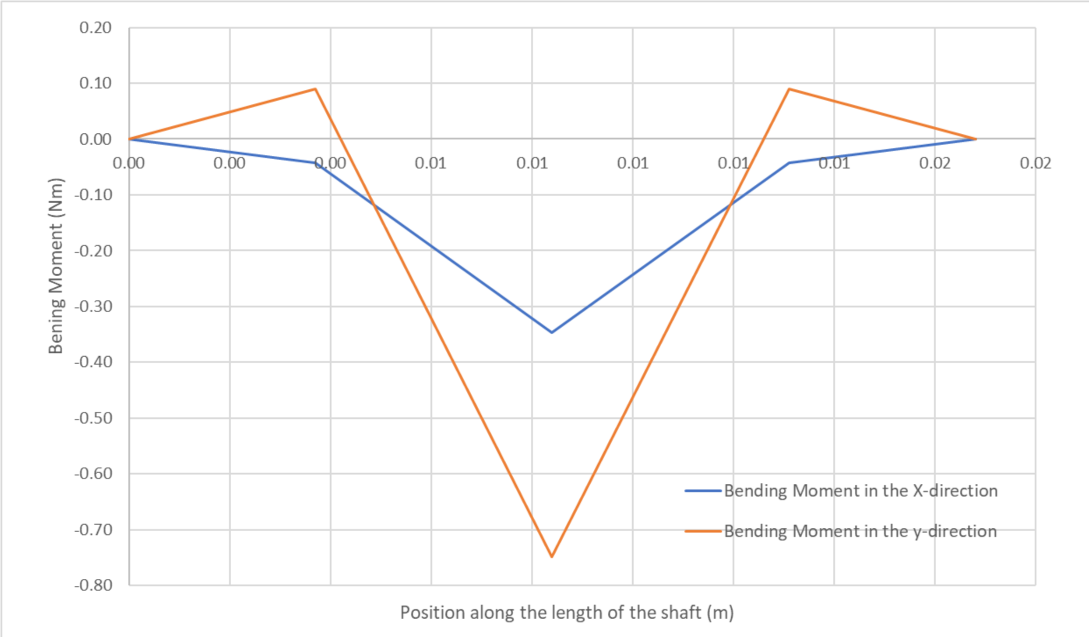

Figure G.3: The bending-moment diagram of the thumb CMC joint in the x- and y- directions, when θ_{T_4} is -25°

Consequently, normal stress, σ, and/or shear stress, τ, builds up in the cross-section of the shaft. For circular shafts, the maximum σ at the surface of the shaft, due to M_b in both the x- and y- direction, $\sigma_{b_{max}}$, was determined using Equation G.7 [322]:

$$\sigma_{b_{max}} = \frac{M_{b_{max_{\{x,y\}}}} y}{I} \tag{G.7}$$

Where,

- $M_{b_{max_{\{x,y\}}}}$ is the maximum M_b observed in both the x- and y-directions, Nm.
- y is the vertical distance away from the neutral axis, m, which in this case should be R_{shaft}.
- I is the moment of inertia around the neutral axis, m^4, which is defined as $\frac{\pi R_{shaft}^4}{4}$ for circular cross-section [322].

Meanwhile, $\tau_{V_{\{x,y\}}}$, the maximum τ that is applied on the cross-section of the shaft due to $V_{\{x,y\}}$, acts along the neutral axis (i.e., the axis in the cross-section of the shaft where no longitudinal stresses or strains are present). It was determined using Equation G.8 [322]:

$$\tau_{V_{\{x,y\}}} = \frac{V_{\{x,y\}}\, Q}{I\, t} \tag{G.8}$$

Where,

- Q is the first moment of area of the section above the point of shear stress with reference to the neutral axis, m^3, for maximum shear Q is defined as $\frac{2R_{shaft}^3}{3}$ for circular cross-section.
- t is the thickness of the shaft at a particular point of shear stress, m; in this case it is the diameter of the shaft.

Meanwhile, τ_T, the maximum τ build up due to T_p, is located at the surface of the shaft. It was determined using the following equation [322]:

$$\tau_T = \frac{T\ R_{shaft}}{J} \tag{G.9}$$

Where,

- J is the polar second moment of area, m^4, which is defined as $\frac{\pi R_{shaft}^4}{2}$ for circles [322].

The maximum τ that the shaft would need to withstand as a result of both $V_{\{x,y\}}$ and T was determined by adding $\tau_{V_{\{x,y\}}}$ and τ_T.

The material chosen for the shaft must have a yield strength and a shear strength greater than the maximum σ and τ calculated, by at least a factor of 1.5 (i.e., the required SF specified in Chapter 3 (on p.44)). Its density must also be taken into consideration. Depending on the design of the shaft, the R_s can be optimized to reduce its weight, as long as the maximum σ and τ present in the shaft remain within the limits.

APPENDIX H: TESTING THE STRENGTH OF A 3D-PRINTED PART

An experiment was carried out on the weaker digit, which is the index finger, to confirm whether the structure of the prosthetic hand when printed with the specified material and printing settings has enough strength to withstand the required loads.

A force is applied and sustained on the structure of the prosthetic hand every time it grasps an object. Each time, stress builds up on the different parts of the prototype. This means that the part may fail from a combination of static loading and fatigue. The latter is difficult to evaluate with a simple experiment, since the parts should fail after a significant number of cycles. Hence, the objective of this experiment was to determine whether the parts of the index finger can withstand a static load being loaded and unloaded on the structure for four times, where each time the load is held for 15 minutes.

The stress that builds up in the structure is a function of the magnitude, the direction, and the position of the load, as well as the angular position of the digit. In the case of the finger, the structure must be able to sustain a load that is applied both laterally and perpendicularly to the active joint, where for most objects, this load is applied by the distal phalange. Hence, the following three scenarios were proposed for the experiment, taking into consideration a SF of 1.5 and the specifications of the worm wheel and the thumb motor:

1. A perpendicular load of $43N$ applied at the fingertip when fully open;
2. A lateral load of $27N$ applied at the fingertip when the index finger is in the P-grasp position;
3. A perpendicular load of $65N$ applied at the fingertip when fully closed.

For each scenario, the structure of the finger was secured in a g-clamp, with the hanger (on which to hang the required loads) hooked at the required position and hung perpendicular to the ground. Given that only a part of the palm was printed for this experiment, a wheel with various holes at different angular positions, mounted instead of the worm wheel, was used to secure the finger in the correct position. Depending on the angular position required, a screw inserted from the back of the palm was tightened inside one of these holes. A deflection gauge was then used to measure the deflection of the structure at the point of contact, Figure H.1. For each scenario, the deflection observed at each loading was noted and listed in Table H.1.

(a)

(b)

Figure H.1: Testing the strength of the part in (a) scenario 1 and (b) scenario 2

Table H.1: The deflections noted for scenarios 1 and 2 after each loading

	Deflection 1 (mm)	***Deflection 2 (mm)***	***Deflection 3 (mm)***	***Deflection 4 (mm)***
Scenario 1	10	17	18.6	18.5
Scenario 2	16	17.7	19.3	24
Scenario 3	/	/	/	/

From the above table, one can observe that some deflection was observed in scenarios 1 and 2, but this should not hinder the overall function of the prosthetic hand. However, the same cannot be said for scenario 3, where the deflection observed was significant, such that when the load was applied, the finger ended up in the open position. This means that while the structure had sufficient strength to sustain the required load, the finger was not able to maintain its position in the presence of such loads. This could be due to the method used to secure the finger in place in the absence of the worm and wheel. Furthermore, some deformation was observed in the interface keys mounted on the Index MCP shaft, as shown in Figure H.1, which would have allowed the proximal phalanx to rotate relative to the corresponding shaft.

Figure H.2: The observed deformation in the interface keys mounted on the Index MCP shaft

APPENDIX I: DETERMINING THE COEFFICIENT OF FRICTION OF THE FRICTIONAL COVERS

An experiment was carried out to estimate μ_{rubber}, the coefficient of friction between the rubber chosen for the frictional covers and the different materials applicable to day-to-day activities.

The set-up shown in Figure I.1 was used, where ten objects of varied materials, as applicable to day-to-day activities (e.g., a body cream container, a wooden block, and a purse), were placed on a rubber plane. The inclination angle of this plane, θ_{slope}, was then increased gradually with a motor until the object was on the verge of slipping. At this point, the driving force (i.e., the component of the weight of the object, W_{object}, along the plane) is equal to the maximum frictional force, $F_{F_{max}}$, present between the two materials. Using Coulomb's Law of friction [192], μ_{rubber} was then calculated using the following equation:

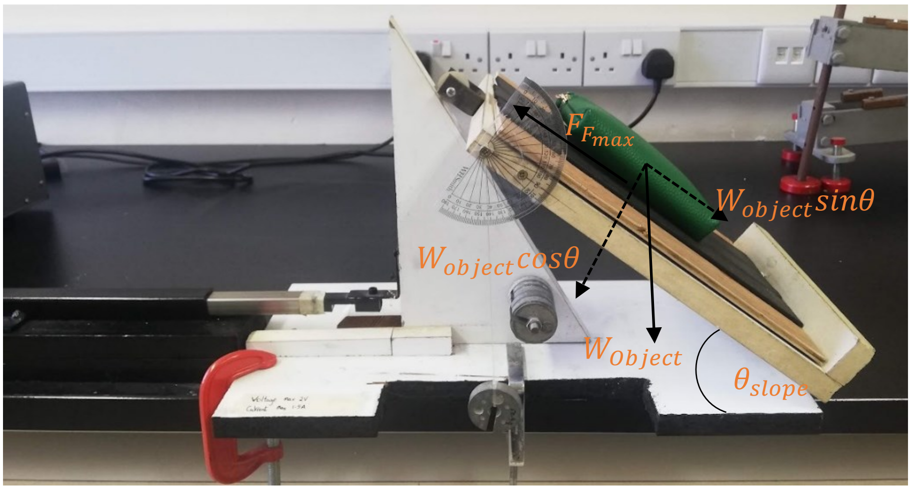

Figure I.1: The set-up used to determine the coefficient of friction of rubber with the different materials

$$\mu_{rubber} = tan\,\theta_{slope} \qquad \text{I.1}$$

This was repeated ten times for each object, with the average μ_{rubber} observed for the different objects listed in Table I.1. From this table, one can observe that the μ_{rubber} ranged from 0.75, for a piece of glass, to 1.19, for a wooden block. On average the μ_{rubber} was 1.01$\pm$ 0.14, which is greater than the μ_s assumed during the force analysis discussed in Section 5.3 (on p.89), which was 0.5. However, while the necessary precautions were taken to minimise errors present during the experiment, such as taking repeated readings and reading the protractor at eye level, some errors might still occur, such as parallax error and human error.

Table I.1: The friction coefficient between the rubber and different day-to-day materials

Object	***Material***	***Coefficient of Friction***	***Standard Deviation***
Body cream container	Plastic	1.11	0.07
Packet	Plastic	1.13	0.04
Wooden Block	Wood	1.19	0.06
Piece of a can of Beverage	Aluminium	1.01	0.04
Jar Cap	Metal	1.12	0.06
Small cereal Box	Paper	0.94	0.04
Purse	Fabric	0.99	0.04
Mobile Phone	Glass	0.82	0.04
Piece of Glass	Glass	0.75	0.03
Piece of Rubber	Rubber	1.1	0.04